Exploitation of stable nanostructures based on the Mouse polyomavirus for development of a recombinant vaccine against Porcine circovirus 2.

Martin Fraiberk[a], Michaela Hajková[a], Magdalena Krulová[a], Martina Kojzarová[a], Alena Drda Morávkova[a], Ivan Pšikal[b] and Jitka Forstová[a*]

[a] Charles University, Faculty of Science, Albertov 6, 128 40 Prague, Czech Republic

[b] Dyntec spol s r.o., Pražská 328, 411 55 Terezín, Czech Republic

[*] Corresponding author

E-mail: jitkaf@natur.cuni.cz

Abstract

The aim of this study was to develop a suitable vaccine antigen against porcine circovirus 2 (PCV2), the causative agent of post-weaning multi-systemic wasting syndrome, which causes significant economic losses in swine breeding. Chimeric antigens containing PCV2b Cap protein sequences based on the mouse polyomavirus (MPyV) nanostructures were developed. First, universal vectors for baculovirus-directed production of chimeric MPyV VLPs or pentamers of the major capsid protein, VP1, were designed for their exploitation as vaccines against other pathogens. Different strategies were employed based on: A) exposure of selected immunogenic epitopes on the surface of MPyV VLPs by inserting them into a surface loop of the VP1 protein, B) insertion of foreign protein molecules inside the VLPs, or C) fusion of a foreign protein or its part with the C-terminus of VP1 protein, thus forming giant pentamers of a chimeric protein. We evaluated the strategies by development of a recombinant vaccine against porcine circovirus 2. All candidate vaccines induced production of antibodies against the capsid protein of porcine circovirus after immunization of mice. The candidate vaccine, Var C, based on fusion of mouse polyomavirus and porcine circovirus capsid proteins, was able to induce production of antibodies with the highest PCV2 neutralizing capacity. Its ability to induce production of neutralization antibodies was verified after immunization of pigs. The advantage of this vaccine, apart from its efficient production in insect cells and easy purification, is that it represents a DIVA (differentiating infected from vaccinated animals) vaccine, also inducing an immune response against the mouse polyoma VP1 protein, thus able to distinguish between vaccinated and naturally infected animals.

Introduction

Most antiviral vaccines are based on killed or attenuated viruses. These vaccines, although relatively safe, still represent a non-negligible risk of reversion to a virulent phenotype *in vivo*. VLPs (virus-like particles), which lack infectious genetic material, represent a modern and safe alternative to the classical vaccines. Similarly to native virions, VLP nanostructures, due to their symmetry and repetitive structure, are able to cross-link surface immunoglobulins on the surface of B-cells, thus inducing a strong activation signal leading to B-cell proliferation and antibody production (1,2). They can serve as direct immunogens stimulating humoral and cellular immune responses. Also, they are internalized by cells as efficiently as native virus particles and have comparable intracellular trafficking (3). Capsid proteins of some viruses can form stable structures of empty capsids spontaneously (4–6). On the other hand, in the absence of viral nucleic acid, VLPs of some viruses are formed inefficiently and/or are unstable (7,8). Stable VLP structures and possibly other viral protein assemblies can serve as scaffolds for preparation of chimeric nanostructures carrying foreign epitopes that may induce a similarly strong humoral response.

Various studies on the exploitation of VLPs of polyomaviruses, including MPyV VLPs as carriers of foreign epitopes, proteins as well as nucleic acids, are reviewed in Teunissen et al or in Suchanova et al (9,10). Previously, we and others studied the potential of MPyV VLPs to carry DNA or proteins inside the MPyV VLPs (11–15).

Mouse polyomavirus is a small non-enveloped DNA virus with a circular 5.3 kbp genome, which encodes three structural proteins, VP1, VP2 and VP3. The capsid shell with icosahedral symmetry is composed of 72 pentameric capsomeres of the major structural protein, VP1. Two minor capsid proteins, longer (VP2) and shorter (VP3) versions synthesized from the same open

59 reading frame, are not exposed on the surface of the virion. Their common C-terminus interacts
60 with the central cavity of VP1 pentamers and the N-terminus of either VP2 or VP3 and is
61 oriented into the capsid interior. The structure of VP1 can be divided into three parts. The N-
62 terminal part includes the nuclear localization signal (first 12 amino acids) and the DNA-
63 binding domain, which interacts with DNA non-specifically (16,17). The central part of the
64 VP1 molecule is formed by α-helixes and β-sheets that are connected with loops. BC, DE and
65 HI loops are exposed on the surface of the capsid. The C-terminal part of VP1 is very flexible
66 and is responsible for inter-capsomeric contacts within the virus particle. VP1, the major capsid
67 architecture protein, is responsible for recognition of the sialysed ganglioside receptor on the
68 cell surface. Importantly, VP1 is able to self-assemble spontaneously and efficiently into VLPs
69 in the cell nucleus when expressed in mammalian, insect or yeast cells, or *in vitro* from VP1
70 pentamers produced in *E. coli*. (18–20). VP2 and VP3 are not required for MPyV VLP
71 formation. MPyV VLPs, as well as capsomeres (VP1 pentamers), are stable, can be easily
72 purified and, as the crystal structure of VP1 has been revealed, they can be easily modified (21).

73 In this study, we designed and prepared vectors for development of chimeric vaccines based on
74 stable VLPs and pentameric capsomeres of the mouse polyomavirus (MPyV) and tested the
75 feasibility and immunogenic properties of MPyV-based chimeric structures by developing a
76 vaccine against porcine circovirus 2 (PCV2).

77 Porcine circovirus type 2 (PCV2), first described in 1998 (22), is a non-enveloped single-
78 stranded DNA virus, a member of the genus *Circovirus*, family *Circoviridae*. PCV2 exists in
79 four genotypes, PCV2a, PCV2b, PCV2c and PCV2d (23). While PCV2a was the dominant
80 genotype in Europe until the year 2000, later, PCV2b has become prevalent (24). PCV2c was
81 identified in archived Danish tissues (25) of foetal pigs from Brazil (26) and PCV2d was
82 identified in China and in the USA (27,28).

PCV2 is considered as an infectious agent that causes several porcine circovirus-associated diseases (PCVAD). The clinical manifestation of PCVAD, post-weaning multi-systemic wasting syndrome (PMWS) (22), is characterized by chronic wasting and severely impaired weight gain in piglets 6 to 11 weeks old. The illness causes severe economic losses in swine industry. Although the presence of PCV2 is essential, only a few studies have been able to reproduce PMWS by inoculating with PCV2 only (29). Thus, another infectious or non-infectious factor must be present to develop PMWS (30). The most successful method to reproduce the disease is coinfection with pathogens such a porcine parvovirus (PPV) (31,32), porcine reproductive and respiratory syndrome virus (PRRSV) (33,34), torque teno virus TTV (35), *Mycoplasma hyopneumoniae* (36) or the use of immunostimulants, e.g. keyhole limpet hemocyanin in incomplete Freund's adjuvant (KLH-ICFA) (37,38).

PCV2 virions display icosahedral symmetry and a diameter around 17 nm (39,40). They are assembled from a single capsid protein. The PCV2 genome is approx. 1.8 kb long and contains four open reading frames (ORFs). ORF1 encodes proteins Rep and Rep', both necessary for replication (41). The ORF3 product plays a role in apoptosis induction and is not essential for virus replication (42,43). ORF4 influences the function of ORF3 and antagonizes apoptosis (44). ORF2 encodes one capsid protein (Cap) – the major antigenic determinant of the virus and the target for vaccine development. The capsid protein comprises three main areas, which contain immunogenic epitopes and are targets of the humoral immune response (45). Amino acids in positions 131, 151, 190 and the last three amino acids are involved in the conformation of neutralizing epitopes (46,47). The non-protective immunogenic epitope, amino acid positions 169-180, which is located inside the PCV2 capsid, seems to be a decoy epitope for the immune response. Pigs developing antibodies against this decoy epitope have significantly lower amounts of neutralizing antibodies (48). The crystal structure of PCV2 (49) allows location of previously determined immunogenic epitopes in the context of the capsid. The Cap

protein is able to assemble into VLP structures in insect (50) or yeast cells (51); however, the efficiency of assembly is much lower in comparison with that of MPyV VLPs. Moreover, self-assembled Cap VLPs were often less ordered than those in the purified PCV2 preparation (Nawagitgul et al (50) and our observations).

Here, we described preparation of several variants of chimeric nanostructures based on MPyV VLP and capsomere scaffolds, carrying epitopes or the entire sequence of PCV2 Cap protein. Further, we compared the abilities of the nanostructures to induce Cap-specific humoral and cellular immune responses in mice. The candidate vaccines exhibiting the best results in virus neutralization assay were further used for immunization of pigs and their immunogenic properties were compared with those of the Circoflex commercial vaccine.

Material and Methods

Cells, viruses

Porcine kidney cells PK15 (ATCC CCL-33), kindly provided by the Dyntec company (www.dyntec.cz), were cultivated in Dulbecco's modified Eagle's medium (DMEM; Sigma) containing 5% FCS (foetal calf serum; Gibco) in humidified incubator at 37°C in 5% CO_2 atmosphere. SF9 (*Spodoptera frugiperda)* insect cells (ThermoFisher Scientific) were cultivated as adherent culture at 27°C in TNM-FH medium (Sigma) containing 10% FCS, supplemented with 4mM L-glutamine (Gibco). The inoculum ($TCID_{50} = 10^5$) of PCV2b was kindly provided by the Dyntec company. PCV2b was originally identified in the Czech Republic by RT PCR performed in the inguinal lymph node (sample L14181) of a pig with clinical manifestation of PMWS (52). The sequence of the Cap gene is given in supporting information S1.

Construction of universal baculovirus transfer vectors for insertions of foreign sequences

The transfer vector for production of VLP-A nanostructures (with foreign epitopes exposed on the VP1 VLP surface) is based on pFastBacI (ThermoFisher Scientific). First, the restriction site for BamHI was deleted from multiple cloning sites (MCS) of pFastBacI as follows: the transfer vector was digested with BamHI, overlapping ends blunted by the Klenow fragment of DNA polymerase I (ThermoFisher Scientific), the vector was circularized by T4 DNA ligase (ThermoFisher Scientific) and then reopened by EcoRI and KpnI. The MPyV VP1 gene was amplified in two parts (VP1a and VP1b). The pMJG plasmid (53) containing the entire MPyV genome served as a template. Primers for amplification were designed so that seven amino acids in the MPyV VP1 DE loop were deleted and replaced by insertion of a BamHI site surrounded by flexible glycine-serine $(G\text{-}S)_3$ linkers. Manipulations in the DE loop have no effect on the stability of VP1 protein (54). Also, EcoRI and KpnI sides were added to 5´end and 3´end of the VP1 gene, respectively. The modified fragments of VP1 gene were connected through BamHI and inserted into the pFastBacI vector via EcoRI and KpnI restriction sites. The resulting construct pFastBacI-$VP1_{DE\Delta7}$ can serve as a universal cloning vector for insertions of sequences of different foreign immunogenic epitopes (through the BamHI restriction site) into the VP1 DE loop (Fig. 1A).

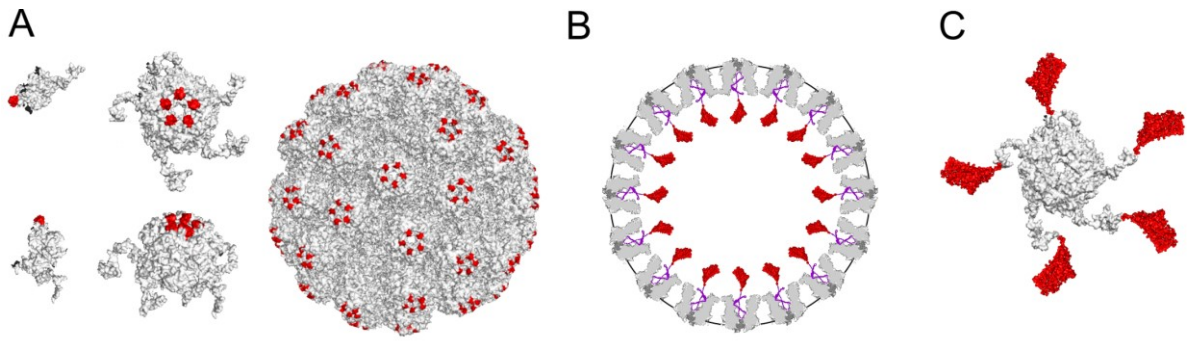

Fig. 1. Design of chimeric structures based on MPyV capsid proteins, carrying sequences of PCV2- Cap.

(A): Monomers, pentamers and VLP of MPyV (grey) with immunogenic epitopes of PCV2 Cap (red) inserted into the DE loop of MPyV VP1 (VLP-A structure). (**B):** Entire PCV2 Cap (red) fused with truncated MPyV minor capsid protein, VP3 (violet) is situated inside the MPyV VLP (VLP-B structure). Cross-section of VLP (grey) is presented. **(C):** Entire PCV2 Cap (red) fused with the C terminus of MPyV VP1 (grey) forming a pentameric capsomere (Capsomere C).

The transfer vector for production of VLP-B nanostructures (with foreign protein or its parts enclosed inside VP1 VLPs), based on the pFastBacDual transfer vector (ThermoFisher Scientific) allowing expression of two foreign genes from two baculovirus promoters, was constructed in our laboratory previously. Briefly, the MPyV VP1 gene was inserted into the plasmid through EcoRI and XmaI under the polyhedrin promoter. The truncated MPyV VP3 gene (tVP3; last 3′end 99 amino acids) was amplified and inserted under the control of baculovirus P_{10} promoter through SmaI and NheI sites. Both MPyV gene sequences were amplified from pMJG plasmid. The resulting construct pFastBacDual-VP1/tVP3 can serve as a universal cloning vector for fusion of sequences of foreign proteins with the 3′terminus of the tVP3 gene (Fig. 1B). VLPs produced by the recombinant baculovirus prepared by this transfer vector contain a foreign protein in their interior, connected via VP3 sequences with the central cavities of pentameric VP1 capsomeres (Fig. 1B).

For construction of the transfer vector for Capsomere-C nanostructures, the MPyV VP1 gene was amplified from the pMJG plasmid using primers designed to remove the stop codon and equip the gene with a BglII restriction site at the 5′end and BamHI and SalI restriction sites at the 3′end. VP1 sequences were then introduced into the pFastBacI vector opened with BamHI and SalI (transfer vector pFastBac1-VP1). Sequences of a foreign protein can be inserted in

frame into several restriction sites (e.g., BamHI, XbaI, PstI, KpnI, or HindIII). The recombinant baculovirus based on this transfer vector should express the VP1 protein fused at its flexible C-terminus with a foreign protein in the form of giant pentamers or their higher complexes (Fig. 1C).

Primers used for construction of baculovirus transfer vectors are given in Supporting information S2.

Insertion of sequences of the capsid protein of porcine circovirus 2b (PCV2b) into universal baculovirus transfer vectors

For VLP-A (VarA1 – A5) nanostructures, phosphorylated synthetic oligonucleotides (synthesized by the IDT company) encoding selected PCV2 Cap epitopes (Fig. 2) were inserted via BamHI restriction sites into the pFastBacI-VP1$_{DE\Delta7}$ transfer vector. For VLP-B (VarB) structures, the entire PCV2 Cap gene was amplified by PCR using the bacterial pET28b-Cap-His plasmid carrying the Cap gene (52) as a template. The FLAG epitope sequence was introduced upstream of Cap via PCR primers. The FLAG-Cap sequence was fused in frame with tVP3 via SmaI and SacI restriction sites with pFastBacDual-VP1/tVP3. The resulting vector was termed pFastBacDual-VP1/FLAG-Cap-tVP3. For Capsomere-C (VarC) nanostructures, the entire PCV2b Cap sequence was amplified using PCR primers introducing BamHI sites to the 5′ end and a His-tag (6 x His) and KpnI to the 3′end and cloned into the pFastBac1-VP1 vector opened by BamHI and KpnI. The resulting transfer vectors were termed pFastBac1-VP1-Cap-His. All these transfer vectors were further used for preparation of recombinant baculoviruses.

A

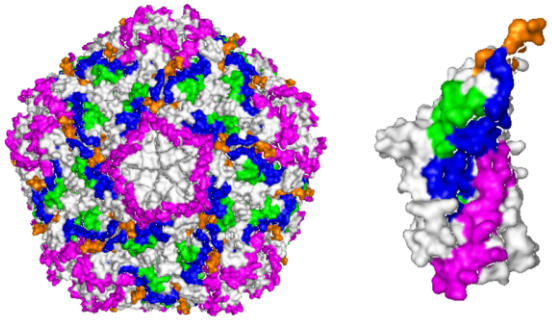

B

Name		PCV2 Cap sequence amino acid position
VLP-A	VarA1	50-66
	VarA2	69-82
	VarA3	185-202
	VarA4	224-233
	VarA5	224-233 (2x)
VLP-B	VarB	1-233 (entire protein)
Capsomere-C	VarC	1-233 (entire protein)

Fig. 2. Model of PCV2 capsid.

(A) Position of selected PCV2 Cap epitopes (coloured) on the surface of PCV2 particle (left) or Cap monomer (right). **(B)** Table of Cap sequences used for construction of individual nanostructure variants.

Phosphorylated oligonucleotides used for construction of baculovirus transfer vectors are given in Supporting information S3.

Recombinant baculovirus preparation

Recombinant baculoviruses were produced according to the manufacturer's instructions (ThermoFisher Scientific, Bac to Bac system). Briefly, *E. coli* DH10Bac containing a bacmid and helper vector were transformed by individual transfer vectors. Recombinant bacmids from positive bacterial colonies were isolated (ThermoFisher Scientific, PureLink™ HiPure Plasmid DNA Miniprep Kit) and verified by PCR. SF9 insect cells were transfected with bacmids by lipofection (ThermoFisher Scientific, Celfectin II reagent). Recombinant baculoviruses released into the growth media were harvested 72 hours after transfection and used for further multiplications by infection of insect cells to generate high-titre viral stocks.

SDS protein electrophoresis (SDS-PAGE) and Western blot analysis

Purified chimeric VLPs and nanostructures were boiled in Laemmli sample buffer for 5 minutes and resolved in 10% SDS-polyacrylamide gel (55). Separated proteins were stained by Gelcode stain (ThermoFisher Scientific). For Western blot analysis, proteins were electro-transferred onto nitrocellulose membrane (Serva) in cold blotting buffer (0.3% Tris, 1.44% glycine, 20% methanol) at 2.5 mA/cm^2 for 3 hours. The membranes were incubated in 5% skim milk in PBS for 1 h. Immunostaining with primary and secondary antibodies was carried out for 1 h and 40 min, respectively, and the membranes washed (3x10minutes) in PBS after each incubation. Membranes were developed using Pierce ECL Western Blotting Substrate reagent (ThermoFisher Scientific) and exposed to X-ray films (Agfa).

Blue native polyacrylamide electrophoresis (BN-PAGE)

The method was adapted from Hornikova et al (56). Briefly, purified nanostructures VarC were mixed with native PAGE sample buffer (ThermoFisher Scientific) and separated in native 3-12% gradient gel. The separated complexes were visualized by Gelcode staining.

Mass spectrometry

The bands of interest were cut out of the gel and chopped into 1x1x1 mm pieces. The pieces were destained, and DTT and iodoacetamide were applied to reduce and block cysteines. The samples were trypsinized as described previously (57). The dried-droplet method of sample preparation was employed and spectra were acquired in a 4800 Plus MALDI TOF/TOF analyzer (AB Sciex). Data were analysed using in-house running Mascot server 2.2.07 and

matched against a database composed of the following background databases: baculovirus expression system, insect SF9 cell proteome database of common contaminants, and MPyV VP1 sequences. Cysteine carbamidomethylation was set as fixed modification, and methionine oxidation and N, Q deamination were set as variable modifications. One missed cleavage site was allowed. Precursor accuracy was set to 50ppm and the accuracy for MS/MS spectra to 0.25 Da.

Immunofluorescence

PK15 cells grown on coverslips in 24-well plates were fixed with 3% formaldehyde for 30 minutes. Cells were permeabilized by 5-minute incubation in 0.1% Triton X-100 in PBS and then washed (three times, 10 minutes) with PBS. Free epitopes were blocked by 1-hour incubation in 1% BSA in PBS. Cells were immunostained by 1-hour incubation in primary antibody, washed (three times, 10 minutes) with PBS and incubated (30 minutes) with secondary antibody. After washing in PBS, the coverslips with cells were briefly washed in deionized water, dried-out and mounted in DAPI Gold solution (ThermoFisher Scientific).

Immunizations of mice and pigs

Mice were divided into groups (5 mice/group) and animals in each group were immunized subcutaneously with three doses (in two-week intervals) of one of the prepared nanostructures. The amount of protein used for immunization was 50 μg per dose. Fourteen days after the last immunization, animals were bled under total anaesthesia with Halothane (Sigma) and then sacrificed. Six-week-old pigs were divided into three groups. A group of seven pigs was immunized by the VarC nanostructure, a group of three pigs by a commercial vaccine, Circoflex (Boehringer-Ingelheim), and the control group of three pigs received adjuvants in PBS. Immunization was performed two times in a 3-week interval into the cervical muscle. The

single 1 ml dose contained 100 µg of antigen and 30 % of Polygen adjuvants (MVP Technologies). The immunization with commercial vaccine Circoflex was performed according to the manufacturer's instructions.

Before pig immunization, the candidate vaccine VarC was inactivated by binary ethylenimine prepared according to Rueda et al (58).

ELISA analyses

The PCV2b virus was propagated in PK15 cells. The cells were infected by multiplicity MOI = 0.01 and 6 days after infection. The cells including growth medium were harvested and subjected to three-fold freezing and melting. Cell lysate was clarified by centrifugation (15000×g, 10 minutes, 4°C) and the virus concentrated by ultracentrifugation at 25,000 rpm, 3 hours, 4°C, Beckman rotor SW28. Sediment was resuspended in cold PBS and protein concentration was measured by the Bradford assay (59). ELISA 96-well plates (Nunc) containing 25 µg of crude PCV2 virus in 50 µl of PBS were incubated overnight at 4°C. The plates were washed five times with PBS containing 0.05% Tween-20 (Sigma) and blocked by 2-hour incubation in 2% skim milk in PBS. Then, 100 µl of serum (diluted as indicated) of control or immunized mice was applied to the wells and incubated for 1 hour. Anti PCV2 Cap monoclonal antibody was used as a positive control. After washing with PBS containing 0.05% Tween-20, 50 µl horseradish peroxidase (HRP)-conjugated secondary antibody, diluted according to the manufacturer's recommendation, was added for 1 hour. Wells were washed with PBS/Tween-20 (0.05%) and overlaid with 100 µl of substrate solution (ABTS, Sigma). The absorbance of each well was determined at 415 nm using a microplate reader (Epoch, BioTec Instruments).

The ELISA commercial set INgezim CIRCO IgG (Ingenasa) was used according to the manufacturer's instructions for measurement of anti PCV2 antibody development in immunized pigs.

Electron microscopy

Parlodion-carbon-coated grids were applied on top of a 5-µl drop of the sample and left to absorb the sample for 5 min. The grids were then rinsed twice in a drop of filtered distilled water for 30 seconds and negatively stained twice by one-minute incubation on a drop of 2% phosphothungustic acid (PTA, pH 7.3, Sigma), left for 1 min and then dried. Electron micrographs were recorded in a JEM-1011 electron microscope (JEOL) operating at 80 kV.

Antibodies

The following primary antibodies were used in this study: mouse monoclonal antibody against MPyV VP1 (7), mouse monoclonal antibody against FLAG (Sigma), mouse monoclonal antibody against PCV2 Cap (Median Diagnostics) and mouse monoclonal antibody Penta His (Sigma) against Histag. The following secondary antibodies were used: goat antibody against mouse immunoglobulins conjugated with HRP (Bio-Rad) and with Alexa Fluor-488 (ThermoFisher Scientific) and donkey antibody against swine immunoglobulins conjugated with HRP (Santa Cruz Biotechnology).

Animals

Charles River BALB/c female mice at the age of 8 weeks were purchased from the breeding unit of the Institute of Molecular Genetics, CAS, Prague, or Velaz company, Prague. Pigs (MeLiM strain) at the age of six weeks were purchased from the Institute of Animal Physiology

and Genetics CAS, Libechov. The use of animals was approved by the local Animal Ethics Committee.

Isolation and quantitative determination of PCV2 DNA

Total genomic DNA was extracted from 200 µl of each serum sample using a NucleoSpin Blood isolation kit (Macherey-Nagel) according to the manufacturer's instructions.

Quantification of PCV2 DNA levels was performed using real-time PCR in a Step One Plus instrument (Applied Biotechnologies) in TaqMan format as previously described by Brunborg et al (60). In short, the TaqMan probe was labelled with 5'-FAM and 3'-BHQ1 fluorophores (Generi Biotech) and the primers were designed to amplify a 100 bp DNA fragment within the selected nucleotide sequence of the PCV2 Cap gene. Absolute quantification of PCV2 DNA was carried out using calibration curves generated by means of external standard DNA obtained by cloning of the PCV2 cap gene in a pCR 2.1 vector (ThermoFisher Scientific). Standard curves for PCV2 DNA quantification were generated using tenfold dilution of the linearized plasmids in the range of 8 log10.

Serum neutralization assay

PCV2-neutralizing antibodies were detected using the serum neutralization assay adapted from Meerts et al (61) and Lefebre et al (62). Porcine PK15 kidney cells were seeded into a 24-well plate at the density of 1.5×10^5/well. Sera originating from the groups of animals (mice or pigs) immunized with the same nanostructure were mixed at equal volume and inactivated at 56°C for 1 hour. Then, 1 ml of PCV2 ($TCID_{50} = 10^5$) in DMEM medium containing 5% FCS was added to individual serum mixtures and incubated for 1 hour at 37°C to allow antibodies to attach to the virus. The mixtures were then used to infect PK15 cells growing on coverslips.

After 1 hour of incubation at 37°C, the mixtures were removed, the cells were washed by medium without serum and then incubated with complete DMEM medium (5% FCS) for 36 hours. After fixation, indirect immunofluorescence assay was performed (using primary antibody against PCV2 Cap and Alexa Fluor-488 secondary antibody). The numbers of infected cells in the samples were calculated and compared with the number of infected cells obtained with controls (cells infected with the virus mixed with sera of control group animals).

Evaluation of cell immune responses

Lymphocyte stimulation

Single-cell suspension of spleen cells from BALB/c mice was prepared in RPMI 1640 medium (Sigma) containing 10% foetal calf serum (FCS, Sigma), antibiotics (100 u/ml of penicillin, 100 μg/ml streptomycin), 10mM HEPES buffer and 5×10^{-5}M 2-mercaptoethanol (hereafter referred to as complete RPMI 1640 medium). The cells (75×10^5 cells/ml) were cultured in a volume of 1 ml of complete RPMI 1640 medium in 24-well tissue culture plates (Nunc) unstimulated or stimulated with 50 μg/ml of nanastructuresVarA4, VarB, VarC and $VP1_{Con}$ for 48-h incubation period.

Detection of activation markers

To characterize the capacity of nanostructures VarA4, VarB and VarC to trigger immune activation, the cultured spleen cells were harvested and washed with PBS containing 0.5% bovine serum albumin (BSA) and centrifuged (250 x *g*, 8 min). Cells were stained for 30 min on ice with the following monoclonal antibodies (mAbs): fluorescein isothiocyanate (FITC)-labelled anti-CD4 antibody (clone GK1.5, BD Pharmingen), phycoerythrin (PE)-labelled anti-CD4 antibody (clone GK1.5, BD Pharmingen), allophycocyanine (APC)-labelled anti-CD8a

antibody (clone 53-6.7, BioLegend), FITC-labelled anti-CD25 antibody (clone PC61, eBioscience), APC-labelled anti-CD25 antibody (clone PC61, BioLegend), Alexa Fluor 700-labelled anti-CD45 antibody (clone 30-F11, BioLegend), PE-labelled anti-CD69 antibody (clone H1.2F3, BioLegend). Dead cells were stained using Hoechst 33258 dye (Sigma) added to samples 15 min before flow cytometry analysis. Data were collected using a LSRII flow cytometer (BD Biosciences) and analysed using Gatelogic 400.2A software (Invai).

Intracellular staining of cytokines

To evaluate the ratio of cytokine-producing lymphocytes, spleen cells were cultivated in the absence or presence of nanostructures VarA4, VarB, VarC and VP1 control ($VP1_{Con}$) (50 μg/ml), and PMA (20 ng/ml Sigma), inonomycin (500 ng/ml, Sigma) and brefeldin A (5 μg/ml, eBioscience) were added to the cultures for the last 5 h of the 48-h incubation period. The cells were harvested and washed with PBS containing 0.5% BSA. Before intracellular staining, the cells were incubated for 30 min on ice with Alexa Fluor 700-labelled anti-CD45 antibody (clone 30-F11, BioLegend) and Live/Dead Fixable Violet Dead Cell Stain Kit (Molecular probes, Eugene, OR) for the staining of dead cells. For intracellular staining, the cells were fixed and permeabilized using a Fixation/permeabilization Buffer Staining Kit (eBioscience) according to the manufacturer's instruction. For detection of cytokine-producing lymphocytes, the cells were stained with the following mAbs: FITC-labelled anti-IFNγ antibody (clone, XMG1.2, BioLegend) and PE-labelled anti IL-4 antibody (clone 11B11, eBiosciences) for 30 min at 25°C. Data were collected using a LSRII flow cytometer (BD Biosciences) and analysed using Gatelogic 400.2A software.

Statistics

All results are expressed as means ± SD, or as SEM. The statistical significance of differences between the means of individual groups was calculated using one way analysis of variance (ANOVA). A value of $P \leq 0.05$ was considered statistically significant.

Results and Discussion

Design and preparation of universal vectors for chimeric nanostructure production

Three types of chimeric structures based on structural proteins of the mouse polyomavirus carrying foreign epitopes or entire proteins were designed (Fig. 1): A) MPyV virus-like particles (VLPs), composed of MPyV major capsid protein, VP1, carrying a foreign epitope on their surface (VLP-A), B) MPyV VLPs carrying sequences of a foreign protein inside the particle (VLP-B), and C) MPyV pentameric capsomeres composed of pentamers of VP1 fused at its C-terminus with foreign protein sequences (Capsomere C). For production of chimeric structures, universal baculovirus transfer vectors were prepared (for detailed description, see Material and Methods). Briefly, for production of VLP-A structures, sequences of top seven amino acids of the DE loop of MPyV VP1 were replaced by a cloning site for insertion of a foreign epitope surrounded by sequences of a glycine-serine linker (pFastBac1 $VP1_{DE\Delta 7}$). For production of VLP-B structures, a transfer vector ensuring expression of the VP1 gene (for VLP formation) and the C-terminal part of VP3 (responsible for interaction of MPyV minor capsid proteins with the central cavity of VP1 capsomere) was prepared. Cloning sites prior to truncated VP3 gene sequences allow fusion of foreign gene sequences with the sequences of truncated VP3. The fused protein should be situated inside VLPs (pFastBacDual VP1/tVP3). Finally, a baculovirus

transfer vector (pFastBac1 VP1) for production of the capsomere C structure carries the VP1 gene with eliminated stop codon and several restriction sites for fusion with the N-terminus of a foreign gene. Fusion of foreign sequences to the 3´terminus of VP1 gene prevents VLP formation while oligomerization into pentameric VP1 capsomeres should not be affected.

The universal vectors were used for construction of baculoviruses producing candidate chimeric antigens for development of vaccines against porcine circovirus 2.

Preparation and characterization of nanostructures carrying the capsid protein of porcine circovirus 2 or its epitopes

First, we prepared chimeric MPyV VLPs carrying selected immunogenic epitopes of PCV2 Cap protein on their surface (VLP-A). For this, we synthetized four epitopes designed according to those previously described by Lekcharoensuk et al (45) and refined by Shang et al (47). Lekcharoensuk et al (45) mapped conformational epitopes of the PCV2 capsid protein by analyses of PCV1-PCV2 ORF2 (open reading frame 2) chimeras in the context of the non-pathogenic PCV1 infectious genome, using seven PCV2 monoclonal antibodies recognizing conformational epitopes. We selected four linear sequences and refined them according to their accessibility on the capsid surface, taking advantage of PCV2 capsid structure determination (42). The selected epitopes (1 – 4) shown by four different colours on the model of PCV2 capsid (Fig. 2A) and Cap monomer (Fig. 2B) were inserted into baculovirus transfer vector pFastBac1 $VP1_{DE\Delta 7}$. Insertions of epitope sequences into the DE loop of MPyV VP1 were confirmed by sequencing. The fourth (yellow) epitope sequence (see Fig. 2) was inserted into the transfer vector as a monomer (4) or dimer (5). From all five constructs, recombinant baculoviruses were prepared for production of VLPs carrying different epitopes (VarA1 – VarA5) in insect cells.

Further, entire Cap protein-coding sequences (provided by the FLAG tag connected with 5'terminus of the Cap gene) were fused with tVP3 in the pFastBacDual VP1/tVP3 transfer vector, and recombinant baculovirus was prepared for production of VLPs with Cap sequences inside VLPs (VarB). We did not expect a high level of Cap-specific humoral response induced by this nanostructure but were interested in whether this nanostructure can induce cellular responses. Previous study performed by Tegerstedt et al (15) showed that MPyV-VLPs carrying inside a fusion protein between MPyV-VP2 and the extracellular and transmembrane domains of human Her2/neu (a proto-oncogene overexpressed in many epithelial carcinomas) induced a rejection response against a tumour inoculum, as well as inhibition of the spontaneous tumour outgrowth in a mutant Her2 transgenic mouse model.

Finally, the cap gene connected at its 3'end with His tag sequences was fused with the 3'end of VP1 gene in the pFastBac1 VP1 transfer vector, and recombinant baculovirus for production of chimeric VP1 capsomeres (VarC) was prepared. FLAG (in VarB) and His tag (in VarC) were inserted for detection of Cap fusion proteins by immune analysis (antibody against the Cap protein for western blot analyses is not available) and for isolation of VarC nanostructures.

Lysates of insect cells infected with individual recombinant baculoviruses were used for isolation of chimeric structures. The presence of epitopes inserted in the DE loop region of all five variants was verified by mass spectroscopy. Electron microscopy (EM) revealed that VarA1, VarA3, VarA4 of chimeric VP1 protein efficiently formed VLP structures, similarly to $VP1_{DE\Delta7}$ (Fig. 3). On the other hand, production of VP1 VarA2 did not yield stable VLPs. The EM picture of VarA2 shows pentamers of non-assembled VLPs or complexed into irregular higher assemblies. VP1 VarA5 is assembled into VLPs and into filamentous structures of different diameters. VLPs were observed in the picture of VarB designed to carry the Cap protein inside. VarC formed VP1-Cap fusion protein complexes with regular morphology,

reminding giant VP1 pentamers by the central hole. These structures formed large aggregates. Apart from the ability of MPyV VP1 to form stable pentamers, the Cap-Cap interaction can apparently cause further complexing of the fusion protein structures. The Cap protein was shown to produce stable dimers (63).

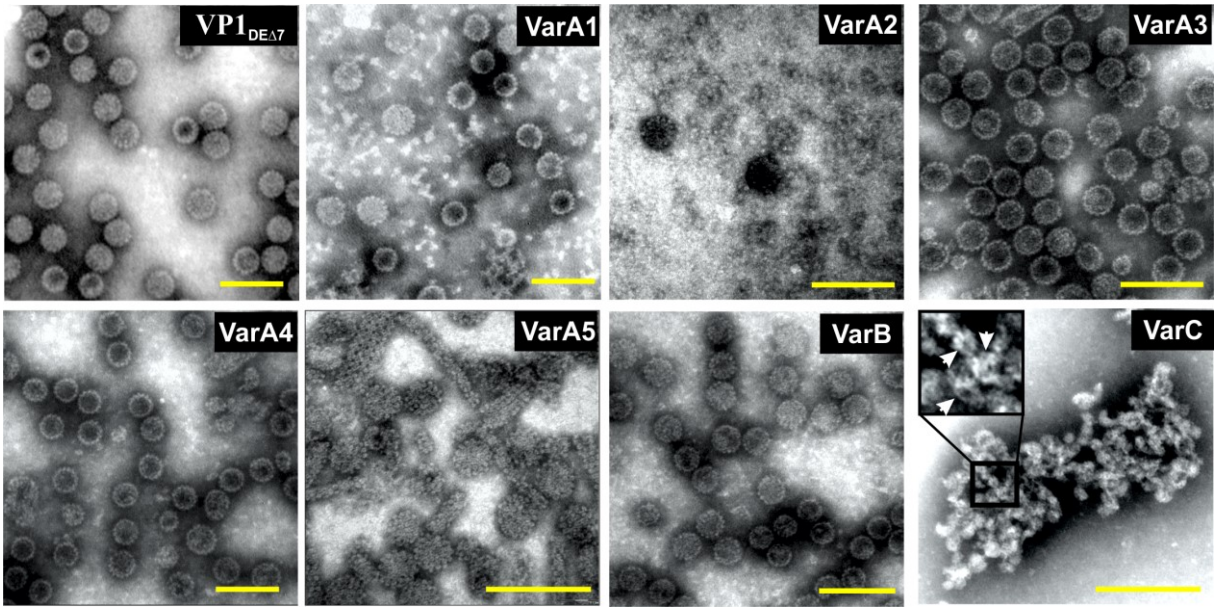

Fig. 3. Electron microscopy of isolated structures.

Negative staining with 2% PTA. The bars represent 100 nm.

The yields of chimeric nanostructure production ranged from 48 mg /L to 80 mg/L.

Isolated structures were further examined by SDS PAGE and Western blot analysis (Fig. 4). Gelcode-stained SDS PAGE (Fig. 4Aa) revealed that all variants of VP1 protein with Cap epitopes inserted into the DE loop (VarA1 – VarA5) were stable and their mobilities corresponded approximately to that of VP1 (45 kDa). No degraded VP1 was observed on western blot stained with VP1 antibody (Fig. 4Ab). Fig. 4B shows SDS PAGE (a) and Western blot analyses (b,c) of the VarB structure. Beside the band corresponding to VP1 protein (Fig. 4Ba,b), a band with mobility corresponding to the FLAG-Cap-tVP3 fusion protein (37 kDa)

and interacting with antibody against FLAG was detected in the lysate of purified VLPs VarB (Fig. 4Bc). In theory, a maximum of 72 molecules of FLAG-Cap-tVP3 can be incorporated into one particle (one molecule into the central cavity of each VP1 capsomere). For rough estimation of the number of fused Cap molecules incorporated into one VLP, the densities of VP1 and FLAG-Cap-tVP3 bands of purified VLPs separated in SDS-PAGE and stained with Coomassie dye were measured. The estimated number was 12 FLAG-Cap-tVP3 molecules per one particle. Analysis of the VP1-Cap fusion protein (VarC) is presented in Fig. 4C. The band with expected mobility for the fusion protein (71 kDa) was detected on SDS-PAGE (Fig. 4Ca) and its identity proved by antibodies against VP1 (Fig. 4Cb) and His tag (Fig. 4Cc). BN-PAGE (blue native electrophoresis) was employed to reveal high-molecular complexes of VarC (Fig. 4Cd). As MPyV VP1 forms immediately after translation of pentamers, we expected to see, among others, pentameric complexes. The molecular weight of VP1-Cap-HIS pentamer is 356 kDa. Surprisingly, the only band detected in the PAGE gel corresponded by its mobility to a decamer (2x pentamer) of the fused VP1-Cap protein. A substantial part of the loaded material did not enter the gel, confirming high aggregate formation.

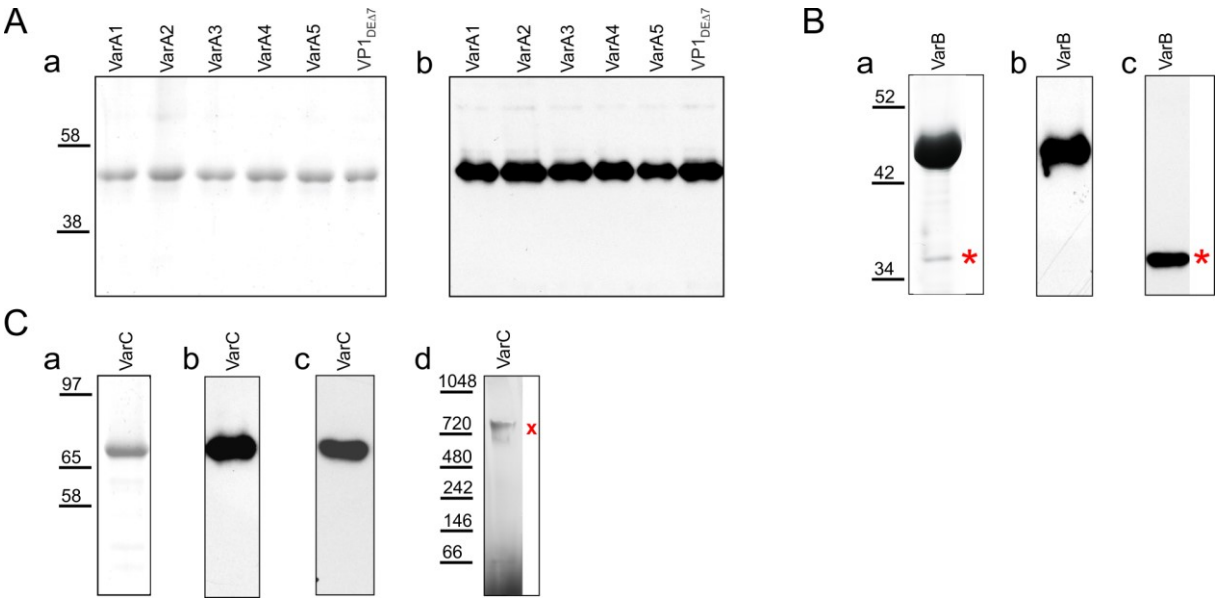

Fig. 4. SDS PAGE and Western blot analyses of purified structures.

Lysates of isolated structures resolved by SDS PAGE followed by Coomassie brilliant blue staining **(a)**, Western blot analyses **(b, c)**. Lysate of VarC resolved on Blue native electrophoresis stained by Gelcode stain. **(d)**. **(A)** VLP-A (Var A1 – A5) and control VLPs composed of $VP1_{DEA7}$. **(B)** VLP-B (VarB). **(C)** Capsomere C (VarC). Antibodies used: antibody against VP1 **(Ab, Bb, Cb)**, antibody against FLAG **(Bc)** and antibody against His tag **(Cc)**. *****mark: Cap-tVP3 band **(Ba, c)**, **x** mark: band corresponding to double pentamer of VP1-Cap-His **(Cd)**.

Immunization by chimeric nanostructures induced specific antibody responses in mice

Mice (five per group) were immunized with individual structures as described in Materials and Methods. Their humoral responses were tested by ELISA (using PCV2 virus as antigen) 14 days after the last immunization. In accordance with our previous findings (12,64), high titres of antibodies against the VP1 protein were detected in all immunized mice (S4). Importantly, all immunized mice (except those of control groups) developed antibodies specific for the PCV2 virus (Fig. 5). As expected, the lowest level of Cap-specific antibodies was induced by VarB VLPs carrying the Cap protein inside the particles. A relatively lower antibody response was also induced with the Cap epitope carried by VarA1 VLP.

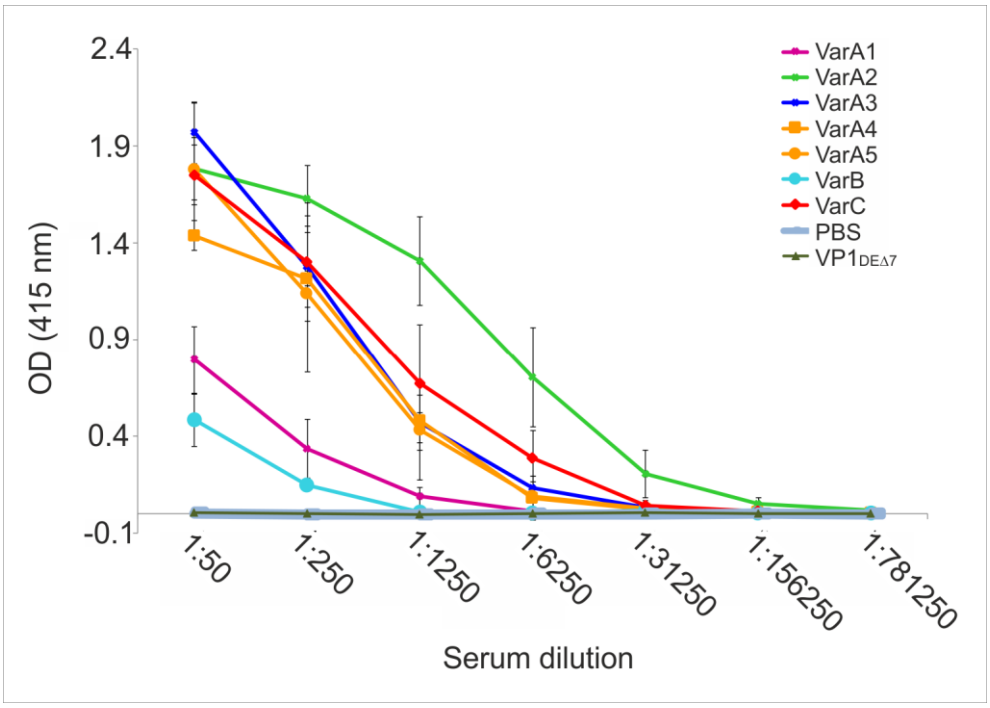

Fig. 5. Cap-specific antibody response induced by candidate vaccine structures in mice.

Groups of mice were immunized three times with individual candidate vaccine structures (50 µg/dose), or with PBS or VLPs composed of $VP1_{DE\Delta7}$ controls. The presence of specific antiPCV2 antibodies was examined by ELISA. Concentrated lysate of PCV2-infected PK15 cells was used as coating material.

Next, we were interested in whether Cap-specific antibodies induced in mice by the prepared nanostructures are able to block PCV2 infection. PCV2 virus inoculum was mixed with inactivated mice sera and after 1 h incubation at 37°C used for infection of PK15 cells. After 36 h, cells were fixed and the numbers of Cap-positive cells were counted. The sera containing Cap-specific antibodies were tested in the neutralization assay. Each serum mixture of mice immunized with VLPs carrying a Cap epitope (VarA) (in dilution 1:50) caused approx. 50% decrease of infected cells in comparison with the control serum. This result reflects the fact that all selected epitopes are part of one dominant conformation epitope on the capsid surface (49). Introduction of a dimer of epitope 4 into VLPs (VarA5) did not significantly affect either

antibody production or virus neutralization. The best results of virus neutralization were achieved after immunization with the VarC structure. The sera of the mice immunized by VarC exhibited 85% neutralization activity in dilution 1:50 (Fig. 6).

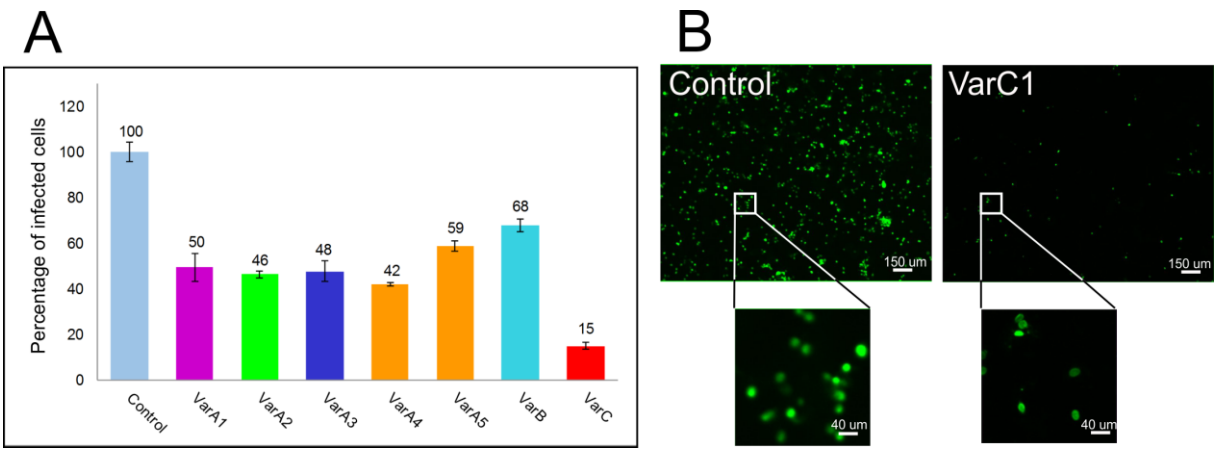

Fig. 6. PCV2 virus neutralization by antibodies induced in mice.

PK15 cells were inoculated with a mixture of 50-fold diluted sera collected from immunized pigs and PCV2 virus (final concentration $TCID_{50} = 10^5$). Control cells were infected with the same amount of the virus mixed with 50-fold diluted serum of mice immunized with PBS. Infected cells were detected 36 hpi by immunofluorescence assay with specific antiCap PCV2 antibody and the number of Cap PCV2-positive cells (green) was calculated. The columns represent percentage of infected cells relative to control. **(A)** Graph of neutralizing activity of mouse sera, **(B)** representative example of immunofluorescence staining of control cells and cells infected with virus incubated with sera of mice immunized by VarC. Error bars represent standard error of three independent experiments. Bars represent 50 µm.

VarC candidate vaccine induces cellular responses *in vitro*

Cell-mediated immunity is an important mechanism in protection of organisms against viral infections. To elucidate whether the prepared nanostructures were able to modulate the cellular

immune response, one representative of VarA nanostructures, Var A4, and VarB and Var C were tested in *in vitro* assays for changes in the population of leukocytes, their activation and cytokine production. To this aim, spleen cells were cultured in the presence or absence of individual nanostructures and cell populations were phenotypically characterized by flow cytometry. As shown in Fig. 7A, VarC by itself significantly increased the proportion of $CD19^+$ cells (Fig. 7Ac), whereas populations of $CD4^+$ (Fig. 7Aa) and $CD8^+$ (Fig. 7Ab) cells remained unaltered by the presence of any tested candidate vaccines. This finding is consistent with the increased production of antibodies specific for the PCV2 virus.

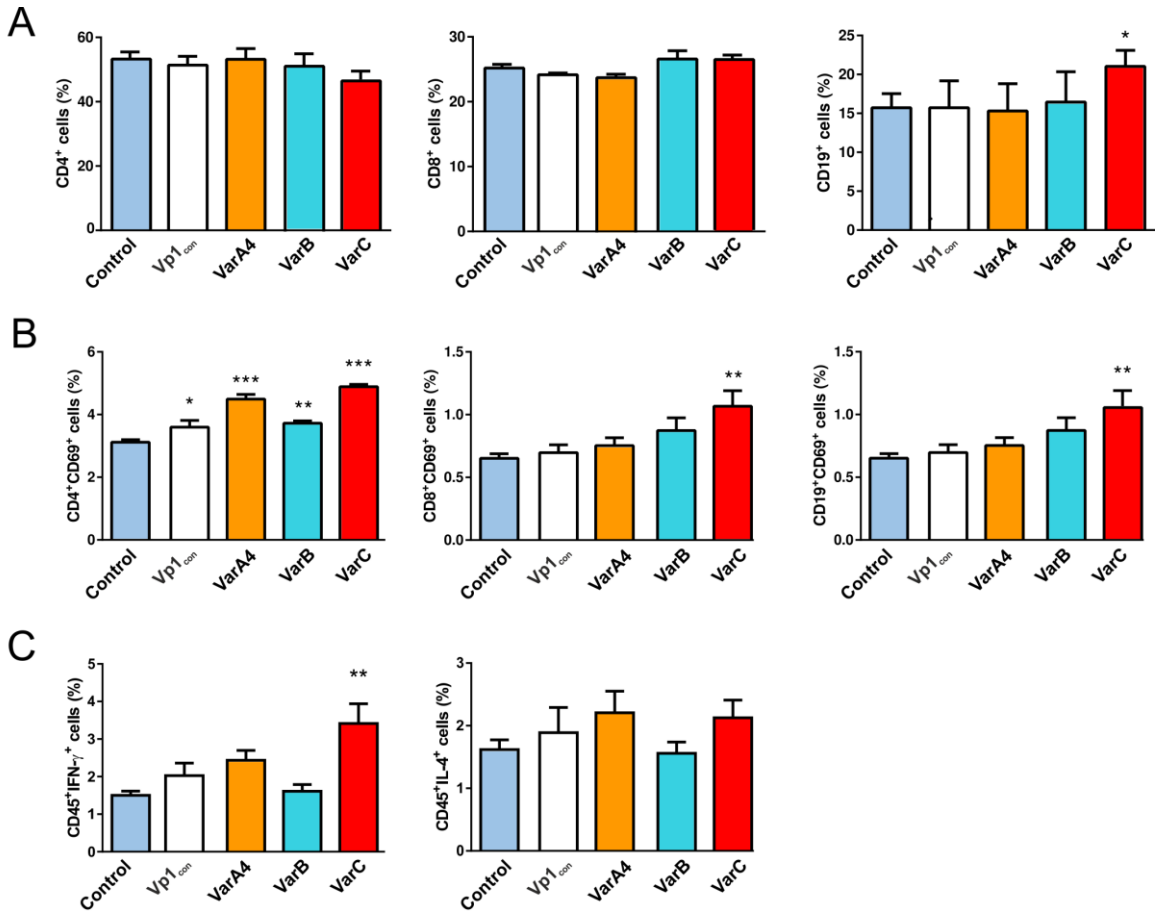

Fig. 7. Cellular immune responses induced by candidate vaccines in mice tested *in vitro*.

522 **(A)** Relative representation of Th $CD4^+$, Tc $CD8^+$ and B lymphocytes $CD19^+$ in mouse
523 splenocyte population after *in vitro* incubation with VarA4, VarB and VarC nanostructures. **(B)**
524 Activation of Th $CD4^+$, Tc $CD8^+$ and B lymphocytes $CD19^+$ in the mouse splenocyte population
525 after *in vitro* incubation with VarA4, VarB and VarC nanostructures. **(C)** The IFNγ and IL-4
526 intracellular level of mouse splenocyte $CD45^+$ population after *in vitro* incubation with VarA4,
527 VarB and VarC nanostructures. White columns represent controls – splenocytes without added
528 nanostructures, $VP1_{Con}$ – MPyV VLPs without inserted PCV2 epitopes, scaffold only. Error
529 bars represent standard error of the mean, SEM, *P <0.05, ** P<0.005, *** P < 0.0005.

530 Then, activation of T and B cell populations in the spleen cell culture by tested candidate
531 vaccines was determined. As demonstrated in Fig. 7B, all tested candidate vaccines activated
532 $CD4^+$ lymphocytes. A more apparent increase was observed when the cells were cultured in the
533 presence of VarA4 and VarC (Fig. 7Ba). The frequency of CD8 (Fig. 7Bb) and CD19 cells
534 expressing early activation marker CD69 (Fig. 7Bc) were significantly increased only in the
535 presence of VarC in the culture. Up-regulation of activation marker CD69 on a large proportion
536 of T and B cells after acute viral infection has been documented (65). As all lymphocyte
537 populations contribute to the specific anti-viral response (66), it is important that the tested
538 populations of T and B lymphocytes are activated by the candidate vaccine. CD69 has also been
539 confirmed as a marker of functionality of leukocytes after *in vitro* expansion (67).

540 To determine whether the candidate vaccines by themselves may prime a Th1-polarized
541 response in the splenocyte culture, we analysed (by intracellular staining) production of IFN-γ
542 and IL-4 by $CD45^+$ cells. A significant increase in the number of $CD45^+$IFN-γ^+ cells was
543 detected in the presence of VarC in the culture (Fig. 7Ca). As the number of $CD45^+$IL-4^+ cells
544 did not show any decrease (Fig. 7 Cb), polarization of the culture in Th-1 direction was not
545 confirmed. A mixed Th1/Th2 response was also induced after immunization of BALB/c mice

546 with chimeric VLPs prepared by insertion of a short-sized epitope at four different sites of
547 yeast-expressed hamster polyomavirus major capsid protein VP1 (68) and in the mouse model
548 of vaccination by a JEV (Japanese encephalitis virus) live-attenuated vaccine or recombinant
549 modified vaccinia virus Ankara (69). However, in both of these models, the proportion of
550 Th1/Th2 population was established according to the immunoglobulin subclass distribution.
551 Our results confirmed this finding by *in vitro* assay.

552 VarC induces efficient production of antibodies including
553 virus neutralization antibody against PCV2 in pigs

554 The candidate vaccine VarC inducing antibodies in mice with the highest ability to neutralize
555 the PCV2 virus was selected for immunization of pigs. Prior to immunization, piglets (aged 6
556 weeks) were tested for the presence of PCV2 DNA in the blood by qPCR to reveal their possible
557 infection by PCV2. No virus DNA copies were detected. The animals were immunized as
558 described in Methods: one group (7 pigs) was immunized by VarC, one group of three pigs
559 with the commercial Circoflex vaccine for comparison, and a control group (three pigs) was
560 immunized using PBS and adjuvants only. The humoral response was tested by commercial
561 ELISA kit Ingezim Circo IgG. At the time of the first immunization (0 days), slightly elevated
562 levels of antibodies specific for PCV2 were detected in all groups of animals (Fig. 8). The levels
563 apparently represent the presence of maternal antibodies in the tested piglets. On day 28 after
564 the first immunization, a significant rise of PCV2-specific antibodies was detected in the sera
565 of pigs immunized by VarC or Circoflex vaccine, but not in the sera of control pigs. The level
566 of PCV2-specific antibodies induced by VarC was significantly higher than that obtained by
567 the Circoflex vaccine. However, 49 days after the first immunization (and 28 days after the
568 second immunization), the level of antibodies induced by VarC decreased, so that the antibody
569 levels induced by both experimental and commercial vaccines became statistically equal. We

suppose that the decrease of antibody level detected on 49th day post immunization by the VarC vaccine can be overcome by optimization of adjuvants. The levels of PCV2-specific antibodies of non-immunized controls decreased over time to the levels that are not considered as positive serum.

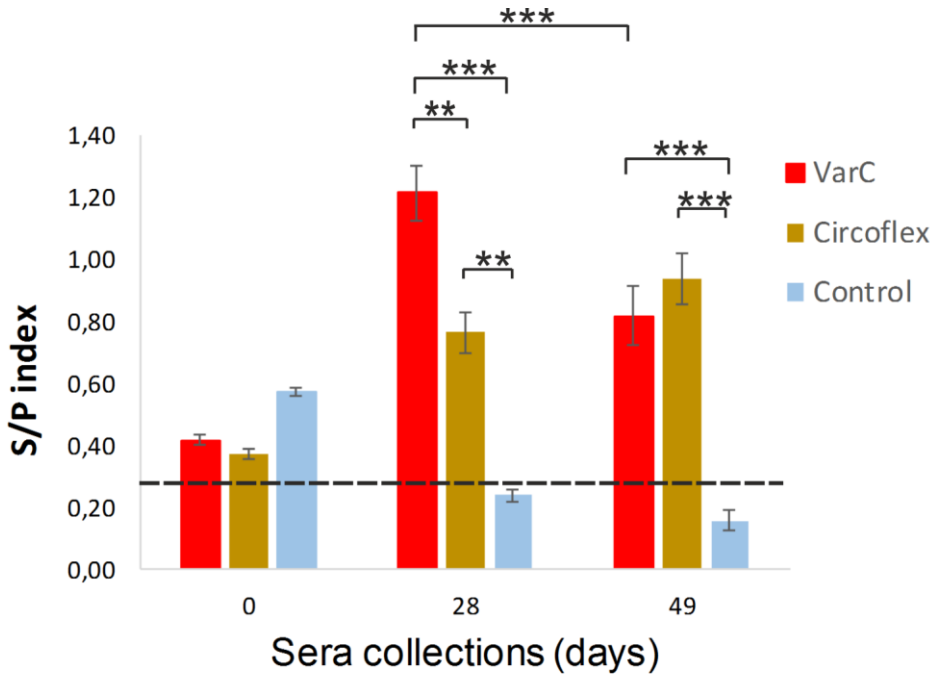

Fig. 8. Comparison of PCV2-specific antibody responses induced by the VarC candidate vaccine with those induced by commercial Circoflex vaccine.

Two groups of pigs were immunized two times (days 0 and 21) with nanostructure VarC or Circoflex vaccine according to the manufacturer's instructions or with PBS containing 30% Polygen adjuvant. The levels of antiPCV2 antibodies were measured by a commercial ELISA kit (Ingezim Circo IgG) according to the manufacturer's instructions. S/P index – index expressing the amount of antiPCV2-specific antibodies, ratio between OD415nm of the sample / OD415nm of the control, which is part of the ELISA kit. Dashed line represents the borderline of S/P index (0,285) between sera negative and positive for PCV2-specific antibodies

584 (calculated according to the ELISA kit manual). Error bars represent standard error of the
585 mean, SEM, *P <0.05, ** P<0.005, *** P < 0.0005.

586 For the viral clearance and recovery of pigs from infection, the presence of neutralizing
587 antibodies is crucial. With the development of PMWS, the absence or impaired production of
588 PCV2-specific neutralizing antibodies was observed (61,70). A decrease in viremia coincides
589 with an increase in neutralizing antibody titres in infected pigs inoculated with PCV2 (70).
590 Therefore, we further investigated whether Cap-specific antibodies induced in pigs are able to
591 block PCV2 infection. The PCV2 virus inoculum was mixed with different concentrations of
592 inactivated pig sera (collected 28 days after the first immunization) and after 1 h incubation at
593 37°C, PK15 pig cells were infected. Cells were fixed 36 hpi, and stained for indirect
594 immunofluorescence. The numbers of Cap-positive cells were counted. The results obtained
595 with 100-fold diluted sera are presented in Fig. 8. Comparable virus neutralization results were
596 obtained for both VarC and Circoflex vaccines.

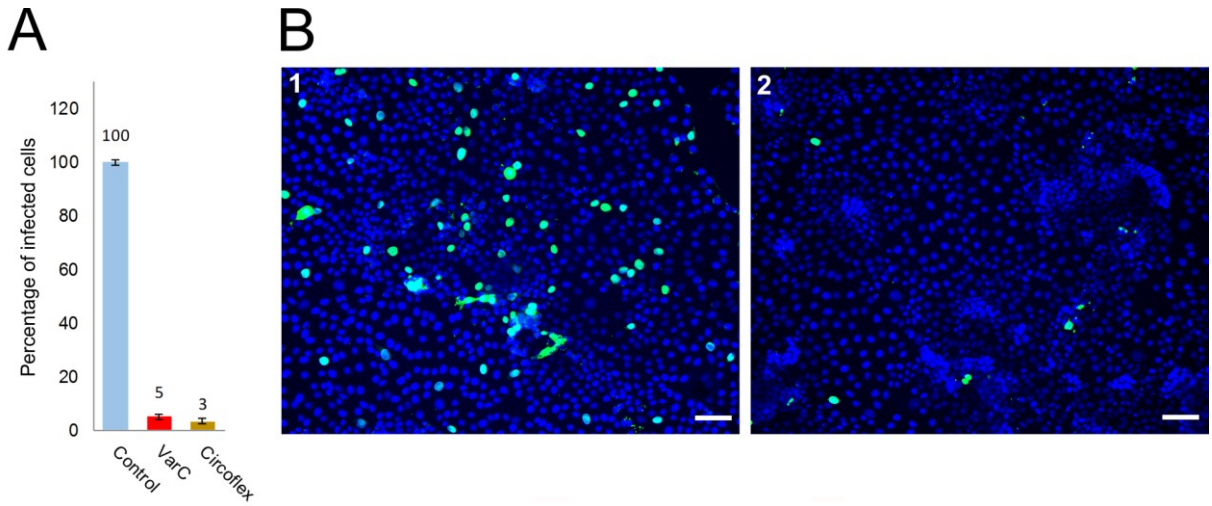

597

598 **Fig. 9. Pig serum neutralization assay.**

599 PK15 cells were inoculated with a mixture of 100-fold diluted sera collected from immunized
600 pigs and PCV2 virus (final concentration $TCID_{50} = 10^5$). Control cells were infected with the

same amount of the virus mixed with 100-fold diluted serum of gnotobiotic pig. Infected cells were detected 36 hpi by immunofluorescence assay with antibody against the Cap protein and the numbers of PCV2-positive cells were calculated. (**A)** Plot of neutralizing activity of pig sera. The plots represent the percentage of infected cells relative to control. Cells from 17 optical fields (approx. 1500 infected cells for the control sample) were counted in each experiment. Error bars represent standard error of three independent experiments. **(B)** Representative fields of counted cells. Control cells **(1)** and cells infected with the virus neutralized by VarC-induced antibodies **(2)**. Blue - DAPI, green - PCV2 Cap protein. Bars represent 50 μm.

The first commercial PCV2 vaccine (Circovac, Merial), introduced in 2006, is based on an inactivated oil-adjuvanted vaccine. The Cap protein of PCV2a expressed in the baculovirus system is the antigen of other three vaccines (Circoflex, Boehringer Ingelheim; Circumvent, Intervet/Merck; Porcillis PCV, Schering-Plough/Merck). Another two vaccines, Suvaxyn (Fort Dodge Animal Health) and Fostera PCV (Pfizer Animal Health) are based on a chimeric PCV1/2 virus containing the genomic backbone of the non-pathogenic PCV1, with the cap gene replaced by that of PCV2. All the vaccines are directed against the PCV2a subtype. Although an improvement in the expression of self-contained Cap protein in insect cells has been achieved (71,72), in our hands, the production and isolation of VarC chimeric structures carrying the fused Cap protein of PCV2b subtype was more efficient and easy. Another advantage of the VarC chimeric vaccine is that it represents a so-called DIVA (differentiating infected from vaccinated animals) vaccine, which also induces an immune response that differs from the response induced by natural infection, in this case antibodies against the mouse polyoma VP1 protein.

Acknowledgment

Acknowledgment to Karel Harant from Mass Spectrometry and Proteomics Service Laboratory of Charles University, Faculty of Science, Biological Section, where the proteomic and mass spectrometric part of this work was done. This work was supported by Technology Agency of the Czech Republic, TACR, project no. TA03010700, Specific University Research Grant of the Ministry of Education, Youth and Sports of CR, project no. SVV-2017-260426 and by the Ministry of Education, Youth and Sports of CR within the National Sustainability Program II (Project BIOCEV-FAR) LQ1604 and by the project ‘‘BIOCEV’’(CZ.1.05/1.1.00/02.0109).”

References

1. Jegerlehner A, Storni T, Lipowsky G, Schmid M, Pumpens P, Bachmann MF. Regulation of IgG antibody responses by epitope density and CD21-mediated costimulation. Eur J Immunol. 2002 Nov;32(11):3305–14.

2. Jegerlehner A, Tissot A, Lechner F, Sebbel P, Erdmann I, Kündig T, et al. A molecular assembly system that renders antigens of choice highly repetitive for induction of protective B cell responses. Vaccine. 2002 Aug 19;20(25–26):3104–12.

3. Richterová Z, Liebl D, Horák M, Palková Z, Stokrová J, Hozák P, et al. Caveolae are involved in the trafficking of mouse polyomavirus virions and artificial VP1 pseudocapsids toward cell nuclei. J Virol. 2001 Nov;75(22):10880–91.

4. Kushnir N, Streatfield SJ, Yusibov V. Virus-like particles as a highly efficient vaccine platform: Diversity of targets and production systems and advances in clinical development. Vaccine. 2012 Dec 17;31(1):58–83.

5. Pushko P, Pumpens P, Grens E. Development of Virus-Like Particle Technology from Small Highly Symmetric to Large Complex Virus-Like Particle Structures. Intervirology. 2013;56(3):141–65.

6. Crisci E, Bárcena J, Montoya M. Virus-like particles: The new frontier of vaccines for animal viral infections. Vet Immunol Immunopathol. 2012 Aug 15;148(3–4):211–25.

7. Meshram CD, Baviskar PS, Ognibene CM, Oomens AGP. The Respiratory Syncytial Virus Phosphoprotein, Matrix Protein, and Fusion Protein Carboxy-Terminal Domain Drive Efficient Filamentous Virus-Like Particle Formation. J Virol. 2016 Sep 21;JVI.01193-16.

8. Adeyemi OO, Nicol C, Stonehouse NJ, Rowlands DJ. Increasing Type 1 Poliovirus Capsid Stability by Thermal Selection. J Virol [Internet]. 2017 Jan 31 [cited 2017 Mar 23];91(4). Available from: http://www.ncbi.nlm.nih.gov/pmc/articles/PMC5286869/

9. Teunissen EA, de Raad M, Mastrobattista E. Production and biomedical applications of virus-like particles derived from polyomaviruses. J Controlled Release. 2013 Nov 28;172(1):305–21.

10. Suchanová J, Španielová H, Forstová J. Applications of Viral Nanoparticles Based on Polyomavirus and Papillomavirus Structures. In: Viral Nanotechnology [Internet]. CRC Press; 2015 [cited 2017 Mar 27]. p. 303–62. Available from: http://www.crcnetbase.com/doi/abs/10.1201/b18596-23

11. Boura E, Liebl D, Spísek R, Fric J, Marek M, Stokrová J, et al. Polyomavirus EGFP-pseudocapsids: analysis of model particles for introduction of proteins and peptides into mammalian cells. FEBS Lett. 2005 Dec 5;579(29):6549–58.

12. Hrusková V, Morávková A, Babiarová K, Ludvíková V, Fric J, Vonka V, et al. Bcr-Abl fusion sequences do not induce immune responses in mice when administered in mouse polyomavirus based virus-like particles. Int J Oncol. 2009 Dec;35(6):1247–56.

13. Forstová J, Krauzewicz N, Sandig V, Elliott J, Palková Z, Strauss M, et al. Polyoma virus pseudocapsids as efficient carriers of heterologous DNA into mammalian cells. Hum Gene Ther. 1995 Mar;6(3):297–306.

14. Stokrová J, Palková Z, Fischer L, Richterová Z, Korb J, Griffin BE, et al. Interactions of heterologous DNA with polyomavirus major structural protein, VP1. FEBS Lett. 1999 Feb 19;445(1):119–25.

15. Tegerstedt K, Lindencrona JA, Curcio C, Andreasson K, Tullus C, Forni G, et al. A single vaccination with polyomavirus VP1/VP2Her2 virus-like particles prevents outgrowth of HER-2/neu-expressing tumors. Cancer Res. 2005 Jul 1;65(13):5953–7.

16. Chang D, Haynes JI, Brady JN, Consigli RA. The use of additive and subtractive approaches to examine the nuclear localization sequence of the polyomavirus major capsid protein VP1. Virology. 1992 Aug;189(2):821–7.

17. Chang D, Cai X, Consigli RA. Characterization of the DNA binding properties of polyomavirus capsid protein. J Virol. 1993 Oct;67(10):6327–31.

18. Forstová J, Krauzewicz N, Wallace S, Street AJ, Dilworth SM, Beard S, et al. Cooperation of structural proteins during late events in the life cycle of polyomavirus. J Virol. 1993 Mar;67(3):1405–13.

19. Montross L, Watkins S, Moreland RB, Mamon H, Caspar DL, Garcea RL. Nuclear assembly of polyomavirus capsids in insect cells expressing the major capsid protein VP1. J Virol. 1991 Sep;65(9):4991–8.

20. Salunke DM, Caspar DL, Garcea RL. Self-assembly of purified polyomavirus capsid protein VP1. Cell. 1986 Sep 12;46(6):895–904.

21. Stehle T, Harrison SC. Crystal structures of murine polyomavirus in complex with straight-chain and branched-chain sialyloligosaccharide receptor fragments. Struct Lond Engl 1993. 1996 Feb 15;4(2):183–94.

22. Meehan BM, McNeilly F, Todd D, Kennedy S, Jewhurst VA, Ellis JA, et al. Characterization of novel circovirus DNAs associated with wasting syndromes in pigs. J Gen Virol. 1998 Sep;79 (Pt 9):2171–9.

23. Franzo G, Cortey M, Olvera A, Novosel D, Castro AMMGD, Biagini P, et al. Revisiting the taxonomical classification of Porcine Circovirus type 2 (PCV2): still a real challenge. Virol J. 2015;12:131.

24. Cortey M, Olvera A, Grau-Roma L, Segalés J. Further comments on porcine circovirus type 2 (PCV2) genotype definition and nomenclature. Vet Microbiol. 2011 May 5;149(3–4):522–3.

25. Dupont K, Nielsen EO, Baekbo P, Larsen LE. Genomic analysis of PCV2 isolates from Danish archives and a current PMWS case-control study supports a shift in genotypes with time. Vet Microbiol. 2008 Apr 1;128(1–2):56–64.

26. Franzo G, Cortey M, de Castro AMMG, Piovezan U, Szabo MPJ, Drigo M, et al. Genetic characterisation of Porcine circovirus type 2 (PCV2) strains from feral pigs in the Brazilian Pantanal: An opportunity to reconstruct the history of PCV2 evolution. Vet Microbiol. 2015 Jul 9;178(1–2):158–62.

27. Guo LJ, Lu YH, Wei YW, Huang LP, Liu CM. Porcine circovirus type 2 (PCV2): genetic variation and newly emerging genotypes in China. Virol J. 2010;7:273.

28. Xiao C-T, Halbur PG, Opriessnig T. Global molecular genetic analysis of porcine circovirus type 2 (PCV2) sequences confirms the presence of four main PCV2 genotypes and reveals a rapid increase of PCV2d. J Gen Virol. 2015 Jul;96(Pt 7):1830–41.

29. Harms PA, Sorden SD, Halbur PG, Bolin SR, Lager KM, Morozov I, et al. Experimental reproduction of severe disease in CD/CD pigs concurrently infected with type 2 porcine circovirus and porcine reproductive and respiratory syndrome virus. Vet Pathol. 2001 Sep;38(5):528–39.

30. Segalés J. Porcine circovirus type 2 (PCV2) infections: Clinical signs, pathology and laboratory diagnosis. Virus Res. 2012 Mar;164(1–2):10–9.

31. Allan GM, Kennedy S, McNeilly F, Foster JC, Ellis JA, Krakowka SJ, et al. Experimental Reproduction of Severe Wasting Disease by Co-infection of Pigs with Porcine Circovirus and Porcine Parvovirus. J Comp Pathol. 1999 ervenec;121(1):1–11.

32. Kennedy S, Moffett D, McNeilly F, Meehan B, Ellis J, Krakowka S, et al. Reproduction of lesions of postweaning multisystemic wasting syndrome by infection of conventional pigs with porcine circovirus type 2 alone or in combination with porcine parvovirus. J Comp Pathol. 2000 Jan;122(1):9–24.

33. Allan GM, McNeilly F, Ellis J, Krakowka S, Meehan B, McNair I, et al. Experimental infection of colostrum deprived piglets with porcine circovirus 2 (PCV2) and porcine reproductive and respiratory syndrome virus (PRRSV) potentiates PCV2 replication. Arch Virol. 2000;145(11):2421–9.

34. Rovira A, Balasch M, Segalés J, García L, Plana-Durán J, Rosell C, et al. Experimental inoculation of conventional pigs with porcine reproductive and respiratory syndrome virus and porcine circovirus 2. J Virol. 2002 Apr;76(7):3232–9.

35. Ellis JA, Allan G, Krakowka S. Effect of coinfection with genogroup 1 porcine torque teno virus on porcine circovirus type 2-associated postweaning multisystemic wasting syndrome in gnotobiotic pigs. Am J Vet Res. 2008 Dec;69(12):1608–14.

36. Opriessnig T, Thacker EL, Yu S, Fenaux M, Meng X-J, Halbur PG. Experimental reproduction of postweaning multisystemic wasting syndrome in pigs by dual infection with Mycoplasma hyopneumoniae and porcine circovirus type 2. Vet Pathol. 2004 Nov;41(6):624–40.

37. Grasland B, Loizel C, Blanchard P, Oger A, Nignol A-C, Bigarré L, et al. Reproduction of PMWS in immunostimulated SPF piglets transfected with infectious cloned genomic DNA of type 2 porcine circovirus. Vet Res. 2005 Dec;36(5–6):685–97.

38. Krakowka S, Ellis JA, McNeilly F, Ringler S, Rings DM, Allan G. Activation of the immune system is the pivotal event in the production of wasting disease in pigs infected with porcine circovirus-2 (PCV-2). Vet Pathol. 2001 Jan;38(1):31–42.

39. Hines RK, Lukert PD. Porcine circovirus:A serological survey of swine in the United States.

40. Tischer I, Gelderblom H, Vettermann W, Koch MA. A very small porcine virus with circular single-stranded DNA. Nature. 1982 Jan 7;295(5844):64–6.

41. Finsterbusch T, Mankertz A. Porcine circoviruses--small but powerful. Virus Res. 2009 Aug;143(2):177–83.

42. Liu J, Chen I, Du Q, Chua H, Kwang J. The ORF3 Protein of Porcine Circovirus Type 2 Is Involved in Viral Pathogenesis In Vivo. J Virol. 2006 May 15;80(10):5065–73.

43. Karuppannan AK, Liu S, Jia Q, Selvaraj M, Kwang J. Porcine circovirus type 2 ORF3 protein competes with p53 in binding to Pirh2 and mediates the deregulation of p53 homeostasis. Virology. 2010 Mar 1;398(1):1–11.

44. Gao Z, Dong Q, Jiang Y, Opriessnig T, Wang J, Quan Y, et al. ORF4-protein deficient PCV2 mutants enhance virus-induced apoptosis and show differential expression of mRNAs in vitro. Virus Res. 2014 Apr;183:56–62.

45. Lekcharoensuk P, Morozov I, Paul PS, Thangthumniyom N, Wajjawalku W, Meng XJ. Epitope mapping of the major capsid protein of type 2 porcine circovirus (PCV2) by using chimeric PCV1 and PCV2. J Virol. 2004 Aug;78(15):8135–45.

46. Saha D, Lefebvre DJ, Ooms K, Huang L, Delputte PL, Van Doorsselaere J, et al. Single amino acid mutations in the capsid switch the neutralization phenotype of porcine circovirus 2. J Gen Virol. 2012 Jul;93(Pt 7):1548–55.

47. Shang S-B, Jin Y-L, Jiang X, Zhou J-Y, Zhang X, Xing G, et al. Fine mapping of antigenic epitopes on capsid proteins of porcine circovirus, and antigenic phenotype of porcine circovirus type 2. Mol Immunol. 2009 Jan;46(3):327–34.

48. Trible BR, Rowland RRR. Genetic variation of porcine circovirus type 2 (PCV2) and its relevance to vaccination, pathogenesis and diagnosis. Virus Res. 2012 Mar;164(1–2):68–77.

49. Khayat R, Brunn N, Speir JA, Hardham JM, Ankenbauer RG, Schneemann A, et al. The 2.3-Angstrom Structure of Porcine Circovirus 2. J Virol. 2011 Aug 1;85(15):7856–62.

50. Nawagitgul P, Morozov I, Bolin SR, Harms PA, Sorden SD, Paul PS. Open reading frame 2 of porcine circovirus type 2 encodes a major capsid protein. J Gen Virol. 2000 Sep;81(Pt 9):2281–7.

51. Bucarey SA, Noriega J, Reyes P, Tapia C, Sáenz L, Zuñiga A, et al. The optimized capsid gene of porcine circovirus type 2 expressed in yeast forms virus-like particles and elicits antibody responses in mice fed with recombinant yeast extracts. Vaccine. 2009 Sep 25;27(42):5781–90.

52. Marcekova Z, Psikal I, Kosinova E, Benada O, Sebo P, Bumba L. Heterologous expression of full-length capsid protein of porcine circovirus 2 in Escherichia coli and its potential use for detection of antibodies. J Virol Methods. 2009 Dec;162(1–2):133–41.

53. Krauzewicz N, Streuli CH, Stuart-Smith N, Jones MD, Wallace S, Griffin BE. Myristylated polyomavirus VP2: role in the life cycle of the virus. J Virol. 1990 Sep;64(9):4414–20.

54. Garcia MI, Perez M, Caruso M, Sthandier O, Ferreira R, Cermola M, et al. A mutation in the DE loop of the VP1 protein that prevents polyomavirus transcription and replication. Virology. 2000 Jul 5;272(2):293–301.

55. Laemmli UK. Cleavage of structural proteins during the assembly of the head of bacteriophage T4. Nature. 1970 Aug 15;227(5259):680–5.

788 56. Horníková L, Man P, Forstová J. Blue native protein electrophoresis for studies of mouse
789 polyomavirus morphogenesis and interactions between the major capsid protein VP1 and
790 cellular proteins. J Virol Methods. 2011 Dec;178(1–2):229–34.

791 57. Shevchenko A, Tomas H, Havlis J, Olsen JV, Mann M. In-gel digestion for mass spectrometric
792 characterization of proteins and proteomes. Nat Protoc. 2006;1(6):2856–60.

793 58. Rueda P, Fominaya J, Langeveld JPM, Bruschke C, Vela C, Casal JI. Effect of different baculovirus
794 inactivation procedures on the integrity and immunogenicity of porcine parvovirus-like
795 particles. Vaccine. 2000 Nov 22;19(7–8):726–34.

796 59. Bradford MM. A rapid and sensitive method for the quantitation of microgram quantities of
797 protein utilizing the principle of protein-dye binding. Anal Biochem. 1976 May 7;72:248–54.

798 60. Brunborg IM, Moldal T, Jonassen CM. Quantitation of porcine circovirus type 2 isolated from
799 serum/plasma and tissue samples of healthy pigs and pigs with postweaning multisystemic
800 wasting syndrome using a TaqMan-based real-time PCR. J Virol Methods. 2004 Dec
801 15;122(2):171–8.

802 61. Meerts P, Misinzo G, Lefebvre D, Nielsen J, Bøtner A, Kristensen CS, et al. Correlation between
803 the presence of neutralizing antibodies against porcine circovirus 2 (PCV2) and protection
804 against replication of the virus and development of PCV2-associated disease. BMC Vet Res.
805 2006;2:6.

806 62. Lefebvre DJ, Costers S, Van Doorsselaere J, Misinzo G, Delputte PL, Nauwynck HJ. Antigenic
807 differences among porcine circovirus type 2 strains, as demonstrated by the use of monoclonal
808 antibodies. J Gen Virol. 2008 Jan;89(Pt 1):177–87.

809 63. Wu P-C, Lin W-L, Wu C-M, Chi J-N, Chien M-S, Huang C. Characterization of porcine circovirus
810 type 2 (PCV2) capsid particle assembly and its application to virus-like particle vaccine
811 development. Appl Microbiol Biotechnol. 2012 Sep;95(6):1501–7.

812 64. Fric J, Marek M, Hrusková V, Holán V, Forstová J. Cellular and humoral immune responses to
813 chimeric EGFP-pseudocapsids derived from the mouse polyomavirus after their intranasal
814 administration. Vaccine. 2008 Jun 19;26(26):3242–51.

815 65. Alsharifi M, Regner M, Blanden R, Lobigs M, Lee E, Koskinen A, et al. Exhaustion of Type I
816 Interferon Response following an Acute Viral Infection. J Immunol. 2006 Sep 1;177(5):3235–41.

817 66. Swanson II PA, Lukacher AE, Szomolanyi-Tsuda E. Immunity to polyomavirus infection: The
818 polyomavirus–mouse model. Semin Cancer Biol. 2009 Aug;19(4):244–51.

819 67. Nielsen SD, Afzelius P, Ersbøll AK, Nielsen JO, Hansen JE. Expression of the activation antigen
820 CD69 predicts functionality of in vitro expanded peripheral blood mononuclear cells (PBMC)
821 from healthy donors and HIV-infected patients. Clin Exp Immunol. 1998 Oct;114(1):66–72.

822 68. Gedvilaite A, Zvirbliene A, Staniulis J, Sasnauskas K, Krüger DH, Ulrich R. Segments of puumala
823 hantavirus nucleocapsid protein inserted into chimeric polyomavirus-derived virus-like particles
824 induce a strong immune response in mice. Viral Immunol. 2004;17(1):51–68.

825 69. Lee E-Y, Kim J-Y, Lee D-K, Yoon I-S, Ko HL, Chung J-W, et al. Sublingual immunization with
826 Japanese encephalitis virus vaccine effectively induces immunity through both cellular and
827 humoral immune responses in mice. Microbiol Immunol. 2016 Dec;60(12):846–53.

828 70. Fort M, Olvera A, Sibila M, Segalés J, Mateu E. Detection of neutralizing antibodies in
829 postweaning multisystemic wasting syndrome (PMWS)-affected and non-PMWS-affected pigs.
830 Vet Microbiol. 2007 Dec 15;125(3–4):244–55.

831 71. López-Vidal J, Gómez-Sebastián S, Bárcena J, Nuñez M del C, Martínez-Alonso D, Dudognon B,
832 et al. Improved Production Efficiency of Virus-Like Particles by the Baculovirus Expression
833 Vector System. PLoS ONE [Internet]. 2015 Oct 12 [cited 2017 Mar 23];10(10). Available from:
834 http://www.ncbi.nlm.nih.gov/pmc/articles/PMC4601761/

835 72. Liu Y, Zhang Y, Yao L, Hao H, Fu X, Yang Z, et al. Enhanced production of porcine circovirus type
836 2 (PCV2) virus-like particles in Sf9 cells by translational enhancers. Biotechnol Lett. 2015
837 Sep;37(9):1765–71.

838

The FEBS Journal

FEBS PRESS science publishing by scientists

VP1, the major capsid protein of the mouse polyomavirus, binds microtubules, promotes their acetylation and blocks the host cell cycle

Lenka Horníková[1], Martin Fraiberk[1], Petr Man[2,3], Václav Janovec[1] and Jitka Forstová[1]

1 Department of Genetics and Microbiology, Faculty of Science, Charles University, Prague, Czech Republic
2 Laboratory of Structural Biology and Cell Signaling, Institute of Microbiology, Academy of Science of the Czech Republic, Prague, Czech Republic
3 Department of Biochemistry, Faculty of Science, Charles University, Prague, Czech Republic

Keywords
cell cycle arrest; chaperone Hsp90; microtubules; mouse polyomavirus; VP1

Correspondence
J. Forstová, Vinicna 5, Prague 2 12844, Czech Republic
Fax: +42 0221951724
Tel: +42 0221951730
E-mail: jitkaf@natur.cuni.cz

(Received 31 May 2016, revised 15 November 2016, accepted 22 November 2016)

doi:10.1111/febs.13977

VP1, the major structural protein of the mouse polyomavirus (MPyV), is the major architectural component of the viral capsid. Its pentamers are able to self-assemble into capsid-like particles and to non-specifically bind DNA. Surface loops of the protein interact with sialic acid of ganglioside receptors. Although the replication cycle of the virus, including virion morphogenesis, proceeds in the cell nucleus, a substantial fraction of the protein is detected in the cytoplasm of late-phase MPyV-infected cells. In this work, we detected VP1 mainly in the cytoplasm of mammalian cells transfected with plasmid expressing VP1. In the cytoplasm, VP1-bound microtubules, including the mitotic spindle, and the interaction of VP1 with microtubules resulted in cell cycle block at the G2/M phase. Furthermore, in the late phase of MPyV infection and in cells expressing VP1, microtubules were found to be hyperacetylated. We then sought to understand how VP1 interacts with microtubules. Dynein is not responsible for the VP1–microtubule association, as neither overexpression of p53/dynamitin nor treatment with ciliobrevin-D (an inhibitor of dynein activity) prevented binding of VP1 to microtubules. A pull-down assay for VP1-interacting proteins identified the heat shock protein 90 (Hsp90) chaperone, and Hsp90 was also detected in the VP1–microtubule complexes. Although Hsp90 is known to be associated with acetylated microtubules, it does not mediate the interaction between VP1 and microtubules. Our study provides insight into the role of the major structural protein in MPyV replication, indicating that VP1 is a multifunctional protein that participates in the regulation of cell cycle progression in MPyV-infected cells.

Introduction

Mouse polyomavirus (MPyV) is a small non-enveloped DNA virus that belongs to the Polyomaviridae family. MPyV virion consists of a genomic circular molecule of dsDNA associated with cellular histones (except

Abbreviations
αTAT1, α-tubulin acetyltransferase; 17-AAG, 17-allylamino-17-demethoxygeldanamycin; EGFP, enhanced green fluorescent protein; FACS, fluorescence-activated cell sorting; GAPDH, glyceraldehyde 3-phosphate dehydrogenase; HDAC6, histone deacetylase 6; hpt, hours post-transfection; Hsc70, heat shock cognate 70; Hsp90, heat shock protein 90; HSV-1, herpes simplex virus 1; LT, large T antigen; MPyV, mouse polyomavirus; NLS, nuclear localization signal; PARP1, poly(ADP-ribose) polymerase 1; sT, small T antigen; SV40, simian virus 40; VP1-BE-CT, major capsid protein VP1 fused with a biotin tag at its C terminus; VP1-BE-NT, major capsid protein VP1 fused with a biotin tag at its N terminus.

histone H1) encased within an icosahedral protein capsid. MPyV genomic DNA encodes three early antigens (large, middle and small T) and three structural proteins – the major capsid protein, VP1, and the minor capsid proteins, VP2 and VP3. VP2 is a larger variant of VP3 with a unique prolonged N terminus. Early antigens deregulate infected cells to ensure a suitable environment for progression of the virus replication cycle and are involved in virus DNA replication and transcription. MPyV capsid is composed of 72 externally exposed VP1 pentamers with one molecule of VP2 or VP3 associated internally with each pentamer [1]. Pentamers are formed immediately after VP1 synthesis in the cytoplasm; they interact with one molecule of the minor capsid protein, and the complex (capsomere) is transported to the nucleus, where virions are assembled. Both major and minor structural proteins possess their own nuclear localization signal (NLS). The NLS of the minor structural proteins was identified at their common C terminus [2], whereas the first five N-terminal amino acids of VP1 were described as the NLS [3]. It was shown previously that the NLS of the minor proteins does not ensure their complete localization in the cell nucleus when the proteins are expressed individually [4,5]. Individual expression of VP1 in insect cells resulted in efficient nuclear localization of the protein. For nuclear localization of the minor proteins, coexpression with VP1 was required [4].

According to X-ray diffraction studies of VP1's tertiary structure [6], the VP1 molecule can be divided into three modules: (a) an N-terminal arm, (b) an antiparallel L-sandwich core and (c) a long, flexible C-terminal arm. Four loops come out the L-sheet framework and are exposed at the surface of the capsomeric structure, and they are therefore the main interaction sites and antigenic determinants of MPyV virions. The flexible C-terminal arm forms interpentameric contacts, and the basic amino acids of the N-terminal arm are responsible, apart from nuclear localization, for the non-specific DNA binding activity of VP1 [7].

Several host cell proteins have been described as interacting with VP1. Cellular chaperone heat shock cognate protein 70 (Hsc70) was shown to bind VP1 immediately after its synthesis and translocate in complex with MPyV capsomeres to the cell nucleus [8]. It was suggested that Hsc70 prevents VP1 from forming empty capsids in the cytoplasm. In the cell nucleus, it helps the virion assembly [9]. Another VP1-interacting host protein is multifunctional cellular transcription factor YY1 [10]. Its function in the virus life cycle is not yet clear; it may be involved in transcription or replication of the virus genome and/or virion morphogenesis [11]. Interaction of VP1 with poly(ADP-ribose) polymerase 1 (PARP1) was described by Carbone *et al.* [12]. These authors hypothesized that PARP1 mediates dissociation of VP1 from uncoated MPyV minichromosome and helps to initialize virus transcription [12]. Bird *et al.* [13] identified *in vitro* interaction of VP1 with karyopherins [13].

VP1 protein is not only the basic building block of the capsid; it mediates virus entry into host cells by interaction with the ganglioside receptor [14]. Moreover, there is some evidence indicating its possible regulative roles in the virus life cycle. Virus mutated in the DE loop of VP1 exhibited a lower replication rate and decreased DNA encapsidation [11].

In this study, we focused on screening and characterization of the cellular proteins and structures that interact with the major capsid protein, VP1, during the late phase of virus infection. Our findings implicate VP1 as a protein that, besides its structural functions, possesses regulatory functions affecting cell cycle progression.

Results

VP1 is not efficiently transported into the cell nucleus when expressed without the minor structural proteins

The distribution of VP1 protein in cells transfected with VP1-expressing plasmid was analyzed by confocal microscopy of fixed cells stained by polyclonal antibody against VP1. Even when VP1 possesses an NLS at its N terminus, most of the VP1 was found in the cytoplasm of 3T3 mouse fibroblasts, and only faint VP1 staining was visible in the nucleus (Fig. 1). A similar staining pattern was observed in NMuMG mouse epithelial cells, human epithelial HeLa cells and human embryonic kidney 293 cells. The nuclear localization of VP1 protein of the closely related SV40 virus was described as being positively affected by the presence of large T (LT) antigen [15]. However, in WOP cells (constitutively producing LT antigen of MPyV), VP1 was also found predominantly in the cytoplasm.

Next, we were interested in the proportion of VP1 protein in the nucleus and cytoplasm and whether there are any differences in VP1 localization between cells expressing or not expressing LT antigen. WOP and 3T3 cells expressing VP1 were fractionated, and the amount of VP1 in the cytoplasmic, nuclear and insoluble fractions was measured by western blot by densitometry analysis of bands stained with specific

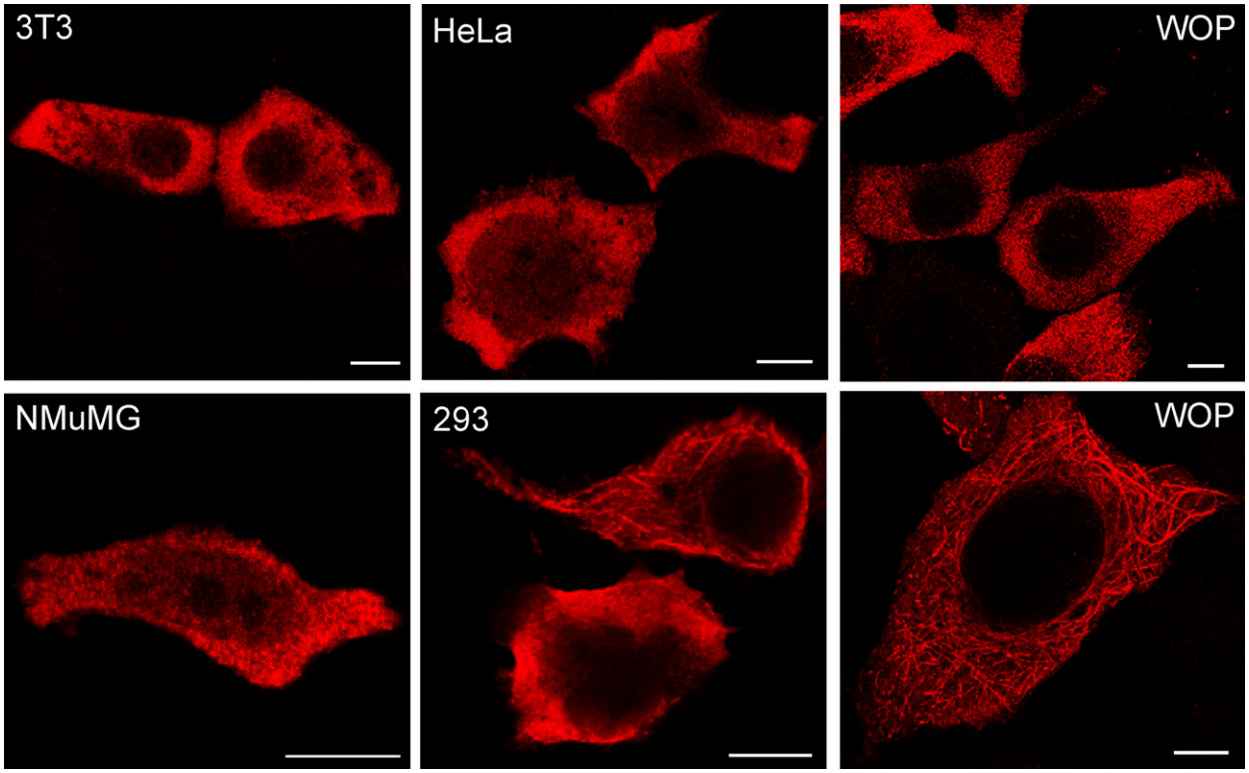

Fig. 1. VP1 is located mainly in the cytoplasm. Mouse 3T3, NMuMG or WOP cells and human HeLa or 293 cells were transfected with pVP1 plasmid and fixed 24 h post-transfection, and VP1 was stained. Shown are selected confocal sections of indicated cells. Bar: 8 μm.

antibody. In both cell types, the majority of VP1 was detected in the cytoplasmic fraction (70% in 3T3 and 60% in WOP cells). Approximately 20% of VP1 was found in the nuclear fraction in both cell types. Residual VP1 was present in insoluble fractions and represented 10% and 20% of VP1 in 3T3 and WOP cells, respectively (Fig. 2A,B). It was shown in a previous study [4] that VP1 helped the minor proteins VP2 and VP3 reach the insect cell nucleus. Therefore, we tested whether in mammalian cells cooperation of VP1 pentamer with VP2 or VP3 would also result in efficient transport of the complex into the nucleus. As shown in Fig. 2C, coexpression of VP1 with VP2 or VP3 resulted in exclusive nuclear localization of both VP1 and the minor protein (Fig. 2C).

These data indicate that the N-terminal sequence of basic amino acids of VP1, determined to be the NLS, is not sufficient for VP1 delivery into the cell nucleus. Efficient delivery of structural proteins into the nucleus can be achieved by their transport as a complex of VP1 pentamer with one molecule of the minor protein. The presence of LT antigen does not substantially affect their transport into the nucleus.

VP1 forms insoluble fibers in the cytoplasm

In 293 and WOP cells, two VP1 staining patterns in the cytoplasm were observed – cells with diffuse VP1 cytoplasmic localization and cells where VP1 formed filamentous structures (Fig. 1). We used *in situ* fractionation [16] of cells exhibiting the diffuse VP1 pattern to obtain more information about the VP1 status in the cytoplasm. This method is designed to avoid alterations in the morphology of non-extracted cellular structures. It is based on successive washing out of proteins according to their solubility in different buffers and may be used for studying proteins washed out in every step as well as for studying the cellular structures remaining in the dish. The first buffer contains detergent NP-40 and washes out all soluble proteins (cytoplasmic and nuclear). The second buffer contains DNase I. In this step, DNA accessible to DNase I treatment and DNA-binding proteins are washed out. The third buffer is of high ionic strength (containing 2 M NaCl) and it removes mainly polysomes, DNA, histones and cytoskeletal proteins (tubulin, actin) from the cells. The last fractionation buffer contains DNase I and RNase A and washes out the rest of the DNA

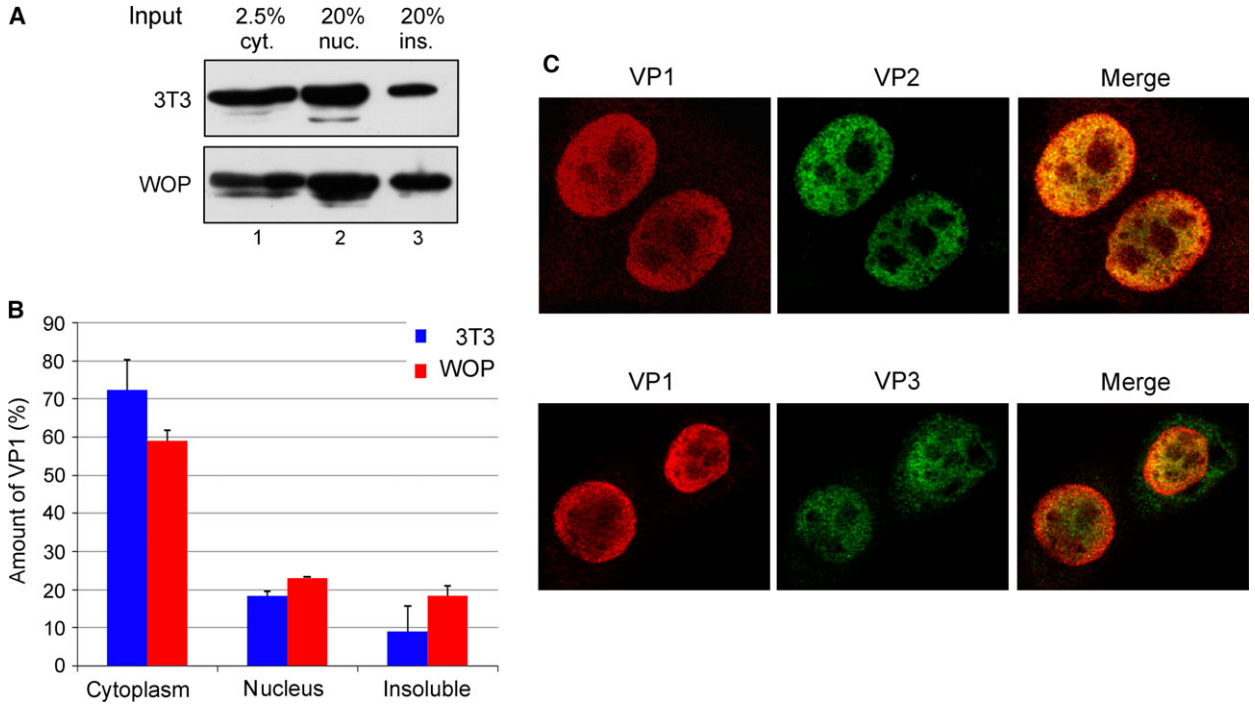

Fig. 2. LT antigen does not improve nuclear import of VP1 into the cell nucleus, in contrast to the minor structural proteins. (A) VP1-expressing 3T3 or WOP cells were fractionated into cytoplasmic, nuclear and insoluble fractions and applied to SDS/PAGE in amounts corresponding to 2.5%, 20% and 20% of fraction volume, respectively. Separated proteins were transferred to the membrane and VP1 protein was detected by specific antibody. Cyt, cytoplasm; ins, insoluble; nuc, nucleus. (B) Graphic illustration of densitometry analysis of the digital images of western blots from three independent experiments, shown as means ± SD. The amount of VP1 in each fraction is shown as the percentage of total VP1 amount. (C) 3T3 cells were cotransfected with plasmid pVP1 and pVP2 or pVP3. Cells were fixed 24 h post-transection and VP1 (red) and VP2/3 (green) were stained by specific antibodies.

and RNA. In this step, only a few residual cellular proteins are solubilized. After *in situ* fractionation, structures made of highly insoluble proteins remain in the dish. These proteins include lamins, vimentin, cytokeratines and the rest of the actin (no tubulin).

WOP and 3T3 cells expressing VP1 were fractionated *in situ* and after each step, VP1 protein in the structures remaining on the coverslip was stained by specific antibody. After the first fractionation step, tiny VP1 fibers appeared even in cells that exhibited originally diffused cytoplasmic VP1 localization (Fig. 3); the same staining pattern of VP1 was seen after DNase I treatment. VP1 fibers were clearly visible in all cells after the third and the last fractionation steps (Fig. 3). Figure 3 presents the results of *in situ* fractionation of 3T3 cells. In all the following experiments, WOP cell were used.

VP1 binds microtubules

Confocal microscopy of MPyV infected cells, or cells transiently expressing VP1 did not showed any colocalization of VP1 with cytoskeleton components, actin or vimentin (not shown). As the VP1 pattern reminded us of the microtubule network, we further focused on the analysis of VP1 colocalization with microtubules. After staining of cells with antibodies against VP1 and α-tubulin, we observed decreased ability of the tubulin-specific antibody to stain microtubules in VP1-positive cells, whereas in cells not expressing VP1, microtubules were stained well (Fig. 4A). However, after the third and the last steps of *in situ* fractionation, when distinct VP1 fibers were clearly visible, colocalization of VP1 with microtubules became more obvious (Fig. 4A). We did not see abundant colocalization; rather, we observed areas that were stained with VP1 antibody and areas that were marked by the tubulin antibody at the same filament (Fig. 4A). In control cells not expressing VP1, where microtubules were strongly stained by tubulin-specific antibody, the tubulin signal totally disappeared after the third fractionation step. This suggests that microtubules are petrified by bound VP1 and the whole complex becomes insoluble. Results of analysis of the washed out material after each fractionation step are in agreement (Fig. 4B).

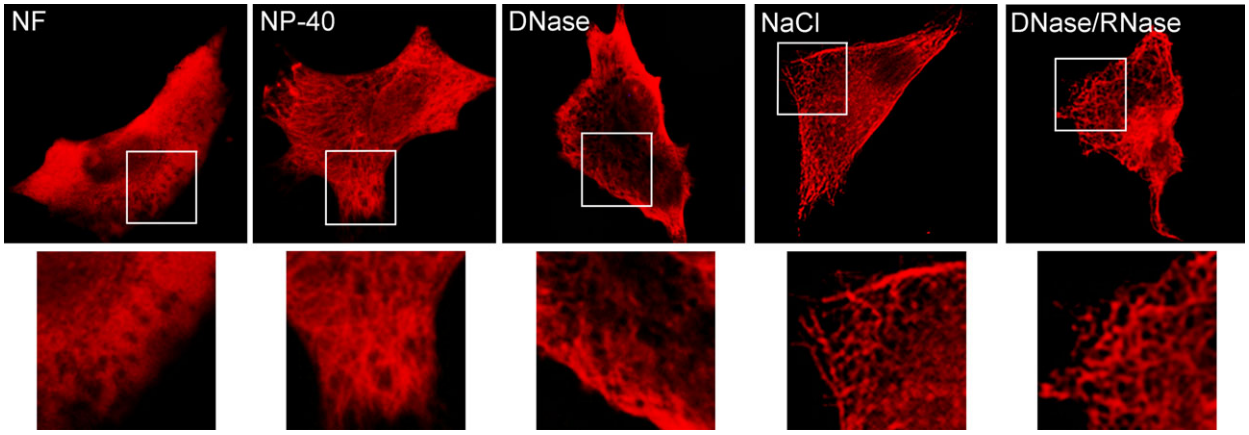

Fig. 3. VP1 forms fibers in VP1-expressing cells. VP1-producing 3T3 cells were fractionated *in situ* and VP1 was stained by specific VP1 antibody. Briefly, cells were gradually incubated in buffers containing: NP-40 detergent (NP-40 fraction); DNase I (DNase fraction); 2 M NaCl (NaCl fraction); and DNase I and RNase A (DNase/RNase fraction). Enlarged details of the cells are presented in lower panels. Microscopy was performed using an Olympus IX71 fluorescence microscope.

VP1 protein was detected in each fraction. Tubulin was solubilized in the first and third fractionation buffers both in VP1-expressing cells and in control cells (Fig. 4B). However, in contrast to control cells, tubulin (and VP1) appeared in the highly insoluble fraction in VP1-producing cells (Fig. 4B). Association of VP1 with microtubules was also verified by immuno-electron microscopy of transfected cells. Areas of colocalization of specific VP1 (5 nm gold particles) and tubulin (10 nm gold particles) staining could be found along the tubular structures (Fig. 4C).

In infected cells, although complexes of VP1 with the minor structural proteins are efficiently transported into the cell nucleus, a substantial fraction of VP1 can be detected in the cytoplasm in late stages of infection. We were interested in whether similar VP1 fibers can be detected in the cytoplasm of infected cells. Mouse fibroblast 3T6 cells were infected, and 40 h post-infection cells were fractionated *in situ*. After each fractionation step, VP1 and tubulin were stained by specific antibodies in structures remaining on the coverslip. Indeed, similar distinct VP1 fibers were visible in the cytoplasm of infected cells partially stainable by tubulin antibody (Fig. 4D). Likewise, western blot analysis of the presence of VP1 and tubulin in washed out material copied the distribution obtained in VP1-expressing cells (Fig. 4E).

Exposure of VP1-expressing cells to a non-toxic concentration of microtubule-destabilizing drug, nocodazole, led to loss of VP1 fibers. VP1 signal was equally distributed in the cytoplasm of these cells (Fig. 5B). After fractionation, most of VP1 was washed out; only a residual signal of VP1 was observed (Fig. 5E). To find out whether removal of nocodazole from the drug-treated cells would restore the VP1 fiber pattern, cells after nocodazole treatment were incubated for 1 h in medium without the drug. Fibers of VP1 became again visible both in the cells before fractionation and in cell residues after fractionation (Fig. 5).

These findings demonstrate that the VP1 fiber pattern is microtubule dependent. VP1 binds to microtubules, covers them and makes them highly insoluble. Interaction of VP1 and microtubules is not an artefact of transient expression of VP1 in the cells. Similar interactions take place in infected cells and may play an important role in the MPyV life cycle.

VP1 interacts with chaperone Hsp90

Next, we were interested in character of VP1–microtubule association. Immunoprecipitation with antibodies specific for VP1 or α-tubulin suggested that VP1 does not bind tubulin dimers (not shown). Also, VP1 is not directed massively to microtubules using dynein, the microtubular motor that transports various cellular components toward the minus ends of microtubules. Dynein binds to its cargo through another large protein complex called dynactin. Neither overexpression of p53/dynamitin (which disrupts the dynactin complex and thus blocks the dynein activity) nor ciliobrevin-D (an inhibitor of dynein activity [17]) abolished the VP1 fiber pattern (Fig. 6).

To identify the putative protein that possibly participates in VP1–microtubule binding, we performed the pull-down assay using N- or C-terminal VP1 fusion with BioEase™ Tag (Thermo Fisher Scientific).

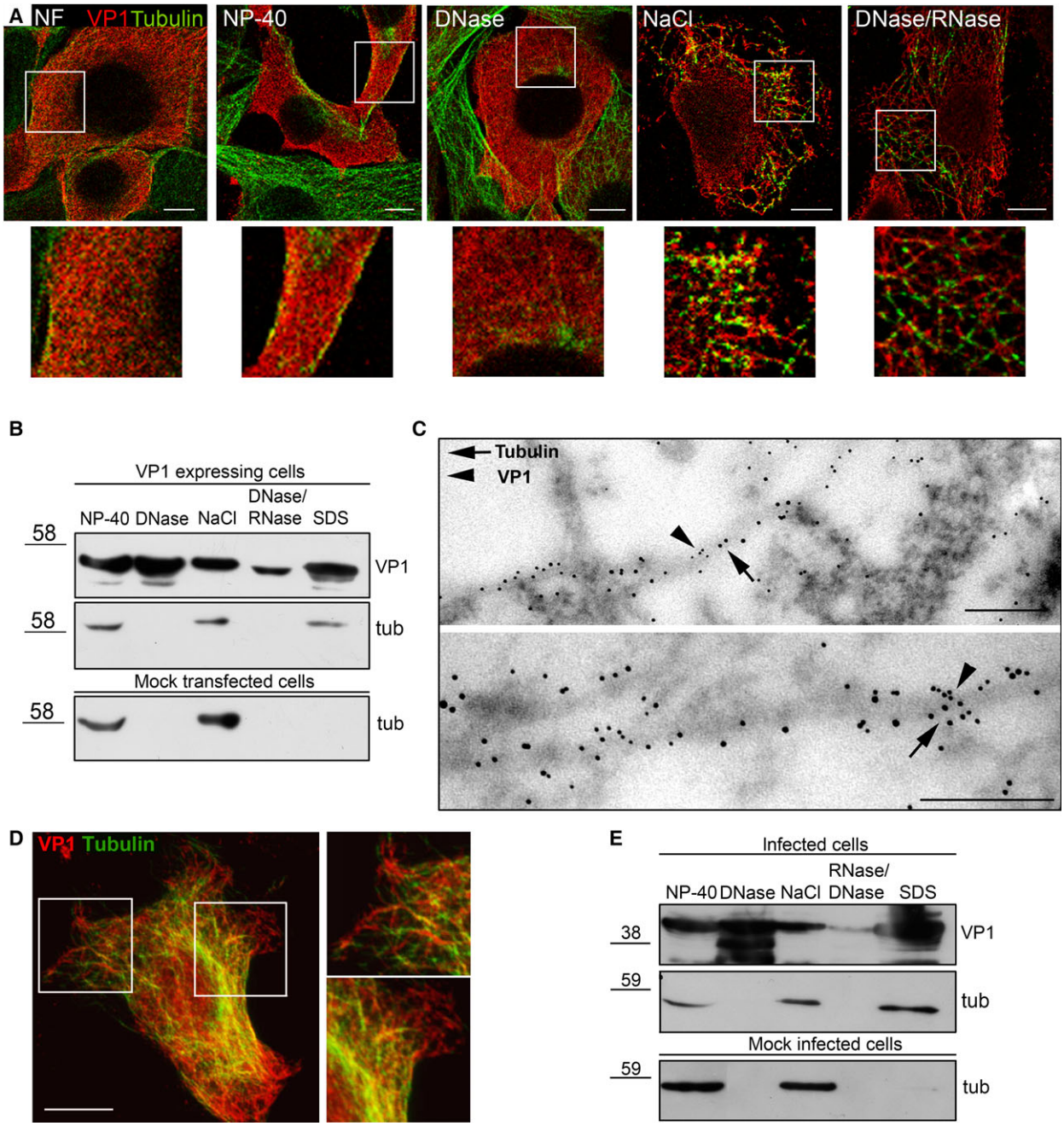

Fig. 4. VP1 binds to microtubules. (A) VP1-producing cells were fractionated *in situ* and VP1 (red) and tubulin (green) were stained by specific antibodies. Enlarged details of the cells are presented in lower panels. Shown are selected confocal sections. Bar: 8 μm. (B) VP1-expressing WOP cells and mock transfected cells were fractionated *in situ*, and washed out material from each fraction was separated by 10% SDS/PAGE and transferred onto PVDF membrane. The presence of VP1 or α-tubulin in each washed out fraction was determined by specific antibodies. (C) Immuno-electron microscopy of cells expressing VP1. Cells expressing VP1 were incubated with buffer containing NP-40 and embedded in resin. VP1 (black arrowhead, 5 nm gold particles) and α-tubulin (black arrows, 10 nm gold particles) were stained by specific antibodies. Bar: 200 nm. (D) 3T6 cells were infected, fractionated *in situ* 40 h post-infection, and VP1 (red) and tubulin (green) were stained by specific antibodies. Enlarged details of the cell are presented in the right panel. Shown is a selected confocal section of a cell after fractionation. Bar: 10 μm. (E) 3T6 cells were infected and fractionated *in situ* 40 h post-infection. Washed out material from each fraction was separated by 10% SDS/PAGE and transferred onto PVDF membrane. The presence of VP1 or α-tubulin in each washed out fraction was determined by specific antibodies.

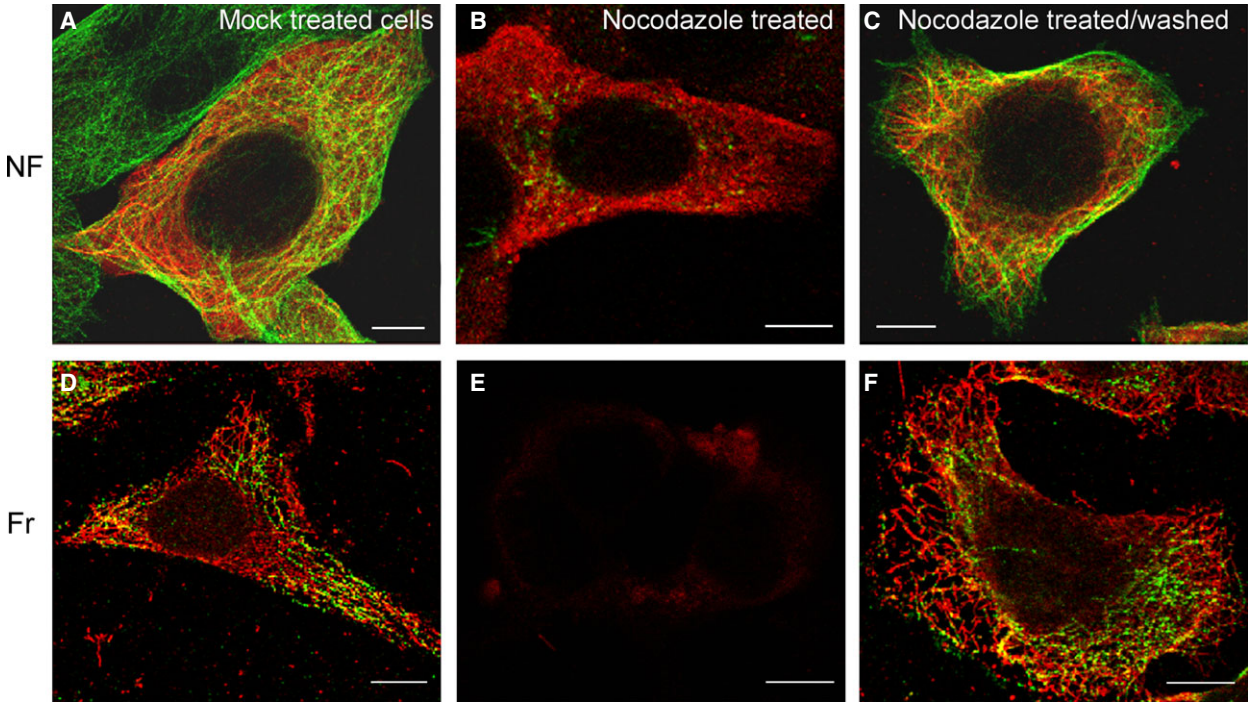

Fig. 5. Exposure to microtubule-destabilizing drug nocodazole abolished the VP1 filamentous pattern. VP1-expressing WOP cells were treated with nocodazole (5 μM) for 1 h (B, E), followed by wash out and microtubule reconstitution (C, F). (A, D) Mock treated VP1 expressing cells. Cells were fractionated *in situ* and VP1 (red) and tubulin (green) were stained by specific antibodies. Shown are selected confocal sections of non-fractionated cells (NF) (A–C) and cells after the last fractionation step (Fr) (D–F). Bar: 8 μm.

Production of the fusion proteins was confirmed by western blot analysis with specific antibodies against VP1 or biotin (not shown). The fused proteins recognized by both antibodies migrated with the expected sizes (57 kDa for VP1-BE-NT and 60 kDa for VP1-BE-CT). After transfection of human embryonal kidney 293T cells with plasmids encoding VP1 fused with the tag on its N or C terminus, VP1-interacting proteins were isolated and resolved in SDS/PAGE gel (Fig. 7). Following gel staining, the most abundant bands were identified by mass spectrometry. Apart from different ubiquitinylated or degraded VP1 sequences, cellular chaperone heat shock protein 90 (Hsp90) was identified in both isolations. Interaction of VP1 and Hsp90 was verified by immunoprecipitation of VP1 using specific Hsp90 antibody and vice versa, by immunoprecipitation of Hsp90 with VP1-specific antibody. As shown in Fig. 7B, positive results of coimmunoprecipitation were obtained in lysates of infected cells as well as of cells transiently expressing VP1. These data indicate that VP1 association with Hsp90 is specific.

Chaperone Hsp90 is known to be a microtubule binding protein mediating association of its client proteins with microtubules [18]. Therefore, we further examined whether this chaperone is involved in interaction of VP1 with microtubules. In experiments of *in situ* fractionation, Hsp90 followed profiles of VP1 and tubulin (Fig. 7C).

We further examined the effect of the Hsp90 inhibitor, 17-allylamino-17-demethoxygeldanamycin (17-AAG; an inhibitor of ATPase activity of Hsp90) [19], on VP1–microtubule interaction. As seen in Fig. 8A, inhibitor treatment of cells expressing VP1 did not prevent VP1–microtubule interaction. VP1 fibers were observed both in control and treated cells. To determine whether the inhibitor decreases the amount of VP1 bound to microtubules, cells were treated with the inhibitor 17-AAG, and the quantities of VP1 and Hsp90 in the last insoluble fraction were determined. In the treated cells, the relative amounts of VP1 and Hsp90 proteins, detected in the last insoluble fraction, decreased by half in comparison with those in control cells (Fig. 8B,C). These data indicate that Hsp90 is involved in VP1-mictotubule interaction. To confirm the involvement of Hsp90 in VP1–microtubule binding, we examined whether the amount of VP1 in the last insoluble fraction would be affected by Hsp90 knock-down. In Hsp90 knock-down cells, the total amount of Hsp90 decreased in two independent experiments by

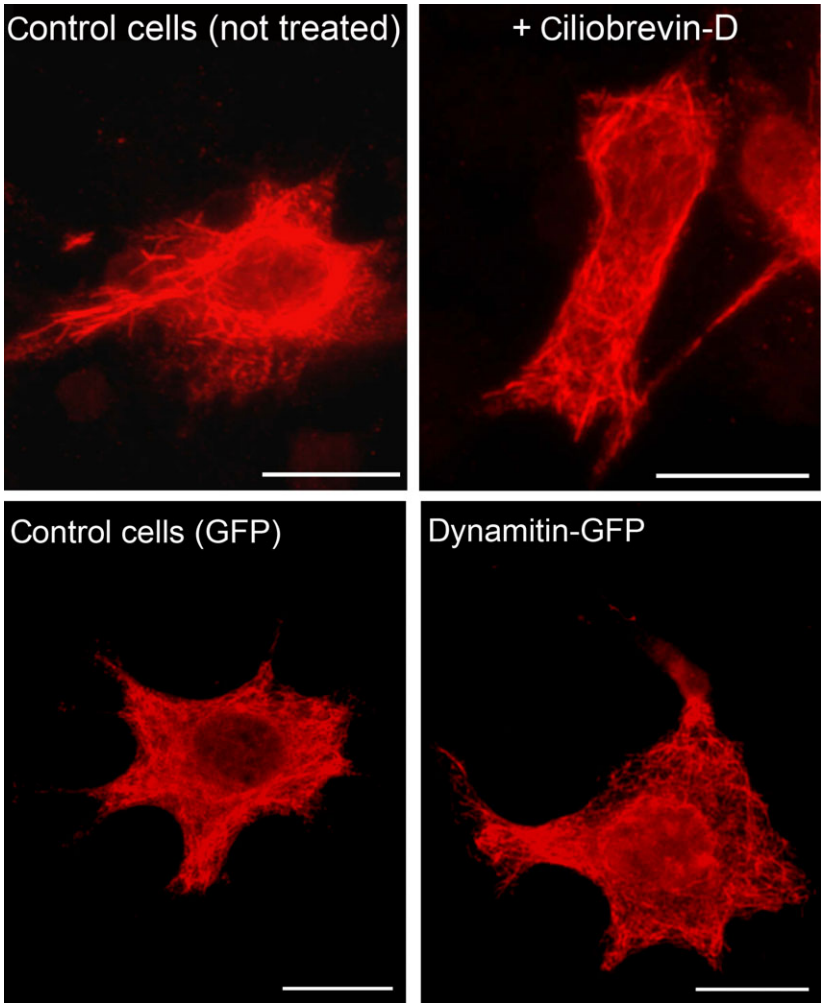

Fig. 6. Dynein does not mediate the VP1–microtubule binding. WOP cells were transfected with pVP1 and treated with ciliobrevin D for 1 h (upper panel) or cotransfected with pVP1 and pdynamitin–green fluorescent protein (GFP) or pGFP (control cells; lower panel). After 24 h, cells were fractionated *in situ* and VP1 was stained by specific antibody. Shown are selected confocal sections of cells after fractionation. Bar: 10 μm.

70% and 50% (Fig. 8D,E) and the relative amount of VP1 in the last insoluble fraction decreased by 40% and 20%, respectively (Fig. 8F,G). The amount of Hsp90 in the last insoluble fraction in Hsp90 knock-down cells decreased under the detection limit of the western blot method (Fig. 8F).

As Hsp90 is known to bind preferentially acetylated microtubules [18], we further addressed the role of microtubule acetylation in VP1–microtubule interaction. We examined the amount of VP1 protein in the last insoluble fraction in TAT KO cells, which do not express the major tubulin acetyltransferase [20–22], tubulin acetyltransferase 1 (αTAT1), and lack acetylated microtubules [23]. The absence of acetylated α-tubulin in TAT KO cells was confirmed by western blot analysis of cell lysates using antibody specific to acetylated α-tubulin (Fig. 9A). As seen in Fig. 9B,C, the relative amounts of VP1 and Hsp90 proteins in the last insoluble fraction did not significantly change in TAT KO cells in comparison with those in control 3T3-wt (wild-type) cells. The results of the experiment indicate that microtubule acetylation is dispensable for VP1–microtubule binding. Moreover, unchanged amounts of VP1 and Hsp90 in insoluble fraction of TAT KO cells also suggest that Hsp90 does not play the role of a mediator of VP1–microtubule association, as Hsp90 prefers to bind acetylated microtubules [18].

Taken together, these data show that the microtubule binding protein, Hsp90 chaperone, is a

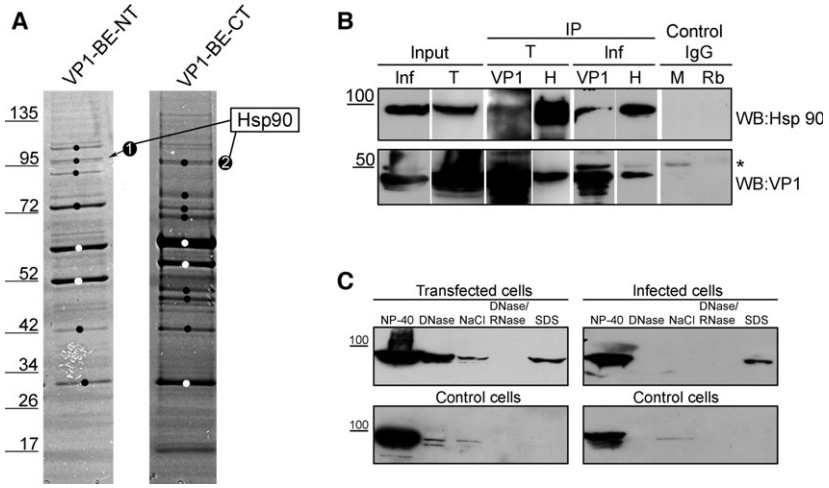

Fig. 7. Identification of proteins interacting with VP1. (A) 293T cells were transfected with pVP1-BE-NT or pVP1-BE-CT and 36 h post-transfection the complexes were isolated by affinity chromatography and separated by 4–12% SDS/PAGE. Separated proteins were visualized by Coomassie staining and the most abundant bands (marked with dot) were identified by mass spectrometry. (B) Immunocomplexes of infected 3T6 cells (40 h post-infection) or VP1-expressing WOP cells (24 h post-transfection) were isolated by specific antibodies, and separated by SDS/PAGE. Proteins were transferred to the membrane and detected by specific antibodies. T, transfected lysates; inf, infected lysates; H, Hsp90 antibody; M, non-specific mouse control IgG; Rb, non-specific control rabbit IgG; *, heavy chain of antibody. (C) Infected 3T6 cells or VP1-expressing WOP cells were fractionated *in situ* 40 h post-infection or 24 h post-transfection, respectively, and each fraction was separated by 10% SDS/PAGE. Proteins were transferred to the membrane and Hsp90 was detected by specific antibody. Control cells: mock-infected/transfected cells.

component of the VP1–microtubule complex. Finding that VP1 interacts with microtubules regardless of their acetylation status suggests that Hsp90 does not function as a mediator of VP1 association with microtubules and is rather recruited to the complex by VP1. However, less efficient binding of VP1 to microtubules after Hsp90 knockdown or inhibition of its chaperone function accounts for some role of Hsp90 in the complex formation. The chaperone function of Hsp90 may help to organize VP1 binding along microtubules.

The level of acetylated α-tubulin is increased in MPyV-infected cells and cells expressing VP1

In situ fractionation of cells suggested that VP1 binding to microtubules stabilizes them. It is known that acetylation of α-tubulin is a well-established marker of microtubule stability [24]. We were further interested in whether VP1 expression and/or MPyV infection affects the level of α-tubulin acetylation. Cells were infected with MPyV or transfected with VP1-expressing plasmid and the amount of acetylated α-tubulin in lysates was quantified by western blot and densitometry analysis. The level of acetylated α-tubulin in infected cells in the late stage of infection (40 h) was 8-fold higher than that in mock-infected cells (Fig. 10A,B). Only a minor change of acetylated α-tubulin level was observed in the cells in the early stage of infection. These data show that in the late phase of infection, when structural proteins are expressed, the level of microtubule acetylation increases dramatically. The level of acetylated α-tubulin in the lysates of transfected cells expressing VP1 was 5-fold higher than that in mock-transfected cells and only a minor increase of acetylated α-tubulin level was detected in cells transfected with a control vector expressing enhanced green fluorescent protein (EGFP) only (Fig. 10A,C). In transfected WOP cells, expression of VP1 was lower than that in infected cells. To find out whether the increasing level of VP1 in the cells would result in increasing level of acetylated α-tubulin, the plasmid carrying the VP1 gene was expressed in cells that differ in their endogenous production of SV40 LT antigen. Human 293 cells that do not express SV40 LT antigen and 293T cells expressing SV40 LT antigen were used for transfection by VP1-expressing and control plasmids carrying the sequence of SV40 origin of replication, thus enabling replication of the plasmids in 293T cells. Therefore, the level of VP1 in 293T cells should be much higher than that in 293 cells. The levels of acetylated α-tubulin and VP1 were quantified by western blot and densitometry analysis. As shown in Fig. 10, the level of acetylated α-tubulin correlated with the amount of VP1 in the cells. These

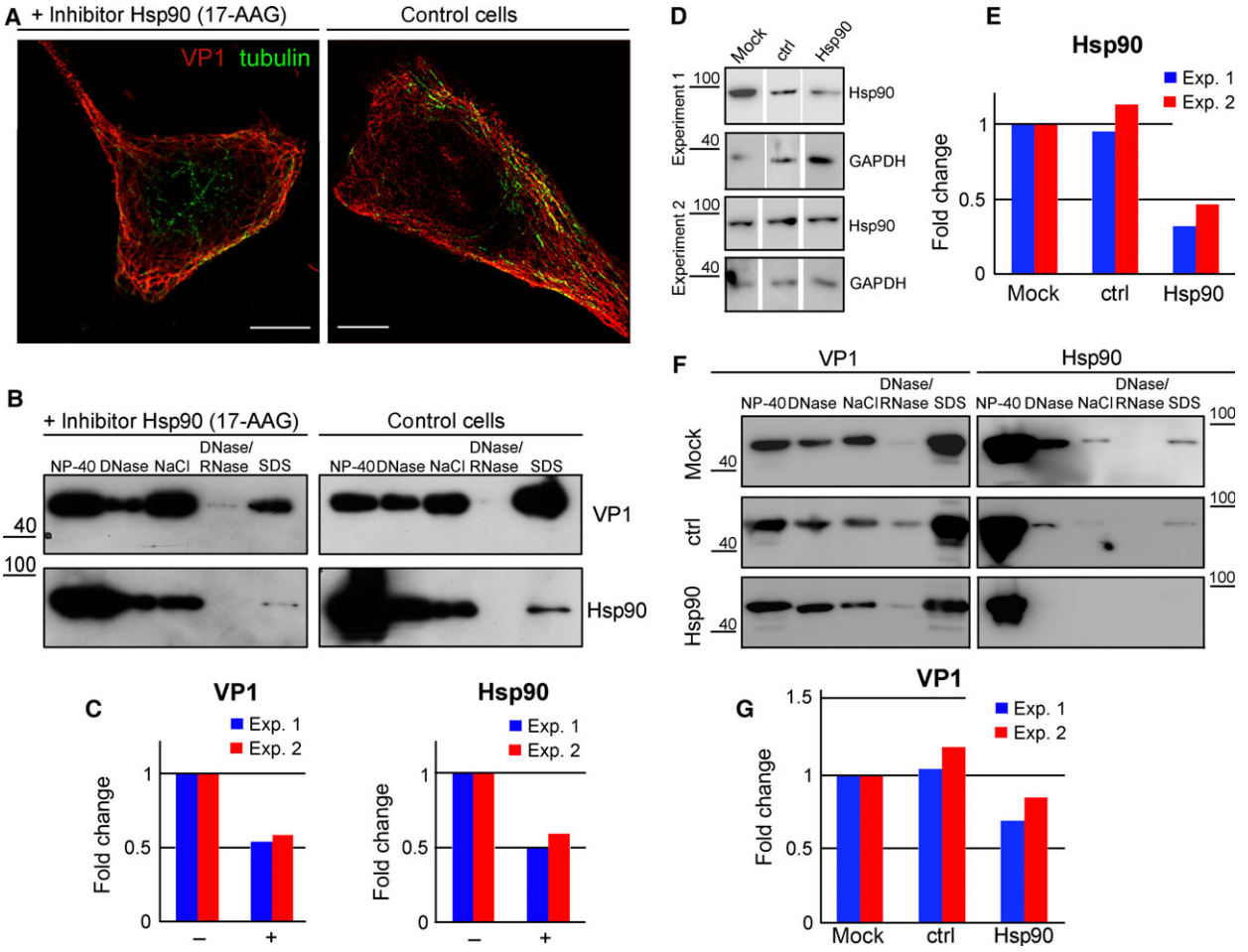

Fig. 8. Inhibition or down-regulation of Hsp90 decreases the amount of VP1 in the insoluble fraction. (A, B) WOP cells were transfected with pVP1 and immediately after transfection, 17-AAG (10 μM) was added. After 24 h treatment, cells were fractionated *in situ* and Hsp90 and VP1 were stained by specific antibodies (A), or the presence of VP1 and Hsp90 in each fraction was detected by specific antibodies (B). (C) Graphic illustration of densitometry analysis of the digital images of western blots from two independent experiments. The amount of VP1 or Hsp90 was measured. Presented is fold change of VP1 or Hsp90 in the last fraction, which was compared with the mock-treated cells expressing VP1. Bar: 8 μm. (D, F) WOP cells were transfected with pVP1 and immediately after transfection, re-transfected with control (ctrl) or Hsp90 specific (Hsp90) siRNA. After 24 h treatment, cells were fractionated *in situ* and total amount of Hsp90 in combined fractions (D) or the presence of VP1 and Hsp90 in each fraction (F) was measured by specific antibodies staining. (E) Graphic illustration of densitometry analysis of the digital images of western blots from two independent experiments. Presented are fold changes of Hsp90 relative to mock siRNA transfected cells expressing VP1. (G) Graphic illustration of densitometry analysis of the digital images of western blots from two independent experiments. Presented are fold changes of VP1 in the last fraction, which was compared with the mock siRNA transfected cells expressing VP1.

data support the hypothesis that VP1 increases the acetylation level of α-tubulin.

Interaction of VP1 with microtubules affects cell proliferation

Microtubules are indispensable cellular structures for ensuring cell division, mainly for chromosome segregation during mitosis. We addressed the question whether VP1 binds also mitotic microtubules. We could hardly find mitotic cells expressing VP1 (Fig. 11Aa). To enrich the number of cells in mitosis, we treated them with taxol, a drug stabilizing microtubules. In taxol-treated mitotic cells, VP1 exhibited affinity to the mitotic spindle body and we could observe also VP1 fibers protruding from the spindle body, apparently as part of spindle (Fig. 11Ab).

Since disturbance of microtubule stability results in cell cycle arrest or cell death, we were interested in whether VP1's interaction with microtubules, resulting

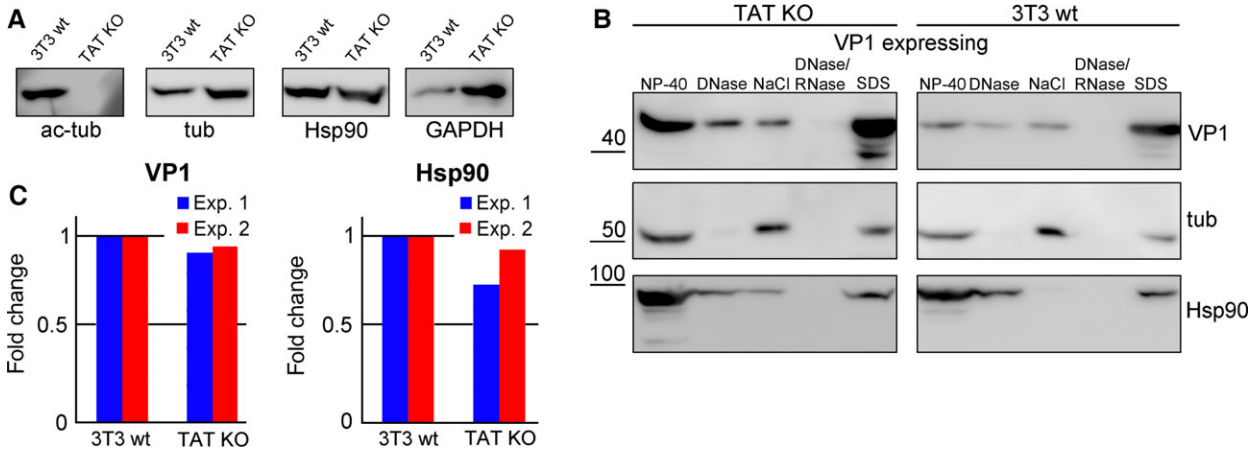

Fig. 9. Microtubule acetylation is not necessary for VP1 interaction. (A) Lysates of TAT KO cells and 3T3-wt cells were separated by 10% SDS/PAGE, transferred onto PVDF membrane, and acetylated α-tubulin (ac-tub), tubulin (tub), Hsp90 and GAPDH were stained by specific antibodies. (B) TAT KO and 3T3-wt cells were transfected with pVP1 and after 24 h, cells were fractionated *in situ*. Presence of VP1, tubulin and Hsp90 in each fraction was detected by specific antibodies. (C) Graphic illustration of densitometry analysis of the digital images of western blots from two independent experiments. Presented are fold changes of VP1 or Hsp90 in the last fraction of TAT KO cells that were compared with the 3T3-wt cells expressing VP1.

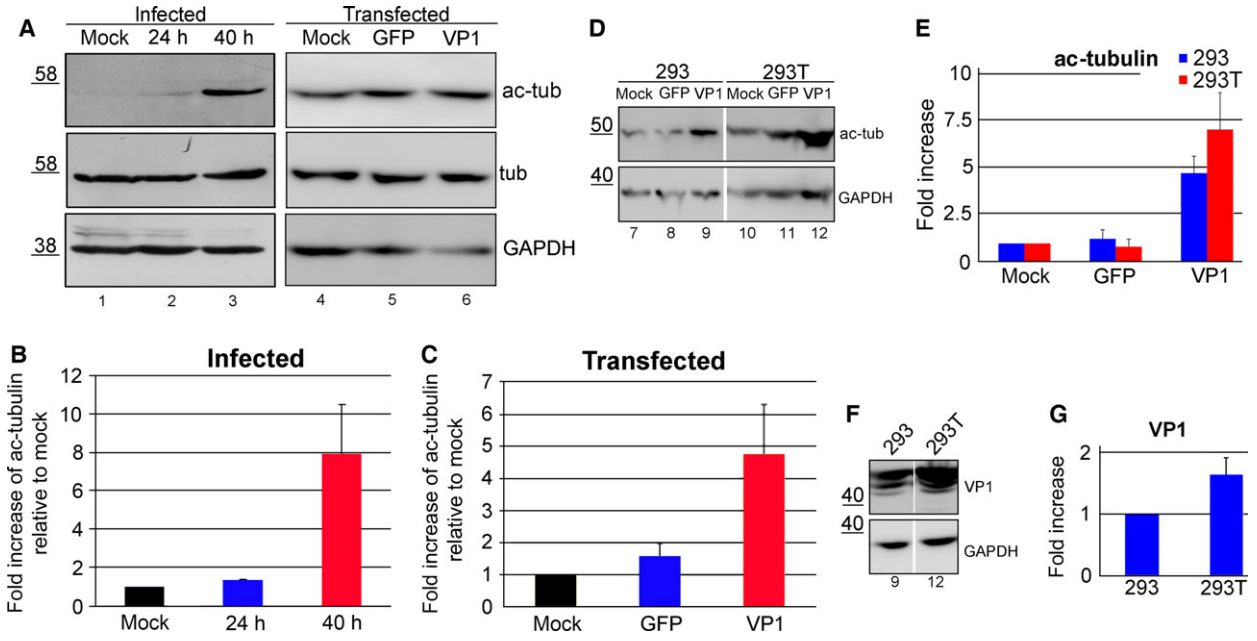

Fig. 10. The amount of acetylated tubulin is increased in cells expressing VP1. (A) WOP cells were infected with MPyV (multiplicity of infection (MOI) = 10 pfu per cell) and lysed at indicated time post-infection (lanes 1–3) or transfected with plasmid expressing EGFP (GFP) or with plasmid expressing VP1 (VP1) (lanes 4–6). Cells were lysed 24 h post-transfection, lysates were separated by 10% SDS/PAGE, transferred onto PVDF membrane, and acetylated tubulin (ac-tub), tubulin (tub) and GAPDH were stained by specific antibodies. (B, C) Graphic illustration of densitometry analysis of the digital images of western blots from three independent experiments. Shown is fold increase relative to mock-infected or transfected cells ± SD. (D, F) 293 (lanes 7–9) and 293T (lanes 10–12) cells were transfected with plasmid expressing EGFP (GFP) or with plasmid expressing VP1 (VP1). Cells were lysed 48 h post-transfection, lysates were separated by 10% SDS/PAGE, transferred onto PVDF membrane, and acetylated tubulin (ac-tub), VP1 and GAPDH were stained by specific antibodies. (E, G) Graphic illustration of densitometry analysis of the digital images of western blots from three independent experiments ± SD. Shown is fold increase relative to mock transfected cells (E) or fold increase relative to 293 cells (G). Mock, mock-transfected or infected cells.

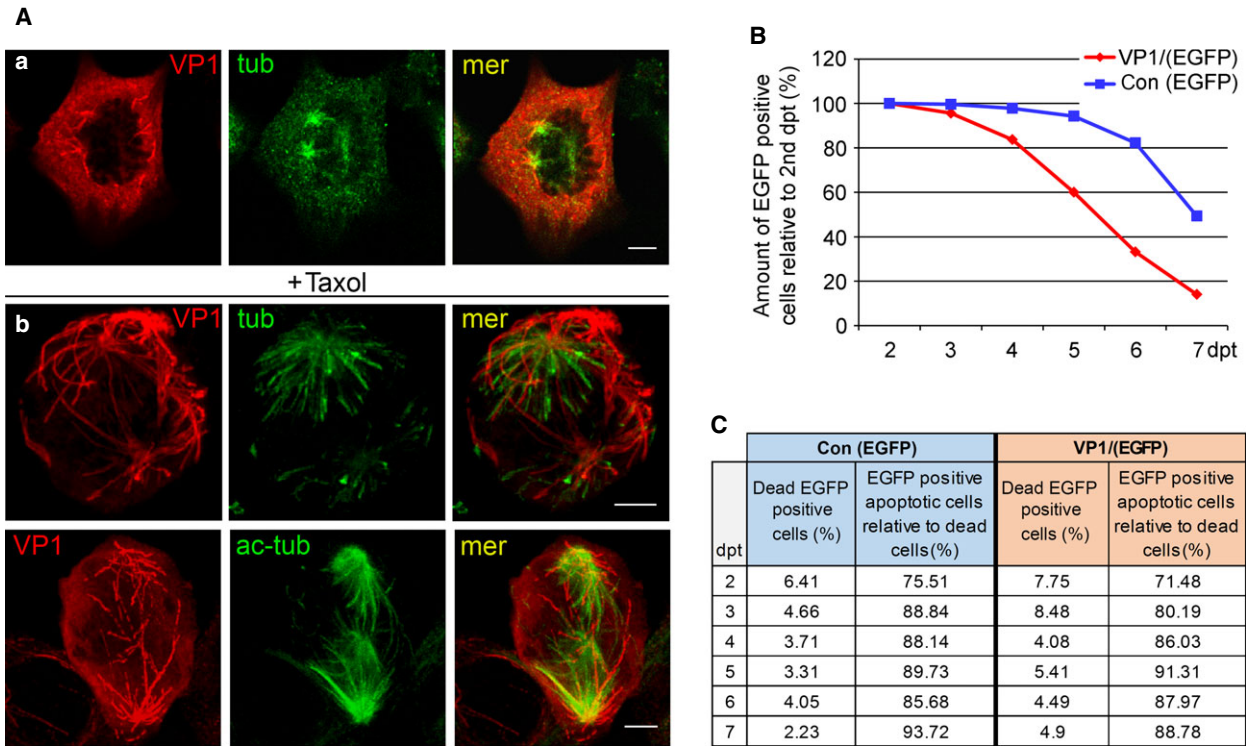

C

dpt	Con (EGFP)		VP1/(EGFP)	
	Dead EGFP positive cells (%)	EGFP positive apoptotic cells relative to dead cells(%)	Dead EGFP positive cells (%)	EGFP positive apoptotic cells relative to dead cells(%)
2	6.41	75.51	7.75	71.48
3	4.66	88.84	8.48	80.19
4	3.71	88.14	4.08	86.03
5	3.31	89.73	5.41	91.31
6	4.05	85.68	4.49	87.97
7	2.23	93.72	4.9	88.78

Fig. 11. VP1 affects cell proliferation. (A) WOP cells were transfected with pVP1 and immediately after transfection, 1 μL of DMSO (a) or 1 μL of taxol in DMSO to final concentration of taxol 10 μM (b) was added. After 24 h incubation, cells were fixed and VP1, tubulin or acetylated α-tubulin was stained by specific antibodies. Shown are maximal projections of 35 sections; bar: 8 μm. (B, C) WOP cells were transfected with pWP (expressing EGFP and VP1) or pCont (expressing EGFP only). Cells were incubated for 2 days and from this starting point, the relative proportion of EGFP-positive cells (B) or dead cells stained by DAPI or apoptotic cells stained by annexin V (C) was measured by flow cytometry. One of two independent experiments is shown (for raw data of both experiments, Fig. S1). dpt, days post-transfection.

in their petrification, may affect proliferation of cells. Therefore, we monitored the numbers of cells expressing VP1 (and EGFP under the control of a different promotor) and control cells (expressing EGFP only) in time. For plasmid introduction to the cells, we used nucleofection, known to give high efficiency of transfection and very fast expression of the desired gene. Because DNA delivered into cells by this method induces interferon expression that affects transiently cell proliferation [25], we began to monitor cells numbers from the second day post-transfection. We expected that if VP1 does not affect the cell cycle, VP1 positive cell and control EGFP-expressing cells in culture should decline by the same rate. However, the number of VP1-expressing cells decreased more precipitously in comparison with the number of control EGFP-expressing cells (Fig. 11B), suggesting disturbed proliferation of VP1-expressing cells. Next, we examined by fluorescence-activated cell sorting (FACS) analysis proportions of dead cells expressing VP1 or control EGFP expressing cells with time (Fig. 11B) and also, whether the cells die by apoptosis (Fig. 11C). Amounts of dead cells decreased with time and their proportion ranged from 6.4% (2 days post-transfection) to 2.2% (7 days post-transfection) for control cells and 7.7% to 4.9% for VP1 expressing cells. The table in Fig. 11C shows that the majority of dead cells (~ 70–90%), both control and VP1 expressing, died by apoptosis.

We further determined by FACS analysis the amount of cells in G2/M phase of the cell cycle. The analysis revealed that VP1-expressing cells accumulated in G2/M phase during the incubation period (Fig. 12). Altogether, these data suggest that VP1 protein promotes cell cycle arrest after S phase in the late phase of MPyV infection and impedes cell division.

Discussion

Gene products of 'small' viruses with limited genome size are usually multifunctional. For example, early gene product of polyomaviruses, LT antigen, possesses

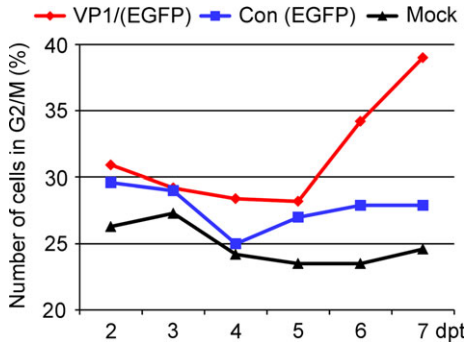

Fig. 12. VP1 affects the progression of the cell cycle. WOP cells were transfected with pWP (expressing EGFP and VP1) or pCont (expressing EGFP only). Cells were incubated for 2 days and from this starting point, the amount of cells in G2/M was measured by flow cytometry. One representation of two independent experiments is shown (for raw data of both experiments, Fig. S1). dpt, days post-transfection.

several functions (pRb- and p53-binding protein, transcription factor, replication initiator) for which larger DNA viruses (such as papillomaviruses or adenoviruses) have at least four gene products. Also, capsid proteins of small viruses were found to have additional functions in translation [26], cell cycle regulation [27], or regulation of viral transcription [28].

A great deal is known about the functions of the MPyV capsid proteins in the virion structure as well as in early stages of virus infection. However, interactions of these proteins with cellular proteins and structures in late stages of infection have not been well characterized. There are several unanswered questions about the mechanism of virion assembly and putative cellular proteins participating in it. Also, additional functions of capsid proteins cannot be excluded. In this work, we searched for new cellular interaction partners and functions of VP1.

Since VP1 possesses the NLS at its N terminus, we expected its accumulation in the cell nucleus after its individual expression in mammalian cells; however, VP1 was surprisingly found mainly in the cytoplasm. Accordingly, VP1 pentamers of another member of the Polyomaviridae family, JC virus, exhibited similar behavior; their individual production led to VP1 accumulation in the cytoplasm [29]. In previous works, MPyV VP1 expressed from recombinant vaccinia virus [30] or baculovirus [4] was detected predominantly in the cell nucleus. These expression systems are based on large DNA virus vectors that, apart from MPyV VP1, express many viral proteins. Thus, the possibility that some of these proteins could help VP1 to be efficiently transported to the cell nucleus cannot be excluded. Li *et al.* [15] were interested in the transport of SV40 VP1 pentamers to the cell nucleus. They proposed that the LT antigen is necessary for efficient nuclear translocation of VP1. They postulated that binding of LT to VP1 pentamers is mediated by cellular chaperones and the resulting complex helps the VP1 pentamer to create the proper conformation for importin recognition. However, our results showed that coexpression of VP1 and LT antigen did not significantly affect VP1 localization. We found that MPyV VP1 is efficiently transported into the cell nucleus when coexpressed with VP2 or VP3. The interchangeability of the NLS of polyomaviral structural proteins was described previously [31,32]; however, our results indicate that the NLS of the minor protein (VP2 or VP3) is absolutely indispensable for efficient VP1 nuclear localization. During infection, the complex of VP1 pentamer with one of the minor proteins is formed in the cytoplasm and then transported to the cell nucleus, where the virion assembly takes place. This mechanism apparently ensures transport of capsid proteins to the cell nucleus in proper stoichiometric concentrations – one molecule of the minor structural protein per one VP1 pentamer. Both minor proteins are necessary for efficient virus infectivity [33] and this mechanism may prevent incorporation of VP1 pentamers lacking minor proteins into viral capsids, thus ensuring virus infectivity.

However, in late phases of MPyV infection, a considerable amount of VP1 stays in the cytoplasm. We have shown that there, VP1 massively binds fiber structures that were identified as microtubules. This interaction was found not to be mediated by the microtubular motor, dynein. Screening of other possible cellular proteins interacting with VP1 identified cellular chaperone, Hsp90, as the MPyV VP1 interaction partner. Hsp90 is an abundant cellular chaperone that interacts with many proteins, including transcription factors, kinases, E3-ligases, structural proteins, ribosomal components and metabolic enzymes [34]. Interaction of polyomaviral proteins with another member of chaperone family, Hsp 70, was characterized previously [8,15]. It was shown for many viruses that Hsp90 is involved in their life cycles; it participates in virus replication, viral structural protein folding and virion assembly [35]. It is likely that Hsp90 takes part also in MPyV infection. As Hsp90 is known to be a microtubule binding protein [18,36,37], we were interested in whether this chaperone mediates VP1–microtubule interaction. Giustiniani *et al.* [18] demonstrated that Hsp90 preferentially binds acetylated microtubules and suggested that it mediates interaction of Hsp90 client proteins with microtubules. This conclusion came from the observation that upon microtubule hyperacetylation, binding of Hsp90 client proteins to

microtubules significantly increased [18]. It was also demonstrated that Hsp90 is important for the transport of herpes simplex virus 1 (HSV-1) capsids to the nucleus in early stages of infection. The transport was dependent on the acetylation status of microtubules and it was proposed that Hsp90 mediates interaction between the capsid protein and microtubules [38]. Our results indicate that Hsp90 is involved in VP1–microtubule interaction. First, after *in situ* fractionation of infected or VP1 producing cells, Hsp90 appeared together with VP1 and tubulin in the last, insoluble fraction. Second, Hsp90 inhibition or down-regulation decreased the VP1–microtubule binding. However, in TAT KO cells, lacking acetylated α-tubulin (knockout of αTAT1), VP1 bound microtubules with an efficiency comparable with that in control cells. Thus, acetylation of microtubules is apparently dispensable for VP1 binding. Also, the fact that we did not detect any significant decrease of amounts of Hsp90 and VP1 associated with microtubules in TAT KO cells suggests that Hsp90 does not function as a mediator of VP1–microtubule association. Instead, it seems to be recruited to microtubules by VP1. Its chaperone activity might assist VP1 to assemble along microtubules. Further research is necessary to clarify the exact mechanism of Hsp90's role in VP1–microtubule complex formation.

Although acetylation of microtubules is not required for VP1–microtubules binding, we showed that in VP1-producing cells, the level of microtubule acetylation was elevated. The real meaning of α-tubulin acetylation is still elusive. Although the relationship between acetylation of microtubules and their increased stability has been described [39–41], the precise relationship between microtubule acetylation and stability is still unclear. There is much evidence supporting as well as denying the hypothesis that acetylation positively affects microtubule stability [39–43]. Microtubule acetylation is a marker of their stability, irrespective of whether acetylation is a cause or a consequence of the stability.

Stabilization of microtubules may have several consequences both for the cell and for the virus life cycle. VP1 binding to microtubules may contribute to maintaining the cell shape and mechanics. These properties are determined by the interplay of three parts of the cytoskeletal network – actin filaments, microtubules and intermediate filaments [44]. Disturbance of one component of the cytoskeletal network leads to changes of other components. Early antigens of members of the Polyomaviridae family were shown to be able to affect the cytoskeletal network. Rathje *et al.* [45] demonstrated that cells constitutively expressing LT antigen of SV40 exhibited reorganization of vimentin filaments (belonging to intermediate filament family) and also that expression of LT decreased the level of α-tubulin acetylation. Reduced α-tubulin acetylation was caused by elevation of histone deacetylase 6 (HDAC6), which also led to vimentin destabilization [45]. Investigators hypothesized that these changes of cytoskeletal network resulted in increased cellular stiffness at the cell periphery and supported cell invasion. Likewise, small T (sT) antigen of Merkel cell polyomavirus promotes lowered α-tubulin acetylation and mediates microtubule destabilization leading to increased cellular motility and migration [46]. Middle T antigen of MPyV is able to deplete acetylation of microtubules and mediate loss of focal adhesions and actin stress fibers [47]. VP1 fibers might compensate for the loss of one cytoskeletal network component by strengthening another and thus maintain the cell shape, having thus an opposite effect to T antigens. It was shown that contact inhibition and adhesion was impaired in cells lacking αTAT1 [23]. VP1 indirectly increases microtubule acetylation, and thereby can promote cell adhesion and contact inhibition.

An increased level of acetylated α-tubulin was described for infection by many viruses, including human immunodeficiency virus 1 [48], influenza A [49] and HSV-1 [50]. It has been shown that microtubule hyperacetylation is important for virus infectivity, namely for virus entry into and egress from host cells [48,51,52]. These studies propose that the role of α-tubulin acetylation is connected with the movement of viruses or virus components in the cells. Tubulin acetylation favors motor binding, which results in enhanced trafficking along the microtubules [53]. Although the involvement of microtubules in MPyV virus egress has not yet been described, increased acetylation may be important for enhancement of trafficking of virus components into the nucleus in the late phase of infection. The increased level of α-tubulin acetylation points to down- or upregulation of αTAT1 and HDAC6 [54], ensuring α-tubulin acetylation and deacetylation, respectively. These proteins interact with several different substrates, thus being also involved in other cellular processes such as autophagy or aggregozome formation [55]. Reduction of the HDAC6 level by viruses can inhibit these processes. It was demonstrated that influenza virus decreases the level of HDAC6 [56]. Experiments are now underway to reveal the mechanisms leading to increased microtubule acetylation upon MPyV infection.

Importantly, we showed that VP1 binding to microtubules resulted in accumulation of cells in the G2/M phase of the cell cycle. The ability of VP1 to interfere with cell cycle progression was already suggested by

several observations. We showed previously that VP1 produced in *Saccharomyces cerevisiae* blocked the growth of colonies for several days by encasing the mitotic spindle [57]. Yeast cells were able to overcome the block by assembly of a new spindle [57]. VP1 was also found to interact with microtubules and spindle bodies in early MPyV-induced epithelial tumors where VP1 was expressed. It was suggested that such VP1-producing cells may be important in the development of aneuploidy in tumors [58]. Later in tumor progression, the VP1 gene was found to be silenced [59]. The association between VP1 and cell cycle arrest was also postulated by Spink and Fluck [60]. Their hypothesis came from the studies of MPyV host range mutants. One of them did not produce MT and sT antigen, but VP1 protein was highly overexpressed. Most of the cells from the infected cell population exhibited block in the first G2/M phase of the cell cycle [60]. Whether increased acetylation of microtubules in cells expressing VP1 is involved in their G2/M block is unclear. Several studies demonstrated that acetylation of spindle is important for its proper formation [61,62]. On the other hand, no problem with division of TAT KO cells was observed, and moreover, they were found to proliferate more efficiently than their parental line [23]. Nevertheless, irrespective of spindle acetylation status, VP1 itself can act as a mitotic poison by petrifying microtubules and mitotic spindle.

Cells infected by polyomaviruses accumulate in S and G2 phases of the cell cycle [63,64]. A later study of cell cycle progression in MPyV-infected cells revealed that infected cells go through at least two cell cycles [65]. They exhibit prolonged S phase and no G2→M transition [66]. Dahl *et al*. [66] also showed that cell cycle arrest is connected with replication of viral DNA, which activates the ATM (protein kinase ataxia telangiectasia mutated) pathway leading to inactivation of CDK1 and thus induces cell cycle arrest. Recently, it was shown that over-expressed sT antigen is able to arrest cells in mitosis [67]. It is possible that early antigens (sT antigen and indirectly LT antigen that mediates virus genome replication) and VP1 protein contribute to the block of cell division. While early antigens are apparently involved in the first cell cycle block, VP1 may contribute to blocking the second cell cycle, thus enabling completion of the virus assembly.

Material and methods

Cells and virus

NIH 3T3 (ATCC, Manassas, VA, USA; CRL-1658) and 3T6 (ATCC; CCL-96) mouse fibroblasts, NMuMG (ATCC; CRL-1636) mouse gland mammary cells, WOP [68], mouse fibroblasts constitutively producing early T antigens of the MPyV, 293 human embryonic kidney cells (ATCC; CRL-1573), 293T human embryonic kidney cells with integrated SV40 virus genome and constitutively expressing LT and sT antigen of SV40 virus (ATCC; CRL-11268) and HeLa cells (ATCC; CCL-13) were grown at 37 °C in a 5% CO_2-air humidified incubator using Dulbecco's modified Eagle's medium (DMEM; Sigma-Aldrich, Saint Louis, MO, USA) supplemented with 10% fetal bovine serum (Thermo Fisher Scientific, Waltham, MA, USA) and 2 mM glutamax (Thermo Fisher Scientific). TAT KO cells [23], mouse fibroblasts with αTAT knock out, and their wild-type counterparts, 3T3-wt cells, were grown at 37 °C in a 5% CO_2-air humidified incubator using DMEM (Sigma-Aldrich) supplemented with 10% fetal bovine serum (Thermo Fisher Scientific), 2 mM glutamine (Thermo Fisher Scientific), 1% non-essential amino acids (Sigma-Aldrich) and 5 mM β-mercaptoethanol (Sigma-Aldrich). MPyV (BG strain) was isolated and purified from infected 3T6 cells using a standard protocol [69]. For infection, 3T6 cells were synchronized in DMEM media for 24 h followed by 1 h incubation with virus inoculum at multiplicity of infection (MOI) 10.

Plasmids

For expression of VP1, plasmids pwP (a gift from C. Buck; Addgene plasmid no. 22519, Addgene, Cambridge, MA, USA) [70] and pVP1 [71] were used. For expression of VP2 and VP3, plasmids pVP2 and pVP3 [25] were used. The list of used plasmids and primers is summarized in Tables S1 and S2.

Plasmid pCont

Plasmid pCont is derived from pwP and carries the sequence of polylinker instead of the VP1 sequence. This plasmid was created by LR recombination of a donor vector (pENTR/D-TOPO-Pol) and destination vector pGwf (a gift from C. Buck, Addgene plasmid no. 22517) [72]. The donor plasmid pENTR/D-TOPO-Pol was constructed as follows. The sequence of polylinker was amplified from plasmid pBluescript SK– (Stratagene, Santa Clara, CA, USA) using primers Pol-F: 5′-CAC CGG GCG AAT TGG GTA CCG GGC-3′ and Pol-R: 5′-CAC TAA AGG GAA CAA AAG CTG GAG C-3′, and inserted into plasmid pENTR/D-TOPO (Thermo Fisher Scientific) using TOPO cloning according to the manufacturer's protocol.

Plasmids pcDNA3.2/VP1-BE-NT and pcDNA3.2/VP1-BE-CT

Plasmids pcDNA3.2/VP1-BE-NT and pcDNA3.2/VP1-BE-CT carrying the sequence for VP1 protein fused with

BioEase Tag (Thermo Fisher Scientific) at its N terminus (VP1-BE-NT) or C terminus (VP1-BE-CT) under the control of cytomegalovirus promoter were constructed using LR recombination. Donor vectors pENTR-VP1 and pENTR-VP1ΔSTOP were constructed as follows. The sequence of VP1 gene was amplified by PCR from plasmid pMJG, carrying the whole MPyV genome [73], using primers VP1-F: 5′-CAC CAT GGC CCC AAA AAG AAA AAG-3′, VP1-R: 5′-TTA ATT TCC AGG AAA TAC AGT C-3′ (VP1-BE-NT) and VP1ΔSTOP-R: 5′-ATT TCC AGG AAA TAC AGT CTT TG-3′ (VP1-BE-CT). VP1 sequences were inserted by TOPO cloning to plasmid pENTR/D-TOPO (according to the manufacturer's instructions). These plasmids were used as donor vectors in an LR recombination reaction with destination vectors pcDNA3.2/capTEV-CT/V5-DEST or pcDNA3.2/capTEV-NT/V5-DEST (Thermo Fisher Scientific, according to the manufacturer's instructions) resulting in creation of the plasmids.

Vector pGwfΔATG-GFP

Vector pGwfΔATG-GFP is a derivative of pGwf plasmid where the start codon for GFP was mutated by site-directed mutagenesis using QuikChange II XL Site-Directed Mutagenesis Kit (Stratagene). Primers used for mutagenesis were GFPΔATG-F: 5′-GGA TCC ACC GGT CGC ACG CGT CGC GAG CAA GGG CGA GG-3′ and GFPΔATG-R: 5′-CCT CGC CCT TGC TCG CGA CGC GTG CGA CCG GTG GAT CC-3′, according to the manufacturer's instructions.

Plasmids pVP1-BE-NT and pVP1-BE-CT

Plasmids pVP1-BE-NT and pVP1-BE-CT carry the sequence of VP1 protein fused with BioEase Tag at its N terminus (VP1-BE-NT) or C terminus (VP1-BE-CT). These sequences are under the control of strong mammalian constitutively expressed promoter EF1α and the sequence WPRE for stabilizing mRNA is also present in these plasmids. The plasmids were constructed using LR recombination. Donor plasmids pENTR-VP1-BE-NT and pENTR-VP1-BE-CT were prepared as follows. The sequence of VP1 fused with BioEase Tag was amplified by PCR from plasmids pcDNA3.2/capTEV-CT/V5-DEST or pcDNA3.2/capTEV-NT/V5-DEST using primers VP1-BE-NT-F: 5′-CAC CAT GGG CGC CGG CAC CCC GGT GAC C-3′ and VP1-R: 5′-TTA ATT TCC AGG AAA TAC AGT C-3′ for VP1-BE-NT or VP1-F: 5′-CAC CAT GGC CCC AAA AAG AAA AAG-3′ and VP1-BE-CT-R: 5′-CTA TCA TTA CTA GGA TCC AGA GC-3′ for VP1-BE-CT. The sequences were inserted by TOPO cloning into plasmid pENTR/D-TOPO according to the manufacturer's instructions. These plasmids were used as donor vectors in LR recombination reaction with destination vector pGwfΔATG-GFP according to the manufacturer's instructions.

Plasmids were isolated by EndoFree Plasmid Maxi kit (Qiagen, Hilden, Germany) and used for transfections.

Antibodies

The primary antibodies used were mouse monoclonal antibody to VP1 [4], mouse monoclonal antibody recognizing the common region of VP2 and VP3 [4], rabbit polyclonal antibody to VP1 (prepared in our laboratory), mouse monoclonal antibody to α-tubulin (Exbio, Prague, Czech Republic or Sigma-Aldrich), mouse monoclonal to acetylated α-tubulin (Sigma-Aldrich), rabbit polyclonal to glyceraldehyde 3-phosphate dehydrogenase (GAPDH; Santa Cruz Biotechnology, Dallas, TX, USA) and rabbit monoclonal to Hsp90α/β (Abcam, Cambridge, UK).

Secondary antibodies used were goat anti-rabbit conjugated with Alexa Fluor-546, donkey anti-mouse conjugated with Alexa Fluor-488 (all from Thermo Fisher Scientific), goat anti-mouse and goat anti-rabbit conjugated with peroxidase (all from Bio-Rad, Hercules, CA, USA), goat anti-rabbit conjugated with 5 nm gold particles, goat anti-mouse conjugated with 10 nm gold particles (all from BBI Solutions, Cardiff, UK).

Transfection of cells

Transfection of NIH 3T3, WOP, TAT KO and 3T3-wt cells was performed by electroporation in the Nucleofector™ device using Nucleofector V solution (Lonza, Basel, Switzerland) according to the manufacturer's instructions. Briefly, 4×10^6 exponentially growing cells were mixed with 6 μg of plasmid DNA and 100 μL of Nucleofector V solution and electroporated (program U-030). Tranfection of NMuMG, 293, 293T and HeLa cells was performed by lipofection using TurboFect™ transfection reagent (Thermo Fisher Scientific). Cells (1×10^6 per six-well plate) were seeded and 24 h later were transfected according to the manufacturer's protocol. Transfection of WOP cells with siRNA was performed by reverse transfection using Lipofectamine RNAiMax transfection reagent (Thermo Fisher Scientific). Cells (2.5×10^5 per well of six-well plate) were transfected with 50 pmol of siRNA according to the manufacturer's protocol.

Cell fractionation

Cells were fractionated to cytoplasmic, nuclear and insoluble fractions according to [74]. Briefly, 1×10^6 cells were washed with PBS and resuspended in 400 μL ice-cold buffer A (10 mM Hepes pH 7.9, 10 mM KCl, 0.1 mM EDTA, 0.1 mM EGTA, 1 mM DTT and a cocktail of protease inhibitors (Roche, Basel, Switzerland) and incubated for

15 min on ice. Then, 25 μL of 10% NP-40 was added and the solution was vigorously vortexed for 10 s. Nuclei were pelleted by centrifugation and the supernatant was designated as the cytoplasmic fraction. The nuclear pellet was resuspended in 50 μL ice-cold buffer C [20 mM Hepes pH 7.9, 400 mM NaCl, 1 mM EDTA, 1 mM EGTA, 1 mM DTT and a cocktail of protease inhibitors (Roche)] and incubated at a rocking platform (250 r.p.m.) for 15 min at 4 °C. The suspension was centrifuged (5 min, 20 000 ***g***, 4 °C) and the supernatant was removed and designated as the nuclear fraction. The pellet, which did not contain unbroken nuclei (as tested by microscopy), was resuspended in 50 μL of Laemmli buffer (1% SDS, 10 mM Tris/HCl, pH 6.8, 5% β-mercaptoethanol, 10% glycerol, 0.001% bromophenol blue) and designated as the insoluble fraction. Proteins from each fraction were separated by 10% SDS/PAGE, transferred onto a membrane, and VP1 protein was detected by specific antibody. The amount of protein in each fraction was determined by measurement of band density and expressed as a ratio to the total protein amount (amount of proteins in all fractions).

In situ fractionation (according to [16])

Cells growing on 10 cm Petri dishes were washed three times with KM buffer [10 mM Mes, pH 6.2, 10 mM NaCl, 1.5 mM $MgCl_2$, 10% glycerol and a cocktail of protease inhibitors (Roche)]. For the first extraction step, KM buffer supplemented with 1% NP-40, 1 mM EGTA and 5 mM DTT was used. Two milliliters of buffer was added to the dish, incubated for 3 min on ice and removed. Another 4 mL of buffer was added to the dish, incubated for 27 min on ice, and the extract was combined with the previous one and designated as the NP-40 fraction. After the first extraction step, structures on the dish were washed three times with KM buffer and incubated with 2 mL of KM buffer supplemented with DNase I (100 $u \cdot mL^{-1}$; Roche) for 15 min at 37 °C. The extract was removed and designated as the DNase fraction. Structures on the dish were washed three times with KM buffer and incubated for 30 min on ice in 2 mL of KM buffer containing 2 M NaCl, 1 mM EGTA and 5 mM DTT. The extract was removed and designated as the NaCl fraction. After the third extraction step, structures on the dish were washed three times with KM buffer and incubated for 30 min at 37 °C in 3 mL of KM buffer supplemented with DNase I (100 $u \cdot mL^{-1}$; Roche) and RNase A (5 $u \cdot mL^{-1}$; Serva Electrophoresis GmbH, Heidelberg, Germany). The extract was removed and designated as the DNase/RNase fraction. After the final step of extraction, the structures were washed three times with KM buffer and the remaining highly insoluble structures were dissolved in KM buffer containing 1% SDS and designated as the SDS fraction. Proteins in the extracted fractions were precipitated by acetone, dissolved in Laemmli buffer and analyzed by SDS/PAGE.

For light microscopy studies, cells were seeded onto coverslips and fractionated as above (the amounts of solutions were adapted accordingly). Structures remaining on the coverslip after each fractionation step were fixed and labeled as described hereafter.

Immunofluorescence staining

Intact cells or cells after *in situ* fractionation growing on the coverslips were washed three times in PBS (Lonza) or KM buffer, respectively. Then, samples were fixed with 3% paraformaldehyde in PBS for 30 min and permeabilized in 0.5% Triton X-100 in PBS for 5 min. After washing in PBS (3 × 10 min), the samples were blocked with 0.25% gelatin and 0.25% bovine serum albumin in PBS for 30 min. Immunostaining with primary and secondary antibodies was carried out for 1 h and 30 min, respectively, with extensive washing in PBS after incubation. Then the coverslips were briefly washed in deionized water, air dried and mounted in DAPI Gold solution (Thermo Fisher Scientific). Samples were observed using an Olympus IX71 microscope (Olympus, Tokyo, Japan) or Leica TCS SP2 AOBS confocal microscope (Leica Microsystems, Wetzlar, Germany).

Electron microscopy (flat embedding)

WOP cells were transfected with pVP1, and 24 h post-transfection (hpt) the first extraction step of *in situ* fractionation was performed. After that, the cells on the coverslips were fixed with 3% formaldehyde, 0.01% glutaraldehyde in 0.2 M Hepes buffer pH 7.4 for 30 min, RT, followed by washing in 0.2 M Hepes buffer, 0.02 M glycine pH 7.4 two times. Then, proteins were immunolabeled using the pre-embedding method. Briefly, samples were blocked for 30 min in 1% normal goat serum (Sigma-Aldrich). Immunostaining with primary and secondary antibodies was carried out for 1 h and 30 min, respectively, with extensive washing in 0.2 M Hepes buffer pH 7.4 after incubation. After immunolabeling, cells on the coverslips were dehydrated with an increasing ethanol series (30%, 50%, 70%, 96%), each for 15 min on ice. Dehydrated cells were infiltrated with an increasing series of LR White resin (London Resin Company, London, UK) in ethanol [100% ethanol: LR White, 2 : 1 (20 min, 4 °C), 1 : 2 (20 min, 4 °C)] followed by incubation in pure resin at 4 °C for 1 h, then overnight with fresh resin and additional 2 h after repeated resin exchange. Polymerization was performed at 4 °C for 48 h. Sections (70 nm thick) were contrasted with a saturated water solution of uranyl acetate for 5 min. Electron micrographs were recorded in a JEM-1011 electron microscope (JEOL, Tokio, Japan) operating at 80 kV.

Western blot analysis

Attached cells were harvested at indicated times post-transfection or post-infection, washed with PBS and resuspended

in ice-cold RIPA buffer (150 mM NaCl, 5 mM EDTA, 50 mM Tris/HCl pH 7.4, 0.05% NP-40, 1% sodium deoxycholate, 1% Triton X-100 and 0.1% SDS) supplemented with a cocktail of protease inhibitors (Roche). Cell lysis was carried out by incubating the cells for 20 min on ice. Cellular debris was removed by centrifugation (20 000 ***g***, 30 min, 4 °C).

Protein samples were resolved by 10% SDS/PAGE [75] and electrotransferred onto Hybond-P membrane (GE Healthcare, Chicago, IL, USA) in cooled blotting buffer (0.3% Tris, 1.44% glycine, 20% methanol) at 2.5 $mA \cdot cm^{-2}$ for 90 min. The membranes were blocked in 5% non-fat milk in PBS for 1 h. Immunostaining with primary and secondary antibodies was carried out for 1 h and 30 min, respectively, with extensive washing in PBS after incubation. Membranes were developed using an enhanced chemiluminescence reagent (Thermo Fisher Scientific) and exposed to X-ray films. When desired, the membrane was re-probed according to [76]. Briefly, the membrane was washed in PBS, incubated in 30% peroxide for 15 min at 37 °C, washed twice in water (15 min each washing), then incubated for 15 min in PBS, 45 min in 5% non-fat milk in PBS, and stained with antibodies. Band intensities were assessed using a densitometer (GS-800; Bio-Rad) and QUANTITY ONE software (Bio-Rad).

Effect of nocodazole on cells expressing VP1

WOP cells were transfected, and 24 hpt they were incubated with 5 μM nocodazole (Merck Millipore, Billerica, MA, USA) for 1 h. Then the cells were fractionated (nocodazole was present in each fractionation buffer) or the drug was washed out with medium. The cells were incubated for 1 h with medium not containing the drug and fractionated. Control cells were maintained similarly to the treated cells but with medium not containing the drug. After each fractionation step, the structures remaining on coverslips were fixed, and VP1 and tubulin were stained by specific antibody.

Role of dynein in binding of VP1 to microtubules

WOP cells were transfected with pVP1, and 24 hpt they were incubated for 1 h with 40 μM ciliobrevin-D (Merck Millipore) and fractionated *in situ*. As an alternative, the cells were cotransfected with VP1 and p50/dynamitin-GFP [77], and 24 hpt they were fractionated *in situ*. To asses VP1 distribution, the protein was stained by specific antibody.

Immunoprecipitation

Infected cells and WOP cells expressing VP1 were lysed 40 h post-infection and 24 hpt, respectively. Cells were incubated in lysis buffer [50 mM Tris/HCl pH 8.0, 250 mM NaCl, 1% NP-40, 0.5% Tween 20, 0.1% SDS and protease inhibitors (Roche)] for 30 min on ice. Cellular debris was removed by centrifugation for 30 min at 20 000 ***g***, 4 °C and supernatant was used for immunoprecipitation. Immunoprecipitation was performed using Dynabeads Protein G (Thermo Fisher Scientific) according to the manufacturer's protocol. Immunocomplexes were resolved by 10% SDS/PAGE, transferred to PVDF membrane, and proteins were detected by specific antibodies.

Effect of 17-AAG on VP1 distribution in the fractions

WOP cells were transfected with pVP1 and immediately after transfection, 17-AAG (Sigma-Aldrich) was added to a concentration of 10 μM. Cells were treated with the drug for 24 h, then fractionated *in situ*. Proteins in the fractions were resolved by 10% SDS/PAGE, transferred to PVDF membrane, and detected by specific antibodies. The amount of protein in each fraction was determined by measurement of band density and expressed as a ratio to the total protein amount (amount of proteins in all fractions). The fold change of protein in each fraction was compared with the mock-treated cells expressing VP1.

Effect of Hsp90 knock-down on VP1 distribution in the fractions

WOP cells were transfected with pVP1 and immediately re-transfected by control siRNA (Silencer Select Negative Control No. 1 siRNA; Thermo Fisher Scientific) or siRNA specific to Hsp90 (s67902; Thermo Fisher Scientific). After 24 h, cells were *in situ* fractionated. To determine the level of Hsp90 down-regulation, 0.1 volumes of each fraction were combined, resolved by 10% SDS/PAGE, transferred to PVDF membrane, and Hsp90 and GAPDH were stained by specific antibodies. The band intensity of each protein was determined using QUANTITY ONE software and normalized to GAPDH levels. The fold change of Hsp90 was compared with mock re-transfected cells expressing VP1. Proteins of each fraction were resolved by 10% SDS/PAGE, transferred to PVDF membrane, and Hsp90 and VP1 were detected by specific antibodies. The amount of Hsp90 or VP1 was determined by measurement of band density and expressed as a ratio to the total protein amount of all fractions. The fold change of protein in each fraction was compared with the transfected cells expressing VP1.

Amount of acetylated α-tubulin in cells expressing VP1

WOP cells were infected with MPyV (MOI = 10 pfu per cell) and lysates were prepared at indicated times post-infection. WOP cells were transfected with pVP1 or pCont and lysed 24 hpt. Lysates were separated by 10% SDS/

PAGE, transferred to PVDF membrane, and proteins were detected by specific antibodies. The band intensity of each protein was determined using QUANTITY ONE software and normalized to GAPDH levels and transfection efficiency. The fold increase of protein was compared with mock-infected or transfected control cells.

Amount of acetylated tubulin in cells with increased levels of VP1

293 and 293T cells were transfected with plasmid pVP1 or pCont, respectively, and lysed 48 hpt. Lysates were resolved by 10% SDS/PAGE, transferred to PVDF membrane, and proteins were detected by specific antibodies. The band intensity of each protein was determined using QUANTITY ONE software and normalized to the GAPDH level and transfection efficiency. The fold increase of protein was compared with mock transfected control cells.

Identification of cellular proteins interacting with VP1

Human embryonic kidney cells 293T were transfected with plasmids pVP1-BE-NT or pVP1-BE-CT and lysed 30 hpt. Cells were washed twice with ice-cold PBS, resuspended in lysis buffer [100 mM Tris/HCl pH 8, 100 mM KCl, 200 μM EDTA, 1.5 mM $MgCl_2$, 1% Triton X-100, cocktail of protease inhibitors (Roche), 700 ng·mL^{-1} pepstatin (Sigma-Aldrich)], and three freeze–thaw cycles were performed to lyse the cells. Lysate was cleared by centrifugation (20 000 ***g***, 20 min, 4 °C) and the supernatant was used for affinity purification.

The clarified lysate (20–30 mg of proteins in 8 mL) was loaded onto a column with 0.5 mL streptavidin agarose (Thermo Fisher Scientific) and incubated for 3 h at 4 °C. Unbound proteins were washed out by 8 mL of binding buffer (100 mM Tris/HCl pH 8, 100 mM KCl, 200 μM EDTA, 1.5 mM $MgCl_2$, 0.1% NP-40, cocktail of protease inhibitors, 700 ng·mL^{-1} pepstatin) and the column was then washed three times with 8 mL of TEV cleavage buffer (10 mM Tris/HCl pH 8, 150 mM NaCl, 500 μM EDTA, 0.1% NP-40). Streptavidin agarose was resuspended in 1 mL of TEV cleavage buffer supplemented with DTT to the final concentration 1 mM and 400 U TEV protease (Thermo Fisher Scientific) and incubated for 22 h at 4 °C. Cleaved proteins were eluted with 3 mL of elution buffer (10 mM Tris/HCl pH 8, 150 mM NaCl, 500 μM EDTA), concentrated by ultra-filtration to the final volume of 20 μL and separated by SDS/PAGE using 4–12% gradient gel (Thermo Fisher Scientific). The most abundant bands were identified by mass spectrometry as described in [78].

Binding of VP1 to the mitotic spindle

WOP cells were transfected, and 6 h after transfection taxol (Sigma-Aldrich) was added to the medium at 10 μM concentration. After 16 h treatment, cells were fixed and VP1, α-tubulin or acetylated α-tubulin was stained with specific antibodies.

Effect of VP1 on the cell cycle

WOP cells were transfected with pwP or pCont. Cells were seeded in decreasing concentration so as not to reach confluence in the eight following days: 1.6×10^6, 1.2×10^6, 6×10^5, 4×10^5, 3.2×10^5, 2.2×10^5 or 1.2×10^5 per 10 cm Petri dish.

From the next day (1 day post-transfection), floating and adherent cells were collected and the number of EGFP-positive cells, number of dead cells and apoptotic cells and amount of DNA in the cells was assessed for 6 days. For analysis of the cell cycle, 1×10^6 cells were resuspended in DMEM containing 8 μg·mL^{-1} Hoechst 33342 dye (Thermo Fisher Scientific), incubated for 40 min at 37 °C, 5% CO_2 and amount of DNA was measured. To measure the number of apoptotic cells, externalization of phosphatidylserine using Annexin V-Cy3 (BioVision, Milpitas, CA, USA) was assessed. Briefly, cells (5×10^5) were stained according to the manufacturer's protocol. Dead cells were stained by DAPI dye (900 ng·mL^{-1}) added to the cells just before measurement.

Samples were analyzed using a BD LSR FORTESSA cytometer (BD Biosciences, San Jose, CA, USA) and data were processed using FLOWJO software (Treestar, San Carlos, CA, USA) with the Dean–Jett–Fox model for cell cycle analysis.

Acknowledgements

We are grateful to Christopher Buck and Beate Sodeik for providing valuable plasmids and to Maxence V. Nachury for the kind gift of TAT KO cells. We wish to thank Kateřina Schwarzerová for the kind gift of acetylated α-tubulin antibody and Šárka Takáčová for assistance in preparation of the manuscript. This work was supported by the European Social Fund and the State Budget of the Czech Republic, Project no. CZ. 1.07/2.3.00/30.0061 (LH), by the Grant Agency of Czech Republic, Projects P302/13-26115S and Project 16-07977S (LH, JF), by project BIOCEV – Biotechnology and Biomedicine Centre of the Academy of Sciences and Charles University (CZ.1.05/1.1.00/02.0109), from the European Regional Development Fund (MF) and by the Charles University in Prague (Project UNCE 204013 (LH) and SVV-2016-260314 (VJ)). Access to the MS facility was enabled by the Operational Program Prague – Competitiveness (project CZ.2.16/3.1.00/24023) and by project LO1509 of the Ministry of Education, Youth and Sports of the Czech Republic (PM). The funders had no role in

study design, data collection and analysis, decision to publish, or preparation of the manuscript.

Author contributions

Conception and design of the experiments: LH, MF, JF. Performance of the experiments: LH, MF. Analysis of the data: LH, MF, JF. Mass spectroscopy: PM. Flow cytometry design and data analysis: VJ. Writing of the paper: LH, JF.

Conflict of interest

The authors have declared that no competing interests exist.

References

1 Barouch DH & Harrison SC (1994) Interactions among the major and minor coat proteins of polyomavirus. *J Virol* **68**, 3982–3989.

2 Chang D, Haynes JI, Brady JN & Consigli RA (1992) Identification of a nuclear localization sequence in the polyomavirus capsid protein VP2. *Virology* **191**, 978–983.

3 Moreland RB & Garcea RL (1991) Characterization of a nuclear localization sequence in the polyomavirus capsid protein VP1. *Virology* **185**, 513–518.

4 Forstova J, Krauzewicz N, Wallace S, Street AJ, Dilworth SM, Beard S & Griffin BE (1993) Cooperation of structural proteins during late events in the life cycle of polyomavirus. *J Virol* **67**, 1405–1413.

5 Huerfano S, Žíla V, Bouřa E, Španielová H, Štokrová J & Forstová J (2010) Minor capsid proteins of mouse polyomavirus are inducers of apoptosis when produced individually but are only moderate contributors to cell death during the late phase of viral infection. *FEBS J* **277**, 1270–1283.

6 Liddington RC, Yan Y, Moulain J, Sahli R, Benjamin TL & Harrison SC (1991) Structure of simian virus 40 at 3.8-A resolution. *Nature* **354**, 278–294.

7 Chang D, Cai X & Consigli RA (1993) Characterization of the DNA binding properties of polyomavirus capsid proteins. *J Virol* **67**, 6327–6331.

8 Cripe TP, Delos SE, Estes PA & Garcea RL (1995) In vivo and in vitro association of hsc70 with polyomavirus capsid proteins. *J Virol* **69**, 7807–7813.

9 Chromy LR, Pipas JM & Garcea RL (2003) Chaperone-mediated in vitro assembly of polyomavirus capsids. *Proc Natl Acad Sci USA* **100**, 10477–10482.

10 Palková Z, Španielová H, Gottifredi V, Hollanderová D, Forstová J & Amati A (2000) The polyomavirus major capsid protein VP1 interacts with the nuclear matrix regulatory protein YY1. *FEBS Lett* **467**, 359–364.

11 Garcia M-I, Perez M, Caruso M, Sthandier O, Ferreira R, Cermola M, Macchia C & Amati P (2000) A mutation in the DE loop of the VP1 protein that prevents polyomavirus transcription and replication. *Virology* **272**, 293–301.

12 Carbone M, Reale A, Di Sauro A, Sthandier O, Garcia MI, Maione R, Caiafa P & Amati P (2006) PARP-1 interaction with VP1 capsid protein regulates polyomavirus early gene expression. *J Mol Biol* **363**, 773–785.

13 Bird G, O'Donnell M, Moroianu J & Garcea RL (2008) Possible role for cellular karyopherins in regulating polyomavirus and papillomavirus capsid assembly. *J Virol* **82**, 9848–9857.

14 Tsai B, Gilbert JM, Stehle T, Lencer W, Benjamin TL & Rapoport TA (2003) Gangliosides are receptors for murine polyoma virus and SV40. *EMBO J* **22**, 4346–4355.

15 Li PP, Itoh N, Watanabe M, Shi Y, Liu P, Yang HJ & Kasamatsu H (2009) Association of Simian virus 40 VP1 with 70-kilodalton heat shock proteins and viral tumor antigens. *J Virol* **83**, 37–46.

16 Staufenbiel M & Deppert W (1984) Preparation of nuclear matrices from cultured cells: subfractionation of nuclei in situ. *J Cell Biol* **98**, 1886–1894.

17 Firestone AJ, Weinger JS, Maldonado M, Barlan K, Langston LD, O'Donnell M, Gelfand VI, Kapoor TM & Chen JK (2012) Small-molecule inhibitors of the AAA+ ATPase motor cytoplasmic dynein. *Nature* **484**, 125–129.

18 Giustiniani J, Daire V, Cantaloube I, Durand G, Poüs C, Perdiz D & Baillet A (2009) Tubulin acetylation favors Hsp90 recruitment to microtubules and stimulates the signaling function of the Hsp90 clients Akt/PKB and p53. *Cell Signal* **21**, 529–539.

19 Schulte TW & Neckers LM (1998) The benzoquinone ansamycin 17-allylamino-17-demethoxygeldanamycin binds to HSP90 and shares important biologic activities with geldanamycin. *Cancer Chemother Pharmacol* **42**, 273–279.

20 Akella JS, Wloga D, Kim J, Starostina NG, Lyons-Abbott S, Morrissette NS, Dougan ST, Kipreos ET & Gaertig J (2010) MEC-17 is an alpha-tubulin acetyltransferase. *Nature* **467**, 218–222.

21 Shida T, Cueva JG, Xu Z, Goodman MB & Nachury MV (2010) The major alpha-tubulin K40 acetyltransferase alphaTAT1 promotes rapid ciliogenesis and efficient mechanosensation. *Proc Natl Acad Sci USA* **107**, 21517–21522.

22 Kalebic N, Sorrentino S, Perlas E, Bolasco G, Martinez C & Heppenstall PA (2013) αTAT1 is the major α-tubulin acetyltransferase in mice. *Nat Commun* **4**, 1962.

23 Aguilar A, Becker L, Tedeschi T, Heller S, Iomini C & Nachury MV (2014) A-tubulin K40 acetylation is

required for contact inhibition of proliferation and cell-substrate adhesion. *Mol Biol Cell* **25**, 1854–1866.
24 Webster DR & Borisy GG (1989) Microtubules are acetylated in domains that turn over slowly. *J Cell Sci* **92**, 57–65.
25 Huerfano S, Ryabchenko B & Forstová J (2013) Nucleofection of expression vectors induces a robust interferon response and inhibition of cell proliferation. *DNA Cell Biol* **32**, 467–479.
26 Boni S, Lavergne JP, Boulant S & Cahour A (2005) Hepatitis C virus core protein acts as a trans-modulating factor on internal translation initiation of the viral RNA. *J Biol Chem* **280**, 17737–17748.
27 Wang T, Yu B, Lin L, Zhai X, Han Y, Qin Y, Guo Z, Wu S, Zhong X, Wang Y *et al.* (2012) A functional nuclear localization sequence in the VP1 capsid protein of coxsackievirus B3. *Virology* **433**, 513–521.
28 Guo YH, Li YN, Zhao JR, Zhang J & Yan Z (2011) HBc binds to the CpG islands of HBV cccDNA and promotes an epigenetic permissive state. *Epigenetics* **6**, 720–726.
29 Shishido-Hara Y, Ichinose S, Higuchi K, Hara Y & Yasuj K (2004) Major and minor capsid proteins of human polyomavirus JC cooperatively accumulate to nuclear domain 10 for assembly into virions. *J Virol* **78**, 9890–9903.
30 Stamatos NM, Chakrabarti S, Moss B & Hare JD (1987) Expression of polyomavirus virion proteins by a vaccinia virus vector: association of VP1 and VP2 with the nuclear framework. *J Virol* **61**, 516–525.
31 Cai X, Chang D, Rottinghaus S & Consigli RA (1994) Expression and purification of recombinant polyomavirus VP2 protein and its interactions with polyomavirus proteins. *J Virol* **68**, 7609–7613.
32 Ishii N, Nakanishi A, Yamada M, Macalalad MH & Kasamatsu H (1994) Functional complementation of nuclear targeting-defective mutants of simian virus 40 structural proteins. *J Virol* **68**, 8209–8216.
33 Mannová P, Liebl D, Krauzewicz N, Fejtová A, Štokrová J, Palková Z, Griffin BE & Forstová J (2002) Analysis of mouse polyomavirus mutants with lesions in the minor capsid proteins. *J Gen Virol* **83**, 2309–2319.
34 Zuehlke AD, Beebe K, Neckers L & Prince T (2015) Regulation and function of the human *HSP90AA1* gene. *Gene* **570**, 8–16.
35 Geller R, Taguwa S & Frydman J (2012) Broad action of Hsp90 as a host chaperone required for viral replication. *Biochim Biophys Acta* **1823**, 698–706.
36 Fostinis Y, Theodoropoulos PA, Gravanis A & Stournaras C (1992) Heat shock protein HSP90 and its association with the cytoskeleton: a morphological study. *Biochem Cell Biol* **70**, 779–786.
37 Echeverria PC & Picard D (2010) Molecular chaperones, essential partners of steroid hormone receptors for activity and mobility. *Biochim Biophys Acta* **1803**, 641–649.
38 Zhong M, Zheng K, Chen M, Xiang Y, Jin F, Ma K, Qiu X, Wang Q, Peng T, Kitazato K *et al.* (2014) Heat-shock protein 90 promotes nuclear transport of herpes simplex virus 1 capsid protein by interacting with acetylated tubulin. *PLoS One* **9**, e99425.
39 Dasgupta D, Rajgopalan R & Gurnani S (1983) Involvement of colchicine binding site of tubulin in the polymerisation process. *FEBS Lett* **152**, 101–104.
40 Black MM & Keyser P (1987) Acetylation of alpha-tubulin in cultured neurons and the induction of alpha-tubulin acetylation in PC12 cells by treatment with nerve growth factor. *J Neurosci* **7**, 1833–1842.
41 Cueva JG, Hsin J, Huang KC & Goodman MB (2012) Posttranslational acetylation of α-tubulin constrains protofilament number in native microtubules. *Curr Biol* **22**, 1066–1074.
42 Cambray-Deakin MA & Burgoyne RD (1987) Posttranslational modifications of alpha-tubulin: acetylated and detyrosinated forms in axons of rat cerebellum. *J Cell Biol* **104**, 1569–1574.
43 Belmadani S, Poüs C, Fischmeister R & Méry PF (2004) Post-translational modifications of tubulin and microtubule stability in adult rat ventricular myocytes and immortalized HL-1 cardiomyocytes. *Mol Cell Biochem* **258**, 35–48.
44 Huber F, Boire A, López MP & Koenderink GH (2015) Cytoskeletal crosstalk: when three different personalities team up. *Curr Opin Cell Biol* **32**, 39–47.
45 Rathje LS, Nordgren N, Pettersson T, Rönnlund D, Widengren J, Aspenström P & Gad AK (2014) Oncogenes induce a vimentin filament collapse mediated by HDAC6 that is linked to cell stiffness. *Proc Natl Acad Sci USA* **111**, 1515–1520.
46 Knight LM, Stakaityte G, Wood JJ, Abdul-Sada H, Griffiths DA, Howell GJ, Wheat R, Blair GE, Steven NM, Macdonald A *et al.* (2015) Merkel cell polyomavirus small T antigen mediates microtubule destabilization to promote cell motility and migration. *J Virol* **89**, 35–47.
47 Da Costa SR, Wang Y, Vilalta PM, Schönthal AH & Hamm-Alvarez SF (2000) Changes in cytoskeletal organization in polyoma middle T antigen-transformed fibroblasts: involvement of protein phosphatase 2A and src tyrosine kinases. *Cell Motil Cytoskeleton* **47**, 253–268.
48 Valenzuela-Fernández A, Alvarez S, Gordon-Alonso M, Barrero M, Ursa A, Cabrero JR, Fernández G, Naranjo-Suárez S, Yáñez-Mo M, Serrador JM *et al.* (2005) Histone deacetylase 6 regulates human immunodeficiency virus type 1 infection. *Mol Biol Cell* **16**, 5445–5454.

49 Husain M & Harrod KS (2011) Enhanced acetylation of alpha-tubulin in influenza A virus infected epithelial cells. *FEBS Lett* **585**, 128–132.

50 Elliott G & O'Hare P (1998) Herpes simplex virus type 1 tegument protein VP22 induces the stabilization and hyperacetylation of microtubules. *J Virol* **72**, 6448–6455.

51 Kotsakis A, Pomeranz LE, Blouin A & Blaho JA (2001) Microtubule reorganization during herpes simplex virus type 1 infection facilitates the nuclear localization of VP22, a major virion tegument protein. *J Virol* **75**, 8697–8711.

52 Husain M & Cheung CY (2014) Histone deacetylase 6 inhibits influenza A virus release by downregulating the trafficking of viral components to the plasma membrane via its substrate, acetylated microtubules. *J Virol* **88**, 11229–11239.

53 Dompierre JP, Godin JD, Charrin BC, Cordelières FP, King SJ, Humbert S & Saudou F (2007) Histone deacetylase 6 inhibition compensates for the transport deficit in Huntington's disease by increasing tubulin acetylation. *J Neurosci* **27**, 3571–3583.

54 Hubbert C, Guardiola A, Shao R, Kawaguchi Y, Ito A, Nixon A, Yoshida M, Wang XF & Yao TP (2002) HDAC6 is a microtubule-associated deacetylase. *Nature* **417**, 455–458.

55 Aldana-Masangkay GI & Sakamoto KM (2011) The role of HDAC6 in cancer. *J Biomed Biotechnol* **2011**, 875824, doi: 10.1155/2011/875824.

56 Husain M & Harrod KS (2009) Influenza A virus-induced caspase-3 cleaves the histone deacetylase 6 in infected epithelial cells. *FEBS Lett* **583**, 2517–2520.

57 Palková Z, Adamec T, Liebl D, Stokrová J & Forstová J (2000) Production of polyomavirus structural protein VP1 in yeast cells and its interaction with cell structures. *FEBS Lett* **478**, 281–289.

58 Talmage DA, Freund R, Dubensky T, Salcedo M, Gariglio P, Rangel LM, Dawe CJ & Benjamin TL (1992) Heterogeneity in state and expression of viral DNA in polyoma virus-induced tumors of the mouse. *Virology* **187**, 734–747.

59 Holländerová D, Raslová H, Blangy D, Forstová J & Berebbi M (2003) Interference of mouse polyomavirus with the c-myc gene and its product in mouse mammary adenocarcinomas. *Int J Oncol* **23**, 333–341.

60 Spink KM & Fluck MM (2003) Polyomavirus hr-t mutant-specific induction of a G2/M cell-cycle arrest that is not overcome by the expression of middle T and/or small T. *Virology* **307**, 191–203.

61 Varberg JM, Padgett LR, Arrizabalaga G & Sullivan WJ Jr (2016) TgATAT-mediated α-tubulin acetylation is required for division of the protozoan parasite *Toxoplasma gondii*. *mSphere* **1**. pii: e00088-15. doi: 10.1128/mSphere.00088-15.

62 Patel H, Stavrou I, Shrestha RL, Draviam V, Frame MC & Brunton VG (2016) Kindlin1 regulates microtubule function to ensure normal mitosis. *J Mol Cell Biol* **8**, 338–348.

63 Schlegel R & Benjamin TL (1978) Cellular alterations dependent upon the polyoma virus Hr-t function: separation of mitogenic from transforming capacities. *Cell* **14**, 587–599.

64 Lehman JM, Laffin J & Friedrich TD (1994) DNA content distribution of mouse cells following infection with polyoma virus. *Cytometry* **16**, 138–143.

65 Chen L & Fluck M (2001) Kinetic analysis of the steps of the polyomavirus lytic cycle. *J Virol* **75**, 8368–8379.

66 Dahl J, You J & Benjamin TL (2005) Induction and utilization of an ATM signaling pathway by polyomavirus. *J Virol* **79**, 13007–13017.

67 Pores Fernando AT, Andrabi S, Cizmecioglu O, Zhu C, Livingston DM, Higgins JM, Schaffhausen BS & Roberts TM (2015) Polyoma small T antigen triggers cell death via mitotic catastrophe. *Oncogene* **34**, 2483–2492.

68 Dailey L & Basilico C (1985) Sequences in the polyomavirus DNA regulatory region involved in viral DNA replication and early gene expression. *J Virol* **54**, 739–749.

69 Horníková L, Žíla V, Španielová H & Forstová J (2015) Mouse polyomavirus: propagation, purification, quantification, and storage. *Curr Protoc Microbiol* **38**, 14F.1.1–14F.1.26.

70 Tolstov YL, Pastrana DV, Feng H, Becker JC, Jenkins FJ, Moschos S, Chang Y, Buck CB & Moore PS (2009) Human Merkel cell polyomavirus infection II. MCV is a common human infection that can be detected by conformational capsid epitope immunoassays. *Int J Cancer* **125**, 1250–1256.

71 Horníková L, Man P & Forstová J (2011) Blue native protein electrophoresis for studies of mouse polyomavirus morphogenesis and interactions between the major capsid protein VP1 and cellular proteins. *J Virol Methods* **178**, 229–234.

72 Buck CB, Day PM, Thompson CD, Lubkowski J, Lu W, Lowy DR & Schiller JT (2006) Human alpha-defensins block papillomavirus infection. *Proc Natl Acad Sci USA* **103**, 1516–1521.

73 Krauzewicz N, Streuli CH, Stuart-Smith N, Jones MD, Wallace S & Griffin BE (1990) Myristylated polyomavirus VP2: role in the life cycle of the virus. *J Virol* **64**, 4414–4420.

74 Schreiber E, Matthias P, Müller MM & Schaffner W (1989) Rapid detection of octamer binding proteins with 'mini-extracts', prepared from a small number of cells. *Nucleic Acids Res* **17**, 6419.

75 Laemmli UK (1970) Cleavage of structural proteins during the assembly of the head of bacteriophage T4. *Nature* **227**, 680–685.
76 Sennepin AD, Charpentier S, Normand T, Sarré C, Legrand A & Mollet LM (2009) Multiple reprobing of western blots after inactivation of peroxidase activity by its substrate, hydrogen peroxide. *Anal Biochem* **393**, 129–131.
77 Dohner K, Wolfstein A, Prank U, Echeverri C, Dujardin D, Vallee R & Sodeik B (2002) Function of dynein and dynactin in herpes simplex virus capsid transport. *Mol Biol Cell* **13**, 2795–2809.
78 Mrázek H, Benada O, Man P, Vaněk O, Křen V, Bezouška K & Weignerová L (2012) Facile production of *Aspergillus niger* α-N-acetylgalactosaminidase in yeast. *Protein Expr Purif* **81**, 106–114.

Supporting information

Additional Supporting Information may be found online in the supporting information tab for this article:
Fig. S1. FACS analysis of VP1 expressing cells (cell death, apoptosis and cell cycle).
Table S1. Plasmids used in this study.
Table S2. List of primers.

ACS APPLIED MATERIALS & INTERFACES

Research Article

www.acsami.org

Antibacterial, Antiviral, and Oxygen-Sensing Nanoparticles Prepared from Electrospun Materials

Petr Henke,[†] Kaplan Kirakci,[‡] Pavel Kubát,[§] Martin Fraiberk,[†] Jitka Forstová,[†] and Jiří Mosinger*[,†,‡]

[†]Faculty of Science, Charles University in Prague, Hlavova 2030, 128 43 Prague 2, Czech Republic

[‡]Institute of Inorganic Chemistry, v.v.i., Academy of Sciences of the Czech Republic, 250 68 Řež, Czech Republic

[§]J. Heyrovský Institute of Physical Chemistry, v.v.i., Czech Academy of Sciences, Dolejškova 3, 182 23 Praha 8, Czech Republic

Supporting Information

ABSTRACT: A simple nanoprecipitation method was used for preparation of stable photoactive polystyrene nanoparticles (NPs, diameter 30 ± 10 nm) from sulfonated electrospun polystyrene nanofiber membranes with encapsulated 5,10,15,20-tetraphenylporphyrin (TPP) or platinum octaethylporphyrin (Pt-OEP). The NPs prepared with TPP have strong antibacterial and antiviral properties and can be applied to the photooxidation of external substrates based on photogenerated singlet oxygen. In contrast to nanofiber membranes, which have limited photooxidation ability near the surface, NPs are able to travel toward target species/structures. NPs with Pt-OEP were used for oxygen sensing in aqueous media, and they presented strong linear responses to a broad range of oxygen concentrations. The nanofiber membranes can be applied not only as a source of NPs but also as an effective filter for their removal from solution.

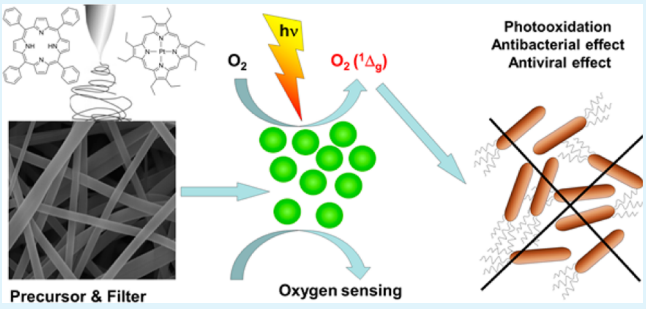

KEYWORDS: *nanoparticles, nanofiber, singlet oxygen, antibacterial, antiviral, oxygen-sensing*

INTRODUCTION

Functional nanoscopic materials with antibacterial and antiviral properties are attracting increasing interest for medicinal[1] and water treatment[2] applications. Among such materials, those based on photogeneration of the short-lived and highly oxidative singlet oxygen, $O_2(^1\Delta_g)$, are the most attractive.[3−5]

Excitation of photosensitizers (typically porphyrins or phthalocyanines) encapsulated in electrospun nanofiber membranes by visible light leads to the formation of $O_2(^1\Delta_g)$, which can efficiently kill bacteria[6−8] and viruses[9] (Figure S1). The membranes are characterized by high surface area, transparency to light, high oxygen diffusion coefficient, and nanoporous structure,[10] which prevent the passage of bacteria and other pathogens through the nanofiber membranes because they are detained on the surface.[11] The main drawbacks of these polymeric nanofiber membranes with encapsulated photosensitizers are the short lifetime ($\tau_\Delta \approx 3.5$ μs in aqueous solution)[12] and the diffusion length of $O_2(^1\Delta_g)$ (typically tens to hundreds of nanometers),[13] which limit efficient photooxidation to chemical/biological targets in close proximity to nanofiber surfaces.[8]

This limitation can be overcome by increasing the wettability of the electrospun nanofiber surface by postprocessing modification,[14] binding of a photosensitizer directly to the surface,[11,15] or photogeneration of long-lived antibacterial species, such as nitric oxide,[16] hydrogen peroxide,[7] and triiodide.[15] In this respect, polymeric nanoparticles (NPs) are advantageous due to size effects, which can overcome the singlet oxygen diffusion limitations. Antibacterial NPs are considered an alternative to antibiotics and have strong potential to solve the problem of bacterial multidrug resistance.[17] Among the variety of nanocarriers useful for biological applications, polystyrene NPs have high efficiencies due to their biocompatibility, good uptake properties, low toxicity, permeability to oxygen, and slow excretion.[18]

In this paper, we describe the fabrication and properties of polystyrene NPs with high antimicrobial activity and smaller environmental impact than the commonly used silver NPs.[19,20] Polystyrene NPs were prepared by simple nanoprecipitation from pristine electrospun nanofiber membranes with encapsulated photosensitizers. The encapsulation of 5,10,15,20-tetraphenylporphyrin (TPP) allows photogeneration of $O_2(^1\Delta_g)$ with high efficiency.[21] Alternatively, the encapsulation of platinum octaethylporphyrin (Pt-OEP) provides NPs for oxygen sensing.[22]

The resulting NPs have a negatively charged surface due to extensive sulfonation, which prevents aggregation in aqueous environments and allows the travel and release of $O_2(^1\Delta_g)$ in close proximity to chemical/biological targets. The polystyrene core is transparent to visible light and has a high oxygen

Received: July 6, 2016
Accepted: September 2, 2016
Published: September 2, 2016

DOI: 10.1021/acsami.6b08234
ACS Appl. Mater. Interfaces 2016, 8, 25127−25136

diffusion coefficient,[7] and the oxygen concentration can be easily monitored by luminescence of the encapsulated Pt-OEP. An important feature, with possible high impact in nanotechnology, is the fact that nanofiber membranes can be used as an efficient filter for bacteria and prepared NPs.

EXPERIMENTAL SECTION

Chemicals. 5,10,15,20-Tetraphenylporphyrin (TPP), 5,10,15,20-tetrakis(4-sulfonatophenyl)porphyrin (TPPS), platinum(II) 2,3,7,8,12,13,17,18-octaethyl-21*H*,23*H*-porphyrin (Pt-OEP), uric acid, cyclohexanone, dimethylacetamide (DMAc), toluene, tetraethylammonium bromide (TEAB), TNM-FH medium, Dulbecco's modified Eagle's medium (DMEM), gelatin, bovine serum albumin, ampicillin sodium, 4′,6-diamidine-2′-phenylindole dihydrochloride (DAPI), paraformaldehyde, sulfuric acid, KI, and other inorganic salts were purchased from Sigma−Aldrich and were used as received. Fetal calf serum (FCS) and glutamine were obtained from ThermoFisher Scientific (Gibco). Triton X-100 was purchased from Serva Electrophoresis GmbH. Luria−Bertani (LB) agar and LB medium (Lennox) were purchased from Carl Roth GmbH & Co. Phosphate-buffered saline solution (PBS) was purchased from Lonza Biotec. Sodium tetraborate, hydrochloric acid, and sodium hydroxide were purchased from Lach-Ner, s.r.o. Krasten 137 polystyrene and Tecophilic polyurethane were purchased from Synthos Kralupy a.s. and from Lubrizol Advanced Materials. Tetrahydrofuran (THF, HPLC-grade) was dried with a PureSolv MD5 solvent purification system (Innovative Technology).

Antibodies. Primary antibodies were a mouse monoclonal antibody against the mouse polyomavirus VP1 protein[23] and a rat monoclonal antibody against the mouse polyomavirus large T (LT) antigen.[24] Alexa Fluor 488 (green) conjugated with goat anti-mouse or donkey anti-rat immunoglobulin antibody (ThermoFisher Scientific) was used as a secondary antibody.

Viruses and Cells. *Spodoptera frugiperda* cells (Sf9; Invitrogen) were cultured as a monolayer at 27 °C in TNM-FH medium containing 10% FCS, as described by Hink.[25] The recombinant baculovirus pVLVP1, carrying the mouse polyomavirus VP1 gene driven by a polyhedrin promoter, was used to infect insect cells.[23] Swiss Albino mouse 3T6 fibroblasts (ATCC CCL-96) were grown at 37 °C in a 5% CO_2 humidified incubator and were supplemented with 2 mM glutamine and 10% FCS. Mouse polyomavirus (strain A2) was propagated for 7 days in 3T6 fibroblasts [0.05 plaque-forming unit (PFU)/cell]. Virions were purified as previously described.[26]

Electrospinning. A mixture of 0.07 wt % TEAB and 99.93 wt % polystyrene (PS) was dissolved in cyclohexanone to prepare a 17% solution for the fabrication of polystyrene nanofiber material. Similarly, a mixture of 0.07 wt % TEAB, 98.93 wt % PS, and 1 wt % TPP or 0.5% Pt-OEP in cyclohexanone was used for fabrication of polystyrene nanofiber material with 1% TPP or 0.5% Pt-OEP. For fabrication of polyurethane nanofiber material, the polymer solution contained 8% (w/w) Tecophilic polyurethane [thermoplastic elastomer consisting of segmented block copolymers synthesized from 4,4′-diisocyanatodicyclohexylmethane, 1,4-butanediol, and poly(ethylene glycol)] in DMAc/toluene, 2:1 (w/w). The conductivity of the solution was enhanced by TEAB (0.12 g/kg). All nanofiber membranes were produced via the modified Nanospider electrospinning industrial technology[27] by simultaneous formation of charged liquid jets on the surface of a thin wire electrode, where the number and location of the jets was set to their optimal positions (Figure S2).[28] The nanofiber diameters were measured by NIS Elements 4.0 image analysis software (Laboratory Imaging).

Preparation of Nanoparticles. Electrospun polystyrene nanofiber membranes (250 cm^2, 150 mg) fixed on quartz substrates were treated by immersion in 96% sulfuric acid[29] at room temperature for 54 h. In special cases, to observe the effect of sulfonation time, the membranes were not treated with sulfuric acid or were treated for a limited time (2, 6, 24, or 36 h). The materials were washed with deionized water until a neutral pH was reached and were then stored in water. Typically, a wet, sulfonated nanofiber membrane was immersed in 16 mL of dry THF for 60 s with stirring, and then deionized water (80 mL) was added. THF was removed by evaporation under vacuum. The resulting dispersion of NPs in water was centrifuged for 10 min at 4700*g* to remove microparticles and was dialyzed by use of Float-A-Lyzer G2 with a molecular weight cutoff of 50 000 for 18 h in deionized water at room temperature to remove traces of sulfuric acid and THF.

Gravimetric Analysis. Twenty-milliliter samples of NPs were dried at 50 °C to a constant weight. The weight was determined on a precision weighing balance GR-200 (A&D Instruments Ltd.).

Ion Exchange Capacity. The ion-exchange capacity (IEC) of sulfonated NPs was determined by titration. Approximately 20 mL ($\sim 1.2 \times 10^{14}$ NPs/mL) of dialyzed NPs was treated with 10 mL of 0.2 M NaOH solution for 1 h to completely replace the H^+ with Na^+. The remaining NaOH was titrated potentiometrically with 0.1 M HCl. The concentration of HCl was determined by use of a primary standard of sodium tetraborate. The IECs were related to the mass of the dried NPs.

Dynamic Light Scattering. Particle size and size distributions in water were determined by dynamic light scattering (DLS) on a Zetasizer Nano ZS particle-size analyzer from Malvern.

Scanning Electron Microscopy. Nanofiber and NP morphology was studied with a scanning electron Quanta 200 field emission gun (FEG) microscope (SEM; FEI).

UV/Vis Absorption and Fluorescence Spectroscopy. UV/vis absorption spectra were recorded on Unicam 340 and Varian 4000 spectrometers. Steady-state fluorescence spectra were monitored on an FLS 980 (Edinburgh Instruments) spectrofluorometer.

Dissolved Oxygen Sensing. An FLS 980 (Edinburgh Instruments) spectrofluorometer with a flow-through luminescence cell equipped with an InPro 6880i oxygen sensor (Mettler Toledo), magnetic stirring, and connections to nitrogen and oxygen gas bottles was used to measure the luminescence response of NPs with encapsulated Pt-OEP (**2**@PS-SO_3) to dissolved oxygen in water. The cell contained 40 mL of **2**@PS-SO_3 (concentration $\sim 1.2 \times 10^{13}$ NPs/mL) in water. Different dissolved oxygen contents were maintained by bubbling by nitrogen or oxygen.

Laser Flash Photolysis Experiments. Laser flash photolysis experiments were performed with a Lambda Physik FL 3002 dye laser (wavelength 425 nm, pulse width 28 ns) on a LKS 20 laser kinetic spectrometer (Applied Photophysics). Kinetics of the TPP triplet states were measured by their transient absorption at 460 nm by use of a 150 W Xe lamp and a R928 photomultiplier (Hamamatsu). Rate constants k_{O_2} for quenching of the triplet states by oxygen were calculated from the linear Stern−Volmer equation: $1/\tau_T = 1/\tau_T^{Ar} + k_{O_2}[O_2]$, where τ_T is the lifetime of triplet states in oxygen-, air-, or argon-saturated D_2O. The average lifetime from double-exponential decay, τ_T^{av}, and the fraction of porphyrin triplets trapped by oxygen in air-saturated D_2O, $F_T^{O_2}$, were calculated respectively as $\tau_T^{av} = (a_1\tau_{T1} + a_1\tau_{T1})/(a_1 + a_2)$ and $F_T^{O_2} = (\tau_T^{Ar} - \tau_T^{air})/\tau_T^{Ar}$. The concentration of molecular oxygen, $[O_2]$, was 0.28 mM in air-saturated water at 20 °C.

Singlet Oxygen Luminescence. The samples were excited by a Lambda Physik Compex 100 (λ_{exc} = 308 nm) or FL3002 dye laser (λ_{exc} = 421 nm). The luminescence spectra of singlet oxygen, $O_2(^1\Delta_g)$, formed after irradiation of nanofiber material with TPP were published previously.[11,13] The kinetics of $O_2(^1\Delta_g)$ luminescence was monitored by use of a Judson Ge diode (Judson J16-8SP-R05M-HS) after being selected by a 1270 nm band-pass filter (Laser Components, Olching, Germany). The signal from the detector was averaged and collected by a 600 MHz oscilloscope (Agilent Infiniium). The rising part of the signals can fail due to scattered light/prompt fluorescence of TPP and saturation of the detector. The luminescence profiles of $O_2(^1\Delta_g)$ were calculated as the difference between signals in air-/oxygen- and argon-saturated D_2O [no generation of $O_2(^1\Delta_g)$]. Individual traces were fitted to a single-exponential decay function $I = I_0 \exp(-t/\tau_\Delta)$, where τ_Δ is the lifetime of $O_2(^1\Delta_g)$ and I and I_0 denote luminescence intensity of $O_2(^1\Delta_g)$ at time t and after excitation ($t = 0$), respectively. The initial portion of the plot, which was affected by formation of $O_2(^1\Delta_g)$ from the TPP triplets, was excluded. This approximation is

DOI: 10.1021/acsami.6b08234
ACS Appl. Mater. Interfaces 2016, 8, 25127−25136

valid for $\tau_\Delta \gg \tau_T$. Details of the measurements can be found in our previous papers.[3,11,13]

Photooxidation of External Substrates. A suspension of NPs with or without encapsulated TPP (~6.0×10^{13} NPs/mL) was placed in a thermostated 10 mm quartz cell (22 °C) that contained 2×10^{-4} M uric acid in 0.02 M phosphate buffer (pH = 7.0) or a 0.1 M iodide detection solution. The cell was irradiated with visible light by use of a stabilized xenon lamp (500 W, Newport) with a long-pass filter ($\lambda \geq$ 400 nm, Newport). UV/vis absorbance changes at 292 nm (attributed to photodegradation of uric acid)[30] and at 287 or 351 nm (attributed to formation of I_3^- in the iodide test)[31] were recorded at regular intervals and compared to a blank solution of the same composition that was stored in the dark.

Antibacterial Tests. A culture of *Escherichia coli* DH5α (Invitrogen, CA) with plasmid pGEM11Z (Promega, WI) was incubated at 37 °C with stirring in LB medium after addition of ampicillin. Incubation was terminated when the absorbance at 560 nm reached approximately 1. The prepared culture was diluted 10 000× to the desired concentration in PBS. NPs from stock suspensions (1.2×10^{14} NPs/mL) with or without encapsulated TPP were mixed with diluted culture in a ratio of 1:1. Two milliliters of this suspension was placed in a thermostated 10 mm quartz cell (25 °C). The cell was irradiated while stirring with visible light produced by a stabilized xenon lamp (500 W, Newport) with a long-pass filter (λ > 400 nm, Newport). At regular time intervals, 150 μL of the irradiated suspension was placed on an agar plate. The plates were incubated for 20 h in darkness at 37 °C to allow the individual bacteria to grow and form colonies.

Antiviral Tests. Nonenveloped mouse polyomavirus (MPyV), propagated in mouse 3T6 fibroblasts, and enveloped recombinant baculovirus pVL-VP1 expressing MPyV VP1 gene, propagated in Sf9 cells, were used for testing the antiviral effect of the NPs.

MPyV stock (100 μL; 5×10^8 virus particles) or pVL-VP1 baculovirus stock (100 μL; 2×10^6 infectious particles) was mixed with 5 μL of stock suspension of NPs (~1.2×10^{14} NPs/mL) with encapsulated TPP (**1**@PS-SO_3) or without TPP (@PS-SO_3). The resulting mixtures in Eppendorf tubes were either placed on ice and exposed to visible light (xenon lamp, 300 W, Kaiser) from 30 cm distance for 30 min or kept in the dark. The samples were then used for infection of cells growing on coverslips placed in 24-well dishes.

3T6 fibroblasts were grown at 37 °C overnight. Adsorption of MPyV to the surface of the 3T6 cells was performed by incubating the virus/NP mixtures (100 μL) and cells together for 1 h at 37 °C. Then 1 mL of prewarmed DMEM with 10% fetal calf serum (FCS) was added to each well, and the cells were grown at 37 °C in 5% CO_2 for 24 h and were finally fixed.

Sf9 cells (1.5×10^5) were seeded and incubated for 1 h at 27 °C in serum-free TNM-FH medium. Adsorption of the baculovirus to the surface of the Sf9 cells was performed by incubating the virus mixture and cells together for 1 h at room temperature. Then 1 mL of prewarmed TNM-FH medium with 10% FCS was added to each well, and the cells were grown at 27 °C for 42 h before fixing. Virus and NP mixtures were added to the host cells before incubating (until the fixation step) in the dark.

Fixation of cells was performed by a 30 min incubation with 3% formaldehyde (freshly made from paraformaldehyde), followed by incubation with 0.5% Triton X-100 for 5 min at room temperature. Nonspecific antibody binding sites were blocked via a 30 min incubation in PBS buffer containing 0.25% gelatin and 0.25% bovine serum albumin. Then the cells were incubated for 30 min with virus-specific antibodies, directed either against the MPyV large T (LT) antigen[24] (for detection of MPyV infectivity in 3T6 fibroblasts) or against the VP1 protein produced by recombinant baculovirus[23] (for detection of baculovirus infection in Sf9 cells). Unbound antibodies were removed by washing with PBS (3 × 10 min), and the cells were then incubated for 30 min with secondary antibody directed against rat or mouse immunoglobulin and conjugated with Alexa Fluor 488. The cells were finally washed with PBS buffer (3 × 10 min), and coverslips were mounted with glycerol containing DAPI. Infected cells were visualized by fluorescence microscopy (Olympus BX60) and counted.

3. RESULTS AND DISCUSSION

Preparation of Nanofiber Membranes and Nanoparticles. New top-down technology was used for the preparation of stable polystyrene NPs from electrospun nanofiber membranes. Membranes were fabricated by the industrial electrospinning method (see Experimental Section and Figure S2), and they served as a precursor for preparation of NPs (free or with encapsulated photoactive porphyrins) after extensive sulfonation by a nanoprecipitation method (Figure 1). The nanofiber character of the pristine polymer ensures

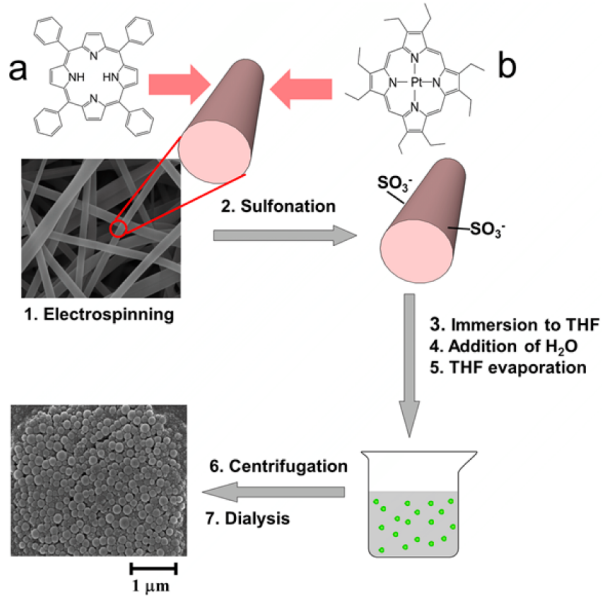

Figure 1. Scheme of NP preparation by nanoprecipitation and structures of encapsulated (a) TPP and (b) Pt-OEP photosensitizers.

extensive sulfonation not only on the surface of thin nanofibers but in the whole volume of the material. Long-term sulfonation (54 h) yielded NPs with an average IEC of NPs ~2.6×10^{-3} mol/g (see Experimental Section and Table S1). A similar value (~4.0×10^{-3} mol/g) of IEC was found on polystyrene nanofiber membranes after fast chlorosulfonation, but chlorosulfonation cannot be applied because it yields insoluble cross-linked membranes.[11]

Extensive sulfonation is necessary to hinder the aggregation of NPs due to repulsive Coulombic forces. In contrast to a similar method we described recently,[32] the photoactive compounds were homogeneously encapsulated in the polystyrene matrix prior to nanoprecipitation, during the electrospinning, which enabled preliminary spectral and photoactivity control of the photoactive material before the next nanoprecipitation. The method is suitable for hydrophobic compounds that are shielded by the polystyrene shell from the surroundings, which efficiently prevents leakage of the encapsulated compounds into the aqueous media.

Two types of NPs with different functionality were prepared: sulfonated NPs with encapsulated 1% TPP photosensitizer (**1**@PS-SO_3) and sulfonated NPs with encapsulated 0.5% Pt-OEP oxygen sensor (**2**@PS-SO_3). NPs without encapsulated porphyrin (@PS-SO_3) were also prepared as a control. On the basis of gravimetric analysis of NPs with encapsulated porphyrins, the average concentration of the prepared NPs (stock suspension) was ~1.2×10^{14} NPs/mL (Table S1).

DOI: 10.1021/acsami.6b08234
ACS Appl. Mater. Interfaces 2016, 8, 25127−25136

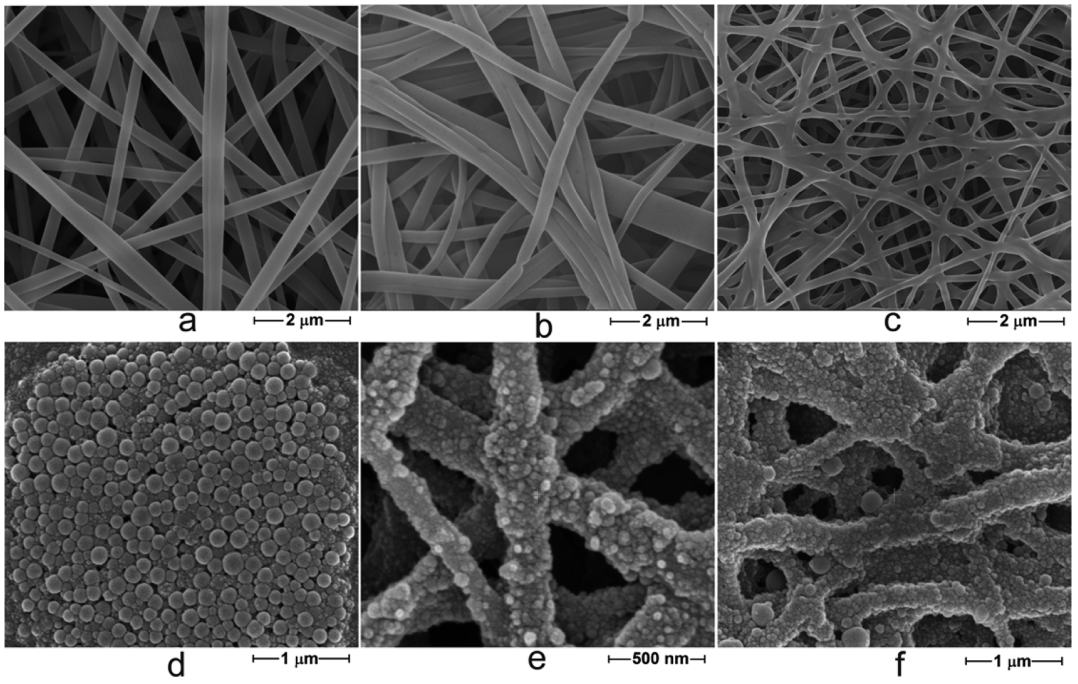

Figure 2. SEM micrographs: pristine polystyrene nanofiber membrane for the preparation of NPs (a) before and (b) after 54 h of sulfonation. (c) Polyurethane (Tecophilic) nanofiber membrane as a filter. Suspensions of (d) **1**@PS-SO_3 and (e, f) **1**@PS-SO_3 on the surface of a polyurethane nanofiber membrane.

Table 1. Influence of Sulfonation Time during Preparation, Aging Time, and Addition of NaCl on Average Diameter of Nanoparticles[a]

avg hydrodynamic diameter (nm)				after 54 h of sulfonation	
sulfonation time (h)	without NaCl	0.1 M NaCl	0.5 M NaCl	aging time (days)	avg hydrodynamic diameter (nm)
0	230 ± 26	*b*	*b*	0	29 ± 5
2	156 ± 32	*b*	*b*	10	27 ± 6
6	150 ± 17	*b*	*b*	20	30 ± 5
24	31 ± 5	*b*	*b*	30	27 ± 7
36	25 ± 6	86 ± 17	*b*	40	31 ± 5
54	29 ± 5	36 ± 7	80 ± 10	270	28 ± 8

[a]Based on three independent measurements. [b]Precipitated.

In addition to transparency to light, the polystyrene matrix has high oxygen permeability [$P(O_2) = 1.9 \times 10^{-13}$ cm^3cm cm^{-2} s^{-1} Pa^{-1}] and oxygen diffusion [$D(O_2) = 2.8 \times 10^{-7}$ $cm^2 \cdot s^{-1}$].[33,7] Therefore, we focused on applications utilizing efficient oxygen transport, namely, photogeneration of $O_2(^1\Delta_g)$ (with **1**@PS-SO_3) and oxygen sensing (with **2**@PS-SO_3).

Morphology of Nanoparticles and Nanofiber Materials. The structure of the original electrospun polystyrene nanofiber materials was visualized by SEM (Figure 2a). The typical nanofiber diameter was in the range 100−400 nm (average diameter of 253 nm).

Sulfonation of the electrospun nanofiber materials led to formation of negative charges on the nanofiber surfaces. As described previously, sulfonation was accompanied by a slight increase of the nanofiber diameter (average diameter 262 nm), but the nanofibrous character of the materials was not changed (Figure 2b).[11]

The nanoprecipitation method led to mostly spherical NPs, as observed in the SEM images of their dried suspensions (Figure 2d and Figure S3), where larger NPs are more visible, in contrast to the majority of small NPs revealed by dynamic light scattering (DLS).

DLS experiments were conducted on suspensions of NPs to evaluate the effect of sulfonation on their size and dispersibility (Table 1). Water dispersions of NPs prepared from pristine polystyrene nanofibers displayed hydrodynamic diameters peaking at approximately 230 nm (Figure S4a). Sulfonation of the nanofibers led to a decrease in size of the NPs. The sulfonated NPs had average hydrodynamic diameters of approximately 30 nm, associated with low polydispersity (PDI index of 0.2−0.3; Figure S4c), in contrast to non-sulfonated NPs, where the freshly prepared NPs were characterized, in some cases, as polydispersed (Figure S4b). The presence of encapsulated porphyrins had no influence on the morphology or size of the NPs.

Due to sulfonation of the pristine nanofiber material, NPs possessing negative charges have a low tendency to precipitate, even long-term (more than 270 days) and at high ionic strength, due to electrostatic repulsions. In contrast, freshly prepared nonsulfonated NPs had a tendency to aggregate (Table 1). Increasing sulfonation time during preparation of the NPs decreased their size and increased their resistance to aggregation in environments with high ionic strength (Table 1) due to the high number of sulfo groups per NP (up to 2.48 ×

DOI: 10.1021/acsami.6b08234
ACS Appl. Mater. Interfaces 2016, 8, 25127−25136

10^4, Table S1). For advanced characterization, only NPs prepared by long-time sulfonation (54 h) were used.

An aqueous suspension of both sulfonated and non-sulfonated NPs can be easily filtered through the hydrophilic polyurethane Tecophilic nanofiber membrane with highly efficient NP removal, despite the fact that the spaces between the nanofibers (more than 150 nm) exceed the size of the sulfonated NPs. The Tecophilic nanofiber membrane (average nanofiber diameter of 110 ± 50 nm, thickness of 0.03 mm, 2.5 g/m^2) removed the majority of the NPs (>99%), as proved by UV/vis spectra of a **1**@PS-SO_3 suspension (Figure 3). DLS

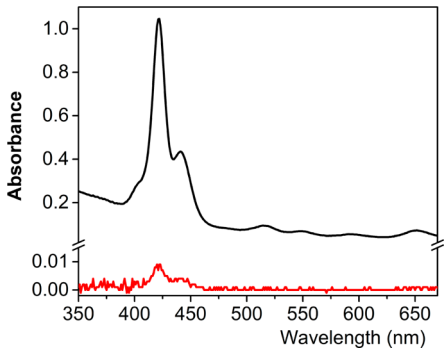

Figure 3. Ability to detain NPs (**1**@PS-SO_3) on the surface of a polyurethane (Tecophilic) membrane. UV−vis spectra of **1**@PS-SO_3 in H_2O before (black) and after (red) filtration through the polyurethane (Tecophilic) nanofiber membrane are shown.

analyses revealed that the small amount of NPs able to pass through the membrane have the same size distribution as before filtration. The test also confirmed the assumption that hydrophobic TPP (insoluble in water) was encapsulated in polystyrene NPs, where it exhibited its monomeric absorption spectrum. This form is removable by membrane filtration, whereas water-soluble TPPS, a possible product of TPP sulfonation, freely passes through the membrane.

NPs are not only wrapped in the space between the nanofibers but also stuck to the surface of the nanofibers (Figure 2e,f). The pristine Tecophilic nanofiber membrane (Figure 2c) was completely covered by NPs. This feature is important from a nanotechnology point of view; the nanofiber materials can serve not only as a simple and huge source of NPs but also for their efficient removal from aqueous media.

UV−Visible Spectra. UV−vis absorption and emission spectra were measured to evaluate the effect of NP preparation on spectra of the encapsulated photoactive compounds TPP and Pt-OEP. **1**@PS-SO_3 and **2**@PS-SO_3 had spectra similar to those of the original materials (polystyrene nanofiber membranes with TPP or Pt-OEP; Figure 4). TPP in **1**@PS-SO_3 was partly protonated (Soret band with a shoulder at 440 nm) due to acidic sulfonation (Figure 4a). UV−vis spectra of the pristine nanofiber membrane with encapsulated Pt-OEP before and after sulfonation revealed slight acidic demetalation of Pt-OEP, which was not detected in the case of **2**@PS-SO_3 due to the high scattering effect (Figure 4d).

All absorption, emission, and excitation spectra indicated that most of the porphyrin molecules were in the monomeric state, well-encapsulated in the polystyrene bulk and protected from the aqueous surroundings, where hydrophobic TPP and Pt-OEP are otherwise in aggregated, nonphotoactive states.[34]

Photophysical Properties. Photophysical properties of **1**@PS-SO_3, **2**@PS-SO_3, and TPPS standard in D_2O are summarized in Table 2.

Formation of singlet oxygen, $O_2(^1\Delta_g)$, inside **1**@PS-SO_3 involves excitation of the ground state of tetraphenylporphyrin ($^1TPP_0$), formation and decay of its excited singlet (^1TPP) and triplet states (^3TPP) (eq 1), and their quenching by molecular oxygen (Figure S1 and eq 2):

$$^1TPP_0 + h\nu \rightarrow {}^1TPP \rightarrow {}^3TPP \quad (1)$$

$$^3TPP + O_2 \rightarrow O_2(^1\Delta_g) \quad (2)$$

Porphyrin triplet states, ^3TPP, in **1**@PS-SO_3 were efficiently quenched by oxygen (Table 2). Traces in argon-, air-, and oxygen-saturated D_2O can be fitted by two exponential decays. The deviation from single-exponential decay observed for ^3TPPS indicates different environments of TPP molecules

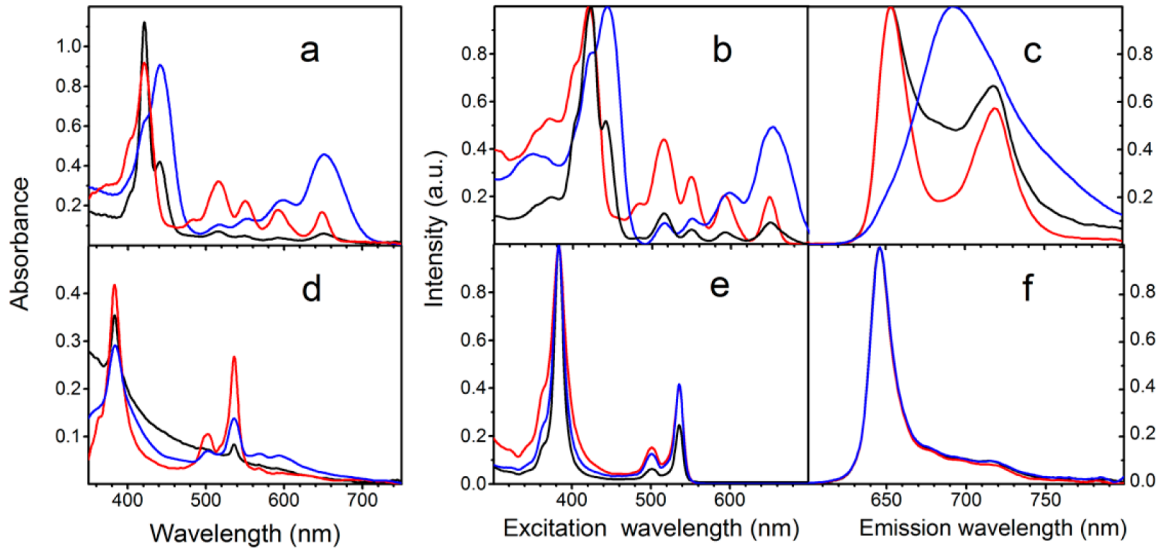

Figure 4. UV−vis excitation and emission spectra of (a−c) **1**@PS-SO_3 and (d−f) **2**@PS-SO_3 (black) and corresponding electrospun polystyrene nanofiber membranes with TPP or Pt-OEP before (red) and after sulfonation (blue). Nanomaterials with TPP were excited at λ_{exc} = 422 nm and emission was detected at λ_{em} = 717 nm. Nanomaterials with Pt-OEP were excited at λ_{exc} = 383 nm and emission was detected at λ_{em} = 646 nm.

DOI: 10.1021/acsami.6b08234
ACS Appl. Mater. Interfaces 2016, 8, 25127−25136

Table 2. Photophysical Properties of 1@PS-SO_3, 2@PS-SO_3, and TPPS Standard in D_2O[a]

triplet states					$O_2(^1\Delta_g)$	
τ_T in oxygen (μs)	τ_T in air (μs)	τ_T in argon (μs)	k_{O_2} (L·mol^{-1}·s^{-1})	$F_T^{O_2}$	amp	τ_Δ (μs)
			TPPS			
0.417	2.01	649	1.7×10^9	0.997	3.1	59.9
			1@PS-SO_3[b]			
1.02 (41%)	6.02 (39%)	1880 (47%)		0.997	1.6	44.3
6.00 (59%)	25.2 (61%)	6560 (53%)				
			2@PS-SO_3[b]			
0.85 (35%)	4.5 (32%)	16.8 (26%)		0.806		
1.16 (65%)	20.1 (68%)	99.3 (74%)				

[a] τ_T, triplet lifetimes; k_{O_2}, rate constant for triplet-state quenching by oxygen; $F_T^{O_2}$, fraction of triplet states trapped by oxygen in air-saturated solution; amp, amplitude of singlet oxygen luminescence; τ_Δ, lifetime of $O_2(^1\Delta_g)$ in D_2O. [b] Biexponential decay.

within the NPs (Figures S5 and S6). The average lifetimes (τ_{Tav} of 22.6 μs for 1@PS-SO_3) in air-saturated dispersion correspond to the lifetime of ^{3}TPP in the original polystyrene nanofiber material in air atmosphere ($\tau_T \sim 22$ μs).[7] High values of τ_T (approximately several ms) were measured for 1@PS-SO_3 in argon-saturated D_2O, similarly to polystyrene nanofiber membranes with TPP. The quenching of ^{3}TPP by oxygen in 1@PS-SO_3 was significantly lower than that of ^{3}TPPS in water (Figures S5 and S6), reflecting the oxygen diffusion coefficient in polystyrene, which is approximately 2 orders of magnitude lower than that in water.[35]

The fraction of triplet states quenched by oxygen in air-saturated solution, $F_T^{O_2}$, is an important parameter to evaluate the efficiency of singlet oxygen photogeneration. It may also include other processes induced by the collision/interaction of oxygen with ^{3}TPP. High values of $F_T^{O_2} = 0.997$ for 1@PS-SO_3, which were the same as that for TPPS, suggest highly efficient $O_2(^1\Delta_g)$ formation. Short lifetimes of ^{3}Pt-OEP in 2@PS-SO_3 (Table 2 and Figure S8) reflect the presence of luminescence as a competitive deactivation process (Figure S9).[18]

Singlet oxygen, $O_2(^1\Delta_g)$, was directly evidenced by its characteristic luminescence centered at 1270 nm. Upon irradiation with blue light, 1@PS-SO_3 in D_2O displayed long-lived $O_2(^1\Delta_g)$ luminescence with the lifetime typical for D_2O (Figure 5a). To compare the behavior of $O_2(^1\Delta_g)$ inside and outside the polystyrene nanoparticles, we measured the luminescence of $O_2(^1\Delta_g)$ in oxygen-saturated D_2O (Figure 5a and Figure S7) and H_2O (Figure 5b).

Formation of $O_2(^1\Delta_g)$ from ^{3}TPP (eq 2) was independent of the solvent and was nearly completed 15 μs after excitation (Figure 5c). Excluding this time interval, the luminescence trace of $O_2(^1\Delta_g)$ in H_2O can be fitted by a single-exponential function with lifetime $\tau_\Delta = 8.4$ μs, whereas the decay in D_2O is biexponential, with lifetimes $\tau_{\Delta1} = \sim 8.4$ μs and $\tau_{\Delta2} = \sim 43$ μs. The lifetime in H_2O ($\tau_\Delta = 8.4$ μs) reflects the predominant contribution of $O_2(^1\Delta_g)$ luminescence inside the NPs. The $O_2(^1\Delta_g)$ outside the NPs in an H_2O environment is deactivated more rapidly ($\tau_\Delta = 3.5$ μs).[12] In D_2O, contributions from both polystyrene NPs and the D_2O environment ($\tau_\Delta \approx 45$ μs) can be resolved, which indicates that the $O_2(^1\Delta_g)$ formed inside 1@PS-SO_3 is released to the aqueous environment, where it can be used as a photooxidation agent.

Longer lifetime of ^{3}TPP in air-saturated D_2O (Table 2) is the reason for slower kinetics of $O_2(^1\Delta_g)$ and lower amplitude than that in oxygen-saturated medium (eq 2 and Figure S7c,d). The photophysical behavior of TPP and $O_2(^1\Delta_g)$ inside and outside polystyrene and other polymeric matrices was described in our previous papers in detail.[3,7,13,14]

Photooxidation of External Substrates. The near-infrared luminescence of the 1@PS-SO_3 dispersion in water (see above) revealed the efficient generation of $O_2(^1\Delta_g)$, which is sufficient to oxidize external substrates in aqueous media. To prove this assumption, we used uric acid, a known specific acceptor of $O_2(^1\Delta_g)$,[36] as the model substrate. Irradiation of the 1@PS-SO_3 suspension in the presence of uric acid led to photobleaching of the substrate, as shown by the gradually decreasing absorbance at 291 nm during the irradiation, in contrast to the behavior in the dark (Figure 6).

No photobleaching was observed during irradiation in the presence of 0.01 mol·L^{-1} NaN_3, a known physical quencher of $O_2(^1\Delta_g)$[37] [quenching rate constant, k_q, of $(2.3-7.0) \times 10^8$ L·mol^{-1}·s^{-1}] or in N_2-saturated solutions or when NPs without a photosensitizer (@PS-SO_3) were used. Similar results were obtained from the iodide test for $O_2(^1\Delta_g)$ generation (Figure S10),[31] where a linear increase in the I_3^- concentration (detected as UV/vis absorbance change at 287 or 351 nm)

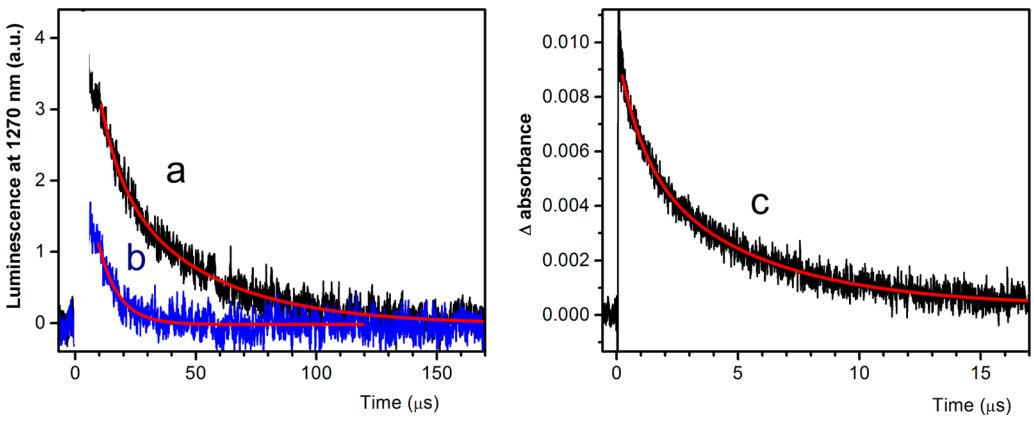

Figure 5. Singlet oxygen generation after excitation by a 421 nm pulse of 1@PS-SO_3 in (a) oxygen-saturated D_2O and (b) H_2O. (c) Corresponding biexponential kinetics of TPP triplet states.

DOI: 10.1021/acsami.6b08234
ACS Appl. Mater. Interfaces 2016, 8, 25127−25136

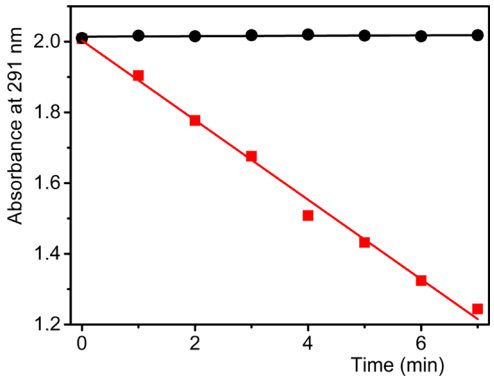

Figure 6. Absorbance at 291 nm of 3 mL of air-saturated 2×10^{-4} mol·L^{-1} uric acid in 0.02 mol·L^{-1} phosphate buffer (pH = 7.0) containing a suspension of **1**@PS-SO_3 during continuous irradiation with visible light (red) or stored in the dark (black). Irradiation source: 500 W Xe lamp with a long-pass filter ($\lambda \geq 400$ nm).

proportional to the photogeneration of $O_2(^1\Delta_g)$ was detected, in contrast to a blank solution of the same composition that was stored in the dark or irradiated in the presence of NaN_3 (Figure S11).

In our previous study, we calculated the effective range of photogenerated $O_2(^1\Delta_g)$ inside polystyrene nanofibers with encapsulated TPP.[14] The mean radial diffusion length, $l_r = [6 D(O_2)\tau_\Delta]^{1/2}$, of $O_2(^1\Delta_g)$ depends on τ_Δ and the diffusion coefficient $D(O_2)$. The distance l_r traveled by $O_2(^1\Delta_g)$ was calculated with the values of τ_Δ obtained from the decay time of $O_2(^1\Delta_g)$ luminescence at 1270 nm and the values of $D(O_2) = 2.8 \times 10^{-7}$ cm^2·s^{-1} in the polystyrene nanofiber material.[33] The effective range of photogenerated $O_2(^1\Delta_g)$ inside the material ($l_r \approx 39-42$ nm) is not significantly influenced by sulfonation. If it is assumed that $D(O_2)$ in $H_2O \approx 2 \times 10^{-5}$ cm^2·s^{-1},[38] the maximum l_r traveled by the photogenerated $O_2(^1\Delta_g)$ from the surface to the aqueous surroundings containing a substrate/target is 205 nm for a typical value of $\tau_\Delta = 3.5$ μs in H_2O.[12] In the case of nanofiber material, the diffusion length is sufficient for photooxidation of a substrate/target only in close proximity to the surface, in contrast to NPs with a photosensitizer, which are homogeneously distributed in the whole volume. If we assume the same l_r (205 nm) traveled by photogenerated $O_2(^1\Delta_g)$ from **1**@PS-SO_3 in stock suspension ($\sim 1.2 \times 10^{14}$ NPs/mL) to the aqueous surroundings, then a simple calculation reveals that photogenerated $O_2(^1\Delta_g)$ reached 100% of the total irradiated volume at a definite time of irradiation (Table S1). Consequently, the photooxidation of a substrate is very efficient. As will be illustrated in the following sections, even diluted suspensions of **1**@PS-SO_3 (6.0×10^{13} NPs/mL for antibacterial study and 5.8×10^{12} NPs/mL for antiviral study) are sufficient for photoinactivation of pathogens.

Antibacterial Activity. The photooxidation experiments revealed that $O_2(^1\Delta_g)$-generating NPs can easily oxidize external substrates in aqueous media. It is generally known that $O_2(^1\Delta_g)$ has a strong cytotoxic effect, although recent studies reported also an opposite effect, the stimulation of cell proliferation by $O_2(^1\Delta_g)$, observed only in some eukaryotic cells with very low concentration of intracellularly generated $O_2(^1\Delta_g)$. Therefore, due to strong external generation of $O_2(^1\Delta_g)$ and prokaryotic cells as a target, antibacterial effect can be expected.[39,40] To test the antibacterial activity, **1**@PS-SO_3 suspensions were added to suspensions of *E. coli* and irradiated or kept in the dark. Then an aliquot of a bacterial suspension was placed on an agar plate and incubated overnight. Figure 7 (see also Table S2) shows very strong bacterial growth inhibition of *E. coli* after 5 min of irradiation by visible light for a bacterial suspension in the presence of **1**@PS-SO_3.

After a short irradiation with visible light, the number of colony-forming units (CFU) drops from approximately 900 to 7. No colonies were found after 10 min of irradiation. **1**@PS-SO_3 suspensions that were kept in the dark and sulfonated NPs that did not contain photosensitizer (@PS-SO_3) did not exhibit bacterial inhibition. Minor antibacterial effects can be attributed to the light itself (see irradiated/nonirradiated sulfonated NPs). Briefly, only the presence of photosensitizer encapsulated in sulfonated NPs exhibited an efficient antibacterial effect due to the formation of cytotoxic $O_2(^1\Delta_g)$.

In contrast to nanofiber materials with encapsulated photosensitizers, which ensure a sterile character only on the surface of the nanofibers due to the short diffusion pathway of $O_2(^1\Delta_g)$, **1**@PS-SO_3 exhibits antibacterial effects in the whole volume. The literature shows that even multiresistant (MRS) bacteria are efficiently inactivated by $O_2(^1\Delta_g)$.[17]

As mentioned above, NPs can be easily removed by filtration through a Tecophilic polyurethane nanofiber membrane with great efficiency. We also found that *E. coli* can be completely removed from aqueous media by use of the same membrane (Figure S12). These facts can be utilized in a new safe and efficient technology for photodisinfection of contaminated

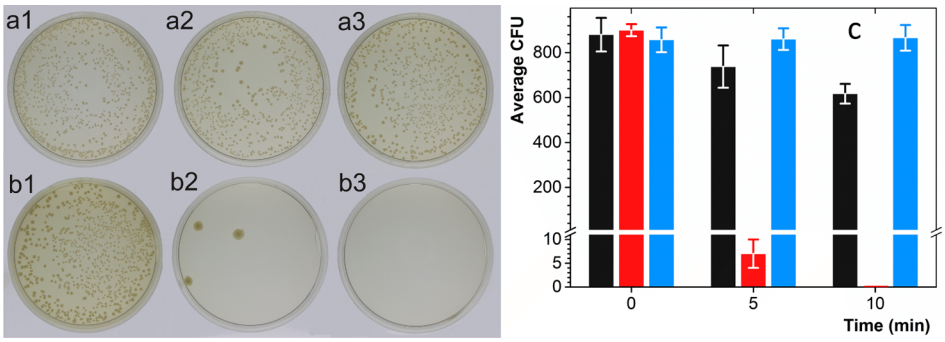

Figure 7. (Photo)antibacterial activity estimated as the average number of colony-forming units (CFU) of *E. coli* observed on agar plates after irradiation with visible light. Pictures of agar plates correspond to (a1, b1) 0 min, (a2, b2) 5 min, and (a3, b3) 10 min of irradiation of (a) @PS-SO_3 nanoparticles without photosensitizer and (b) **1**@PS-SO_3. (c) Average number of CFUs corresponding to treatment with @PS-SO_3 (black) and **1**@PS-SO_3 (red) after 0–10 min of irradiation and of **1**@PS-SO_3 stored in the dark (blue), based on three independent tests.

DOI: 10.1021/acsami.6b08234
ACS Appl. Mater. Interfaces 2016, 8, 25127–25136

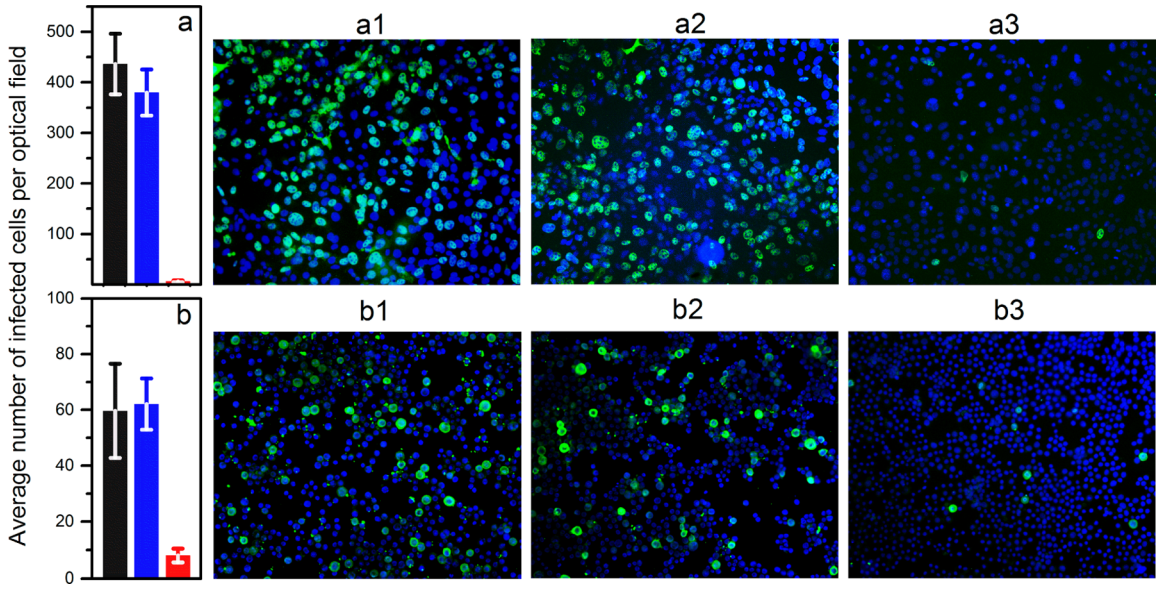

Figure 8. Antiviral activity of light-activated **1**@PS-SO_3, estimated as the average number of cells infected by (a) nonenveloped polyomavirus and (b) enveloped recombinant pVL-VP1 baculovirus. Columns represent the average numbers of infected cells per optical field of the fluorescent microscope, with the standard deviation from three independent experiments. Results for virus stocks with @PS-SO_3 (black) or **1**@PS-SO_3 kept in the dark (blue) or irradiated by visible light for 30 min (red) are shown. (a1−a3, b1−b3) Representative optical fields for individual columns in panels a and b are shown; cell nuclei are stained with DAPI (blue), and infected cells are stained with virus-specific antibodies (green).

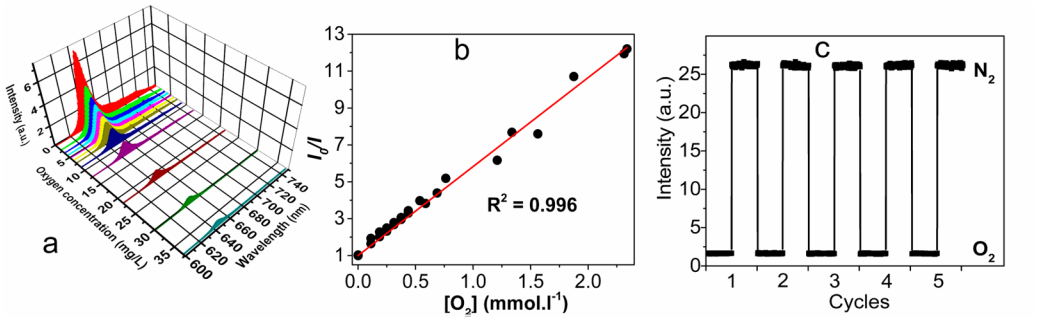

Figure 9. (a) Three-dimensional representation of the spectral response of **2**@PS-SO_3 to dissolved oxygen in water. (b) Corresponding Stern−Volmer plot with different dissolved oxygen concentrations. (c) Reversibility of dissolved oxygen sensing: change in luminescence intensity of **2**@PS-SO_3 (λ_{exc} = 383 nm, λ_{em}= 646 nm) after several cycles of saturation with nitrogen (high luminescence intensity) and oxygen (low intensity).

aqueous media, even when contaminated with MRS, by use of NPs, such as **1**@PS-SO_3, followed by filtration through a nanofiber membrane.

Antiviral Activity. The antiviral effect on the surface of polyurethane and polycaprolactone membranes that generate $O_2(^1\Delta_g)$ was previously described.[9] Similarly to this study, the antiviral effect of **1**@PS-SO_3 was evaluated for nonenveloped mouse polyomavirus and enveloped recombinant pVL-VP1 baculovirus, as described in the Experimental Section. A 100 μL volume of virus stock (5×10^8 MPyV virus particles or 2×10^6 pVL-VP1 baculovirus particles) was mixed with 5 μL of **1**@PS-SO_3 or @PS-SO_3 (both ~1.2×10^{14} NPs/mL) as a control. Mixtures were kept in the dark or irradiated with visible light for 30 min and were then applied to 3T6 fibroblast (MPyV; Figure 8a) or Sf9 cells (pVL-VP1 baculovirus; Figure 8b). Virus infectivity was analyzed by use of specific antibodies directed against virus proteins.

The robust photogeneration and lifetime of $O_2(^1\Delta_g)$ on **1**@PS-SO_3 leads to strong photoinduced antiviral effects on both nonenveloped polyomaviruses and enveloped baculoviruses. In particular, nonenveloped polyomaviruses are extremely sensitive to the presence of irradiated **1**@PS-SO_3, probably due to the higher accessibility of amino acid residues sensitive to $O_2(^1\Delta_g)$, as nonenveloped viruses are enclosed in protective, protein-only capsids.[9] A 2-fold amount of **1**@PS-SO_3 (10 μL), with stronger antiviral effect, or a decreased concentration of viruses (5×10^7 for MPyV or 2×10^5 for pVL-VP1 baculovirus) resulted in complete inhibition of infection (data not shown).

These NPs could be considered for use in a number of biomedical applications utilizing virus inactivity and for the development of $O_2(^1\Delta_g)$ inactivation tests for enveloped and nonenveloped viruses.

Dissolved Oxygen Sensing. Application of NPs with Pt-OEP (**2**@PS-SO_3) for oxygen sensing via phosphorescence of encapsulated Pt-OEP[22,41,42] utilizes the high polystyrene transparency and facile oxygen transport due to the high diffusion coefficient.

For oxygen sensing in water, phosphorescence of the **2**@PS-SO_3 suspension was monitored (see Experimental Section) in H_2O with different concentrations of dissolved oxygen that were maintained by nitrogen or oxygen gas bubbling. The

DOI: 10.1021/acsami.6b08234
ACS Appl. Mater. Interfaces 2016, 8, 25127−25136

intensity of the luminescence at 645 nm was efficiently quenched with increasing oxygen concentration, which was independently recorded by use of a commercial optical sensor. No shift in the luminescence band was observed with increased level of oxygen (Figure 9a). The dynamic quenching of luminescence can be described by the Stern−Volmer equation (eq 3):

$$I_0/I = 1 + k_q\tau_0[O_2] \quad (3)$$

where I_0 and I are luminescence intensity without and with oxygen quencher, $[O_2]$ is oxygen concentration, k_q is the bimolecular rate constant of quenching, and τ_0 is the lifetime of luminescent excited state without quencher.

Considering τ_0 = 99.3 μs from laser flash photolysis experiments (Table 2), the Stern−Volmer plot (eq 3) yields $k_q = 5.4 \times 10^7$ L·mol^{-1}·s^{-1}.[22,41,42] The sensitivity of **2**@PS-SO$_3$ to dissolved oxygen can be expressed by the intensity ratio of **2**@PS-SO$_3$ in oxygen-free water (I_0) and in water saturated with oxygen (I_{max}). The value of 12.2 for I_0/I_{max} ratio and the coefficient for linear fitting (R^2 = 0.996) demonstrate high sensitivity with good calibration fitting over the full range of oxygen content. Even better calibration fitting (R^2 = 0.997) can be obtained in the biologically relevant range (0−0.28 mmol·L^{-1}) of oxygen content in biological media. These data indicate the broad range and good accuracy of **2**@PS-SO$_3$ as an oxygen sensor (Figure 9b) with a reversible luminescent response (Figure 9c).

In conclusion, **2**@PS-SO$_3$ suspensions prepared from electrospun material by a cheap industrial method possess encapsulated Pt-OEP molecules that are protected from the surroundings by a polystyrene shell. However, due to the high oxygen permeability of polystyrene, the luminescence of Pt-OEP is highly sensitive to quenching by dissolved oxygen. Therefore, application of **2**@PS-SO$_3$ for sensing dissolved oxygen is an alternative method to measure the content of oxygen in aqueous (biological) media in compartments where the dimensions are too small to use standard oxygen electrodes and when chemical probes are too toxic (for application in biological environments) and/or are sensitive to the surroundings.

4. CONCLUSIONS

We have demonstrated a fast, simple top-down process for fabrication of stable photoactive polystyrene NPs from sulfonated polystyrene electrospun nanofiber material. Properties of the NPs were tuned by the selection of encapsulated porphyrin derivatives: NPs with TPP photosensitizer had strong antibacterial and antiviral properties due to the formation of highly reactive singlet oxygen, whereas NPs with encapsulated Pt-OEP were applied for oxygen sensing.

NP-photogenerated singlet oxygen, with a short lifetime of several microseconds in aqueous media, can travel within close proximity of chemical/biological targets and allow their more efficient photooxidation compared to electrospun membranes with limited oxygen diffusion to the target structures. NPs with encapsulated Pt-OEP exhibited reversible luminescent response and linear Stern−Volmer quenching behavior over the whole range of dissolved oxygen concentrations. The pristine nanofiber membranes prepared by industrial electrospinning can be used not only as a source of NPs but also as an efficient filter to remove bacteria and prepared NPs.

■ ASSOCIATED CONTENT

Supporting Information

The Supporting Information is available free of charge on the ACS Publications website at DOI: 10.1021/acsami.6b08234.

Twelve figures showing $O_2(^1\Delta_g)$ photogeneration and electrospinning devices, SEM image, DLS measurements, decay kinetics of ^{3}TPPS and ^{3}TPP in **1**@PS-SO$_3$ and ^{3}Pt-OEP in **2**@PS-SO$_3$; time-resolved luminescence of **1**@PS-SO$_3$, iodide tests for generation of $O_2(^1\Delta_g)$, and ability to detain bacteria on the surface of polyurethane membrane; two tables listing properties of NPs and (photo)antibacterial activity (PDF)

■ AUTHOR INFORMATION

Corresponding Author

*E-mail mosinger@natur.cuni.cz.

Notes

The authors declare no competing financial interest.

■ ACKNOWLEDGMENTS

This work was supported by the Czech Science Foundation (16-15020S). We acknowledge the assistance provided by the Research Infrastructure NanoEnviCz, supported by the Ministry of Education,Youth and Sports of the Czech Republic under Project LM2015073. We thank Dr. Lukáš Plíštil for preparation of nanofiber membranes by electrospinning and Dr. Pavel Engst for help with laser flash photolysis experiments.

■ ABBREVIATIONS

TPP, 5,10,15,20-tetraphenylporphyrin
Pt-OEP, platinum(II) 2,3,7,8,12,13,17,18-octaethyl-21*H*,23*H*-porphyrin
NPs, nanoparticles
@PS-SO$_3$, sulfonated nanoparticles without an encapsulated compound
1@PS-SO$_3$, sulfonated nanoparticles with encapsulated 5,10,15,20-tetraphenylporphyrin
2@PS-SO$_3$, sulfonated nanoparticles with encapsulated platinum(II) 2,3,7,8,12,13,17,18-octaethyl-21*H*,23*H*-porphyrin
IEC, ion-exchange capacity

■ REFERENCES

(1) Rizzello, L.; Cingolani, R.; Pompa, P. P. Nanotechnology Tools for Antibacterial Materials. *Nanomedicine (London, U. K.)* **2013**, *8*, 807−821.

(2) Li, Q.; Mahendra, S.; Lyon, D. Y.; Brunet, L.; Liga, M. V.; Li, D.; Alvarez, P. J. J. Antimicrobial Nanomaterials for Water Disinfection and Microbial Control: Potential Applications and Implications. *Water Res.* **2008**, *42*, 4591−4602.

(3) Mosinger, J.; Jirsák, O.; Kubát, P.; Lang, K.; Mosinger, B. Bactericidal Nanofabrics Based on Photoproduction of Singlet Oxygen. *J. Mater. Chem.* **2007**, *17*, 164−166.

(4) Gabriel, D.; Monteiro, I. P.; Huang, D.; Langer, R.; Kohane, D. S. A Photo-Triggered Layered Surface Coating Producing Reactive Oxygen Species. *Biomaterials* **2013**, *34*, 9763−9769.

(5) McCoy, C. P.; O'Neil, E. J.; Cowley, J. F.; Carson, L.; De Baróid, Á. T.; Gdowski, G. T.; Gorman, S. P.; Jones, D. S. Photodynamic Antimicrobial Polymers for Infection Control. *PLoS One* **2014**, *9*, No. e108500.

(6) Mosinger, J.; Lang, K.; Kubát, P.; Sykora, J.; Hof, M.; Plíštil, L.; Mosinger, B. Photofunctional Polyurethane Nanofabrics Doped by

DOI: 10.1021/acsami.6b08234
ACS Appl. Mater. Interfaces 2016, 8, 25127−25136

Zinc Tetraphenylporphyrin and Zinc Phthalocyanine Photosensitizers. *J. Fluoresc.* **2009**, *19*, 705−713.
(7) Jesenská, S.; Plíštil, L.; Kubát, P.; Lang, K.; Brožová, L.; Popelka, S.; Szatmáry, L.; Mosinger, J. Antibacterial Nanofiber Materials Activated by Light. *J. Biomed. Mater. Res., Part A* **2011**, *99*, 676−683.
(8) Arenbergerova, M.; Arenberger, P.; Bednar, M.; Kubat, P.; Mosinger, J. Light-Activated Nanofibre Textiles Exert Antibacterial Effects in the Setting of Chronic Wound Healing. *Exp. Dermatol.* **2012**, *21*, 619−624.
(9) Lhotakova, Y.; Plistil, L.; Moravkova, A.; Kubat, P.; Lang, K.; Forstova, J.; Mosinger, J. Virucidal Nanofiber Textiles Based on Photosensitized Production of Singlet Oxygen. *PLoS One* **2012**, *7*, e49226.
(10) Greiner, A.; Wendorff, J. H. Electrospinning: A Fascinating Method for the Preparation of Ultrathin Fibres. *Angew. Chem., Int. Ed.* **2007**, *46*, 5670−5703.
(11) Henke, P.; Lang, K.; Kubát, P.; Sýkora, J.; Šlouf, M.; Mosinger, J. Polystyrene Nanofiber Materials Modified with an Externally Bound Porphyrin Photosensitizer. *ACS Appl. Mater. Interfaces* **2013**, *5*, 3776−3783.
(12) Hatz, S.; Poulsen, L.; Ogilby, P. R. Time-Resolved Singlet Oxygen Phosphorescence Measurements from Photosensitized Experiments in Single Cells: Effects of Oxygen Diffusion and Oxygen Concentration. *Photochem. Photobiol.* **2008**, *84*, 1284−1290.
(13) Mosinger, J.; Lang, K.; Plístil, L.; Jesenská, S.; Hostomský, J.; Zelinger, Z.; Kubát, P. Fluorescent Polyurethane Nanofabrics: a Source of Singlet Oxygen and Oxygen Sensing. *Langmuir* **2010**, *26*, 10050−10056.
(14) Henke, P.; Kozak, H.; Artemenko, A.; Kubát, P.; Forstová, J.; Mosinger, J. Superhydrophilic Polystyrene Nanofiber Materials Generating O2(1Δg): Postprocessing Surface Modifications toward Efficient Antibacterial Effect. *ACS Appl. Mater. Interfaces* **2014**, *6*, 13007−13014.
(15) Plíštil, L.; Henke, P.; Kubát, P.; Mosinger, J. Anion Exchange Nanofiber Materials Activated by Daylight with a Dual Antibacterial Effect. *Photochem. Photobiol. Sci.* **2014**, *13*, 1321−1329.
(16) Dolanský, J.; Henke, P.; Kubát, P.; Fraix, A.; Sortino, S.; Mosinger, J. Polystyrene Nanofiber Materials for Visible-Light-Driven Dual Antibacterial Action via Simultaneous Photogeneration of NO and $O_2(^1\Delta_g)$. *ACS Appl. Mater. Interfaces* **2015**, *7*, 22980−22989.
(17) Laxminarayan, R.; Duse, A.; Wattal, C.; Zaidi, A. K. M.; Wertheim, H. F. L.; Sumpradit, N.; Vlieghe, E.; Hara, G. L.; Gould, I. M.; Goossens, H.; Greko, C.; So, A. D.; Bigdeli, M.; Tomson, G.; Woodhouse, W.; Ombaka, E.; Peralta, A. Q.; Qamar, F. N.; Mir, F.; Kariuki, S.; Bhutta, Z. A.; Coates, A.; Bergstrom, R.; Wright, G. D.; Brown, E. D.; Cars, O. Antibiotic Resistance-the Need for Global Solutions. *Lancet Infect. Dis.* **2013**, *13*, 1057−1098.
(18) Wolfbeis, O. S. An Overview of Nanoparticles Commonly Used in Fluorescent Bioimaging. *Chem. Soc. Rev.* **2015**, *44*, 4743−4768.
(19) Morones, J. R.; Elechiguerra, J. L.; Camacho, A.; Holt, K.; Kouri, J. B.; Ramírez, J. T.; Yacaman, M. J. The Bactericidal Effect of Silver Nanoparticles. *Nanotechnology* **2005**, *16*, 2346−2353.
(20) Richter, A. P.; Brown, J. S.; Bharti, B.; Wang, A.; Gangwal, S.; Houck, K.; Cohen Hubal, E. A.; Paunov, V. N.; Stoyanov, S. D.; Velev, O. D. An Environmentally Benign Antimicrobial Nanoparticle Based on a Silver-Infused Lignin Core. *Nat. Nanotechnol.* **2015**, *10*, 817−823.
(21) Wilkinson, F.; Helman, W. P.; Ross, A. B. Quantum Yields for the Photosensitized Formation of the Lowest Electronically Excited Singlet-state of Molecular Oxygen in Solution. *J. Phys. Chem. Ref. Data* **1993**, *22*, 113−262.
(22) Mills, A.; Lepre, A. Controlling the Response Characteristics of Luminescent Porphyrin Plastic Film Sensors for Oxygen. *Anal. Chem. (Washington, DC, U. S.)* **1997**, *69*, 4653−4659.
(23) Forstová, J.; Krauzewicz, N.; Wallace, S.; Street, A. J.; Dilworth, S. M.; Beard, S.; Griffin, B. E. Cooperation of Structural Proteins During Late Events in the Life Cycle of Polyomavirus. *J. Virol.* **1993**, *67*, 1405−1413.
(24) Dilworth, S. M.; Griffin, B. E. Monoclonal Antibodies Against Polyomavirus Tumour Antigens. *Proc. Natl. Acad. Sci. U. S. A.* **1982**, *79*, 1059−1063.
(25) Hink, W. F. Established Insect Cell Line from the Cabbage Looper Trichoplusia ni. *Nature (London, U. K.)* **1970**, *226*, 466−467.
(26) Horníková, L.; Žíla, V.; Španielová, H.; Forstová, J. Mouse Polyomavirus: Propagation, Purification, Quantification, and Storage. *Current Protocols in Microbiology* **2015**, *38*, 14F.1.1−14F.1.26.
(27) Jirsák, O.; Sanetrník, F.; Lukáš, D.; Kotek, V.; Martinová, L.; Chaloupek, J. International Patent WO 2005024101 A1, 2005.
(28) Forward, K. M.; Rutledge, G. C. Free Surface Electrospinning from a Wire Electrode. *Chem. Eng. J. (Amsterdam, Neth.)* **2012**, *183*, 492−503.
(29) An, H.; Shin, C.; Chase, G. G. Ion Exchanger Using Electrospun Polystyrene Nanofibers. *J. Membr. Sci.* **2006**, *283*, 84−87.
(30) Fischer, F.; Graschew, G.; Sinn, H. J.; Maier-Borst, W.; Lorenz, W. J.; Schlag, P. M. A Chemical Dosimeter for the Determination of the Photodynamic Activity of Photosensitizers. *Clin. Chim. Acta* **1998**, *274*, 89−104.
(31) Mosinger, J.; Mosinger, B. Photodynamic Sensitizers Assay: Rapid and Sensitive Iodometric Measurement. *Experientia* **1995**, *51*, 106−109.
(32) Kirakci, K.; Kubát, P.; Fejfarová, K.; Martinčík, J.; Nikl, M.; Lang, K. X-ray Inducible Luminescence and Singlet Oxygen Sensitization by an Octahedral Molybdenum Cluster Compound: A New Class of Nanoscintillators. *Inorg. Chem.* **2016**, *55*, 803−809.
(33) Pauly, S. Permeation and Diffusion Data. In *Polymer Handbook*, 4th ed.; Brandrup, J., Immergut, E. H., Grulke, E. A., Eds.; Wiley: New York, 1999; Chapter 6, pp 543−569.
(34) Procházková, K.; Zelinger, Z.; Lang, K.; Kubát, P. Meso-Tetratolylporphyrins Substituted by Pyridinium Groups Aggregation, Photophysical Properties and Complexation with DNA. *J. Phys. Org. Chem.* **2004**, *17*, 890−897.
(35) Gao, Y.; Baca, A. M.; Wang, B.; Ogilby, P. R. Activation Barriers for Oxygen Diffusion in Polystyrene and Polycarbonate Glasses: Effects of Low Molecular Weight Additives. *Macromolecules (Washington, DC, U. S.)* **1994**, *27*, 7041−7048.
(36) Fischer, F.; Graschew, G.; Sinn, H. J.; Maier-Borst, W.; Lorenz, W. J.; Schlag, P. M. A Chemical Dosimeter for the Determination of the Photodynamic Activity of Photosensitizers. *Clin. Chim. Acta* **1998**, *274*, 89−104.
(37) Wilkinson, F.; Helman, W. P.; Ross, A. B. Rate Constants for the Decay and Reactions of the Lowest Electronically Excited Singlet State of Molecular Oxygen in Solution. An Expanded and Revised Compilation. *J. Phys. Chem. Ref. Data* **1995**, *24*, 663−677.
(38) Tsushima, M.; Tokuda, K.; Ohsaka, T. Use of Hydrodynamic Chronocoulometry for Simultaneous Determination of Diffusion Coefficients and Concentrations of Dioxygen in Various Media. *Anal. Chem. (Washington, DC, U. S.)* **1994**, *66*, 4551−4556.
(39) Blázquez-Castro, A.; Breitenbach, T.; Ogilby, P. R. Singlet Oxygen and ROS in a New Light: Low-dose Subcellular Photodynamic Treatment Enhances Proliferation at the Single Cell Level. *Photochem. Photobiol. Sci.* **2014**, *13*, 1235−1240.
(40) Zhou, X.; Wang, Y.; Si, J.; Zhou, R.; Gan, L.; Di, C.; Xie, Y.; Zhang, H. Laser Controlled Singlet Oxygen Generation in Mitochondria to Promote Mitochondrial DNA Replication *in vitro*. *Sci. Rep.* **2015**, *5*, No. 16925.
(41) Chu, C.; Lo, Y. Highly Sensitive and Linear Calibration Optical Fiber Oxygen Sensor Based on Pt(II) Embedded in Sol-Gel Matrix. *Sens. Actuators, B* **2011**, *155*, 53−57.
(42) Baldo, M. A.; O'Brien, D. F.; You, Y.; Shoustikov, A.; Sibley, S.; Thompson, M. E.; Forrest, S. R. Highly Efficient Phosphorescent Emission from Organic Electroluminescent Devices. *Nature (London, U. K.)* **1998**, *395*, 151−154.

DOI: 10.1021/acsami.6b08234
ACS Appl. Mater. Interfaces 2016, 8, 25127−25136

Journal of Medical Virology 86:1560–1568 (2014)

Seroprevalence Rates of BKV, JCV, and MCPyV Polyomaviruses in the General Czech Republic Population

Vojtěch Šroller,[1]* Eva Hamšíková,[1] Viera Ludvíková,[1] Petra Vochozková,[1] Martina Kojzarová,[2] Martin Fraiberk,[2] Martina Saláková,[1] Alena Morávková,[2] Jitka Forstová,[2] and Šárka Němečková[1]

[1]*Department of Experimental Virology, Institute of Hematology and Blood Transfusion (IHBT), Prague, Czech Republic*

[2]*Faculty of Science, Department of Genetics and Microbiology, Charles University in Prague, Prague, Czech Republic*

JC and BK polyomaviruses (JCV and BKV) infect humans and can cause severe illnesses in immunocompromised patients. Merkel cell polyomavirus (MCPyV) can be found in skin carcinomas. In this study, we assessed the occurrence of serum antibodies against MCPyV, BKV, and JCV polyomaviruses in a healthy population of the Czech Republic. Serum samples from 991 healthy individuals (age range: 6–64 years) were examined by enzyme-linked immunoassay (ELISA) using virus-like particles (VLPs) based on the major VP1 capsid proteins of these viruses. Overall, serum antibodies against MCPyV, JCV, and BKV were found in 63%, 57%, and 69%, respectively, of this population. For all three viruses, these rates were associated with age; the occurrence of antibodies against MCPyV and JCV was highest for those older than 59 years, while the occurrence of antibodies against BKV was highest in those aged 10–19 years and 20–29 years. This is the first large study to determine the seroprevalence rates for BKV, JCV, and MCPyV polyomaviruses in the general Czech Republic population. ***J. Med. Virol. 86:1560–1568, 2014.***

KEY WORDS: polyomavirus; epidemiology; antibodies; prevalence

INTRODUCTION

Polyomaviruses are small, non-enveloped DNA viruses that have double-stranded circular genomes of approximately 5,000 base pairs in length. Their icosahedral capsids comprise three proteins, VP1, VP2, and VP3. Members of the *Polyomaviridae* family have been identified in mammals and birds [Imperiale and Major, 2007]. Infections with most polyomaviruses, except for murine pneumotropic polyomavirus and avian polyomaviruses, are asymptomatic and a primary infection follows an inapparent latent infection [zur Hausen, 2008]. However, under conditions of immunosuppression, such as those with AIDS, organ transplantation, or leukemia, these viruses may

Grant sponsor: Czech Science Foundation (GAČR); Grant number: P304/10/1511; Grant sponsor: Charles University in Prague; Grant number: UNCE 204013; Grant sponsor: ERDF OPPK; Grant number: CZ.2.16/3.1.00/24001; Grant sponsor: Czech Ministry of Health; Grant number: MZ(00023736)

Conflict of interest: none to declare.

Ethics approval: Serum samples were from serological surveys conducted in the Czech Republic by the National Institute of Public Health with the aim of providing information regarding the immune status of the population and basic data for decisions on possible changes in vaccination strategies. These surveys have been conducted in the Czech Republic since 1971. People enrolled in these surveys were randomly selected in cooperation with regional and district sanitary offices and with general practitioners who cared for adults, adolescents, and children. Blood samples were collected for various urban and rural populations from healthy individuals 6–64 years of age. Blood samples were obtained from subjects with no acute febrile diseases and no signs of immunodeficiency on the day of sampling. All enrolled subjects signed informed consents. For children, informed consent was signed by parents. Blood samples were coded with regard to region, district, physician, and client. All serum samples were aliquoted, registered in the Serum Bank of the Center for Epidemiology and Microbiology, National Institute of Public Health, and kept frozen. The set of samples analyzed in our study included sera that had been collected in 2001. For the purposes of our study, all serum samples were marked by laboratory ID and no identification of a particular person was possible. This study was approved by the Ethics Committee of the Institute of Hematology and Blood Transfusion.

*Correspondence to: Vojtěch Šroller, Department of Experimental Virology, Institute of Hematology and Blood Transfusion, U Nemocnice 1, CZ-128 20, Prague 2, Czech Republic. E-mail: sroller@uhkt.cz

Accepted 9 October 2013

DOI 10.1002/jmv.23841

Published online 8 November 2013 in Wiley Online Library (wileyonlinelibrary.com).

become reactivated in infected individuals and cause disease [Gardner et al., 1984; Berger, 1988; Koljonen et al., 2009]. Some polyomaviruses can also transform cell lines in vitro [Imperiale and Major, 2007].

To date, 10 human polyomaviruses have been identified. BK virus (BKV) and JC virus (JCV), which were co-discovered in 1971, were the first human polyomaviruses to be described [Gardner et al., 1971; Padgett et al., 1971]. With the recent development of novel molecular biology techniques, other human polyomaviruses have been identified, including WUPyV, KIPyV, Merkel cell polyomavirus (MCPyV), Human polyomaviruses 6 and 7 (HPyV6 and HPyV7), Trichodysplasia spinulosa-associated polyomavirus (TSPyV), HPyV9, and Malawi polyomavirus (MWPyV) [Allander et al., 2007; Gaynor et al., 2007; Feng et al., 2008; Schowalter et al., 2010; van der Meijden et al., 2010; Scuda et al., 2011; Siebrasse et al., 2012].

MCPyV polyomavirus was discovered in 2008 and was the first human polyomavirus to be associated with a human cancer, Merkel cell carcinoma (MCC), which is a rare, but aggressive skin malignancy [Lemos and Nghiem, 2007]. MCPyV DNA is consistently found on the skin surfaces of healthy individuals as well as MCC patients [Schowalter et al., 2010; Arora et al., 2012]. Seroprevalence data suggest that MCPyV infection occurs during early childhood and that this virus is ubiquitous among adults [Kean et al., 2009]. These data are consistent with lifelong MCPyV infections of humans.

Both BK and JC polyomaviruses are ubiquitous among humans. After a primary infection during childhood, these viruses can establish lifelong infections in the urinary tract [Heritage et al., 1981; Chesters et al., 1983]. The fecal–oral route of transmission has been suggested, as occasional reactivation results in these viruses to be shed in urine and both viruses are commonly found in urban sewage systems [Bofill-Mas and Girones, 2003]. The reactivation of BK virus in immunosuppressed patients after renal transplantation can result in virus-induced nephropathy and cause renal graft failure [Ramos et al., 2009]. JC virus reactivation in immunosuppressed patients can result in this virus crossing the blood–brain barrier and cause progressive multifocal encephalopathy (PML) [Berger, 2003]. Several drugs based on monoclonal antibody binding to surface molecules (rituximab, natalizumab) were reported to facilitate JCV reactivation and result in PML [Kappos et al., 2007]. JCV and BKV have been shown to have oncogenic potential in animal models. However, the results of studies linking these viruses to human malignancies are controversial [Laghi et al., 1999; Geetha et al., 2002; Kausman et al., 2004].

The seroprevalence of antibodies against these viruses provides important epidemiological information by establishing the distributions of these viruses in human populations. We sought to determine the frequency of occurrence of antibodies against MCPyV, JCV, and BKV in the general Czech Republic population. To our knowledge, this is the first study of this kind to be done in the Czech Republic, as well as in Central and Eastern Europe.

MATERIALS AND METHODS

Study Subjects

Serum samples were from serological surveys conducted in the Czech Republic by the National Institute of Public Health, Prague, for multi-purpose immunological surveys. People enrolled in these surveys were randomly selected in cooperation with regional and district public health offices and general practitioners who cared for adults, adolescents, and children. Blood samples were collected for various urban and rural populations from healthy individuals aged 1–64 years who had no acute febrile diseases and no signs of immunodeficiency on the day of sampling. Each practitioner was provided with a list of blood samples to be obtained based on subjects' gender and age. All subjects who were enrolled signed informed consent forms. Children's parents signed the informed consent form on their behalf. All serum samples were aliquoted, registered in the Serum Bank of the National Institute of Public Health, and kept frozen at −20°C [Kriz, 2003]. The set of serum samples analyzed in our study were collected in 2001 and included a total of 991 people aged 6–64 years.

Animal Immunizations

Polyclonal VP1 MCPyV specific antibodies were prepared in mice that were immunized with a DNA vaccine. Plasmid used for immunization was constructed by PCR amplification of the MCPyV VP1 gene (codon modified, pwM, Addgene plasmid #22515) [Tolstov et al., 2009] using Pfu polymerase and the primers VP1-IK-Sal 5′-ATAAGTCGACAC-CATGGCCCCGAAGCG-3′ and VP1-T-Bgl 5′-TAATA-GATCTTCATAGCTCCTGCGTCTGT-3′. The MCPyV VP1 gene was inserted into pCR®-Blunt II-TOPO® (Invitrogen, Carlsbad, CA and its identity with the original gene was confirmed by sequencing. The VP1 gene was then transferred into a pBSC plasmid [Smahel et al., 2001] using *Sal*I/*Xho*I and *Bgl*II restriction sites. The resulting plasmid was designated pBSC-VP1-MCPyV. Mice of strain ICR (CD1) were immunized with three doses of pBSC-VP1-MCPyV DNA administered at two-week intervals (1 μg each dose) using the biolistic method [Smahel et al., 2001]. Mice were maintained under standard conditions at the Center for Experimental Biomodels, Charles University, Prague. Serum samples were collected one week after the last immunization. These experiments complied with Acts Nos. 246/92 and 77/2004 on animal protection against cruelty and Decree No. 207/2004 of the Ministry of Agriculture of the Czech Republic on the care and use of experimental

animals. The DNA vaccine induced strong antibody responses against the viral protein VP1. All serum samples collected from immunized mice were reactive to MCPyV VLPs in an ELISA. The majority of mouse sera also reacted with MCPyV VLPs on Western blots (data not shown). Serum samples from mice immunized with empty pBSC plasmids were used as a negative control.

Polyclonal antibodies specific for BKV VP1 and JCV VP1 were prepared from the sera of mice immunized with purified VLPs. Mice of strain C57BL/6 were immunized by subcutaneous administration of three doses of VLPs (100 μg/dose) with Freund's complete adjuvant (first dose) or Freund's incomplete adjuvant (second and third doses). Serum samples were collected 2 weeks after administering the last dose.

Production and Purification of Polyomavirus Virus-Like Particles (VLPs)

The VP1 genes of human BKV, JCV, or MCPyV polyomaviruses were inserted into recombinant baculovirus vectors. The BKV VP1 gene corresponding to the Gardner strain, genotype Ia (GenBank accession number: JF894228) encoded for a VP1 protein 362 amino acids in length. The JCV VP1 gene corresponding to the Mad1 strain (GenBank accession number: J02226) encoded for a VP1 protein 354 amino acids in length. The MCPyV VP1 gene was derived from strain 339, codon modified for expression in human cell lines (Gen Bank accession number: FJ548568) and encoded for a VP1 protein 423 amino acids in length.

Plasmid pBluescript II KS(+)-BK containing the full-length BKV genome was kindly provided by K. Dorries [Vallbracht et al., 1993]. A VP1 gene was amplified using the primers BKV-VP1-I-SmaI 5′-CCAGCACCCGGGATGGCCCCAACCAAAAGA-3′ and BKV-VP1-II-PstI 5′-CTCGTACTGCAGTTAAAGCATT TTGGTTTGCAA-3′. An amplified VP1 gene was digested with *Sma*I and *Pst*I and inserted into a pFactBac™ Dual plasmid (Invitrogen) digested with *Stu*I and *Pst*I downstream of the polyhedrin promoter. The resulting plasmid was designated pBac-VP1-BKV.

Plasmid pBRJCV-MAD-1 containing the full-length genome of JCV, strain Mad1 cloned into a pBR322 *Eco*RI site was kindly provided by Prof. J. S. Butel (Baylor College of Medicine, Houston, TX). The JCV VP1 gene in this plasmid was divided into two fragments that were separated by a vector sequence bordered by an *Eco*RI site. Both VP1 gene fragments were PCR-amplified using Vent polymerase and the primers JCV-I-BamHI 5'-GAAAGAGGATCCATGGC CCCAACAAAAAGAAAAGGA-3' and JCV-II-EcoRI 5'-GATGATGAATTCTGGCCACACTGTAACAAG-3' or JCV-III-EcoRI 5'-GCTGCTGAATTCCACTACCCAATC TAAATGAGG-3' and JCV-IV-HindIII 5'-GATGCCAA GCTTTTACAGCATTTTTGTCTGCAACTGCAACTGT CC-3'. Both of the VP1 gene fragments were joined through an *Eco*RI site and the full-length VP1 gene was subsequently inserted into a baculovirus transfer vector, pFactBac™ Dual, under the control of the polyhedrin promoter using *Bam*HI and *Hin*dIII restriction sites. The accuracy of an inserted gene was confirmed by sequencing. The resulting plasmid was designated pBac-VP1-JCV.

Codon modified MCPyV VP1 gene in plasmid pwM (Addgene plasmid #22515) was obtained from the Addgene exchange collection (Cambridge, MA). The MCPyV VP1 gene was amplified by PCR using Pfu polymerase and the primers VP1-I-Sal 5'-ATAAGTC-GACATGGCCCCGAAGCGCAAG-3' and VP1-T-Xba 5'-ATAATCTAGATCATAGCTCCTGCGTCTGT-3'. A MCPyV VP1 gene was inserted into pCR®—Blunt II-TOPO® (Invitrogen) and its identity with the original gene was confirmed by sequencing. The VP1 gene was then transferred into a pFactBac™ Dual plasmid under control of the polyhedrin promoter using *SalI* and *XbaI* restriction sites. The resulting plasmid was designated pBac-VP1-MCPyV.

Recombinant baculoviruses that expressed a VP1 gene were prepared separately according to the Bac-to-Bac Baculovirus Expression System manual (Invitrogen). Donor plasmids pBac-VP1-MCPyV, pBac-VP1-BKV, or pBac-VP1-JCV were transfected into the bacmid containing DH10Bac™ *Escherichia coli* strain. Colonies with the recombinant bacmids were selected, bacmid DNA was purified, and then used to transfect Sf9 insect cells. Recombinant baculoviruses were plaque purified.

MCPyV, JCV, and BKV VLPs were prepared using previously described protocols [Hrbacek et al., 2011]. Briefly, SF-9 cells were grown to a density of 1×10^6 cells/ml in TNM-FH insect medium (Sigma) supplemented with 10% FBS (Gibco) and infected at an MOI of 10 with BKV-VP1, JCV-VP1, or MCPyV-VP1 baculoviruses. Cells were harvested at 72 h post-infection, pelleted by centrifugation (430*g*, 10 min, 4°C), and then frozen at −20°C. Thawed pellets of about 2×10^9 cells were resuspended in 20 ml of extraction buffer (100 mM $MgCl_2$, 50 mM $CaCl_2$, 150 mM NaCl, 0.01% Triton X-100, and 20 mM Hepes, pH 7.4), disrupted by sonication (3×30 sec on ice), and cell debris was pelleted at 46,328*g* at 4°C for 20 min. The pellet was resuspended in 20 ml of fresh extraction buffer, sonicated, and cell debris was pelleted as above. Both supernatant fractions that contained VLPs were combined and CsCl was added to final concentration of 0.3 g/ml. After centrifugation (195,883*g*, 18°C, 20 h), bands appearing at the position of the buoyant density of empty capsids were collected. These samples were dialyzed against PBS, loaded on a CsCl step gradient (36%–30.5%–16%), and then centrifuged (234,116*g*, 18°C, 4 h). The layer at the 36–30.5% interface containing VLPs was collected. Protein concentration was determined with a NanoDrop spectrophotometer. The sizes of purified VP1 proteins were confirmed by SDS–PAGE stained with Blue BANDit™ (Amresco LLC, Solon, OH). The

identity of VP1 capsid proteins was confirmed by Western blotting using specific antibodies. The integrity of VLPs of individual polyomaviruses was verified by electron microscopy. VLP samples were applied to copper 200-mesh grids covered with parlodion/carbon, stained with 2% phosphotungstic acid, pH 7.3, and examined with a JEOL JEM-1011 electron microscope.

VLP ELISA

VP1 VLP-based ELISAs were prepared in-house as described previously [Hrbacek et al., 2011]. Briefly, ELISA plates were coated with purified MCPyV, BKV, or JCV VLPs, blocked with bovine serum albumin, after which a diluted serum sample (1:25) was incubated in duplicate. Bound antibodies were detected using donkey, anti-human IgG linked to horseradish peroxidase. The reaction was visualized by *o*-phenylenediamine and optical densities were read at 492 and 630 nm. Control sera known to be positive and negative were also tested with each ELISA plate. An optical density cut-off (CO) value was determined separately for each antigen/plate as the mean of the negative control plus two standard deviations (2SD). An ELISA result was the ratio of the absorbance of a sample to the respective CO value (OD index). To confirm these results, samples with values of 10% above the CO value and about ¼ of all serum samples were retested. Only samples with repeat positive results were considered reactive.

Statistical Analysis

Statistical analysis used GraphPad Instat software (V.3.00). Comparisons of two groups were based on a normal approximation for the binomial distribution. A Chi-square test with Yate's correction was used to calculate odds ratios (ORs) and 95% confidence intervals (CIs). Non-parametric Spearman's correlation coefficients (r) were determined to compare OD values obtained from two assays. All statistical tests were two-tailed and *P*-values of <0.05 were considered significant.

RESULTS

Characterization of VLPs

VP1 proteins that were produced in insect cells spontaneously formed VLPs, which were subsequently purified on CsCl gradients. Purified VLPs analyzed by SDS-PAGE were in major bands of mobilities that were predicted based on the respective VP1 protein lengths. The MCPyV VP1 protein was in a band of $\approx$ 44 kDa, and both BKV and JCV VP1 proteins were in bands of $\approx$ 40 kDa (data not shown). Purified VLPs of all three polyomaviruses that corresponded to their VP1 proteins were completely assembled into spherical capsid-like structures of $\approx$ 45 nm in diameter, as observed with electron microscopy (data not shown).

MCPyV, BKV, and JCV Seroreactivity Rates in the General Czech Republic Population

The presence of serum antibodies specific for the MCPyV, BKV, and JCV polyomaviruses was tested using ELISAs. Overall, among a total of 991 subjects, serum antibodies against MCPyV, BKV, and JCV were found in 63.4%, 68.7%, and 56.6%, respectively, of these subjects (Table I). The seroprevalence rates for men and women were not significantly different. Serum antibodies against MCPyV were found in 64.2% of men and 62.5% of women (OR = 1.0; 95% CI: 0.8–1.2; $P = 0.827$), serum antibodies against BKV were found in 67.1% of men and 70.0% of women (OR = 1.0; 95% CI: 0.8–1.2; $P = 0.666$), and serum antibodies against JCV were found in 57.8% of men and 55.4% of women (OR = 1.0; 95% CI: 0.8–1.2; $P = 0.736$). Comparable seroreactivity results for each polyomavirus for men and women were also found among different age groups (data not shown).

We next tested the specificity of the VLP based ELISAs for the respective VP1 proteins. Possible associations between seroresponses to the three polyomaviruses were tested in a subset of 50 serum samples selected at random for those aged 30–39 years for which the seroprevalence rate for all three viruses was >50%. No association was found between the MCPyV and BKV seroresponses in this subgroup

TABLE I. Seroprevalence Rates for Merkel Cell Polyomavirus (MCPyV), BK Polyomavirus (BKV), and JC Polyomavirus (JCV) for Different Age Groups and Among Men and Women

Age group Gender	Number tested	MCPyV seropositive (%)	BKV seropositive (%)	JCV seropositive (%)
6–9	107	63 (58.9)	78 (72.9)	51 (47.7)
10–19	219	109 (49.8)	175 (79.9)	105 (47.9)
20–29	177	107 (60.5)	141 (79.7)	94 (53.1)
30–39	139	96 (69.1)	90 (64.7)	74 (53.2)
40–49	141	105 (74.5)	79 (56.0)	96 (68.1)
50–59	138	95 (68.8)	79 (57.2)	88 (63.8)
>59	70	53 (75.7)	39 (55.7)	53 (75.7)
Men	495	318 (64.2)	332 (67.1)	286 (57.8)
Women	496	310 (62.5)	349 (70.0)	275 (55.4)
Total	991	628 (63.4)	681 (68.7)	561 (56.6)

(r = 0.21; $P = 0.14$; Fig. 1A). Similarly, no associations were found when comparing MCPyV and JCV seroresponses (r = 0.08; $P = 0.57$; Fig. 1B) and BKV and JCV seroresponses (r = 0.11; $P = 0.44$; Fig. 1C).

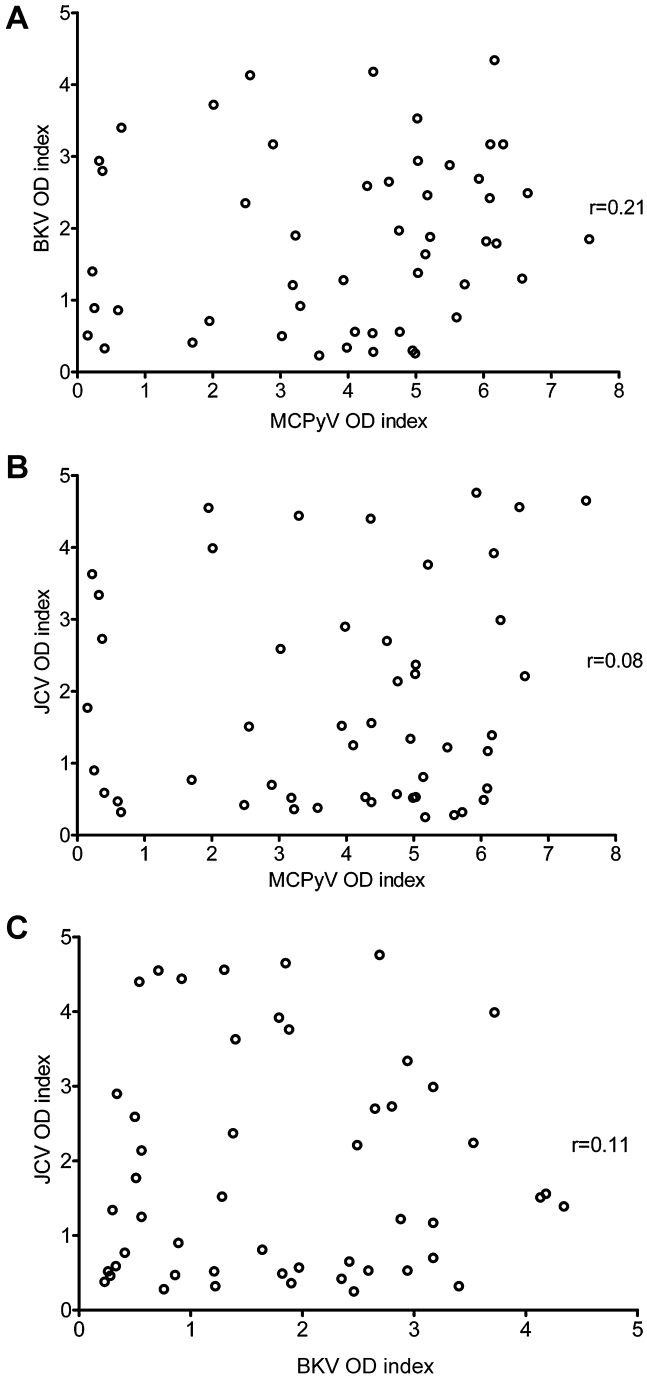

Fig. 1. Cross-reactivity between Merkel cell polyomavirus (MCPyV), BK polyomavirus (BKV), and JC polyomavirus (JCV) VP1 capsid proteins. Correlations between optical density (OD) indices for (**A**) MCPyV and BKV, (**B**) MCPyV and JCV, and (**C**) BKV and JCV are shown for 50 randomly selected serum samples from the age group of 30–39 years. Each circle represents one serum sample; correlation coefficient for each graph (r) is shown.

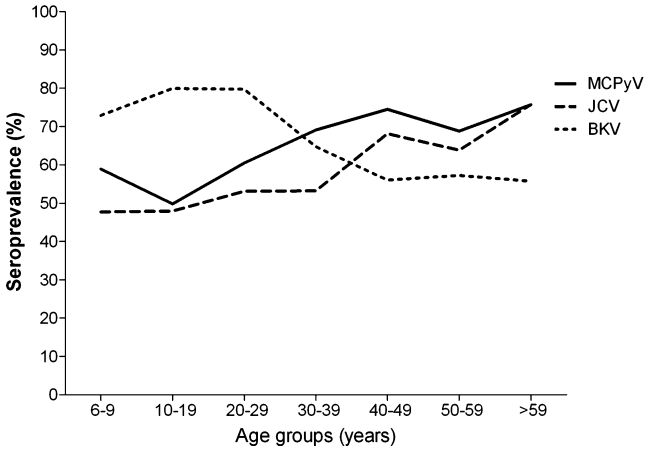

Fig. 2. Age-associated seroprevalence rates of Merkel cell polyomavirus (MCPyV), BK polyomavirus (BKV), and JC polyomavirus (JCV) among 991 serum samples obtained from the general Czech Republic population. Serum samples were diluted 1:25 and assayed using VLP-based ELISAs. The study population was divided into seven age groups.

Age-Associated Seroprevalence Rates

The seroprevalence rates for the group aged 6–9 years (Fig. 2), which included the youngest children in this study, were considerably high. These were 58.9%, 72.9%, and 47.7%, respectively, for MCPyV, BKV, and JCV. With increasing age, MCPyV seroprevalence rates also increased; the highest (72.9%) was found in the group that included those who were older than 59 years (oldest group in this study). The same trend was found for JCV; the highest seroprevalence rate for JCV (75.7%) was also found in the oldest age group (those older than 59 years). In contrast, the seroprevalence rates for BKV were the highest among those aged 10–19 years (79.9%) and 20–29 years (79.7%). With increasing age, BKV seroprevalence rates decreased; the lowest seroprevalence was found among those older than 59 years (55.7%).

Figure 3 shows the levels of specific antibodies in seropositive samples (OD indices for specific polyomaviruses in serum) by age groups. For MCPyV antibodies, the medians of the OD indices of positive sera increased with age due to fewer serum samples with lower OD index values (Fig. 3A). By comparison, the medians of BKV OD indices decreased with increased age because of fewer serum samples with high OD index values (Fig. 3B). For JCV, the medians of OD indices remained comparable across the different age groups (Fig. 3C).

DISCUSSION

In this study, we determined the seroprevalence rates for the polyomavirus MCPyV and the first two human polyomaviruses that were discovered, BKV and JCV, in the general population of the Czech Republic. Seropositivity was determined using ELISAs based on VLPs comprising the respective VP1

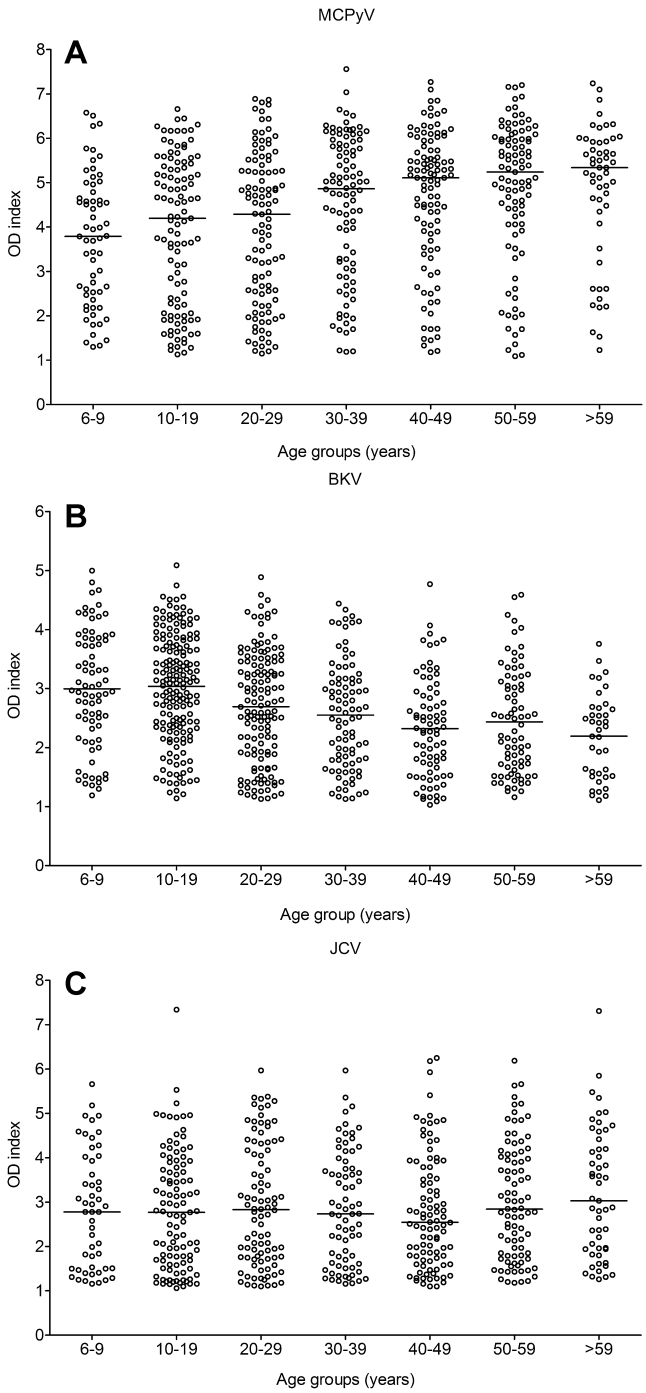

Fig. 3. Optical density (OD) indices of positive sera in age groups using VLP-based ELISAs. An OD index is the ratio between an absorbance reading and a cut-off value. Each open circle represents one serum sample, and the median of each age group is indicated by a horizontal line. Results are OD indices of sera assayed using (**A**) Merkel cell polyomavirus (MCPyV) VLPs, (**B**) BK polyomavirus (BKV) VLPs, and (**C**) JC polyomavirus (JCV) VLPs.

proteins prepared with a baculovirus system. Ours was a large study population to evaluate the general population (N = 991) and included both pediatric (N = 326) and adult subjects (N = 665). To our knowledge, information of this type has not been previously reported for Central and Eastern Europe.

Historically, hemagglutinin inhibition assays were used to evaluate the seroprevalence rates of human polyomaviruses [Taguchi et al., 1982; Hamilton et al., 2000]. Currently, several types of assays are used to detect antibodies specific for human polyomaviruses, including direct ELISAs or multiplex immunoassays with VP1 capsomers expressed in bacteria or VLPs expressed in baculoviruses. Polyomavirus neutralizing antibodies can be determined with in vitro neutralizing assays for which specific neutralizing antibodies block the entry of virions or pseudovirions carrying a reporter genes into target cells [Pastrana et al., 2009]. However, these assays are time consuming and, thus, are not suitable for large epidemiological studies. Further, the seroprevalence data obtained using these assays may not be directly comparable.

In this study, the direct ELISA tests with purified VLPs as antigens could identify neutralizing and non-neutralizing polyclonal antibodies directed against various antigenic epitopes on the surfaces of virus-like particles. ELISAs with VP1 capsomers detect all VP1-reactive antibodies. However, they may miss some antibodies that are specific for conformational epitopes on the surfaces of virions/VLPs [Schiller and Lowy, 2009].

There were some other factors that could have affected the observed seroprevalence results in this population, such as the selection of the study cohort and the demographic characteristics of the enrolled subjects. The serum samples analyzed in this study were originally collected within the scope of immunological surveys organized in the Czech Republic. Thus, the only information available was for age and gender.

A high MCPyV seroprevalence rate of 58.9% was found in children aged 6–9 years. In this age group, the BKV seroprevalence rate was 72.9% and the JCV seroprevalence rate was 47.7%. The mode of transmission for MCPyV is not known and the cellular tropism of MCPyV remains unclear. MCPyV DNA, most likely within virions, is repeatedly detected on the skin surfaces of healthy individuals. For infectious entry into cells, MCPyV sequentially utilizes glycosaminoglycans and sialylated glycans [Schowalter et al., 2011]. Interestingly, the same strategy of infectious entry is used by human papillomaviruses that are exclusively tropic for keratinocytes, which form the epidermal layers of the skin and the mucosa. This observation supports MCPyV cutaneous transmission.

However, MCPyV DNA can also be detected in nasopharyngeal aspirates, tonsil tissues, the digestive system, saliva, and urban sewage systems. Thus, it may also be spread by fecal-oral transmission or a respiratory route [Bialasiewicz et al., 2009; Kantola et al., 2009; Bofill-Mas et al., 2010; Loyo et al., 2010]. Vertical transmission from a mother to her fetus is

not likely due to the absence of viral DNA in fetal autopsy samples [Sadeghi et al., 2010].

No associations were found between the presence of antibodies against BKV, JCV, and MCPyV and gender. These results correspond to those of other studies that reported little variation in the seroprevalence rates between men and women [Knowles et al., 2003; Antonsson et al., 2010]. Comparable high MCPyV seroprevalence rates of about 50% in children were found in other studies, which reported 35–50% seropositivity in young people [Kean et al., 2009; Tolstov et al., 2009; Chen et al., 2011; Viscidi et al., 2011].

For adults older than 20 years of age, there was a trend for increased MCPyV seroprevalence with increased age. MCPyV seroprevalence ranged from 60.5% among those aged 20–29 years to 75.7% among those older than 59 years. These results were consistent with those of other studies in which the reported MCPyV seroprevalence in adults ranged between 46% and 88%. This increase in MCPyV seroprevalence among adults is very likely caused by seroconversion after asymptomatic primary infections [Tolstov et al., 2011].

In addition to the increased seroprevalence among our older age groups, increased levels of MCPyV antibodies (OD indices) in older individuals were also found. In a retrospective study, MCPyV antibodies were detectable up to 25 years after seroconversion. In addition, in 2/3 of those subjects, the levels of MCPyV antibodies slowly increased over time [Tolstov et al., 2011]. MCPyV very likely causes chronic, lifelong infections due to host immune systems being continuously stimulated by viral antigens.

It was found that BKV seropositivity was very common among children, which reached a peak of 79.8% among those aged 10–29 years, and then slowly declined in older aged groups. This finding was in agreement with previous reports in which peak seroprevalence rates ranged from 65% to 95% and with similar age-associated dynamics in terms of the antibodies detected [Knowles et al., 2003; Stolt et al., 2003; Viscidi et al., 2011]. We also observed that a decline in BKV seropositivity was reflected by decreased antibody levels. This phenomenon suggests that BKV transmission is less common later in life and that antigenic stimulation is low.

In the present study, the curve for age-associated JCV seroprevalence was similar to that for MCPyV with low seropositivity of 47.7% in young children, and then increasing with increased age, with 75.7% in the oldest age group. These dynamics are consistent with previous reports in which the highest seropositivity rates (up to 80%) were observed in the oldest age groups [Egli et al., 2009; Kantola et al., 2009; Viscidi et al., 2011]. JCV antibody levels, however, remained comparable across the different age groups. This suggests continuous JCV transmission throughout life. The JC virus is found more frequently in the urine of healthy individuals than is BKV, which suggests more frequent JCV reactivation [Imperiale and Major, 2007]. This JCV reactivation may counteract antibody waning, which was seen in older age groups for BKV antibodies.

Serological cross-reactivity among viruses within the same family can affect the observed seroreactivity. Using competitive inhibition assays, no cross-reactivity was reported among MCPyV, JCV, and BKV VLPs or pseudovirions [Viscidi and Clayman, 2006; Tolstov et al., 2009]. The most closely related VP1 proteins are for BKV and JCV (pair-wise amino acid sequence identity of 78%; NCBI Blast algorithm). BKV/MCPyV and JCV/MCPyV are more distantly related (pair-wise amino acid sequence identities of 48% and 49%, respectively). Cross-reactivity has been observed between HPyV9 and LPyV VLPs; however, their VP1 amino acid sequences are more closely related (87%) [Scuda et al., 2011; Nicol et al., 2012]. In the present study, the specificity of seroreactivity was analyzed using correlation analyses. No evidence of seroreactivity correlations was found among these three viruses. Yet, cross-reactivity with other known or as yet undiscovered human polyomaviruses cannot be excluded.

MCPyV very likely plays a role in the etiology of human Merkel cell carcinoma. Several experimental vaccines have been designed to prevent MCPyV infections, which could consequently limit MCC prevalence [Gomez et al., 2012; Zeng et al., 2012]. Seroepidemiological analyses provide important information on virus epidemiology in different geographical regions and help to identify those populations that would benefit from vaccinations.

ACKNOWLEDGMENTS

We thank Janet Butel for the generous gift of the pBRJCV-MAD-1 plasmid, Christopher Buck for the pwM plasmid deposited in the Addgene collection, and Veronika Hrušková and Marianna Papová for preparing BKV VLPs.

REFERENCES

Allander T, Andreasson K, Gupta S, Bjerkner A, Bogdanovic G, Persson MA, Dalianis T, Ramqvist T, Andersson B. 2007. Identification of a third human polyomavirus. J Virol 81:4130–4136.

Antonsson A, Green AC, Mallitt KA, O'Rourke PK, Pawlita M, Waterboer T, Neale RE. 2010. Prevalence and stability of antibodies to the BK and JC polyomaviruses: A long-term longitudinal study of Australians. J Gen Virol 91:1849–1853.

Arora R, Chang Y, Moore PS. 2012. MCV and Merkel cell carcinoma: A molecular success story. Curr Opin Virol 2:489–498.

Berger JR. 1988. The neurological complications of HIV infection. Acta Neurol Scand Suppl 116:40–76.

Berger JR. 2003. Progressive multifocal leukoencephalopathy in acquired immunodeficiency syndrome: Explaining the high incidence and disproportionate frequency of the illness relative to other immunosuppressive conditions. J Neurovirol 9:38–41.

Bialasiewicz S, Lambert SB, Whiley DM, Nissen MD, Sloots TP. 2009. Merkel cell polyomavirus DNA in respiratory specimens from children and adults. Emerg Infect Dis 15:492–494.

Bofill-Mas S, Girones R. 2003. Role of the environment in the transmission of JC virus. J Neurovirol 9:54–58.

Bofill-Mas S, Rodriguez-Manzano J, Calgua B, Carratala A, Girones R. 2010. Newly described human polyomaviruses Merkel cell, KI and WU are present in urban sewage and may represent potential environmental contaminants. Virol J 7:141–144.

Chen T, Hedman L, Mattila PS, Jartti T, Ruuskanen O, Soderlund-Venermo M, Hedman K. 2011. Serological evidence of Merkel cell polyomavirus primary infections in childhood. J Clin Virol 50:125–129.

Chesters PM, Heritage J, McCance DJ. 1983. Persistence of DNA sequences of BK virus and JC virus in normal human tissues and in diseased tissues. J Infect Dis 147:676–684.

Egli A, Infanti L, Dumoulin A, Buser A, Samaridis J, Stebler C, Gosert R, Hirsch HH. 2009. Prevalence of polyomavirus BK and JC infection and replication in 400 healthy blood donors. J Infect Dis 199:837–846.

Feng H, Shuda M, Chang Y, Moore PS. 2008. Clonal integration of a polyomavirus in human Merkel cell carcinoma. Science 319:1096–1100.

Gardner SD, Field AM, Coleman DV, Hulme B. 1971. New human papovavirus (B.K.) isolated from urine after renal transplantation. Lancet 1:1253–1257.

Gardner SD, MacKenzie EF, Smith C, Porter AA. 1984. Prospective study of the human polyomaviruses BK and JC and cytomegalovirus in renal transplant recipients. J Clin Pathol 37:578–586.

Gaynor AM, Nissen MD, Whiley DM, Mackay IM, Lambert SB, Wu G, Brennan DC, Storch GA, Sloots TP, Wang D. 2007. Identification of a novel polyomavirus from patients with acute respiratory tract infections. PLoS Pathogens 3:e64, 595–604.

Geetha D, Tong BC, Racusen L, Markowitz JS, Westra WH. 2002. Bladder carcinoma in a transplant recipient: Evidence to implicate the BK human polyomavirus as a causal transforming agent. Transplantation 73:1933–1936.

Gomez BP, Wang C, Viscidi RP, Peng S, He L, Wu TC, Hung CF. 2012. Strategy for eliciting antigen-specific CD8+ T cell-mediated immune response against a cryptic CTL epitope of merkel cell polyomavirus large T antigen. Cell Biosci 2:36–45.

Hamilton RS, Gravell M, Major EO. 2000. Comparison of antibody titers determined by hemagglutination inhibition and enzyme immunoassay for JC virus and BK virus. J Clin Microbiol 38:105–109.

Heritage J, Chesters PM, McCance DJ. 1981. The persistence of papovavirus BK DNA sequences in normal human renal tissue. J Med Virol 8:143–150.

Hrbacek J, Urban M, Hamsikova E, Tachezy R, Eis V, Brabec M, Heracek J. 2011. Serum antibodies against genitourinary infectious agents in prostate cancer and benign prostate hyperplasia patients: A case-control study. BMC Cancer 11:53–62.

Imperiale MJ, Major EO. 2007. Polyomaviridae. In: Knipe DM, Howley PM, editors-in-chief: Fields virology, 5th edition. Philadelphia, PA, USA: Lippincott Williams &Wilkins, pp. 2263–2298.

Kantola K, Sadeghi M, Lahtinen A, Koskenvuo M, Aaltonen LM, Mottonen M, Rahiala J, Saarinen-Pihkala U, Riikonen P, Jartti T, Ruuskanen O, Soderlund-Venermo M, Hedman K. 2009. Merkel cell polyomavirus DNA in tumor-free tonsillar tissues and upper respiratory tract samples: Implications for respiratory transmission and latency. J Clin Virol 45:292–295.

Kappos L, Bates D, Hartung HP, Havrdova E, Miller D, Polman CH, Ravnborg M, Hauser SL, Rudick RA, Weiner HL, O'Connor PW, King J, Radue EW, Yousry T, Major EO, Clifford DB. 2007. Natalizumab treatment for multiple sclerosis: Recommendations for patient selection and monitoring. Lancet Neurol 6:431–441.

Kausman JY, Somers GR, Francis DM, Jones CL. 2004. Association of renal adenocarcinoma and BK virus nephropathy post transplantation. Pediatr Nephrol 19:459–462.

Kean JM, Rao S, Wang M, Garcea RL. 2009. Seroepidemiology of human polyomaviruses. PLoS Pathog 5:e1000363, 1–10.

Knowles WA, Pipkin P, Andrews N, Vyse A, Minor P, Brown DW, Miller E. 2003. Population-based study of antibody to the human polyomaviruses BKV and JCV and the simian polyomavirus SV40. J Med Virol 71:115–123.

Koljonen V, Kukko H, Pukkala E, Sankila R, Bohling T, Tukiainen E, Sihto H, Joensuu H. 2009. Chronic lymphocytic leukaemia patients have a high risk of Merkel-cell polyomavirus DNA-positive Merkel-cell carcinoma. Br J Cancer 101:1444–1447.

Kriz B. 2003. Multipurpose serological survey–its philosophy and objectives in the Czech Republic. Cent Eur J Public Health 11: S4–S6.

Laghi L, Randolph AE, Chauhan DP, Marra G, Major EO, Neel JV, Boland CR. 1999. JC virus DNA is present in the mucosa of the human colon and in colorectal cancers. Proc Natl Acad Sci USA 96:7484–7489.

Lemos B, Nghiem P. 2007. Merkel cell carcinoma: More deaths but still no pathway to blame. J Invest Dermatol 127:2100–2103.

Loyo M, Guerrero-Preston R, Brait M, Hoque MO, Chuang A, Kim MS, Sharma R, Liegeois NJ, Koch WM, Califano JA, Westra WH, Sidransky D. 2010. Quantitative detection of Merkel cell virus in human tissues and possible mode of transmission. Int J Cancer 126:2991–2996.

Nicol JT, Touze A, Robinot R, Arnold F, Mazzoni E, Tognon M, Coursaget P. 2012. Seroprevalence and cross-reactivity of human polyomavirus 9. Emerg Infect Dis 18:1329–1332.

Padgett BL, Walker DL, ZuRhein GM, Eckroade RJ, Dessel BH. 1971. Cultivation of papova-like virus from human brain with progressive multifocal leucoencephalopathy. Lancet 1:1257–1260.

Pastrana DV, Tolstov YL, Becker JC, Moore PS, Chang Y, Buck CB. 2009. Quantitation of human seroresponsiveness to Merkel cell polyomavirus. PLoS Pathogens 5:e1000578.

Ramos E, Drachenberg CB, Wali R, Hirsch HH. 2009. The decade of polyomavirus BK-associated nephropathy: State of affairs. Transplantation 87:621–630.

Sadeghi M, Riipinen A, Vaisanen E, Chen T, Kantola K, Surcel HM, Karikoski R, Taskinen H, Soderlund-Venermo M, Hedman K. 2010. Newly discovered KI, WU, and Merkel cell polyomaviruses: No evidence of mother-to-fetus transmission. Virol J 7:251–255.

Schiller JT, Lowy DR. 2009. Immunogenicity testing in human papillomavirus virus-like-particle vaccine trials. J Infect Dis 200:166–171.

Schowalter RM, Pastrana DV, Pumphrey KA, Moyer AL, Buck CB. 2010. Merkel cell polyomavirus and two previously unknown polyomaviruses are chronically shed from human skin. Cell Host Microbe 7:509–515.

Schowalter RM, Pastrana DV, Buck CB. 2011. Glycosaminoglycans and sialylated glycans sequentially facilitate Merkel cell polyomavirus infectious entry. PLoS Pathogens 7:e1002161.

Scuda N, Hofmann J, Calvignac-Spencer S, Ruprecht K, Liman P, Kuhn J, Hengel H, Ehlers B. 2011. A novel human polyomavirus closely related to the african green monkey-derived lymphotropic polyomavirus. J Virol 85:4586–4590.

Siebrasse EA, Reyes A, Lim ES, Zhao G, Mkakosya RS, Manary MJ, Gordon JI, Wang D. 2012. Identification of MW polyomavirus, a novel polyomavirus in human stool. J Virol 86:10321–10326.

Smahel M, Sima P, Ludvikova V, Vonka V. 2001. Modified HPV16 E7 Genes as DNA Vaccine against E7-Containing Oncogenic Cells. Virology 281:231–238.

Stolt A, Sasnauskas K, Koskela P, Lehtinen M, Dillner J. 2003. Seroepidemiology of the human polyomaviruses. J Gen Virol 84:1499–1504.

Taguchi F, Kajioka J, Miyamura T. 1982. Prevalence rate and age of acquisition of antibodies against JC virus and BK virus in human sera. Microbiol Immunol 26:1057–1064.

Tolstov YL, Pastrana DV, Feng H, Becker JC, Jenkins FJ, Moschos S, Chang Y, Buck CB, Moore PS. 2009. Human Merkel cell polyomavirus infection II. MCV is a common human infection that can be detected by conformational capsid epitope immunoassays. Int J Cancer 125:1250–1256.

Tolstov YL, Knauer A, Chen JG, Kensler TW, Kingsley LA, Moore PS, Chang Y. 2011. Asymptomatic primary Merkel cell polyomavirus infection among adults. Emerg Infect Dis 17:1371–1380.

Vallbracht A, Lohler J, Gossmann J, Gluck T, Petersen D, Gerth HJ, Gencic M, Dorries K. 1993. Disseminated BK type polyomavirus infection in an AIDS patient associated with central nervous system disease. Am J Pathol 143:29–39.

van der Meijden E, Janssens RW, Lauber C, Bouwes Bavinck JN, Gorbalenya AE, Feltkamp MC. 2010. Discovery of a new human polyomavirus associated with trichodysplasia spinulosa in an immunocompromized patient. PLoS Pathogens 6:e1001024.

Viscidi RP, Clayman B. 2006. Serological cross reactivity between polyomavirus capsids. Adv Exp Med Biol 577:73–84.

Viscidi RP, Rollison DE, Sondak VK, Silver B, Messina JL, Giuliano AR, Fulp W, Ajidahun A, Rivanera D. 2011. Age-specific seroprevalence of Merkel cell polyomavirus, BK virus, and JC virus. Clin Vaccine Immunol 18:1737–1743.

Zeng Q, Gomez BP, Viscidi RP, Peng S, He L, Ma B, Wu TC, Hung CF. 2012. Development of a DNA vaccine targeting Merkel cell polyomavirus. Vaccine 30:1322–1329.

zur Hausen H. 2008. Novel human polyomaviruses-re-emergence of a well known virus family as possible human carcinogens Int J Cancer 123:247–250.

Virology 450-451 (2014) 122–131

Contents lists available at ScienceDirect

Virology

journal homepage: www.elsevier.com/locate/yviro

The encapsidation of polyomavirus is not defined by a sequence-specific encapsidation signal

Hana Španielová *, Martin Fraiberk, Jiřina Suchanová, Jakub Soukup, Jitka Forstová

Department of Genetics and Microbiology, Faculty of Science, Charles University in Prague, Viničná 5, 128 44 Prague 2, Czech Republic

ARTICLE INFO

Article history:
Received 3 September 2013
Returned to author for revisions
25 September 2013
Accepted 10 December 2013
Available online 31 December 2013

Keywords:
Mouse polyomavirus
Encapsidation signal
Assembly
Pseudovirion
Packaging

ABSTRACT

Mouse polyomavirus (MPyV) is considered a potential tool for the application of gene therapy; however, the current knowledge of the encapsulation of DNA into virions is vague. We used a series of assays based on the encapsidation of a reporter vector into MPyV pseudovirions to identify putative *cis*-acting elements that are involved in DNA encapsidation. None of the sequences that were derived from MPyV have been shown to solely enhance the encapsidation of a reporter vector in the assay. The frequency of encapsidation strongly correlated with the total intracellular amount of the vector after transfection. The encapsidation of target DNA into the pseudovirions was shown to be non-specific, and the packaging of non-replicated DNA was observed. We propose that the actual concentration of target DNA at the sites of virion formation is the primary factor that determines its selection for encapsidation.

Introduction

Mouse polyomavirus (MPyV) and simian virus 40 (SV40) have historically served as molecular biology models and are considered potential gene therapy tools in anticancer therapy. MPyV seems to be superior for this type of application due to the absence of a pre-existing immunity in the human population. Both viruses are members of *Polyomaviridae*, which is a family of small, non-enveloped DNA viruses. The approximately 5.3-kb genome of MPyV circular dsDNA encodes three early regulatory proteins, designated small (ST), middle (MT) and large (LT) tumor antigens, and three late structural proteins, the viral proteins VP1, VP2 and VP3. Viral DNA is assembled with histones of cellular origin (except H1) in the form of a minichromosome and is encapsidated into an icosahedral capsid approximately 45 nm in diameter. The capsid consists of 72 capsomers composed of five monomers of the major capsid protein, VP1 and one of the minor proteins (VP2 or VP3), which faces the internal cavity of the viral shell (Chen et al., 1998). The processes of MPyV virion morphogenesis, genome selection and its encapsidation, albeit important for gene therapy vector design, are not well understood.

For SV40, detailed analyses of deletion mutants of the virus were performed and have revealed that the *cis*-acting DNA signal, which is important for the encapsidation of the SV40 minichromosome, resides in the enhancer region close to the origin of replication (ori) (Oppenheim et al., 1992; DalyotHerman et al., 1996). The signal is called *ses* (SV40 encapsidation signal). The recognition of the SV40 minichromosome during packaging is thought to be achieved via Sp1, a mammalian transcription factor, which binds *ses* within the regulatory region of the genome (Gordon-Shaag et al., 2002). Sp1 recruits the capsid proteins to the viral minichromosome by forming a recruitment complex that is composed of the Sp1 transcription factor and the SV40 capsomere (which is formed by five molecules of VP1 and one molecule of VP2 or VP3). Furthermore, the binding of the recruitment complex to *ses* via the association of VP2/3 with Sp1 leads to the repression of both early and late genes (Gordon-Shaag et al., 1998), thus regulating the transition from replication and transcription to assembly. Sp1 has not been found in mature virions (Roitman-Shemer et al., 2007), which indicates that before assembly, the transcription factor is displaced from the viral genome.

In contrast to SV40, the MPyV *cis*-acting signals and *trans*-acting proteins, which are prerequisites for the encapsidation of its DNA, have not been identified. The similarities in the organization of the regulatory region of both viruses justify the presumption that these elements exist and drive the virion assembly of MPyV. For example, the transcriptional regulator Ying-Yang 1 (YY1), which is a component of the nuclear matrix, has been found to directly interact with the major capsid protein VP1 of MPyV in vivo; however, the biological role of this interaction is not yet understood (Palkova et al., 2000). Three YY1 binding sites are present in the MPyV genome (Martelli et al., 1996, Gendron et al., 1996), and the direct interaction of VP1-YY1 could offer the possibility that YY1 can be involved in virion assembly similar to Sp1 in SV40 morphogenesis.

* Corresponding author. Tel.: +420 221 951 728, fax: +420 221 951 724.
E-mail address: hs@natur.cuni.cz (H. Španielová).

0042-6822/$ - see front matter © 2013 Elsevier Inc. All rights reserved.
http://dx.doi.org/10.1016/j.virol.2013.12.010

In this study, we attempted to identify the encapsidation signal for MPyV. Instead of deleting the viral genome and screening for the alleviation of genome packaging in mutants, we used methods for the efficient intracellular assembly of reporter vector (RV) DNA into pseudovirions, which have been recently developed for both SV40 (Oppenheim and Peleg, 1989) and papillomaviral vectors (Buck et al., 2004). We introduced parts of the MPyV viral genome in the target RVs to enhance their encapsidation. Moreover, by using the SV40 regulatory elements for MPyV encapsidation, we experimentally separated the process of encapsidation from MPyV DNA replication.

Table 1
Description of MPyV regions in reporter vectors.

Reporter vector	Region location (nucleotides)[a]	Landmarks
RV-1	4953–311	Regulatory region
RV-2	292–985	LT/MT/ST, intron
RV-3	971–1635	LT/MT
RV-4	1618–2180	LT
RV-5	2172–2836	LT
RV-6	2816–3496	poly(A) signal, VP1
RV-7	3479–4137	VP1
RV-8	4104–4741	VP2, VP3
RV-9	4748–3	VP2, enhancer

[a] MPyV genome numbering according to the GenBank database.

Results

Design and construction of pseudovirion-based assays

Based on SV40 research (Oppenheim et al., 1992), we reasoned that sequences around the origin of replication (ori) and the enhancer have the highest probability of containing the encapsidation sequence; however, we faced the problem that the importance of viral genome replication during virion assembly has never been systematically analyzed. For MPyV, it has been convincingly shown that the modification of the enhancer region can have an increased effect of one or two orders of magnitude on MPyV compared to SV40 DNA replication (Guo and DePamphilis, 1992) and that the manipulation of the viral genome in the YY1-binding area dramatically reduces genome replication (Spanielová, 2002). We assumed that the construction of an MPyV deletion mutant in a regulatory region would likely lead to restricted replication, decreased DNA copy number and limited encapsidation, regardless of its intrinsic packaging potential. For this reason, we did not use the deletion mutant approach, as performed during the identification of *ses* (Oppenheim et al., 1992). Instead, we developed several assays based on pseudovirion technology. This technology allows for the generation of pseudovirions consisting of capsid proteins and an RV (instead of a viral genome) associated with cellular histones in producer cells.

The first assay, called the Reporter vector Encapsidation into Pseudoivirions system (REPs) is designed to use the pseudovirions for the subsequent experimental infection, which causes the transduction of the reporter gene. The efficacy of the pseudoinfection (transduction) by pseudovirions, which contain different RVs (measured by the activity of the reporter gene product after the gene transduction by each individual vector), then corresponds to the efficacy of their packaging. The RVs that carry the part of MPyV with a putative encapsidation signal sequence would be transduced with the highest frequency. Specifically, the system consists of a series of RVs that serve as target DNAs for encapsidation, helper vector(s) providing the capsid proteins in *trans* and two cell lines: one allowing the production of pseudovirions (producer cells) and the second (detection cells) allowing the sensitive screening of reporter activity after pseudoinfection (transduction).

RVs were constructed from the pGL3-Control vector (Promega), which harbors the luciferase reporter gene under the control of a strong SV40 promoter. The vector also carries the SV40 enhancer and SV40 ori, which ensures the replication in monkey and human cell lines with the constitutive expression of the SV40 large T-antigen. The plasmid pGL3-Control does not contain any MPyV-derived sequences. The plasmid's size corresponds to the size of the MPyV genome (5.3 kb); thus, it serves as the control RV throughout the study. For the construction of RVs, the MPyV genome was divided into nine 650-bp-long fragments that cover the entire viral genome (Table 1), and each fragment was cloned into the multiple cloning site of the shortened pGL3-Control plasmid (pGL3-ΔC, see the section "Materials and methods"). The final size of all RVs was approximately the size of the MPyV genome to allow the unrestrained encapsidation of constructs.

The helper vectors ph2-VP1 (encoding VP1 and VP2) and ph3β (encoding VP3 and β-galactosidase) were constructed from codon-optimized MPyV structural genes (see the section "Materials and methods" for detail). Both helper vectors contain the SV40 origin of replication, and their size exceeds the MPyV genome size by 2.5 kb to prevent their encapsidation. The β-galactosidase gene was included in the system to normalize the transfection efficiency. In some experiments, the pCG-VP1/2/3 vector (6.5 kb) that encoded all three structural proteins under the control of the MPyV late promoter was used. The descriptions of all of the plasmids that were used in the study are shown in the Supplementary Table S2. Human embryonic kidney 293TT cells that stably expressed the SV40 large T-antigen to enhance the replication of SV40 origin-containing plasmids were used as producer cells.

The second assay, called the qPCR assay, is derived from the REPs system. During the qPCR assay, the RVs are isolated directly from pseudovirions and are used for quantitative PCR (qPCR) analysis to determine the most frequently encapsidated RV. This assay eliminates the need to determine the efficacy of packaging by secondary transduction to the screening line, which can be a potential confounding factor. Moreover, due to sequence-specific detection of each RV, it allows direct identification of RV from a mixture of pseudovirions carrying different RVs. There is, however, a potential disadvantage in that fragmented DNA, or DNA of less than unit length, enclosed in so called "empty" capsids can be detected.

The third assay, called the transformation assay, also directly identifies encapsidated RV, but the DNA extracted from pseudovirions is used for the transformation of bacteria. The identification of encapsidated RVs is based on the subsequent sequencing of vectors isolated from bacterial colonies. In contrast to the qPCR assay, this approach ensures the identification of full-length intact encapsidated vectors, thus further increasing the accuracy of the experimental evaluation.

Pseudovirions are generated inside the cell nucleus

To ensure that MPyV pseudovirions can be successfully generated in cells using our system, we co-transfected 293TT producer cells with helper plasmids, ph2-VP1, ph3β and the reporter control vector, pGL3-Control. The transfection efficiency was evaluated by immunofluorescence. Capsid proteins and luciferase genes were coexpressed in 87% of transfected cells (data not shown). At 48 h post-transfection, cells were collected and were then either subjected to a purification procedure or processed directly for electron microscopic examination on ultrathin sections in order to exclude a theoretical possibility that transducing particles are nonspecifically formed in the cell lysate through a self-assembly process.

Electron microscopy confirmed that viral particles could be purified from cell extracts (Fig. 1A) and that the cell-associated viral particles could be detected inside the nuclei of transfected cells (Fig. 1B).

A region of early introns (nucleotides 292–985) in the MPyV genome surpasses other regions in the REPs assay

The REPs assay was designed as a rapid screen for packaging signal. The pseudovirions, which were formed after the transfection of producer cells with helper vectors and with each individual target RV, were not purified, but the whole-cell lysate that was treated with DNase I was used for the transduction of the detection cell line. In this way, the efficiency of the encapsidation of a given RV in producer cells can be estimated from the normalized activity of luciferase that was measured in the corresponding cell extract from transduced detection cells. Initially, MPyV-permissive mouse 3T6 fibroblasts were used as the detection cell line. Using these cells, we failed to detect any luciferase activity in the REPs assay (data not shown). However, high luciferase activity was achieved in COS-1 cells after the transduction of pGL3-Control. COS-1 cells that express the SV40 large T-antigen support the replication of plasmids containing the ori. We concluded that (i) the replication of the RV in detection cell lines is necessary to increase the sensitivity of the assay and (ii) RVs can

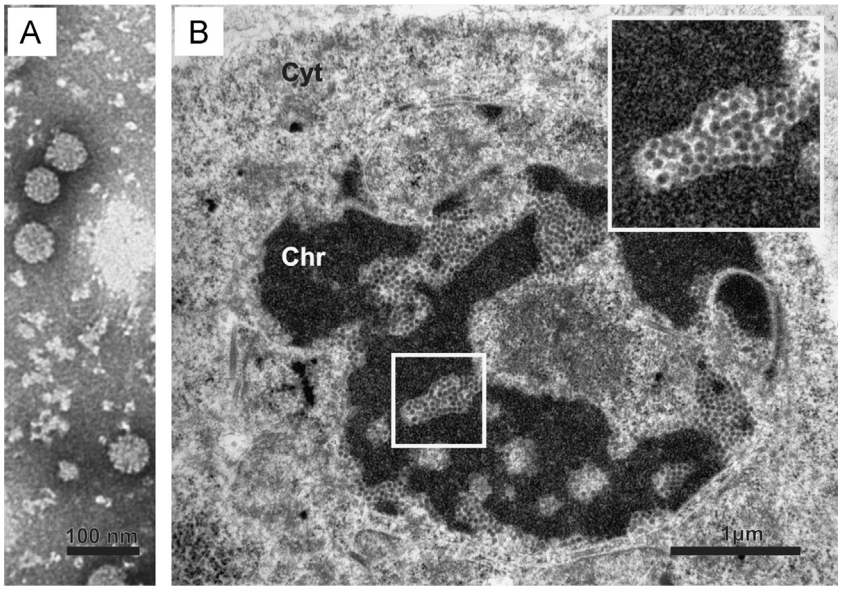

Fig. 1. Electron micrographs of MPyV viral particles that were produced in 293TT cells. (A) Purified viral particles were visualized by negative staining. (B) For transmission electron microscopy on ultrathin (70 nm) resin sections, cells were fixed at 48 h post-transfection. Particles were observed in clusters (as shown in the inset) inside the nucleus in the periphery of the condensed chromatin (Chr). Cyt, cytoplasm.

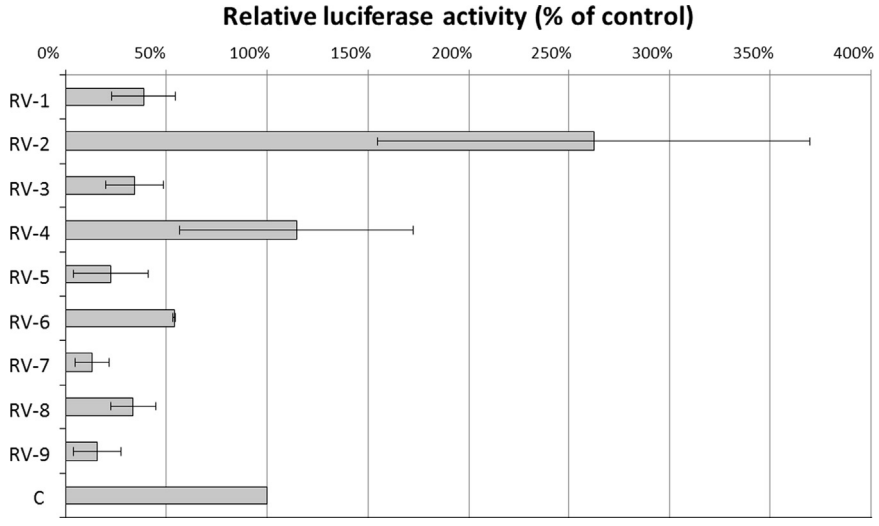

Fig. 2. The REPs assay in COS-1 cells. The 293TT cell line was co-transfected with the helper vectors ph2-VP1 and ph3β and each of the indicated RVs. A cell lysate from the production cell line was used for the transduction of the COS-1 cell line. Luciferase activity was measured in cell lysates that were prepared at 48 h post-transfection and in lysates that were prepared at 48 h post-transduction. Relative luciferase activity was determined for each cell lysate as described in the section Materials and methods, and the final relative luciferase activity was calculated by dividing the relative luciferase activity that was determined in COS-1 cell lysates with the relative luciferase activity that was determined in the corresponding 293TT cell lysates. The graph shows the results of three independent experiments, and the relative luciferase activity that was calculated for each sample is expressed as a percentage of the relative luciferase activity that was determined for the pGL3-Control (C) vector (represented by 100% on *x*-axis). The standard deviations of the mean are indicated by error bars.

be effectively transduced by MPyV pseudovirions. Finally, the COS-1 cell line was employed as a detection cell line in REPs assays.

The results from three separate REPs assay screens are shown in Fig. 2. Out of all RVs, reporter vector 2 (RV-2) was the only vector that was transduced into the COS-1 cell line more efficiently than the control vector. This observation suggested that the RV-2 MPyV genome region (nucleotides 292–985) could enhance the packaging of DNA by MPyV capsids. However, we noted that the transfection of RV-2 always resulted in the highest luciferase activity in producer cells (data not shown). This result may indicate that this MPyV region can convey another quality, such as replication enhancement or plasmid stability, instead of the putative packaging signal. Although this bias was corrected by normalizing the results using β-galactosidase activity in cell lysates used for transduction, the bias could not be avoided during the final screen in the detection cell line that supported replication. For this reason, we decided to verify the data by an independent method and to focus on RV-2 and its unique qualities.

None of the MPyV regions are required for the encapsidation of the reporter vector into the pseudovirions

We decided to trace encapsidated RVs directly in assembled pseudovirions by qPCR assay. We mixed all RVs (including the pGL3-Control) together with helper vectors (ph2-VP1 and ph3β), transfected the entire mixture into the 293TT producer cells and separately analyzed the DNA contents of the pseudovirions and the total extrachromosomal DNA in transfected cells. The transfected producer cells were harvested at 48 h post-transfection and divided; one-half was used for the extraction of total extrachromosomal DNA (by a modified Hirt method), and the second half was used for the extraction of nuclease-resistant (encapsidated) DNA. Both samples were used for qPCR with primers that were specific for each RV. The encapsidation efficiency for each RV was determined as the ratio of the amount of the RV that was detected in the nuclease-resistant pool and in the total extrachromosomal DNA. In two separate experiments, none of the MPyV regions were able to significantly increase the encapsidation efficiency of any RV over the control vector (Fig. 3B). Surprisingly, RV-1, which possessed a complete set of MPyV regulatory elements that included the MPyV ori, repeatedly exhibited the lowest calculated encapsidation efficiency (approximately 40% of the control). This result reflects the fact that the amount of RV-1 reached only the median value in the nuclease-resistant (encapsidated) pool of DNA; whereas its proportion in the total extrachromosomal DNA sample was above the mean of vector amounts (Fig. 3A). RV-2 that positively scored in the REPs assays was over-represented in both DNA samples (Fig. 3B), but the nuclease-resistant-to-total DNA proportion was similar to the control vector. Altogether, the results shown in Fig. 3 suggest that the RV packaging in this experimental system is not enhanced by any distinct MPyV element and that the second MPyV ori region in RV-1 can even negatively influence encapsidation. This result also suggests that the presence of the SV40 ori and *ses* in all RVs may drive the replication and/or packaging, overcome the putative MPyV encapsidation signaling and limit the usage of this experimental design. To dissect the role of these elements in vector packaging, we performed additional experiments in a mouse production cell line.

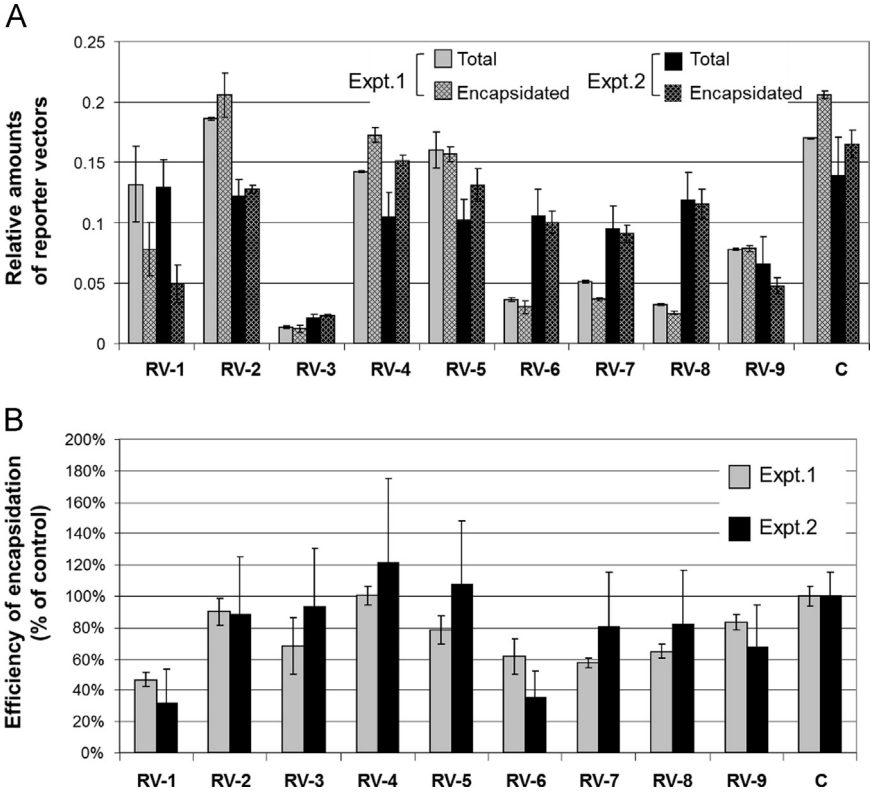

Fig. 3. The determination of reporter vector encapsidation efficiency by qPCR. All 10 RVs (including pGL3-Control) were mixed together with helper vectors ph2-VP1 and ph3β and were transfected into the 293TT cell line. Cells were harvested at 48 h post-transfection. The total extrachromosomal DNA and nuclease-resistant DNA were extracted separately from equivalent numbers of cells. Both DNA samples were used for qPCR with primers that were specific for each RV to determine the amount of each RV. The data were normalized to the luciferase gene to calculate the relative amount of each RV in both DNA pools. (A) The relative amounts of each RV in the extrachromosomal (Total) and nuclease-resistant (Encapsidated) DNA samples are shown for two independent experiments as the means of triplicate samples ± standard deviations (error bars). (B) The encapsidation efficiency was determined from the data that are shown in (A) as a ratio between the relative amounts of each RV that were detected in the nuclease-resistant pool and in the total extrachromosomal DNA. The data are plotted as percentages of encapsidation efficiencies compared to the control (C) RV (set as 100%). Error bars represent the standard deviations of triplicate samples.

Reporter vectors can be encapsidated into MPyV pseudovirions without replication

To separate the driving force of SV40-based replication and the possible influence of *ses* on encapsidation, we performed additional experiments in WOP cells. The WOP cell line is a mouse cell line expressing MPyV T-antigens, which support the replication of plasmids containing the MPyV ori and therefore only RV-1 out of all of the RVs is able to replicate in these cells. Originally, we attempted to produce MPyV pseudovirions using the same reporter and helper vectors as in the REPs assay. However, when the expression of the capsid and reporter genes after co-transfection was assessed using immunofluorescence, we discovered that the co-transfection/expression rate was low in these particular cells (less than 10% of transfected cells expressed luciferase together with all three capsid proteins; data not shown). For this reason, further experiments were performed with the pCG-VP1/2/3 vector, which ensured the weak, but simultaneous, expression of all three capsid genes in one cell. Moreover, the mouse producer cells allowed us to use the MPyV genomic DNA as the helper vector for the production of high levels of all capsid proteins. Pseudovirions generated in WOP cells were further analyzed by transformation assay: the encapsidated plasmids that were extracted as nuclease-resistant DNA were used for the transformation of *Escherichia coli*. To reveal their identity, the RVs were isolated from ampicillin-resistant colonies and then sequenced.

In the initial experiment, we used an equimolar mix of all RVs (including the pGL3-Control) as the target DNA to determine whether any RVs would show preferential encapsidation. In the second set of experiments, only the pGFPmax vector served as the target DNA. The vector pGFPmax does not contain any sequences that were derived from either MPyV or the SV40 genome and has a suitable size (3.8 kb) for encapsidation. Using this target vector, we wanted to determine whether a non-replicating vector without *ses* and MPyV sequences could be successfully encapsidated. Target vectors were used for transfections with either MPyV DNA or pCG-VP1/2/3 as the helper vector (Table 2). Control transfections without the helper vector were also performed (see Table 2). Cells were harvested at 48 h post-transfection, and total extrachromosomal and nuclease-resistant DNAs were extracted from an equivalent number of cells and were used for qPCR quantification and *E. coli* transformation, respectively. The overall results of this assay, which were expressed as numbers of *E. coli* colonies grown after transformation with each sample, are shown in Table 2. The transformation of DNA that was extracted from pseudovirions formed with the use of MPyV DNA as the helper vector led to the emergence of 26 colonies; whereas the pCG-VP1/2/3 vector co-transfection samples yielded 166 colonies. Notably, in contrast to pCG-VP1/2/3, MPyV DNA could compete with the encapsidation of RVs, and the low colony yield was expected. The control reaction without the transfected helper vector yielded no colonies, indicating that the nuclease treatment was effective. Subsequently, plasmid DNA from 52 colonies (all colonies from the MPyV DNA sample and 26 randomly chosen colonies grown from the pCG-VP1/2/3 sample) was extracted and sequenced. In parallel, the total extrachromosomal DNA that was extracted from the same samples of transfected cells was subjected to qPCR to determine the total amount of each individual RV. The frequency of each RV that was found in the nuclease-resistant pool and its proportion relative to the total amount of each vector in the extrachromosomal DNA are shown in Table 3. The data from the sample in which MPyV DNA served as a helper indicate that the high total amount of RV-2 in the transfected cells led to its preferential encapsidation. In contrast, the amplification of RV-1 was likely negatively influenced by the presence of the replicating viral genome, thus decreasing the probability of its encapsidation. However, sequence analysis of 26 clones from randomly chosen colonies that were obtained from the sample in which the pCG-VP1/2/3 vector served as a helper revealed that RV-1 had been encapsidated with the highest frequency. The high total amount of RV-1 in the extrachromosomal DNA fraction also indicated that its replication was not influenced by the pCG-VP1/2/3 helper DNA (as observed for MPyV helper DNA; see Table 3). Although it is impossible to determine the encapsidation efficiency for each vector because of the low number of sequenced clones, the data suggest that encapsidation in the mouse production system does not exhibit a strict sequence preference and reflects the RV amount. Spearman's rank correlation test (Wessa, 2012) confirmed a very strong positive correlation [$\rho(8)=0.852$, $p=0.001$] between the amount and frequency of encapsidation of a given RV in the MPyV DNA helper sample and a strong positive correlation [$\rho(8)=0.705$, $p=0.023$] in the pCG-VP1/2/3 helper sample, which was statistically significant. Moreover, a second set of experiments with the pGFPmax vector as a target DNA (Table 2) was performed to reveal whether the SV40 encapsidation signal is dispensable for packaging. The numbers of colonies that are shown in Table 2 indicate that the pGFPmax vector, which lacks SV40 elements, could be efficiently encapsidated into the viral particles. Taken together, these results suggest that the vector amount is the only important factor in encapsidation and that replication competence, which is connected with the presence of SV40 and MPyV regulatory elements, is not necessary for encapsidation.

Table 2
Summary of transfections performed in WOP cells for the extraction of nuclease-resistant DNA used for *E. coli* transformation.

Vector		Transfection mix					
Helper	MPyV DNA	+	−	−	+	−	−
	pCG-VP1/2/3	−	+	−	−	+	−
Target	RVs mix[a]	+	+	+	−	−	−
	pGFP max	−	−	−	+	+	+
No. of colonies	Expt. 1	**26**[b]	**166**[c]	**0**	**81**	**146**	**0**
	Expt. 2	**ND**	**ND**	**ND**	**65**	**67**	**0**

[a] Equimolar ratios of all RVs were used in the transfection.
[b] All colonies were used for sequencing.
[c] 26 colonies were randomly chosen for sequencing; ND – not done.

Table 3
Encapsidation as determined from transformation assays.

	Helper: MPyV DNA		Helper: pCG-VP1/2/3	
	No. of colonies[a]	Relative amount[b]	No. of colonies[a]	Relative amount[b]
RV-1	0	0.10	19	0.25
RV-2	11	0.23	2	0.17
RV-3	0	0.02	0	0.01
RV-4	1	0.11	0	0.10
RV-5	4	0.13	1	0.11
RV-6	0	0.06	2	0.09
RV-7	3	0.07	0	0.08
RV-8	0	0.03	0	0.03
RV-9	3	0.10	1	0.05
Control	4	0.15	1	0.10
Total	26	1	26	1

[a] Number of colonies that contain a given RV.
[b] The relative amount of each RV in the sample was determined by qPCR.

Some regions of the MPyV genome enhance the stability of DNA after transfection

Finally, we focused on RV-2 and its unique qualities that led to its positive scoring in the REPs assay (Fig. 2) and partly in the

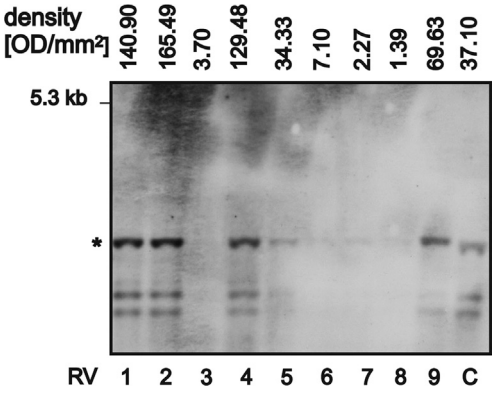

Fig. 4. Determination of the intracellular amounts of reporter vectors. 3T3 cells were transfected with individual RVs. The total extrachromosomal DNA was extracted at 48 h post-transfection and was digested with Sal I and Dpn I enzymes. DNA from each sample (0.5 μg) was separated using agarose electrophoresis, subjected to Southern blotting, hybridized to a DIG-labeled luciferase gene probe, detected with chemiluminescence and recorded by exposure to X-ray film. The optical density of the prominent band (indicated by an asterisk) was determined with a densitometer and is shown in the upper row for each sample.

transformation assay (Table 2). We repeatedly observed that, compared with other RVs, the direct transfection of RV-2 into cells leads to very high luciferase activity in all cell lines tested (NIH-3T3, 3T6, COS-1, 293TT and WOP cells, data not shown). Our results from qPCR (Fig. 3B) also suggested that this effect was more likely caused by an augmented amount of the vector than by the transcriptional upregulation of the activity of the reporter gene in transfected cells. To examine whether the early intron region (nucleotides 292–985) of the MPyV genome can confer some unusual property on RV-2 that leads to the stabilization of the plasmid (due to the plasmid maintenance sequences) or to ori-independent replication, we transfected individual RVs into the mouse NIH-3T3 cell line and followed the reporter activity in several generations of cells. The NIH-3T3 cell line is a parental line for WOP cells and does not normally support the replication of MPyV ori-containing plasmids without the presence of large T-antigen. After the transfection of a full set of RVs into this cell line, RV-2 exhibited the highest luciferase activity, even after three cell passages (data not shown). We performed a replication assay to exclude the possibility that an ori-independent, low level of plasmid replication, which is occasionally observed (Katinka and Yaniv, 1983), is responsible for this effect. The total DNA from cells that were transfected by nucleofection was extracted, digested with Dpn I and analyzed by gel electrophoresis and Southern blotting. Dpn I is a methylation-sensitive enzyme; newly replicated DNA molecules are resistant to Dpn I digestion. The results showed that none of the RVs could be replicated in 3T3 cells (Fig. 4; note complete digestion by Dpn I). More importantly, a great difference in the abundance of individual plasmids was noted, although the transfection was performed with equal amounts of RVs. Because the Amaxa Nucleofector Technology is considered the most reproducible method of transfection, the results suggest that RV-2, RV-1 and RV-4 harbor MPyV elements that are responsible for the increased intracellular stability of DNA after transfection. RV-2 was the most stable (Fig. 4).

Discussion

In this study, we attempted to identify the MPyV encapsidation signal. We used pseudovirion-based approaches for the identification of the polyomavirus-specific sequences that enhance the encapsidation of RVs.

From the series of assays, only the most laborious, transformation assay led to the final conclusion that the encapsidation of target DNA is not driven by any distinct, sequence-specific encapsidation signal. The assay confirmed a strong positive correlation between the amount and frequency of encapsidation of a given RV. Moreover, we used two different helpers (pCG-VP1/2/3 or MPyV DNA) for the production of pseudovirions in WOP cells and both variants brought additional interesting results. The presence of the MPyV DNA as a replicating and transcriptionally active viral genome creates a highly competitive environment in the system. This environment probably negatively affected RV-1 replication because its relative intracellular amount was lower than expected for a vector with an exclusive capacity to replicate. It is well-documented that the presence of wild-type replicons strongly interferes with mutant replication after transfection (Nilsson et al., 1991) and the defect could be at the stage of initiation (Yamaguchi and DePamphilis, 1986). Furthermore, MPyV DNA is undoubtedly efficiently encapsidated into virions but cannot be detected by this type of assay. Therefore, the RVs that were identified with a frequency that was related to their intracellular amounts reflect the minority of successfully encapsulated DNA. In contrast, the encapsidation of pCG-VP1/2/3 is prevented due to a size discrimination mechanism, and the vector did not restrict the replication potential of RV-1, which accumulated in the system. Subsequently, the high relative amount of RV-1 led to its preferential encapsidation. However, in both cases, the non-replicating pGFPmax vector without any viral (MPyV or SV40) sequence could be encapsidated equally well. The results indicated that an intracellular amount of target DNA determines the outcome of the encapsidation process, and virtually any DNA with an appropriate size can be encapsidated. The preferential packaging of a RV with an active regulatory region can be a consequence of the fact that encapsidation is likely interconnected with the processes of replication and/or transcription. According to our observations, at the early stages of the late phase of MPyV infection, the newly expressed VP1 protein accumulates at distinct sites of DNA replication near PML bodies; whereas during the later times, the VP1 protein expands throughout the nucleus (Ryabchenko, unpublished data). Therefore, the organization of the replication foci during the initial phases of virion formation, when capsid proteins are spare, can favor DNA with a highly active ori region for encapsidation. In agreement with this notion, in our mouse production system, where the pCG-VP1/2/3 vector ensures a low level of capsid proteins (thus reminiscent of early events in the late phase of infection), RV-1 containing an active ori was detected as an almost exclusive target of encapsidation (Table 3). In contrast, MPyV helper DNA played a dual role in the mouse system by encapsidating itself as replicating target DNA in the initial phase of virion formation and ensuring high levels of capsid proteins later, thus allowing the encapsidation of other available targets. We propose that by employing such a simple regulation of encapsidation that is based on the spatio-temporal organization of virion formation, MPyV can achieve a reasonable level of encapsidation specificity without employing a sequence-specific signal.

The results from the qPCR assay were also in agreement with this notion. None of the MPyV sequences were able to enhance the encapsidation of RVs and the RV-1 with second MPyV ori region was packaged with the lowest efficiency. It has been shown that SV40 LT can efficiently bind the MPyV ori on LT-binding sites (Bhattacharyya et al., 1995) without triggering DNA replication. We reasoned that SV40 LT binding on a non-active MPyV ori could cause the retention of target DNA on chromatin and limit its encapsidation.

The REPs system, originally designed as an easy and rapid screening method, was unfortunately biased as a result of unexpected obstacles. The idea of the REPs system is based on the

assumption that intracellular levels of each RV in producer cells are comparable due to the similar efficiency of replication driven from a common SV40 origin. Normalizing the transfection efficiency of the system by the co-transfected internal control gene (for β-galactosidase) and by the protein content in the lysate of the producer cell should provide adequate corrections for perturbations during the transduction assay. An analysis of the REPs screening hit (RV-2) revealed that this is not the case. The experiments that took into consideration the levels of copies of individual RVs showed a constant and high level of RV-2 in cells, and consequently, in viral particles in most assays (see Fig. 3B; Table 3). By performing the replication assay with RVs that were transfected into 3T3 cells, we excluded the possibility that the plasmids undergo an ori-independent replication; however, without further analyzing the reasons, we observed completely different intracellular amounts of each RV after transfection. It has previously been shown that the use of a second reporter plasmid as an internal standard to normalize luciferase activity in transient transfection experiments may lead to a systematic error due to the interaction between co-transfected RVs (Huszár et al., 2001, Bergeron et al., 1995). Moreover, it has been shown that coexpression efficiencies among transfected cells are variable, and a significant number of transfected cells express only a single target protein (Ma et al., 2007). This observation points to the difficulties that are connected with the comparison of the quantitative data from parallel transfections in general; however, in our system, the small error in the normalization of the cell lysates of producer cells can be dramatically amplified during the final screen in the detection cell line where the RV replicates. We concluded that this amplification was the case for RV-2 in the REPs assay.

Until now, the SV40 *ses* sequence has been the only identified encapsidation signal in polyomaviruses. Our work surprisingly suggests the fact that the mechanism of the selection of DNA for encapsidation may not be universal within the virus family. We hypothesize that the mechanisms of encapsidation in MPyV and SV40 may likely differ due to the differences in the DNA-binding properties of the minor capsid proteins. The minor proteins of SV40 bind nonspecifically to DNA (Dean et al., 1995), and Sp1 proteins cooperate in *ses*-specific DNA binding with VP2/3 (Gordon-Shaag et al., 2002); whereas MPyV VP2 and VP3 proteins do not bind the DNA (Chang et al., 1993) None of these proteins interact with the MPyV genome in virions (Carbone et al., 2004). However, it should be noted that the SV40 mutant that lacked minor structural proteins is able to encapsidate virus DNA efficiently (Nakanishi et al., 2007), which is similar to the corresponding MPyV mutants (Mannova et al., 2002). Moreover, in vitro experiments have shown that the *ses* sequence itself, in the absence of a large excess of cellular chromatin, does not promote the preferential binding of capsomere VP1(5)VP2/3 complexes to the SV40 genome (Roitman-Shemer et al., 2007). These observations not only suggest that the involvement of these proteins in the encapsidation process may differ between both viruses but also that their importance may depend on the actual context. Further investigation would be needed to evaluate the preferential mode of genome selection during virion assembly for other members of the *Polyomaviridae* family.

Materials and methods

Plasmids and viruses

For the construction of RVs, the plasmid pGL3-Control (Promega, Madison, Wisconsin, USA) was shortened by digestion with the restriction enzyme Ssp I and re-ligation (without the f1 ori sequence). The obtained pGL3-ΔC vector could accommodate polyomaviral sequences without exceeding the size of the MPyV genome. Both vectors, pGL3-Control and pGL3-ΔC, yielded the same level of activity of the reporter luciferase gene that they carried. The genome of the MPyV BG strain (GenBank: AF442959.1) was divided into nine regions of approximately 650 bp each, and each region was cloned using the In-Fusion HD Cloning System (Clontech Laboratories, Mountain View, California, USA) into the Mlu I and Xho I sites of the pGL3-ΔC plasmid. All clones were verified by sequencing. A list of the cloning primers used is available as Supplementary information in Table S1.

The helper vector ph2-VP1 (7802 bp), which carries the codon-modified VP1 and VP2 MPyV genes as described in Tolstov et al. (2009), was constructed from the ph2p vector (Addgene plasmid 22520) (Pastrana et al., 2009) by digestion with the restriction enzymes Stu I and Cla I and re-ligation with the PCR-amplified product, which contains the human elongation factor-1 alpha (hEF1a) promoter, codon-modified VP1 gene, woodchuck hepatitis virus posttranscriptional regulatory element (WPRE) sequence and hEF1a poly(A) signal from the pwP vector (Addgene plasmid 22519) (Pastrana et al., 2009). The vector ph3β (7538 bp), which carries the codon-modified MPyV VP3 and β-galactosidase genes, was constructed from ph3p (Addgene plasmid 22521) (Pastrana et al., 2009) by digestion with the restriction enzymes Stu I and Not I and re-ligation with the β-galactosidase gene, which was obtained via Sma I and Not I digestion of the pCMVβ vector (Clontech Laboratories, Mountain View, California, USA). The vector pCG-VP1/2/3 (6542 bp) was constructed from the pGL3-Control vector by the excision of the luciferase gene using Ehe I and Xba I restriction enzymes and re-ligation with a part of the polyomavirus genome that is composed of the regulatory and late-gene regions (cut by Ehe I and Xba I from MPyV genome DNA). The plasmid pmaxGFP (Lonza, Cologne, Germany), which encodes maxGFP, which is a green fluorescent protein from the copepod *Pontellina plumata*, was used as a negative control vector in the transfections and as a target DNA for some packaging experiments. The plasmid pcDNA3-LT was used for the expression of the MPyV LT antigen in some co-transfection experiments. The summarized description of all plasmids that were used for the production of the pseudovirion is shown in supplementary Table S2.

Cell lines and transfections

Mouse Swiss albino 3T6, NIH 3T3 mouse fibroblasts, SV40-transformed African green monkey kidney cells, COS-1 and WOP cells were maintained in Dulbecco's modified Eagle medium (DMEM) (Sigma-Aldrich, St. Louis, Missouri, USA) that was supplemented with 10% Gibco™ fetal calf serum (Invitrogen, Paisley, UK) and GlutaMAX™ (Invitrogen, Paisley, UK) at 37 °C in a 5% CO_2-air humidified incubator. The mouse WOP cell line that constitutively expresses the MPyV large T-antigen is a 3T3 fibroblast derivative that was transformed using an origin-defective polyomavirus (Dailey and Basilico, 1985). The human embryonic kidney cells 293TT that express the SV40 large T-antigen were kindly provided by John Schiller and Chris Buck (Bethesda, Maryland, USA) and were cultivated as previously described (Buck and Thompson, 2007).

The plasmid DNA that was used for transfections was purified using either the EndoFree Plasmid Maxi Kit (Qiagen, Valencia, California, USA) or the GenBond Plasmid Endofree FlexSpin Kit (Renogen Biolab, Vancouver, Canada). 293TT or COS-1 cells were transfected using the TurboFect Transfection Reagent (Thermo Fisher Scientific, Waltham, Massachusetts, USA) according to the manufacturers' instructions. Briefly, logarithmically growing cells (5×10^5) in 6-well dishes were transfected with 4 μg of DNA. In the REPs assay, 1.5 μg of ph2-VP1 and 0.5 μg of ph3β together with 2 μg of RV were transfected in a production cell line. WOP cells

(for transformation assays) and 3T3 cells (for the replication assay) (both 4×10^6) were transfected (using Amaxa® Nucleofector® Technology [Lonza, Cologne, Germany] according to the manufacturer's instructions) with 6 μg of DNA (total) in solution V using the programs U-030 and T-030, respectively. Specifically, the mixed transfections (all RVs with helper DNA) contained either 2.5 μg of ph2VP1 and 0.5 μg of ph3β or 3 μg of pCG-VP1/2/3 as helper DNA and 0.3 μg of each RV. For the comparative analysis of the encapsidation of the pGFPmax vector, either 3 μg of MPyV DNA or 3 μg of pCG-VP1/2/3 were mixed with 3 μg of the pGFPmax plasmid and were transfected into WOP cells.

Pseudovirion production and purification

Transfected 293TT cells were harvested 48 h post-transfection, and pseudovirions were isolated by three rounds of freeze–thaw cycles as described for polyomavirus (Türler and Beard, 1985), concentrated by pelleting through a 10% sucrose cushion (25,000 r.p.m., Beckman SW28 rotor, 3 h, 4 °C), resuspended in B buffer (150 mM NaCl, 10 mM Tris–HCl [pH 7.4], 0.01 mM $CaCl_2$) and purified by CsCl gradient ultracentrifugation (Beckman SW41 rotor, 35,000 r.p.m., 24 h, 18 °C). Gradient fractions were collected by bottom puncture and were assayed for the presence of the VP1 protein by dot-blot analysis. The fractions that contained a peak amount of VP1 (1.33–1.29 g/cm^3) were dialyzed against B buffer, concentrated by pelleting through a 10% sucrose cushion (Beckman SW41 rotor, 35,000 r.p.m., 2 h, 4 °C) and subjected to electron microscopic examination.

REPs (transduction) assay

Producer 293TT cells (1.5×10^6) were harvested at 48 h post-transfection, washed by PBS and lysed in 100 μl of 250 mM Tris–HCl [pH 7.4] by three rounds of freeze–thaw cycles. Lysates were centrifuged at 10,000*g* for 5 min at 4 °C. The supernatant (50 μl) was supplemented with magnesium chloride (final concentration 10 mM), treated with 0.1 mg/ml DNase I (Roche Diagnostics GmbH, Mannheim, Germany) for 30 min in 25 °C and used for transduction. An aliquot of the original supernatant (20 μl) was used for the parallel determination of the activity of luciferase and β-galactosidase with the Dual-Light System (Applied Biosystems, Bedford, Massachusetts, USA) and for the measurement of the protein concentration (Bradford, 1976). Several cell lines were tested as suitable detection cell lines; COS-1 cells were chosen for the final transduction screen. Exponentially growing COS-1 cells in a 6-well dish (1.5×10^5 cells/well) were washed with 2 ml of serum-free medium, and 50 μl of the lysate supernatant was diluted in 150 μl of serum-free medium, added to cells and incubated for 1.5 h in a thermostat with intermittent agitation. At the end of the incubation, 2.5 ml of complete medium was added to the cells. Transduced COS-1 cells were harvested at 48 h post-transduction and were washed two times with phosphate-buffered saline (PBS). The cell lysate was prepared by three rounds of freeze–thaw cycles, and cellular debris was removed by centrifugation at 14,000*g* and 4 °C for 5 min. Supernatants were used for protein concentration (Bradford, 1976) and luciferase measurement determinations with the Luciferase Assay System (Promega, Madison, Wisconsin, USA) in a Microlite TLX2 luminometer (Dynatech Laboratories, Inc, Chantilly, Virginia, USA). The transduction efficacy, which was expressed as relative luciferase activity (in relative luminescence units) for each sample, was calculated by dividing the relative activity of luciferase that was measured in COS-1 cell lysates by the relative activity of luciferase that was measured in the 2932TT cell lysate. The luciferase activities that were measured in the 2932TT cell lysate were normalized by protein concentrations and β-galactosidase activity (i.e., the relative activity of luciferase in 293TT cells), and the luciferase activities that were measured in COS-1 cells were normalized by protein concentrations only (i.e., the relative activity of luciferase in COS-1 cells). The background activity of luciferase that was measured in the control sample that was transduced with lysates, which were generated from 293TT cells that were transfected with pGL3-Control vector without helper vectors, was subtracted from all measurements before computation.

DNA analysis

Low-molecular-weight (extrachromosomal) DNA was extracted from one million cells using a previously reported neutral lysis method (Arad, 1998). The extraction of nuclease-resistant extrachromosomal DNA from transfected cells was performed exactly as described in (Buck et al., 2004). The viral genomic DNA that was used as helper in transfection assays was extracted according to the classical Hirt procedure (Hirt, 1967). For Southern blot analysis, the purification of total DNA from transfected cells was performed using a DNeasy Blood & Tissue Kit (Qiagen, Valencia, California, USA).

Transformation assay

WOP cells that were transfected with mixed vectors (all RVs and helper DNA) were harvested at 48 h post-transfection; aliquots were then generated by dividing each lysate in half. The extrachromosomal and nuclease-resistant (encapsidated) DNAs were extracted from each aliquot as described above. The nuclease-resistant DNA was used to transform Stellar™ Competent Cells (*E. coli* HST08 strain) (Clontech Laboratories, Mountain View, California, USA). The plasmid DNA from transformed bacterial colonies was extracted using a QIAGEN Plasmid Mini Kit (Qiagen, Valencia, California, USA) and was sequenced with a 3130xl Genetic Analyzer (Applied Biosystems, Bedford, Massachusetts, USA). Extrachromosomal DNA was used for quantitative polymerase chain reaction (qPCR) analysis to determine the total intracellular amounts of each individual RV in WOP cells. For the analysis of the encapsidation of the pGFPmax vector, Stellar™ Competent Cells were transformed with the nuclease-resistant DNAs. Equal amounts of the bacterial suspension were plated on agar plates containing kanamycin and ampicillin to discriminate between pGFPmax (kanamycin resistance) and the helper vector (ampicillin resistance).

Electron microscopy

For the ultrastructural analysis of cell-associated viral particles, the producer cells were washed with PBS at 48 h post-transfection and were fixed with 3% glutaraldehyde in 0.1 M cacodylate buffer on ice for 60 min. Cells were washed two times with cacodylate buffer and were postfixed with 1% osmium tetroxide for 60 min. The postfixation was followed by embedding the cells in 3% low melting point agarose. The solidified agarose blocks were cut into 1 mm^3 pieces and were dehydrated with an increasing ethanol series (30%, 50%, 70%, 90%, 96%, 100% and 100%), each for 15 min. Dehydrated blocks were infiltrated with an increasing series of AGAR 100 resin (Gröpl, Tulln, Austria) in propylene oxide (propylene oxide: AGAR 100-2 × pure propylene oxide 10 min); 2:1 (15 min); 1:1 (30 min); 2:1 (30 min); and pure AGAR 100 overnight; pure AGAR 100 (3 h). Polymerization was performed at 60 °C for 72 h. Sections of 70-nm thickness (Leica ultramicrotome EM UC7, Leica Microsystems, Austria) were contrasted with a saturated water solution of uranyl acetate (5 min) and Reynolds lead citrate solution (3 min).

For the negative staining of purified viral particles, the parlodion-carbon coated grids, which were activated by glow discharge, were put

on the top of a 10 μl-drop of sample and were allowed to adsorb for 5 min; the grids were then rinsed in 2 drops of filtered distilled water and transferred onto 2 drops of 2% phosphotungstic acid (pH 7.3), left for 1 min and then dried.

Electron micrographs were recorded in a JEM-1011 electron microscope (JEOL) operating at 80 kV.

Quantitative PCR

qPCR was performed in a Light Cycler 480 II (Roche Diagnostics GmbH, Mannheim, Germany) using the iQ™ SYBR® Green Supermix (Bio Rad), according to the manufacturer's protocol. The DNA was amplified by PCR using a forward primer from Promega (RVprimer_pGL3), which was common to all RV and reverse primers that were designed for each individual RV as described in the supplementary Table S3. Specific primer pairs were designed for pGL3-Control and the luciferase gene. The quantification of each RV in the extracted DNA samples was performed with the Light Cycler 480 II software for an advanced relative quantification with an efficiency correction using standard curves for each primer pair. The concentration of each RV was normalized to the luciferase gene and was expressed as a proportion of the individual vector in the total amount of DNA.

Replication assay and Southern blotting

The 3T3 cells that were transfected with individual vectors by nucleofection were harvested at 48 h post-transfection for the extraction of total DNA. The DNA from each sample (0.5 μg) was digested with Sal I and Dpn I enzymes, separated by electrophoresis in 0.8% agarose and blotted onto a nylon membrane (Roche Diagnostics GmbH, Mannheim, Germany). Southern blotting was performed with a DIG High Prime DNA Labeling and Detection Starter Kit II (Roche Diagnostics GmbH, Mannheim, Germany) according to the manufacturer's protocol. The hybridization was performed using a DIG-labeled probe that contained the luciferase gene probe. The blots were detected with chemiluminescence and were recorded by exposure to X-ray film. The optical densities of the bands were determined with a GS-800™ Calibrated Densitometer (Bio-Rad Laboratories, Hercules, California, USA).

Immunofluorescence

The cells that were grown on the glass slides were fixed in 3.7% paraformaldehyde (PFA) in PBS for 15 min, permeabilized with 0.5% Triton X-100 in PBS for 5 min, rinsed 3 times with PBS and blocked with PBS containing 0.25% bovine serum albumin and 0.25% porcine skin gelatin for 30 min. Immunostaining with primary and secondary antibodies was performed for 1 h and 30 min, respectively, with extensive washing by PBS after each incubation step. The cells were mounted in 50% glycerol with 4′,6-diamidino-2-phenylindole (DAPI) and were examined using an Olympus BX-60 fluorescence microscope (Olympus; Center Valley, Pennsylvania, USA).

Antibodies

The following primary antibodies were used: rat monoclonal IgG against the MPyV large T-antigen (LT1) (Dilworth and Griffin, 1982), mouse monoclonal anti-MPyV VP1 IgG, mouse monoclonal IgG against the common region of VP2 and VP3 (Forstová et al., 1993) and the goat anti-luciferase polyclonal antibody (pAb) (Promega, Madison, Wisconsin, USA). The following secondary antibodies were used: donkey anti-mouse IgG and donkey anti-rat IgG conjugated with Alexa Fluor 488, goat anti-rat and donkey anti-goat IgGs conjugated with Alexa Fluor 546 and chicken anti-mouse IgG conjugated with Alexa Fluor 647 (all from Molecular Probes®, Invitrogen, Paisley, UK).

Acknowledgments

This work was generously supported by the Grant Agency of Czech Republic GACR, No. P302-10-P118 (H.S.), by SVV-2013-267205 (J.S., J.S.), by TACR No. 213TA0310700 (M.F.), by a project of the Ministry of Education, Youth and Sports of the Czech Republic, MSM0021620858 (J.F.), and by UNCE 204013/2013.

We thank Vlasta Sakařová for excellent technical assistance.

Appendix A. Supplementary information

Supplementary data associated with this article can be found in the online version at http://dx.doi.org/10.1016/j.virol.2013.12.010.

References

Arad, U., 1998. Modified Hirt procedure for rapid purification of extrachromosomal DNA from mammalian cells. Biotechniques 24, 761–762.
Bergeron, D., Barbeau, B., Léger, C., Rassart, E., 1995. Experimental bias in the evaluation of the cellular transient expression in DNA co-transfection experiments. Cell. Mol. Biol. Res. 41, 155–159.
Bhattacharyya, S., Lorimer, H.E., Prives, C., 1995. Murine polyomavirus and simian virus 40 large T antigens produce different structural alterations in viral origin DNA. J. Virol. 69, 7579–7585.
Bradford, M.M., 1976. A rapid and sensitive method for the quantitation of microgram quantities of protein utilizing the principle of protein-dye binding. Anal. Biochem. 72, 248–254.
Buck, C.B., Pastrana, D.V., Lowy, D.R., Schiller, J.T., 2004. Efficient intracellular assembly of papillomaviral vectors. J. Virol. 78, 751–757.
Buck, C.B., Thompson, C.D., 2007. Production of papillomavirus-based gene transfer vectors. Curr. Protoc. Cell. Biol. 37, 26.1.1–26.1.19.
Carbone, M., Ascione, G., Chichiarelli, S., Garcia, M.I., Eufemi, M., Amati, P., 2004. Chromosome-protein interactions in polyomavirus virions. J. Virol. 78, 513–519.
Chang, D., Cai, X., Consigli, R.A., 1993. Characterization of the DNA binding properties of polyomavirus capsid protein. J. Virol. 67, 6327–6331.
Chen, X.J.S., Stehle, T., Harrison, S.C., 1998. Interaction of polyomavirus internal protein VP2 with the major capsid protein VP1 and implications for participation of VP2 in viral entry. EMBO J. 17, 3233–3240.
Dailey, L., Basilico, C., 1985. Sequences in the polyomavirus DNA regulatory region involved in viral DNA replication and early gene expression. J. Virol. 54, 739–749.
Dalyotherman, N., Bennunshaul, O., Gordonshaag, A., Oppenheim, A., 1996. The simian virus 40 packaging signal ses is composed of redundant DNA elements which are partly interchangeable. J. Mol. Biol. 259, 69–80.
Dean, D.A., Li, P.P., Lee, L.M., Kasamatsu, H., 1995. Essential role of the Vp2 and Vp3 DNA-binding domain in simian virus 40 morphogenesis. J. Virol. 69, 1115–1121.
Dilworth, S.M., Griffin, B.E., 1982. Monoclonal antibodies against polyoma virus tumor antigens. Proc. Natl. Acad. Sci. USA 79, 1059–1063.
Forstová, J., Krauzewicz, N., Wallace, S., Street, A.J., Dilworth, S.M., Beard, S., Griffin, B.E., 1993. Cooperation of structural proteins during late events in the life cycle of polyomavirus. J. Virol. 67, 1405–1413.
Gendron, D., Delbecchi, L., Bourgauxramoisy, D., Bourgaux, P., 1996. An enhancer of recombination in polyomavirus DNA. J. Virol. 70, 4748–4760.
Gordon-Shaag, A., Ben-Nun-Shaul, O., Kasamatsu, H., Oppenheim, A.B., Oppenheim, A., 1998. The SV40 capsid protein VP3 cooperates with the cellular transcription factor Sp1 in DNA-binding and in regulating viral promoter activity. J. Mol. Biol. 275, 187–195.
Gordon-Shaag, A., Ben-Nun-Shaul, O., Roitman, V., Yosef, Y., Oppenheim, A., 2002. Cellular transcription factor Sp1 recruits simian virus 40 capsid proteins to the viral packaging signal, ses. J. Virol. 76, 5915–5924.
Guo, Z.S., Depamphilis, M.L., 1992. Specific transcription factors stimulate simian virus 40 and polyomavirus origins of DNA replication. Mol. Cell. Biol. 12, 2514–2524.
Hirt, B., 1967. Selective extraction of polyoma DNA from infected mouse cell cultures. J. Mol. Biol. 26, 365–369.
Huszár, T., Mucsi, I., Terebessy, T., Masszi, A., Adamkó, S., Jeney, C., Rosivall, L., 2001. The use of a second reporter plasmid as an internal standard to normalize luciferase activity in transient transfection experiments may lead to a systematic error. J. Biotechnol. 88, 251–258.
Katinka, M., Yaniv, M., 1983. DNA replication origin of polyoma virus: early proximal boundary. J. Virol. 47, 244–248.
Ma, Z.L., Werner, M., Körber, C., Joshi, I., Hamad, M., Wahle, P., Hollmann, M., 2007. Quantitative analysis of cotransfection efficiencies in studies of ionotropic glutamate receptor complexes. J. Neurosci. Res. 85, 99–115.

Mannova, P., Liebl, D., Krauzewicz, N., Fejtova, A., Stokrova, J., Palkova, Z., Griffin, B. E., Forstova, J., 2002. Analysis of mouse polyomavirus mutants with lesions in the minor capsid proteins. J. Gen. Virol. 83, 2309–2319.

Martelli, F., Iacobini, C., Caruso, M., Felsani, A., 1996. Characterization of two novel YY1 binding sites in the polyomavirus late promoter. J. Virol. 70, 1433–1438.

Nakanishi, A., Itoh, N., Li, P.P., Handa, H., Liddington, R.C., Kasamatsu, H., 2007. Minor capsid proteins of simian virus 40 are dispensable for nucleocapsid assembly and cell entry but are required for nuclear entry of the viral genome. J. Virol. 81, 3778–3785.

Nilsson, M., Osterlund, M., Magnusson, G., 1991. Analysis of polyomavirus enhancer-effect on DNA replication and early gene expression. J. Mol. Biol. 218, 479–483.

Oppenheim, A., Peleg, A., 1989. Helpers for efficient encapsidation of SV40 pseudovirions. Gene 77, 79–86.

Oppenheim, A., Sandalon, Z., Peleg, A., Shaul, O., Nicolis, S., Ottolenghi, S., 1992. A cis-acting DNA signal for encapsidation of simian virus 40. J. Virol. 66, 5320–5328.

Palkova, Z., Spanielova, H., Gottifredi, V., Hollanderova, D., Forstova, J., Amati, P., 2000. The polyomavirus major capsid protein VP1 interacts with the nuclear matrix regulatory protein YY1. FEBS Lett. 467, 359–364.

Pastrana, D.V., Tolstov, Y.L., Becker, J.C., Moore, P.S., Chang, Y., Buck, C.B., 2009. Quantitation of Human Seroresponsiveness to Merkel Cell Polyomavirus. PLoS Pathog., 5.

Roitman-Shemer, V., Stokrova, J., Forstova, J., Oppenheim, A., 2007. Assemblages of simian virus 40 capsid proteins and viral DNA visualized by electron microscopy. Biochem. Biophys. Res. Commun. 353, 424–430.

Spanielová, H., 2002. Analysis of regulation of polyomavirus promoters by a luciferase reporter system. Acta Virol. 46, 219–227.

Tolstov, Y.L., Pastrana, D.V., Feng, H.C., Becker, J.C., jenkins, F.J., Moschos, S., Chang, Y., Buck, C.B., Moore, P.S., 2009. Human Merkel cell polyomavirus infection II. MCV is a common human infection that can be detected by conformational capsid epitope immunoassays. Int. J. Cancer 125, 1250–1256.

Türler, H., Beard, P., 1985. Simian virus 40 and polyoma virus: growth, titration, transformation and purification of viral components. In: mahy, B.W.J. (Ed.), Virology: a Practical Approach. IRL Press, Oxford.

Wessa, P., 2012. Spearman Rank Correlation (v1.0.1) in Free Statistics Software (v1.1.23-r7), Office for Research Development and Education, URL ⟨http://www.wessa.net/rwasp_spearman.wasp/⟩.

Yamaguchi, M., Depamphilis, M.L., 1986. DNA binding site for a factor(s) required to initiate simian virus 40 DNA replication. Proc. Natl. Acad. Sci. USA 83, 1646–1650.

Viruses **2012**, *4*, 325-347; doi:10.3390/v4030325

OPEN ACCESS

viruses

ISSN 1999-4915

www.mdpi.com/journal/viruses

Review

Nuclear Actin and Lamins in Viral Infections

Jakub Cibulka, Martin Fraiberk and Jitka Forstova *

Charles University in Prague, Faculty of Science, Department of Genetics and Microbiology, Vinicna 5, 12844, Prague 2, Czech Republic; E-Mails: jakubcib@gmail.com (J.C.); martin.fraiberk@natur.cuni.cz (M.F.)

* Author to whom correspondence should be addressed; E-Mail: jitkaf@natur.cuni.cz; Tel.: +420-221951730; Fax: +420-221951724.

Received: 24 January 2012; in revised form: 20 February 2012 / Accepted: 21 February 2012 / Published: 28 February 2012

Abstract: Lamins are the best characterized cytoskeletal components of the cell nucleus that help to maintain the nuclear shape and participate in diverse nuclear processes including replication or transcription. Nuclear actin is now widely accepted to be another cytoskeletal protein present in the nucleus that fulfills important functions in the gene expression. Some viruses replicating in the nucleus evolved the ability to interact with and probably utilize nuclear actin for their replication, e.g., for the assembly and transport of capsids or mRNA export. On the other hand, lamins play a role in the propagation of other viruses since nuclear lamina may represent a barrier for virions entering or escaping the nucleus. This review will summarize the current knowledge about the roles of nuclear actin and lamins in viral infections.

Keywords: viruses; nuclear actin; nuclear lamina; lamin; cytoskeleton; nucleus

1. Introduction

Viruses are intracellular pathogens known to employ various host-cell mechanisms to facilitate their replication. The cell cytoskeleton is not an exception. To date, many interactions between viruses and cytoskeleton have been described including virus entry, transport of viral particles in the cytoplasm, and release of progeny virions [1].

It would not be surprising if similar interactions between viruses and cytoskeletal proteins also occurred in the nucleus. In fact, there is growing evidence of interactions between certain viruses and two cytoskeletal constituents of the nucleus–nuclear actin and nuclear lamins. After brief characterization of nuclear actin and lamins, respectively, we discuss their role in the replication of viruses from individual families.

2. Viruses and Nuclear Actin

For a long time, the existence and function of actin in the nucleus had been rather controversial. Although seen as early as in the 1970s in amphibian oocytes [2] and even described as necessary for transcription on salamander lampbrush chromosomes [3], nuclear actin was long considered to be cytoplasmic contamination or experimental artifact. In the last decade, numerous reports not only confirmed the actin presence in the nucleus, but also showed actin involvement in several crucial nuclear processes. Nuclear actin plays an important role in transcription, transcription regulation, and chromatin remodeling [4–6]. Actin is required for the function of all three RNA polymerases [7–9]. Moreover, it was shown to bind some pre-mRNA-binding proteins on the nascent transcripts [10–12], and even recruit histone acetyl transferases to actively transcribed areas [13]. Nuclear actin is also believed to participate in chromatin remodeling complexes, e.g., SWI/SNF-like BAF complex [14].

Interestingly, myosin isoform I is also located in the nucleus [15]. Nuclear myosin I is essential for RNA polymerase I [9] and RNA polymerase II transcription [16,17], and interacts with the chromatin remodeling complex, WSTF-SNF2h, which participates in rRNA gene transcription [18]. Other studies confirmed the roles of nuclear actin and myosin in the RNA polymerase I transcription, and even suggested mutual cooperation of these two proteins [19–21].

Despite the evidence of nuclear actin function, its form remains enigmatic. In normal physiological conditions, actin cannot be detected in the nucleus in its polymeric form (e.g., by phalloidin staining) [22,23]. Actin could be present in the nucleus in its monomeric state, but it may also form some non-traditional oligomeric or polymeric conformations. Indeed, there is indirect evidence that nuclear actin can exist in conformations distinct from the cytoplasmic actin [24–26]. Nuclear actin may also be involved in nucleoskeletal structures, where it could participate in nuclear transport or maintenance of nuclear shape [27–30]. Besides actin, many actin-binding proteins (ABPs) and actin-related proteins (ARPs) are also found in the nucleus, where they take part in nuclear processes [30,31]. Finally, it should be noted that nuclear accumulation of actin is also connected with cellular stresses such as heat shock or DMSO treatment [32]. Viral infection naturally also represents a stressful situation, and this should be remembered when discussing subsequent findings regarding viruses and nuclear actin.

2.1. Herpesviruses

Herpesviruses are large enveloped double-stranded DNA viruses with complex structure. The linear dsDNA genomes are located in capsids with icosahedral symmetry. The entire virions are surrounded by a host-cell derived membrane envelope with a number of viral glycoproteins. The capsid and the envelope are divided by an asymmetrical amorphous proteinaceous layer called tegument [33,34].

Herpesviruses replicate in the cell nucleus. Viral replication, late transcription, and formation of viral capsids take place in the ‘replication compartments’ (RCs) [35–40], intranuclear structures

originally defined by the presence of viral single-strand DNA-binding protein ICP8, and other viral and host factors [39,41,42]. RCs are formed by fusion of smaller pre-replication sites [43] followed by dramatic changes in the nuclear morphology, host chromatin marginalization, and finally nuclear lamina disruption apparently required for virion egress [44–47].

2.1.1. Nuclear Actin in the Assembly and Transport of Viral Capsids

Three members of the *Alphaherpesvirinae* subfamily–herpes simplex virus 1 (HSV-1), herpes simplex virus 2 (HSV-2), and pseudorabies virus (PRV) were shown to induce filament formation in the nuclei of infected cells [48,49]. In the case of PRV infection, the observed filaments had an average length of 3 μm and a diameter of 25–100 nm (rather suggesting bundles of filaments), and associated with the viral capsids, as shown by serial-section block-face scanning electron microscopy (SBFSEM) [48]. Further examination revealed that these filaments consisted of F-actin and their polarity corresponded with the overall polarity of the cell–they formed predominantly on the side of the nucleus facing the Golgi apparatus [48]. The nuclear actin filaments (stained with fluorescent phalloidin) colocalized with the GFP-labeled main capsid protein, VP26, and were required for the formation of GFP-VP26 foci (where the capsids are likely assembled) [48]. The findings of another report suggest that the motion of HSV-1 capsids in the nucleus is active and dependent on actin and myosin [50]. Indeed, nuclear myosin Va strongly colocalized with GFP-labeled capsids of PRV, mainly in the GFP-VP26 foci [48]. Taken together, we can assume that nuclear actin filaments (possibly together with nuclear myosin Va) play a role in the assembly and/or transport of alphaherpesviral capsids.

2.1.2. Nuclear Actin and Morphological Changes of Infected Nuclei

The HSV-1 infection induces dramatic changes in the structure of infected nuclei. Along with the appearance of virus RCs, their growth and fusion, we can also observe marginalization and dispersion of host chromatin and substantial enlargement of infected nuclei (to twice the volume of uninfected nuclei) [44]. Finally, the nuclear lamina is disrupted, and virions escape the nucleus (see later).

In HSV-1-infected cells treated with latrunculin A, reductions in enlargement of nuclei, host chromatin dispersion, and RC maturation were observed in comparison with the untreated control cells. This suggests participation of nuclear actin in the maturation of RCs and accompanying processes. Interestingly, treatment of HSV-1-infected cells with cytochalasin D did not exhibit such reductions (discussed in next subsection) [46]. Besides that, HSV-1 is also able to disrupt the nucleoskeletal structure visualized by GFP-Cdc14B fusion protein [46]. Cdc14B is a phosphatase acting in the cell cycle regulations, which can localize to intranuclear filaments connecting nucleoli and nuclear periphery (and often ending in the vicinity of nuclear pores) [51]. These filaments are about 7 nm in diameter, and their formation is actin dependent [51]. In the course of HSV-1 infection, the filaments are disrupted, and GFP-Cdc14B forms point aggregates in the nuclei [46].

Finally, the sequestration of actin monomers by latrunculin A does not prevent the HSV-1-induced nuclear lamina disruption [46], and this process is therefore probably actin independent.

2.1.3. Monomeric *versus* Polymeric Nuclear Actin

While it seems that the polymeric F-actin plays a certain role in the capsid assembly, it is not clear what form of nuclear actin is responsible for other mentioned phenomena. The morphological changes of HSV-1-infected nuclei are abolished in the presence of latrunculin A but not cytochalasin D [46]. Similarly, latrunculin A but not cytochalasin D was shown to decrease the mobility of HSV-1 capsids in the nucleus [50]. Considering that latrunculin A binds actin monomers (G-actin) and thus inhibits its potential functions, we can assume that the above-mentioned phenomena are G-actin dependent. The disassembly of F-actin by cytochalasin D (binding specifically to the growing end of actin filament) had little effect on the nuclear morphology and capsid mobility [46,50]. Unfortunately, data concerning the effects of actin inhibitors on alphaherpesvirus infectivity are rather inconsistent. Cytochalasin D was shown to reduce PRV infectivity [52], but no reduction in replication after latrunculin A or cytochalasin D treatment was observed for HSV-1 (cytochalasin D in fact markedly increased the infectious titer of HSV-1) [46]. We should also consider the possibility that nuclear actin is distinct in its conformation from the cytoplasmic F-actin, and therefore the effects of these inhibitors may differ. Whatever the functions of nuclear actin, they are rather auxiliary than essential for virus replication, since treatment with actin polymerization inhibitors does not affect replication of HSV-1 [46].

2.1.4. Actin as Part of Herpesviral Virions

Actin can be incorporated into virions of PRV [52,53], human cytomegalovirus (HCMV) [54], murine cytomegalovirus (MCMV) [55], and Kaposi's sarcoma-associated herpesvirus (KSHV) [56,57]. It is localized predominantly in the tegument [53]. In the case of PRV, it was shown that actin can partly replace the main tegument protein, VP22 [53]. Furthermore, filaments similar to F-actin were observed both in the perinuclear [58] and extracellular virions [34] of HSV-1. These filaments appeared to connect the nucleocapsid with the membrane envelope of the virion [34,58]. Despite many evidences of actin presence in the virions of herpesviruses, its function remains unknown.

2.2. Baculoviruses

Baculoviruses are dsDNA viruses infecting invertebrates, mainly insects from orders *Lepidoptera*, *Hymenoptera*, and *Diptera*. Baculoviruses are unique in producing two morphologically distinct infectious viral particles. Budded virions (BV), formed by budding of the nucleocapsid from the host cell cytoplasmic membrane, are responsible for viral spreading between the cells of one individual and inducing systemic infection. Occlusion-derived virus (ODV) gains its envelope in the nucleus of infected cells (most likely from the nuclear membrane invaginations). The virions of ODV are further incorporated into huge paracrystalline proteinaceous matrix formed by protein polyhedrin (nucleopolyhedroviruses) or granulin (granuloviruses). ODV can infect other individuals and is capable of long persistence outside the host cell.

The polyhedral-shaped ODV particle of nucleopolyhedroviruses contains a number of enveloped virions connected by polyhedrin. According to the number of nucleocapsids in one envelope, the nucleopolyhedroviruses are further divided to single nucleopolyhedroviruses (SNPV; one capsid per envelope) and multiple nucleopolyhedroviruses (MNPV; more capsids per one envelope). The

granuloviral ODV particle contains only one virion in the ovicylindrical granulin occlusion (baculovirus biology briefly reviewed at [59]).

Replication, transcription, and morphogenesis of baculoviral capsids take place in the cell nucleus. Viral DNA replication occurs in specific intranuclear domains that grow gradually to form the 'virogenic stroma'. Virogenic stroma occupies most of the nucleus and marginalizes host chromatin [60].

2.2.1. Nuclear Actin Filaments and Nucleocapsid Morphogenesis

More than twenty years ago, cytochalasin D was found to inhibit *Autographa californica* multiple nucleopolyhedrovirus (AcMNPV) replication by preventing proper nucleocapsid assembly in the infected nuclei [61–63]. These results suggested that F-actin is somehow involved in this nuclear process, as it was in fact later confirmed [64–66].

Nuclear actin filaments form in the AcMNPV-infected cells in the late phase of infection (starting 12 hpi) and are located mainly in the area bordering the virogenic stroma, where they colocalize with the main capsid protein, p39 [64,65]. The experiments with mutated actin resistant to cytochalasin D definitely confirmed that inhibition of proper nucleocapsid morphogenesis induced by this inhibitor was caused by nuclear F-actin disassembly [66].

Other nucleopolyhedroviruses–*Spodoptera frugiperda* MNPV, *Bombyx mori* NPV, *Orgyia pseudotsugata* MNPV, *Lymantria dispar* MNPV, *Anticarsia gemmatalis* MNPV, and *Helicoverpa zea* SNPV–are not able to create infective progeny in the presence of either cytochalasin D or latrunculin A [67]. These findings suggest a conserved mechanism of nuclear F-actin employment in the nucleocapsid morphogenesis of nucleopolyhedroviruses.

2.2.2. Actin Relocalization to the Nucleus

The prerequisite for nuclear actin polymerization in late infection is previous accumulation of sufficient amounts of actin monomers in the nucleus. As described for AcMNPV, this happens already in the early phase of infection with participation of products of six viral genes: ie-1, pe38, he65, Ac004, Ac102, and Ac152 [68]. IE1 and PE38 proteins are immediate-early transcription activators, he65 encodes delayed-early protein, and the products of the remaining genes have not been characterized yet. The product of Ac152 is most likely transactivator of Ac102 and he65 genes. The expression of these six genes is sufficient for G-actin nuclear localization but not for its polymerization [68].

2.2.3. Mechanism of Nuclear Actin Polymerization

The AcMNPV nucleocapsids are able to induce actin polymerization *in vitro* [69] and *in vivo* in the early infection after their release from endosomes [70]. Two actin-binding capsid proteins of AcMNPV were identified: p39 and p78/83 [69].

Study of actin polymerization kinetics using fluorescence recovery after photobleaching (FRAP) revealed the dynamic nature of nuclear F-actin in the AcMNPV-infected cells. Jasplakinolide (stabilizing actin filaments and inhibiting further polymerization) prevented fluorescence recovery in FRAP experiments and lowered the viral infectivity substantially [71]. It means that not only F-actin formation but also its dynamic polymerization plays a key role in the AcMNPV life cycle. The Arp2/3

complex (common host cell actin nucleator) is responsible for nuclear actin nucleation in this step of infection. Arp2/3 is recruited to the nucleus and activated by viral capsid protein p78/83 [71]. Protein p78/83 of nucleopolyhedroviruses contains several highly conserved sequences typical for the Wiskott-Aldrich syndrome protein (WASP) family: proline-rich region, G-actin binding WH2 (WASP-homology 2) domain, and Arp2/3 binding CA (connector and acidic) region [72]. The purpose of WASP proteins and related activators of actin nucleation is activation of Arp2/3 and subsequent actin filament nucleation. Protein p78/83 is therefore probably able to mimic the action of cellular proteins from the WASP family [71].

Another viral capsid protein, C42, is essential for nuclear F-actin formation and proper nucleocapsid assembly. This protein mediates translocation of p78/83 into the nucleus using its nuclear localization signal [73]. Moreover, it participates directly in the nuclear actin polymerization, probably via its pocket protein binding sequence (PPBS) [74]. The absence of C42 prevents the nuclear actin filament assembly and correct nucleocapsid morphogenesis even when the nuclear localization of p78/83 is provided artificially [74]. Mutation of the PPBS of C42 does not impair the nuclear translocation of p78/83, Arp2/3, or G-actin, but it blocks the nuclear actin polymerization and reduces viral infectivity [74].

The above-mentioned findings apply to AcMNPV, but the same mechanism of nuclear actin polymerization was also described for *Helicoverpa armigera* MNPV [75]. Taken together with the high level of similarity in WASP-related sequences among different nucleopolyhedroviruses [72], we can assume a general mechanism of nuclear actin utilization valid for all nucleopolyhedroviruses.

2.2.4. F-Actin and the Nuclear Egress of AcMNPV

Recently, one more protein of AcMNPV, VP80, was found to interact with the host nuclear actin [76]. VP80 associates both with nucleocapsids and nuclear actin filaments that connect virogenic stroma and nuclear periphery [76]. VP80 is also indispensable for nuclear export of AcMNPV capsids [77]. Interestingly, this export seems to be actin and myosin dependent. Supported by the fact that VP80 shares sequence homologies with the paramyosin protein family, this may point to nuclear export of nucleocapsids using the actin-myosin complex [76].

2.3. Retroviruses

Besides herpesviruses and baculoviruses, two retroviruses have been shown to use nuclear actin in their life cycle. The first is human immunodeficiency virus type 1 (HIV-1) from the genus lentivirus, the second is Mason-Pzifer monkey virus (MPMV) from the genus betaretrovirus. Both viruses need nuclear actin to transport their unspliced mRNAs from the nucleus to the cytoplasm [28,29].

HIV-1 Rev is a viral protein responsible for transport of unspliced and partially spliced viral mRNAs from the nucleus to the cytoplasm. In its amino-terminal region, Rev contains a sequence that serves as nuclear localization signal and also specifically recognizes the hairpin structure present on unspliced viral mRNAs called Rev response element (RRE). The carboxy-terminus of Rev includes the nuclear export signal that interacts with exportin 1 facilitating (together with Ran GTPase) translocation of Rev with bound mRNA to the cytoplasm through the nuclear pore complex. Another factor essential for Rev-dependent export of HIV-1 mRNAs to the cytoplasm of *Xenopus laevis*

oocytes is translation initiation factor eIF-5A. eIF-5A interacts with exportin 1, Rev, various nucleoporins, and even actin [28]. Mason-Pfizer monkey virus does not encode any protein similar to Rev, and transport of unspliced mRNAs depends on the host cell factors recognizing specific RNA structure, constitutive transport element (CTE) (mRNA export of HIV-1 and MPMV reviewed at [78]). Export of mRNA using CTE is not dependent on eIF-5A [28].

Nuclear actin filament bundles were observed in the nuclei of transfected HeLa cells that expressed HIV-1 RNAs. These bundles, intersecting the nucleus and pointing to the nuclear envelope, colocalized with gag mRNA, Rev protein, exportin 1, and GTPase Ran. Disassembly of the actin bundles with latrunculin B inhibited nuclear export of gag mRNA, but not of completely spliced tat/rev mRNA or cellular mRNA for glyceraldehyde 3-phospahate dehydrogenase [29]. The necessity of nuclear actin for Rev-dependent (HIV-1) as well as Rev-independent (MPMV) transport of unspliced retroviral mRNAs was further confirmed in microinjection experiments performed with *X. laevis* oocytes and Vero cells [28]. Similar results were surprisingly obtained for the host protein kinase inhibitor (PKI) possessing its own nuclear export signal [28]. The nuclear actin involved in this nuclear export could be in its polymeric, filamentous state [29], but experiments with actin inhibitors point to actin monomers or short oligomers rather than to F-actin [28]. This is also supported by labeling with 2G2 antibody [28] that recognizes the actin conformation specific for the nucleus [24]. Whatever is the case, the actual function and form of nuclear actin in retroviral infections will have to be clarified by further research.

3. Viruses and Nuclear Lamins

Lamins are the best known cytoskeletal constituents of the nucleus. They belong to the intermediate filament protein family (class V) and possess the typical structure of intermediate filaments. Mammalian cells produce four main types of lamins: lamin A and lamin C (called A-type lamins) are different splicing products of the same gene, lamin B1 and lamin B2 (B-type lamins) are encoded by two distinct genes. A-type and B-type lamins differ in several characteristics, e.g., isoelectric point and behavior during mitosis. Lamins represent the main components of the nuclear lamina, proteinaceous filamentous layer that is located between chromatin and inner nuclear membrane and contributes significantly to the structural integrity of the nuclear envelope. Nuclear lamina was traditionally described as a regular network of lamin filaments [79], but recent reports revealed more complicated structure dependent on the lamina composition and cell type [80]. Besides the nuclear lamina, lamins were also found as spots in the nucleus interior [81–83] and in the case of lamin A even as a part of intranuclear filaments [84–87]. Today, lamins are recognized to play many roles in different nuclear processes including replication, transcription, chromatin organization, and others [88]. Mutations in genes for nuclear lamina components (mainly lamin A gene) are associated with a variety of human diseases called laminopathies [89].

3.1. Herpesviruses

Thanks to the size of nucleocapsids of herpesviruses (~125 nm in diameter for HSV-1), the nuclear envelope represents a significant barrier on their way out of the nucleus. Only particles up to 39 nm in diameter can be transported through the nuclear pore [90], and the size of nuclear lamina fenestrations

is approximately 15 nm [80]. Thus, either enlargement of nuclear pores or changes in the lamina structure are necessary for successful release of herpesvirus nucleocapsids to the cytoplasm. According to the now widely accepted 'envelopment-deenvelopment-reenvelopment' hypothesis, the nucleocapsids bud through the inner nuclear membrane to perinuclear space. This primary envelope subsequently fuses with the outer nuclear membrane, and naked nucleocapsids escape to the cytoplasm, where they gain a new envelope derived from the endoplasmic reticulum (ER) or Golgi apparatus membranes [91,92]. This model assumes that herpesviruses are able to induce restructuring or disassembly of nuclear lamina that would normally prevent the direct contact of nucleocapsids with the inner nuclear membrane.

Many studies confirmed the involvement of herpesviruses in the changes of nuclear lamina structure. HSV-1, HSV-2, MCMV, HCMV, and Epstein-Barr virus (EBV) use similar mechanisms to disrupt the nuclear lamina and release the virions from the nucleus [93]. These mechanisms utilize viral as well as host factors and will be discussed in detail on the example of HSV-1, and briefly described for other herpesviruses.

3.1.1. HSV-1

Cells infected with HSV-1 exhibit different fluorescent profiles of nuclear lamins and lamin B receptor, suggesting thinning and partial disassembly of the nuclear lamina [45]. These findings were obtained by observing living cells producing proteins lamin B receptor, lamin A, and lamin B2 fused with GFP and also by indirect immunofluorescence using antibodies against lamin A/C, lamin B1, and lamin B2. Furthermore, during infection, the rate of lamin B receptor diffusion in the inner nuclear membrane and solubility of lamin A are significantly increased [45]. HSV-1 infection also induces an overall decrease in the amount of lamins in infected cells [45].

Disruption of nuclear lamina by HSV-1 is coupled with RC maturation [47] and involves action of both viral and host proteins. These include viral proteins associated with the nuclear envelope together with viral as well as cellular kinases. All these proteins form the 'nuclear egress complex' (Figure 1, left) and work in concert to facilitate nuclear lamina breach and thus the egress of new virions from the nucleus.

The viral transmembrane protein necessary for primary envelopment, pUL34 [94], and the viral phosphoprotein found to be associated with the nuclear matrix, pUL31 [95], form together a complex that associates with the inner nuclear membrane [96–98]. This localization of pUL34 and pUL31 is observable only when expressed together (infection with viruses that had deleted either gene led to mislocalization of the remaining protein) [96,97]. Coexpression of UL34 and UL31 genes alone is sufficient for pUL34 and pUL31 localization to the nuclear envelope [96]. However, for even distribution of the complex along the nuclear rim, viral kinase pUS3 is required. When pUS3 is absent, pUL34 and pUL31 are unevenly distributed throughout the nuclear rim and associate with the nuclear membrane invaginations containing clusters of primarily enveloped virions [96,97]. The correct localization of pUL34 also depends on the presence of the lamin A/C itself [99].

Figure 1. Nuclear egress complex of herpes simplex virus 1 (HSV-1) and human cytomegalovirus (HCMV). The lamin proteins are depicted as two layers beneath the nuclear membrane (lamin B in red, lamin A/C in green). The red "P" in circle marks phosphorylated proteins, actions of individual protein kinases are represented by black arrows. The dashed arrow suggests hypothetical phosphorylation of lamins by pUL13 kinase (proved for HSV-2). The lamin B receptor protein is abbreviated as "LBR". Besides PKC, other cellular kinases may be involved in phosphorylation of nuclear lamina components.

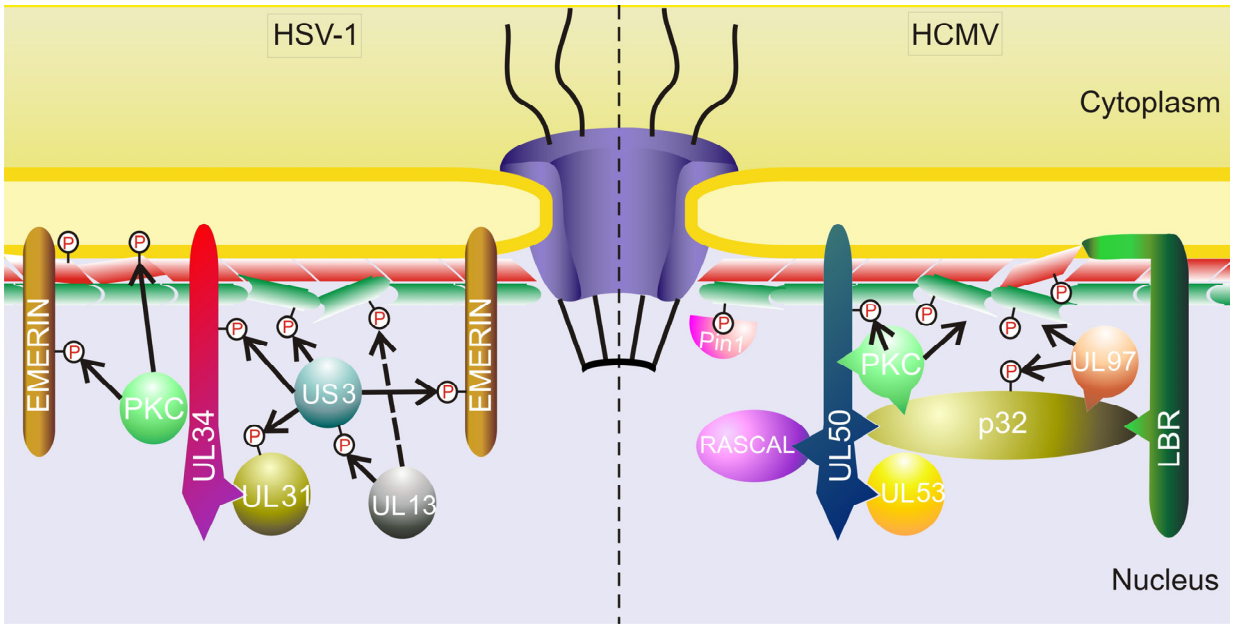

Besides the role in primary envelopment of virions [94,96,97], the pUL34-pUL31 complex is responsible for nuclear lamina disruption. Viruses lacking UL34 or UL31 genes are not capable to induce changes in the immunoreactivity of lamin A/C and lamin-associated polypeptide 2, typical of cells infected with the wild-type virus [47]. Additionally, the UL34 gene is also required for disruption of lamin B [100]. The role of pUL31 and pUL34 in the nuclear lamina rearrangement is further supported by findings that both bind lamin A/C directly and that overexpression of either of them leads to partial lamin A/C relocalization [101].

Whether HSV-1 induces only conformational changes or even disruption of nuclear lamina was examined by different antibodies directed against lamin A/C. Staining with monoclonal antibody against the tail domain of lamin A/C exhibited significant reduction in the infected cells dependent on the pUL34 and pUL31 presence. Polyclonal antibody recognizing epitopes in the rod domain of lamin A/C showed decreased lamin staining even in the absence of pUL31 (but not pUL34). Surprisingly, labeling with the third polyclonal antibody did not exhibit any differences between infected and uninfected cells. Based on these experiments the authors suggested that the alterations in lamin staining during HSV-1 infection were caused by conformational changes in the nuclear lamina rather than its direct disintegration [101]. However, observations in cells producing GFP-lamin A fusion protein showed that HSV-1 caused real perforation of nuclear lamina dependent on the presence of pUL34 and pUL31 [46].

Proteins pUL34 and pUL31 are indispensable not only for nuclear lamina disruption, but also for characteristic nuclei enlargement [46].

In HSV-1-infected cells, viral serine/threonine kinase, pUS3, colocalizes with pUL34 and pUL31 on the nuclear envelope and also associates with perinuclear virions [97]. pUS3 can phosphorylate pUL34 [102] and pUL31 [103] and its activity is needed for even distribution of the pUL34-pUL31 complex in the inner nuclear membrane [96,97]. If pUS3 is missing or catalytically inactive, primarily enveloped virions are concentrated in the invaginations of perinuclear space into the nucleoplasm. In these areas, pUL34 and pUL31 accumulation and large perforations of nuclear lamina can be detected [97,100,104]. This effect is probably caused by prevention of pUS3-mediated phosphorylation of pUL31 [103]. The damage to nuclear lamina is greater in the absence of pUS3, suggesting that some negative regulation between the action of pUS3 and pUL34-pUL31 complex exists. This would be in agreement with findings that coexpression of pUS3 (catalytically active) and pUL34 leads to less dramatic changes in the nuclear lamina than individual expression of either gene [100]. Deletion of US3 gene decreases viral infectivity, although surprisingly not in all cell types [97,102].

Apart from the indirect role in the nuclear lamina disruption via regulation of pUL34 and pUL31 activity, pUS3 was shown to directly phosphorylate lamin A/C on several sites *in vitro* and *in vivo* [104]. Moreover, pUS3 alone can increase lamin A/C solubility and induce some defects in the nuclear lamina [100,104]. Interestingly, its kinase activity is not required to disrupt lamins in transfected cells [100].

HSV-1 also causes structural changes of proteins of the inner nuclear membrane that are associated with nuclear lamina such as lamin B receptor [45] and lamin-associated polypeptide 2 [47]. Another inner nuclear membrane protein affected by HSV-1 infection is emerin. During infection, emerin is delocalized and exhibits increased mobility [105,106]. This is due to its phosphorylation by host protein kinases [105,106], including protein kinase C (PKC) δ [106]. However, the involvement of PKCδ was later disputed [107]. Virus pUS3 kinase participates in emerin phosphorylation too [105,106], although possibly indirectly by modulating cellular kinase(s) activities [105]. Hyperphosphorylation of emerin is also partially dependent on the presence of pUL34, which is able to bind emerin and recruit cellular kinase(s) [106].

Another kinase participating in nuclear lamina disintegration is a product of the UL13 gene, highly conserved herpesviral serine/threonine kinase. pUL13 is capable to phosphorylate the pUS3 kinase and its deletion leads to a similar phenotype as deletion of US3, *i.e.*, changes in the localization of pUL34 and pUL31 in the inner nuclear membrane [108]. Nevertheless, it is not clear whether pUL13 influences pUL34-pUL31 localization directly or via phosphorylation of pUS3 [108]. It is also worth mentioning that pUL13 of HSV-2 directly phosphorylates nuclear lamins and causes their redistribution [109].

In the course of HSV-1 infection, PKC is concentrated in the vicinity of nuclear envelope [110]. This relocalization occurs between 8 and 12 hours post infection and depends on the presence of the pUL34-pUL31 complex in the nuclear envelope [110]. Viral kinase pUS3 is responsible for the even distribution of PKC along the nuclear rim because it influences the distribution of pUL34-pUL31 in the same way [110]. Two isoforms of PKC–PKCα and PKCδ–are relocalized to the nuclear envelope coincidently with increased lamin B phosphorylation [110]. Lamin B could be phosphorylated directly by PKC and/or other cellular or viral kinases [107,110]. The PKC activity is essential for HSV-1 infection since inhibition of all PKC isoforms causes substantial reduction of viral replication, accumulation of virus particles in the nuclei, and overall decrease in the amount of viral capsids in the

infected cells. On the other hand, specific inhibition of conventional PKCs (including PKCα) or PKCδ does not inhibit viral replication [107]. This indicates either functional redundancy of these isoforms or involvement of other PKC forms in the viral life cycle.

3.1.2. Other Herpesviruses

Individual members of the *Herpesviridae* family share substantial resemblance concerning the mechanisms of nuclear lamina disruption. Proteins homological to pUL34 and pUL31 were described for HSV-2 [111,112], PRV [113,114], HCMV [115], MCMV [116], and EBV [117–119]. These proteins are, like in HSV-1, responsible for primary envelopment and release of virions from the nucleus. The direct role in the changes of nuclear lamina, including PKC relocalization, was proved for pUL50 and pUL53 of HCMV [115,120,121], although, unlike HSV-1 pUL34, pUL50 alone is able to recruit PKC [121] and even can be phosphorylated itself by this kinase [120]. During MCMV infection, proteins M50/p35 and M53/p38 recruit PKC to the nuclear rim for lamin phosphorylation and lamina dissolution [116]. BFLF2 and BFRF1 proteins of EBV were shown to interact with lamin B [119].

Homologs of HSV-1 pUL13 kinase ('conserved herpesviral kinases'), pUL13 of HSV-2, pUL97 of HCMV, and BGLF4 of EBV, participate in direct phosphorylation of lamins and disruption of the nuclear lamina [109,121–126]. Remarkably, pUL97 and BGLF4 apparently imitate the activity of cellular cyclin-dependent kinase 1, which is responsible for the nuclear lamina breakdown during mitosis [123,126]. Furthermore, the pUL97-mediated phosphorylation of lamin A/C at Ser22 creates a binding motif for the cellular peptidyl-prolyl cis/trans-isomerase Pin1 [125]. During HCMV infection, Pin1 is concentrated by the nuclear lamina in a manner dependent on the protein kinase activity [125]. Pin1 could contribute to nuclear lamina reorganization by inducing conformational changes of lamins [125].

Another cellular protein involved in the HCMV-induced nuclear lamina disruption is p32 protein. This protein recruits pUL97 kinase to the lamin B receptor and is itself phosphorylated by pUL97 [122]. Moreover, p32 also directly interacts with pUL50 and PKC [120,121]. In addition, the recently characterized protein of HCMV, RASCAL (nuclear rim-associated cytomegaloviral protein), was also identified to be involved in the nuclear egress complex, likely via its interaction with pUL50 [127]. The nuclear egress complex of HCMV is depicted in figure 1, right.

Alphaherpesviruses have homologs of HSV-1 pUS3 kinase as well, and they share some functional similarities – for example, pUS3 of PRV influences pUL34 localization in the same way as its HSV-1 counterpart [128] and pUS3 of HSV-2 changes the pattern of emerin hyperphosphorylation [105]. Interestingly, HSV-2 pUS3 exhibits marked differences from HSV-1 pUS3 in its catalytic functions, e.g., it does not control the localization of the nuclear egress complex [129].

Even though the ways of interactions of viral proteins with nuclear lamins slightly vary between individual herpesviruses, they all result in nuclear lamina disruption, thus confirming the role of nuclear lamina as a major obstacle to herpesviral replication.

3.2. Other Viruses

Although herpesviruses are by far the most extensively studied virus family regarding their interactions with nuclear lamins, studies describing the interplay between lamins and other viruses are

slowly emerging. It seems that, similarly to herpesviruses, the nuclear lamina represents a barrier for all these viruses, and hence they evolved mechanisms to overcome it. However, we have to be more careful about making any definite conclusions since there is only one or a few reports concerning lamins for each below-mentioned virus family.

3.2.1. Retroviruses

HIV-1 requires nuclear actin for nuclear export of its unspliced mRNAs, but there are also evidences for HIV-1 interactions with nuclear lamina. Viral protein Vpr induces perforations in the nuclear envelope corresponding to the sites with defects in nuclear lamina [130]. These perforations lead to mixing of cytoplasmic and nucleoplasmic content, including cell cycle regulators. The authors hence deduce that these defects consequently result in the cell cycle arrest in G2 phase, which is a known effect of the Vpr protein [130]. Apart from that, this action of Vpr could facilitate the nuclear entry of HIV preintegration complex [130,131].

3.2.2. Polyomaviruses

Polyomaviruses are small non-enveloped tumorigenic viruses with circular double-stranded DNA genome. The best studied representatives of the *Polyomaviridae* family are simian virus 40 (SV40), mouse polyomavirus (MPyV), and human pathogens JC virus and BK virus. In the last several years, seven additional human polyomaviruses have been discovered, including Merkel cell polyomavirus associated with rare but aggressive cancer of Merkel cells.

Upon cell entry, polyomaviruses are transported through the endosomal pathway to the ER [132–136]. Infection of MPyV is dependent on acidic pH of the endosomes [137]. Qian *et al*. proposed that MPyV is transported first to the endolysosome, and there the polyomavirus ganglioside receptor stimulates sorting of MPyV to the ER [138]. The precise mechanism controlling the transport of MPyV from the plasma membrane to the ER remains to be clarified. Even less clear is the mechanism by which polyomaviruses deliver their genomes into the cell nucleus. Based on electron microscopy analyses, early papers suggested that SV40 [139] and MPyV [140] enter the cell nucleus bypassing nuclear pores by fusion of vesicles carrying virions directly with the nuclear envelope. At present, two models of polyomavirus trafficking from ER into the nucleus are discussed. The first model presumes that partially disassembled virions are translocated (by an as yet unknown mechanism) from ER to the cytosol and enter the nucleus via nuclear pores. Although it has never been proved, several findings support this hypothesis [141–145].

Alternatively, a recent report on SV40 suggests a model, in which the genomes are delivered from the ER directly to the nucleus. During cell entry, SV40 induces transient changes in the structure of the nuclear envelope accompanied by fluctuations in the lamin A/C protein level, accumulation of lamin A/C in the cytoplasm, and dephosphorylation of a specific lamin A/C epitope [146]. These changes culminate 6-8 hours post infection, just prior to and during nuclear entry of the viral genome, and seem to be caspase-6 dependent. Interestingly, these alterations in nuclear envelope structure occur exclusively during infection of non-proliferating cells, and the pentamers of the major capsid protein, VP1, are sufficient to induce them [146]. Interaction of VP1 protein with nuclear lamina was also observed during the expression of MPyV VP1 in mouse fibroblast cells (our unpublished results).

Along with the lamina, the nuclear membrane represents a natural barrier for polyomavirus infection. *In vitro* studies on the minor structural proteins, VP2 and VP3, of SV40 [147] and of MPyV [148,149] showed that they are able to bind, insert into, perforate and even fuse cell membranes. Thus, in all the above-discussed models, the minor structural proteins might be key actors helping virions pass through ER and/or inner nuclear membrane.

3.2.3. Parvoviruses

The Minute virus of mice (MVM) is a small non-enveloped ssDNA virus that belongs to the *Parvoviridae* family and replicates in the cell nucleus. In the early phase of infection, prior to the nuclear entry, MVM induces transient breaks in the nuclear envelope accompanied by changes in the lamin A/C immunostaining [150]. Moreover, the gaps in lamin staining are coincident with the antibody-labeled virus [150]. Further examination revealed that host caspases are involved in MVM-induced nuclear envelope breakdown. In particular, basally active caspase 3 is relocalized to the nucleus, where it cleaves nuclear lamins (most likely lamin B2) [151]. These findings suggest that parvoviruses, despite their small size (ca 26 nm in diameter), do not import their genome into the nucleus via the nuclear pore, and instead they cause partial breaks in the nuclear envelope to facilitate nuclear entry. Consistently with this unusual model, capsids of adeno-associated virus 2 (AAV2) were shown to enter purified nuclei independently of nuclear pore complexes [152].

4. Conclusions

In this review, we wanted to present the current knowledge on the significance of nuclear actin and lamins for various viruses. Despite the increasing number of reports dealing with this topic, many issues remain unresolved. First of all, we still know very little about the form of nuclear actin even in normal, uninfected cells, and that makes our understanding of its employment by viruses more difficult. Secondly, the most findings presented in this review refer to only two virus families– herpesviruses and baculoviruses. Data on other discussed viruses is based on a few studies only. It would be very surprising if these viruses were the only ones interacting with host nuclear actin or lamins. In fact, it is reasonable to expect that other viruses replicating in the nucleus will soon extend this list. To conclude, the participation of both lamins and nuclear actin in the viral life cycle represents a relatively unexplored but very promising area of research that can tell us much about the ability of viruses to deal with the host cell environment.

Acknowledgments

The work was generously supported by the grant SVV-2012-265202 (J.C.), by the grant of Ministry of Education, Youth and Sports of the Czech Republic, n. MSM0021620858 (J.F.), and by the Grant Agency of the Czech Republic, n. P304/10/1511 (M.F.). We are grateful to Sarka Takacova for her assistance in the preparation of this manuscript.

Conflict of Interest

The authors declare no conflict of interest.

References

1. Radtke, K.; Dohner, K.; Sodeik, B. Viral interactions with the cytoskeleton: A hitchhiker's guide to the cell. *Cell. Microbiol.* **2006**, *8*, 387–400.
2. Clark, T.G.; Rosenbaum, J.L. An actin filament matrix in hand-isolated nuclei of x. Laevis oocytes. *Cell* **1979**, *18*, 1101–1108.
3. Scheer, U.; Hinssen, H.; Franke, W.W.; Jockusch, B.M. Microinjection of actin-binding proteins and actin antibodies demonstrates involvement of nuclear actin in transcription of lampbrush chromosomes. *Cell* **1984**, *39*, 111–122.
4. Miralles, F.; Visa, N. Actin in transcription and transcription regulation. *Curr. Opin. Cell Biol.* **2006**, *18*, 261–266.
5. Zheng, B.; Han, M.; Bernier, M.; Wen, J.K. Nuclear actin and actin-binding proteins in the regulation of transcription and gene expression. *FEBS J.* **2009**, *276*, 2669–2685.
6. Olave, I.A.; Reck-Peterson, S.L.; Crabtree, G.R. Nuclear actin and actin-related proteins in chromatin remodeling. *Annu. Rev. Biochem.* **2002**, *71*, 755–781.
7. Hofmann, W.A.; Stojiljkovic, L.; Fuchsova, B.; Vargas, G.M.; Mavrommatis, E.; Philimonenko, V.; Kysela, K.; Goodrich, J.A.; Lessard, J.L.; Hope, T.J.; *et al.* Actin is part of pre-initiation complexes and is necessary for transcription by rna polymerase ii. *Nat. Cell Biol.* **2004**, *6*, 1094–1101.
8. Hu, P.; Wu, S.; Hernandez, N. A role for beta-actin in rna polymerase iii transcription. *Genes Dev.* **2004**, *18*, 3010–3015.
9. Philimonenko, V.V.; Zhao, J.; Iben, S.; Dingová, H.; Kyselá, K.; Kahle, M.; Zentgraf, H.; Hofmann, W.A.; de Lanerolle, P.; Hozák, P.; *et al.* Nuclear actin and myosin i are required for rna polymerase i transcription. *Nat. Cell Biol.* **2004**, *6*, 1165–1172.
10. Percipalle, P.; Zhao, J.; Pope, B.; Weeds, A.; Lindberg, U.; Daneholt, B. Actin bound to the heterogeneous nuclear ribonucleoprotein hrp36 is associated with balbiani ring mrna from the gene to polysomes. *J. Cell Biol.* **2001**, *153*, 229–236.
11. Percipalle, P.; Jonsson, A.; Nashchekin, D.; Karlsson, C.; Bergman, T.; Guialis, A.; Daneholt, B. Nuclear actin is associated with a specific subset of hnrnp a/b-type proteins. *Nucleic Acids Res.* **2002**, *30*, 1725–1734.
12. Kukalev, A.; Nord, Y.; Palmberg, C.; Bergman, T.; Percipalle, P. Actin and hnrnp u cooperate for productive transcription by rna polymerase ii. *Nat. Struct. Mol. Biol.* **2005**, *12*, 238–244.
13. Sjölinder, M.; Björk, P.; Söderberg, E.; Sabri, N.; Farrants, A.K.; Visa, N. The growing pre-mrna recruits actin and chromatin-modifying factors to transcriptionally active genes. *Genes Dev.* **2005**, *19*, 1871–1884.
14. Zhao, K.; Wang, W.; Rando, O.J.; Xue, Y.; Swiderek, K.; Kuo, A.; Crabtree, G.R. Rapid and phosphoinositol-dependent binding of the swi/snf-like baf complex to chromatin after t lymphocyte receptor signaling. *Cell* **1998**, *95*, 625–636.
15. Nowak, G.; Pestic-Dragovich, L.; Hozák, P.; Philimonenko, A.; Simerly, C.; Schatten, G.; de Lanerolle, P. Evidence for the presence of myosin i in the nucleus. *J. Biol. Chem.* **1997**, *272*, 17176–17181.

16. Pestic-Dragovich, L.; Stojiljkovic, L.; Philimonenko, A.A.; Nowak, G.; Ke, Y.; Settlage, R.E.; Shabanowitz, J.; Hunt, D.F.; Hozak, P.; de Lanerolle, P. A myosin i isoform in the nucleus. *Science* **2000**, *290*, 337–341.
17. Hofmann, W.A.; Vargas, G.M.; Ramchandran, R.; Stojiljkovic, L.; Goodrich, J.A.; de Lanerolle, P. Nuclear myosin i is necessary for the formation of the first phosphodiester bond during transcription initiation by rna polymerase ii. *J. Cell Biochem.* **2006**, *99*, 1001–1009.
18. Percipalle, P.; Fomproix, N.; Cavellán, E.; Voit, R.; Reimer, G.; Krüger, T.; Thyberg, J.; Scheer, U.; Grummt, I.; Farrants, A.K. The chromatin remodelling complex wstf-snf2h interacts with nuclear myosin 1 and has a role in rna polymerase i transcription. *EMBO Rep.* **2006**, *7*, 525–530.
19. Philimonenko, V.V.; Janacek, J.; Harata, M.; Hozak, P. Transcription-dependent rearrangements of actin and nuclear myosin i in the nucleolus. *Histochem. Cell Biol.* **2010**, *134*, 243–249.
20. Fomproix, N.; Percipalle, P. An actin-myosin complex on actively transcribing genes. *Exp. Cell Res.* **2004**, *294*, 140–148.
21. Kyselá, K.; Philimonenko, A.A.; Philimonenko, V.V.; Janácek, J.; Kahle, M.; Hozák, P. Nuclear distribution of actin and myosin i depends on transcriptional activity of the cell. *Histochem. Cell Biol.* **2005**, *124*, 347–358.
22. Pederson, T.; Aebi, U. Actin in the nucleus: What form and what for? *J. Struct. Biol.* **2002**, *140*, 3–9.
23. Bettinger, B.T.; Gilbert, D.M.; Amberg, D.C. Actin up in the nucleus. *Nat. Rev. Mol. Cell Biol.* **2004**, *5*, 410–415.
24. Gonsior, S.M.; Platz, S.; Buchmeier, S.; Scheer, U.; Jockusch, B.M.; Hinssen, H. Conformational difference between nuclear and cytoplasmic actin as detected by a monoclonal antibody. *J. Cell Sci.* **1999**, *112*, 797–809.
25. Schoenenberger, C.A.; Buchmeier, S.; Boerries, M.; Sütterlin, R.; Aebi, U.; Jockusch, B.M. Conformation-specific antibodies reveal distinct actin structures in the nucleus and the cytoplasm. *J. Struct. Biol.* **2005**, *152*, 157–168.
26. McDonald, D.; Carrero, G.; Andrin, C.; de Vries, G.; Hendzel, M.J. Nucleoplasmic beta-actin exists in a dynamic equilibrium between low-mobility polymeric species and rapidly diffusing populations. *J. Cell Biol.* **2006**, *172*, 541–552.
27. Kiseleva, E.; Drummond, S.P.; Goldberg, M.W.; Rutherford, S.A.; Allen, T.D.; Wilson, K.L. Actin- and protein-4.1-containing filaments link nuclear pore complexes to subnuclear organelles in xenopus oocyte nuclei. *J. Cell Sci.* **2004**, *117*, 2481–2490.
28. Hofmann, W.; Reichart, B.; Ewald, A.; Müller, E.; Schmitt, I.; Stauber, R.H.; Lottspeich, F.; Jockusch, B.M.; Scheer, U.; Hauber, J.; *et al.* Cofactor requirements for nuclear export of rev response element (rre)- and constitutive transport element (cte)-containing retroviral rnas. An unexpected role for actin. *J. Cell Biol.* **2001**, *152*, 895–910.
29. Kimura, T.; Hashimoto, I.; Yamamoto, A.; Nishikawa, M.; Fujisawa, J.I. Rev-dependent association of the intron-containing hiv-1 gag mrna with the nuclear actin bundles and the inhibition of its nucleocytoplasmic transport by latrunculin-b. *Genes Cells* **2000**, *5*, 289–307.
30. Castano, E.; Philimonenko, V.V.; Kahle, M.; Fukalová, J.; Kalendová, A.; Yildirim, S.; Dzijak, R.; Dingová-Krásna, H.; Hozák, P. Actin complexes in the cell nucleus: New stones in an old field. *Histochem. Cell Biol.* **2010**, *133*, 607–626.

31. Chen, M.; Shen, X. Nuclear actin and actin-related proteins in chromatin dynamics. *Curr. Opin. Cell Biol.* **2007**, *19*, 326–330.
32. Yahara, I.; Aizawa, H.; Moriyama, K.; Iida, K.; Yonezawa, N.; Nishida, E.; Hatanaka, H.; Inagaki, F. A role of cofilin/destrin in reorganization of actin cytoskeleton in response to stresses and cell stimuli. *Cell Struct. Funct.* **1996**, *21*, 421–424.
33. van Hal, S.J.; Dwyer, D.E. Herpes Simplex: Viruses and Infections. In *Encyclopedia of Life Sciences*; John Wiley & Sons, Ltd.: Hoboken, NJ, USA, 2001.
34. Grünewald, K.; Desai, P.; Winkler, D.C.; Heymann, J.B.; Belnap, D.M.; Baumeister, W.; Steven, A.C. Three-dimensional structure of herpes simplex virus from cryo-electron tomography. *Science* **2003**, *302*, 1396–1398.
35. Randall, R.E.; Dinwoodie, N. Intranuclear localization of herpes simplex virus immediate-early and delayed-early proteins: Evidence that icp 4 is associated with progeny virus DNA. *J. Gen. Virol.* **1986**, *67*, 2163–2177.
36. Knipe, D.M.; Senechek, D.; Rice, S.A.; Smith, J.L. Stages in the nuclear association of the herpes simplex virus transcriptional activator protein icp4. *J. Virol.* **1987**, *61*, 276–284.
37. Phelan, A.; Dunlop, J.; Patel, A.H.; Stow, N.D.; Clements, J.B. Nuclear sites of herpes simplex virus type 1 DNA replication and transcription colocalize at early times postinfection and are largely distinct from rna processing factors. *J. Virol.* **1997**, *71*, 1124–1132.
38. Ward, P.L.; Ogle, W.O.; Roizman, B. Assemblons: Nuclear structures defined by aggregation of immature capsids and some tegument proteins of herpes simplex virus 1. *J. Virol.* **1996**, *70*, 4623–4631.
39. de Bruyn Kops, A.; Uprichard, S.L.; Chen, M.; Knipe, D.M. Comparison of the intranuclear distributions of herpes simplex virus proteins involved in various viral functions. *Virology* **1998**, *252*, 162–178.
40. Leopardi, R.; Ward, P.L.; Ogle, W.O.; Roizman, B. Association of herpes simplex virus regulatory protein icp22 with transcriptional complexes containing eap, icp4, rna polymerase ii, and viral DNA requires posttranslational modification by the u(l)13 proteinkinase. *J. Virol.* **1997**, *71*, 1133–1139.
41. Quinlan, M.P.; Chen, L.B.; Knipe, D.M. The intranuclear location of a herpes simplex virus DNA-binding protein is determined by the status of viral DNA replication. *Cell* **1984**, *36*, 857–868.
42. de Bruyn Kops, A.; Knipe, D.M. Preexisting nuclear architecture defines the intranuclear location of herpesvirus DNA replication structures. *J. Virol.* **1994**, *68*, 3512–3526.
43. Taylor, T.J.; McNamee, E.E.; Day, C.; Knipe, D.M. Herpes simplex virus replication compartments can form by coalescence of smaller compartments. *Virology* **2003**, *309*, 232–247.
44. Monier, K.; Armas, J.C.; Etteldorf, S.; Ghazal, P.; Sullivan, K.F. Annexation of the interchromosomal space during viral infection. *Nat. Cell Biol.* **2000**, *2*, 661–665.
45. Scott, E.S.; O'Hare, P. Fate of the inner nuclear membrane protein lamin b receptor and nuclear lamins in herpes simplex virus type 1 infection. *J. Virol.* **2001**, *75*, 8818–8830.
46. Simpson-Holley, M.; Colgrove, R.C.; Nalepa, G.; Harper, J.W.; Knipe, D.M. Identification and functional evaluation of cellular and viral factors involved in the alteration of nuclear architecture during herpes simplex virus 1 infection. *J. Virol.* **2005**, *79*, 12840–12851.

47. Simpson-Holley, M.; Baines, J.; Roller, R.; Knipe, D.M. Herpes simplex virus 1 u(l)31 and u(l)34 gene products promote the late maturation of viral replication compartments to the nuclear periphery. *J. Virol.* **2004**, *78*, 5591–5600.
48. Feierbach, B.; Piccinotti, S.; Bisher, M.; Denk, W.; Enquist, L.W. Alpha-herpesvirus infection induces the formation of nuclear actin filaments. *PLoS Pathog.* **2006**, *2*, e85.
49. Ecob-Johnston, M.S.; Whetsell, W.O. Host-cell response to herpes virus infection in central and peripheral nervous tissue in vitro. *J. Gen. Virol.* **1979**, *44*, 747–757.
50. Forest, T.; Barnard, S.; Baines, J.D. Active intranuclear movement of herpesvirus capsids. *Nat. Cell Biol.* **2005**, *7*, 429–431.
51. Nalepa, G.; Harper, J.W. Visualization of a highly organized intranuclear network of filaments in living mammalian cells. *Cell Motil. Cytoskelet.* **2004**, *59*, 94–108.
52. Wong, M.L.; Chen, C.H. Evidence for the internal location of actin in the pseudorabies virion. *Virus Res.* **1998**, *56*, 191–197.
53. del Rio, T.; DeCoste, C.J.; Enquist, L.W. Actin is a component of the compensation mechanism in pseudorabies virus virions lacking the major tegument protein vp22. *J. Virol.* **2005**, *79*, 8614–8619.
54. Varnum, S.M.; Streblow, D.N.; Monroe, M.E.; Smith, P.; Auberry, K.J.; Pasa-Tolic, L.; Wang, D.; Camp, D.G.; Rodland, K.; Wiley, S.; *et al.* Identification of proteins in human cytomegalovirus (hcmv) particles: The hcmv proteome. *J. Virol.* **2004**, *78*, 10960–10966.
55. Kattenhorn, L.M.; Mills, R.; Wagner, M.; Lomsadze, A.; Makeev, V.; Borodovsky, M.; Ploegh, H.L.; Kessler, B.M. Identification of proteins associated with murine cytomegalovirus virions. *J. Virol.* **2004**, *78*, 11187–11197.
56. Bechtel, J.T.; Winant, R.C.; Ganem, D. Host and viral proteins in the virion of kaposi's sarcoma-associated herpesvirus. *J. Virol.* **2005**, *79*, 4952–4964.
57. Zhu, F.X.; Chong, J.M.; Wu, L.; Yuan, Y. Virion proteins of kaposi's sarcoma-associated herpesvirus. *J. Virol.* **2005**, *79*, 800–811.
58. Baines, J.D.; Hsieh, C.E.; Wills, E.; Mannella, C.; Marko, M. Electron tomography of nascent herpes simplex virus virions. *J. Virol.* **2007**, *81*, 2726–2735.
59. Guarino, L. Baculoviruses. In *Encyclopedia of Life Sciences*; John Wiley & Sons, Ltd.: Hoboken, NJ, USA, 2001.
60. Nagamine, T.; Kawasaki, Y.; Abe, A.; Matsumoto, S. Nuclear marginalization of host cell chromatin associated with expansion of two discrete virus-induced subnuclear compartments during baculovirus infection. *J. Virol.* **2008**, *82*, 6409–6418.
61. Volkman, L.E.; Goldsmith, P.A.; Hess, R.T. Evidence for microfilament involvement in budded autographa californica nuclear polyhedrosis virus production. *Virology* **1987**, *156*, 32–39.
62. Volkman, L.E. Autographa californica mnpv nucleocapsid assembly: Inhibition by cytochalasin d. *Virology* **1988**, *163*, 547–553.
63. Hess, R.T.; Goldsmith, P.A.; Volkman, L.E. Effect of cytochalasin d on cell morphology and acmnpv replication in a spodoptera frugiperda cell line. *J. Invertebr. Pathol.* **1989**, *53*, 169–182.
64. Volkman, L.E.; Talhouk, S.N.; Oppenheimer, D.I.; Charlton, C.A. Nuclear f-actin - a functional component of baculovirus-infected lepidopteran cells. *J. Cell Sci.* **1992**, *103*, 15–22.

65. Charlton, C.A.; Volkman, L.E. Sequential rearrangement and nuclear polymerization of actin in baculovirus-infected spodoptera frugiperda cells. *J. Virol.* **1991**, *65*, 1219–1227.
66. Ohkawa, T.; Volkman, L.E. Nuclear f-actin is required for acmnpv nucleocapsid morphogenesis. *Virology* **1999**, *264*, 1–4.
67. Kasman, L.M.; Volkman, L.E. Filamentous actin is required for lepidopteran nucleopolyhedrovirus progeny production. *J. Gen. Virol.* **2000**, *81*, 1881–1888.
68. Ohkawa, T.; Rowe, A.R.; Volkman, L.E. Identification of six autographa californica multicapsid nucleopolyhedrovirus early genes that mediate nuclear localization of g-actin. *J. Virol.* **2002**, *76*, 12281–12289.
69. Lanier, L.M.; Volkman, L.E. Actin binding and nucleation by autographa california m nucleopolyhedrovirus. *Virology* **1998**, *243*, 167–177.
70. Charlton, C.A.; Volkman, L.E. Penetration of autographa californica nuclear polyhedrosis virus nucleocapsids into iplb sf 21 cells induces actin cable formation. *Virology* **1993**, *197*, 245–254.
71. Goley, E.D.; Ohkawa, T.; Mancuso, J.; Woodruff, J.B.; D'Alessio, J.A.; Cande, W.Z.; Volkman, L.E.; Welch, M.D. Dynamic nuclear actin assembly by arp2/3 complex and a baculovirus wasp-like protein. *Science* **2006**, *314*, 464–467.
72. Machesky, L.M.; Insall, R.H.; Volkman, L.E. Wasp homology sequences in baculoviruses. *Trends Cell Biol.* **2001**, *11*, 286–287.
73. Wang, Y.; Wang, Q.; Liang, C.; Song, J.; Li, N.; Shi, H.; Chen, X. Autographa californica multiple nucleopolyhedrovirus nucleocapsid protein bv/odv-c42 mediates the nuclear entry of p78/83. *J. Virol.* **2008**, *82*, 4554–4561.
74. Li, K.; Wang, Y.; Bai, H.; Wang, Q.; Song, J.; Zhou, Y.; Wu, C.; Chen, X. The putative pocket protein binding site of autographa californica nucleopolyhedrovirus bv/odv-c42 is required for virus-induced nuclear actin polymerization. *J. Virol.* **2010**, *84*, 7857–7868.
75. Wang, Q.; Liang, C.; Song, J.; Chen, X. Ha2 from the helicoverpa armigera nucleopolyhedrovirus: A wasp-related protein that activates arp2/3-induced actin filament formation. *Virus Res.* **2007**, *127*, 81–87.
76. Marek, M.; Merten, O.W.; Galibert, L.; Vlak, J.M.; van Oers, M.M. Baculovirus vp80 protein and the f-actin cytoskeleton interact connecting the viral replication factory with the nuclear periphery. *J. Virol.* **2011**, *85*, 5350–5362.
77. Marek, M.; van Oers, M.M.; Devaraj, F.F.; Vlak, J.M.; Merten, O.W. Engineering of baculovirus vectors for the manufacture of virion-free biopharmaceuticals. *Biotechnol. Bioeng.* **2011**, *108*, 1056–1067.
78. Cullen, B.R. Nuclear mrna export: Insights from virology. *Trends Biochem. Sci.* **2003**, *28*, 419–424.
79. Aebi, U.; Cohn, J.; Buhle, L.; Gerace, L. The nuclear lamina is a meshwork of intermediate-type filaments. *Nature* **1986**, *323*, 560–564.
80. Goldberg, M.W.; Huttenlauch, I.; Hutchison, C.J.; Stick, R. Filaments made from a- and b-type lamins differ in structure and organization. *J. Cell Sci.* **2008**, *121*, 215–225.
81. Bridger, J.M.; Kill, I.R.; O'Farrell, M.; Hutchison, C.J. Internal lamin structures within g1 nuclei of human dermal fibroblasts. *J. Cell Sci.* **1993**, *104*, 297–306.
82. Goldman, A.E.; Moir, R.D.; Montag-Lowy, M.; Stewart, M.; Goldman, R.D. Pathway of incorporation of microinjected lamin a into the nuclear envelope. *J. Cell Biol.* **1992**, *119*, 725–735.

83. Moir, R.D.; Montag-Lowy, M.; Goldman, R.D. Dynamic properties of nuclear lamins: Lamin b is associated with sites of DNA replication. *J. Cell Biol.* **1994**, *125*, 1201–1212.
84. Hozák, P.; Sasseville, A.M.; Raymond, Y.; Cook, P.R. Lamin proteins form an internal nucleoskeleton as well as a peripheral lamina in human cells. *J. Cell Sci.* **1995**, *108*, 635–644.
85. Barboro, P.; D'Arrigo, C.; Diaspro, A.; Mormino, M.; Alberti, I.; Parodi, S.; Patrone, E.; Balbi, C. Unraveling the organization of the internal nuclear matrix: Rna-dependent anchoring of numa to a lamin scaffold. *Exp. Cell Res.* **2002**, *279*, 202–218.
86. Barboro, P.; D'Arrigo, C.; Mormino, M.; Coradeghini, R.; Parodi, S.; Patrone, E.; Balbi, C. An intranuclear frame for chromatin compartmentalization and higher-order folding. *J. Cell. Biochem.* **2003**, *88*, 113–120.
87. Neri, L.M.; Raymond, Y.; Giordano, A.; Capitani, S.; Martelli, A.M. Lamin a is part of the internal nucleoskeleton of human erythroleukemia cells. *J. Cell. Physiol.* **1999**, *178*, 284–295.
88. Prokocimer, M.; Davidovich, M.; Nissim-Rafinia, M.; Wiesel-Motiuk, N.; Bar, D.Z.; Barkan, R.; Meshorer, E.; Gruenbaum, Y. Nuclear lamins: Key regulators of nuclear structure and activities. *J. Cell. Mol. Med.* **2009**, *13*, 1059–1085.
89. Worman, H.J.; Bonne, G. "Laminopathies": A wide spectrum of human diseases. *Exp. Cell Res.* **2007**, *313*, 2121–2133.
90. Panté, N.; Kann, M. Nuclear pore complex is able to transport macromolecules with diameters of about 39 nm. *Mol. Biol. Cell* **2002**, *13*, 425–434.
91. Skepper, J.N.; Whiteley, A.; Browne, H.; Minson, A. Herpes simplex virus nucleocapsids mature to progeny virions by an envelopment --> deenvelopment --> reenvelopment pathway. *J. Virol.* **2001**, *75*, 5697–5702.
92. Nagel, C.H.; Döhner, K.; Fathollahy, M.; Strive, T.; Borst, E.M.; Messerle, M.; Sodeik, B. Nuclear egress and envelopment of herpes simplex virus capsids analyzed with dual-color fluorescence hsv1(17+). *J. Virol.* **2008**, *82*, 3109–3124.
93. Lee, C.P.; Chen, M.R. Escape of herpesviruses from the nucleus. *Rev. Med. Virol.* **2010**, *20*, 214–230.
94. Roller, R.J.; Zhou, Y.; Schnetzer, R.; Ferguson, J.; DeSalvo, D. Herpes simplex virus type 1 u(l)34 gene product is required for viral envelopment. *J. Virol.* **2000**, *74*, 117–129.
95. Chang, Y.E.; Roizman, B. The product of the ul31 gene of herpes simplex virus 1 is a nuclear phosphoprotein which partitions with the nuclear matrix. *J. Virol.* **1993**, *67*, 6348–6356.
96. Reynolds, A.E.; Ryckman, B.J.; Baines, J.D.; Zhou, Y.; Liang, L.; Roller, R.J. U(l)31 and u(l)34 proteins of herpes simplex virus type 1 form a complex that accumulates at the nuclear rim and is required for envelopment of nucleocapsids. *J. Virol.* **2001**, *75*, 8803–8817.
97. Reynolds, A.E.; Wills, E.G.; Roller, R.J.; Ryckman, B.J.; Baines, J.D. Ultrastructural localization of the herpes simplex virus type 1 ul31, ul34, and us3 proteins suggests specific roles in primary envelopment and egress of nucleocapsids. *J. Virol.* **2002**, *76*, 8939–8952.
98. Liang, L.; Baines, J.D. Identification of an essential domain in the herpes simplex virus 1 ul34 protein that is necessary and sufficient to interact with ul31 protein. *J. Virol.* **2005**, *79*, 3797–3806.
99. Mou, F.; Wills, E.G.; Park, R.; Baines, J.D. Effects of lamin a/c, lamin b1, and viral us3 kinase activity on viral infectivity, virion egress, and the targeting of herpes simplex virus u(l)34-encoded protein to the inner nuclear membrane. *J. Virol.* **2008**, *82*, 8094–8104.

100. Bjerke, S.L.; Roller, R.J. Roles for herpes simplex virus type 1 ul34 and us3 proteins in disrupting the nuclear lamina during herpes simplex virus type 1 egress. *Virology* **2006**, *347*, 261–276.
101. Reynolds, A.E.; Liang, L.; Baines, J.D. Conformational changes in the nuclear lamina induced by herpes simplex virus type 1 require genes u(l)31 and u(l)34. *J. Virol.* **2004**, *78*, 5564–5575.
102. Ryckman, B.J.; Roller, R.J. Herpes simplex virus type 1 primary envelopment: Ul34 protein modification and the us3-ul34 catalytic relationship. *J. Virol.* **2004**, *78*, 399–412.
103. Mou, F.; Wills, E.; Baines, J.D. Phosphorylation of the u(l)31 protein of herpes simplex virus 1 by the u(s)3-encoded kinase regulates localization of the nuclear envelopment complex and egress of nucleocapsids. *J. Virol.* **2009**, *83*, 5181–5191.
104. Mou, F.; Forest, T.; Baines, J.D. Us3 of herpes simplex virus type 1 encodes a promiscuous protein kinase that phosphorylates and alters localization of lamin a/c in infected cells. *J. Virol.* **2007**, *81*, 6459–6470.
105. Morris, J.B.; Hofemeister, H.; O'Hare, P. Herpes simplex virus infection induces phosphorylation and delocalization of emerin, a key inner nuclear membrane protein. *J. Virol.* **2007**, *81*, 4429–4437.
106. Leach, N.; Bjerke, S.L.; Christensen, D.K.; Bouchard, J.M.; Mou, F.; Park, R.; Baines, J.; Haraguchi, T.; Roller, R.J. Emerin is hyperphosphorylated and redistributed in herpes simplex virus type 1-infected cells in a manner dependent on both ul34 and us3. *J. Virol.* **2007**, *81*, 10792–10803.
107. Leach, N.R.; Roller, R.J. Significance of host cell kinases in herpes simplex virus type 1 egress and lamin-associated protein disassembly from the nuclear lamina. *Virology* **2010**, *406*, 127–137.
108. Kato, A.; Yamamoto, M.; Ohno, T.; Tanaka, M.; Sata, T.; Nishiyama, Y.; Kawaguchi, Y. Herpes simplex virus 1-encoded protein kinase ul13 phosphorylates viral us3 protein kinase and regulates nuclear localization of viral envelopment factors ul34 and ul31. *J. Virol.* **2006**, *80*, 1476–1486.
109. Cano-Monreal, G.L.; Wylie, K.M.; Cao, F.; Tavis, J.E.; Morrison, L.A. Herpes simplex virus 2 ul13 protein kinase disrupts nuclear lamins. *Virology* **2009**, *392*, 137–147.
110. Park, R.; Baines, J.D. Herpes simplex virus type 1 infection induces activation and recruitment of protein kinase c to the nuclear membrane and increased phosphorylation of lamin b. *J. Virol.* **2006**, *80*, 494–504.
111. Shiba, C.; Daikoku, T.; Goshima, F.; Takakuwa, H.; Yamauchi, Y.; Koiwai, O.; Nishiyama, Y. The ul34 gene product of herpes simplex virus type 2 is a tail-anchored type ii membrane protein that is significant for virus envelopment. *J. Gen. Virol.* **2000**, *81*, 2397–2405.
112. Yamauchi, Y.; Shiba, C.; Goshima, F.; Nawa, A.; Murata, T.; Nishiyama, Y. Herpes simplex virus type 2 ul34 protein requires ul31 protein for its relocation to the internal nuclear membrane in transfected cells. *J. Gen. Virol.* **2001**, *82*, 1423–1428.
113. Klupp, B.G.; Granzow, H.; Mettenleiter, T.C. Primary envelopment of pseudorabies virus at the nuclear membrane requires the ul34 gene product. *J. Virol.* **2000**, *74*, 10063–10073.
114. Fuchs, W.; Klupp, B.G.; Granzow, H.; Osterrieder, N.; Mettenleiter, T.C. The interacting ul31 and ul34 gene products of pseudorabies virus are involved in egress from the host-cell nucleus and represent components of primary enveloped but not mature virions. *J. Virol.* **2002**, *76*, 364–378.

115. Camozzi, D.; Pignatelli, S.; Valvo, C.; Lattanzi, G.; Capanni, C.; Dal Monte, P.; Landini, M.P. Remodelling of the nuclear lamina during human cytomegalovirus infection: Role of the viral proteins pul50 and pul53. *J. Gen. Virol.* **2008**, *89*, 731–740.
116. Muranyi, W.; Haas, J.; Wagner, M.; Krohne, G.; Koszinowski, U.H. Cytomegalovirus recruitment of cellular kinases to dissolve the nuclear lamina. *Science* **2002**, *297*, 854–857.
117. Lake, C.M.; Hutt-Fletcher, L.M. The epstein-barr virus bfrf1 and bflf2 proteins interact and coexpression alters their cellular localization. *Virology* **2004**, *320*, 99–106.
118. Farina, A.; Feederle, R.; Raffa, S.; Gonnella, R.; Santarelli, R.; Frati, L.; Angeloni, A.; Torrisi, M.R.; Faggioni, A.; Delecluse, H.J. Bfrf1 of epstein-barr virus is essential for efficient primary viral envelopment and egress. *J. Virol.* **2005**, *79*, 3703–3712.
119. Gonnella, R.; Farina, A.; Santarelli, R.; Raffa, S.; Feederle, R.; Bei, R.; Granato, M.; Modesti, A.; Frati, L.; Delecluse, H.J.; *et al.* Characterization and intracellular localization of the epstein-barr virus protein bflf2: Interactions with bfrf1 and with the nuclear lamina. *J. Virol.* **2005**, *79*, 3713–3727.
120. Milbradt, J.; Auerochs, S.; Marschall, M. Cytomegaloviral proteins pul50 and pul53 are associated with the nuclear lamina and interact with cellular protein kinase c. *J. Gen. Virol.* **2007**, *88*, 2642–2650.
121. Milbradt, J.; Auerochs, S.; Sticht, H.; Marschall, M. Cytomegaloviral proteins that associate with the nuclear lamina: Components of a postulated nuclear egress complex. *J. Gen. Virol.* **2009**, *90*, 579–590.
122. Marschall, M.; Marzi, A.; aus dem Siepen, P.; Jochmann, R.; Kalmer, M.; Auerochs, S.; Lischka, P.; Leis, M.; Stamminger, T. Cellular p32 recruits cytomegalovirus kinase pul97 to redistribute the nuclear lamina. *J. Biol. Chem.* **2005**, *280*, 33357–33367.
123. Hamirally, S.; Kamil, J.P.; Ndassa-Colday, Y.M.; Lin, A.J.; Jahng, W.J.; Baek, M.C.; Noton, S.; Silva, L.A.; Simpson-Holley, M.; Knipe, D.M.; *et al.* Viral mimicry of cdc2/cyclin-dependent kinase 1 mediates disruption of nuclear lamina during human cytomegalovirus nuclear egress. *PLoS Pathog.* **2009**, *5*, e1000275.
124. Prichard, M.N. Function of human cytomegalovirus ul97 kinase in viral infection and its inhibition by maribavir. *Rev. Med. Virol.* **2009**, *19*, 215–229.
125. Milbradt, J.; Webel, R.; Auerochs, S.; Sticht, H.; Marschall, M. Novel mode of phosphorylation-triggered reorganization of the nuclear lamina during nuclear egress of human cytomegalovirus. *J. Biol. Chem.* **2010**, *285*, 13979–13989.
126. Lee, C.P.; Huang, Y.H.; Lin, S.F.; Chang, Y.; Chang, Y.H.; Takada, K.; Chen, M.R. Epstein-barr virus bglf4 kinase induces disassembly of the nuclear lamina to facilitate virion production. *J. Virol.* **2008**, *82*, 11913–11926.
127. Miller, M.S.; Furlong, W.E.; Pennell, L.; Geadah, M.; Hertel, L. Rascal is a new human cytomegalovirus-encoded protein that localizes to the nuclear lamina and in cytoplasmic vesicles at late times postinfection. *J. Virol.* **2010**, *84*, 6483–6496.
128. Klupp, B.G.; Granzow, H.; Mettenleiter, T.C. Effect of the pseudorabies virus us3 protein on nuclear membrane localization of the ul34 protein and virus egress from the nucleus. *J. Gen. Virol.* **2001**, *82*, 2363–2371.

129. Morimoto, T.; Arii, J.; Tanaka, M.; Sata, T.; Akashi, H.; Yamada, M.; Nishiyama, Y.; Uema, M.; Kawaguchi, Y. Differences in the regulatory and functional effects of the us3 protein kinase activities of herpes simplex virus 1 and 2. *J. Virol.* **2009**, *83*, 11624–11634.
130. de Noronha, C.M.; Sherman, M.P.; Lin, H.W.; Cavrois, M.V.; Moir, R.D.; Goldman, R.D.; Greene, W.C. Dynamic disruptions in nuclear envelope architecture and integrity induced by hiv-1 vpr. *Science* **2001**, *294*, 1105–1108.
131. Segura-Totten, M.; Wilson, K.L. Virology. Hiv--breaking the rules for nuclear entry. *Science* **2001**, *294*, 1016–1017.
132. Pelkmans, L.; Kartenbeck, J.; Helenius, A. Caveolar endocytosis of simian virus 40 reveals a new two-step vesicular-transport pathway to the er. *Nat. Cell Biol.* **2001**, *3*, 473–483.
133. Gilbert, J.M.; Benjamin, T.L. Early steps of polyomavirus entry into cells. *J. Virol.* **2000**, *74*, 8582–8588.
134. Gilbert, J.M.; Goldberg, I.G.; Benjamin, T.L. Cell penetration and trafficking of polyomavirus. *J. Virol.* **2003**, *77*, 2615–2622.
135. Richterova, Z.; Liebl, D.; Horak, M.; Palkova, Z.; Stokrova, J.; Hozak, P.; Korb, J.; Forstova, J. Caveolae are involved in the trafficking of mouse polyomavirus virions and artificial vp1 pseudocapsids toward cell nuclei. *J. Virol.* **2001**, *75*, 10880–10891.
136. Mannova, P.; Forstova, J. Mouse polyomavirus utilizes recycling endosomes for a traffic pathway independent of copi vesicle transport. *J. Virol.* **2003**, *77*, 1672–1681.
137. Liebl, D.; Difato, F.; Hornikova, L.; Mannova, P.; Stokrova, J.; Forstova, J. Mouse polyomavirus enters early endosomes, requires their acidic ph for productive infection, and meets transferrin cargo in rab11-positive endosomes. *J. Virol.* **2006**, *80*, 4610–4622.
138. Qian, M.; Cai, D.; Verhey, K.J.; Tsai, B. A lipid receptor sorts polyomavirus from the endolysosome to the endoplasmic reticulum to cause infection. *PLoS Pathog.* **2009**, *5*, e1000465.
139. Maul, G.G.; Rovera, G.; Vorbrodt, A.; Abramczuk, J. Membrane fusion as a mechanism of simian virus 40 entry into different cellular compartments. *J. Virol.* **1978**, *28*, 936–944.
140. Mackay, R.L.; Consigli, R.A. Early events in polyoma virus infection: Attachment, penetration, and nuclear entry. *J. Virol.* **1976**, *19*, 620–636.
141. Nakanishi, A.; Shum, D.; Morioka, H.; Otsuka, E.; Kasamatsu, H. Interaction of the vp3 nuclear localization signal with the importin alpha 2/beta heterodimer directs nuclear entry of infecting simian virus 40. *J. Virol.* **2002**, *76*, 9368–9377.
142. Gilbert, J.; Ou, W.; Silver, J.; Benjamin, T. Downregulation of protein disulfide isomerase inhibits infection by the mouse polyomavirus. *J. Virol.* **2006**, *80*, 10868–10870.
143. Lilley, B.N.; Gilbert, J.M.; Ploegh, H.L.; Benjamin, T.L. Murine polyomavirus requires the endoplasmic reticulum protein derlin-2 to initiate infection. *J. Virol.* **2006**, *80*, 8739–8744.
144. Schelhaas, M.; Malmstrom, J.; Pelkmans, L.; Haugstetter, J.; Ellgaard, L.; Grunewald, K.; Helenius, A. Simian virus 40 depends on er protein folding and quality control factors for entry into host cells. *Cell* **2007**, *131*, 516–529.
145. Kuksin, D.; Norkin, L.C. Disassembly of simian virus 40 during passage through the endoplasmic reticulum and in the cytoplasm. *J. Virol.* **2012**, *86*, 1555–1562.

146. Butin-Israeli, V.; Ben-Nun-Shaul, O.; Kopatz, I.; Adam, S.A.; Shimi, T.; Goldman, R.D.; Oppenheim, A. Simian virus 40 induces lamin a/c fluctuations and nuclear envelope deformation during cell entry. *Nucleus* **2011**, *2*, [Epub ahead of print].
147. Daniels, R.; Rusan, N.M.; Wadsworth, P.; Hebert, D.N. Sv40 vp2 and vp3 insertion into er membranes is controlled by the capsid protein vp1: Implications for DNA translocation out of the er. *Mol. Cell* **2006**, *24*, 955–966.
148. Rainey-Barger, E.K.; Magnuson, B.; Tsai, B. A chaperone-activated nonenveloped virus perforates the physiologically relevant endoplasmic reticulum membrane. *J. Virol.* **2007**, *81*, 12996–13004.
149. Huerfano, S.; Zila, V.; Boura, E.; Spanielova, H.; Stokrova, J.; Forstova, J. Minor capsid proteins of mouse polyomavirus are inducers of apoptosis when produced individually but are only moderate contributors to cell death during the late phase of viral infection. *FEBS J.* **2010**, *277*, 1270–1283.
150. Cohen, S.; Behzad, A.R.; Carroll, J.B.; Pante, N. Parvoviral nuclear import: Bypassing the host nuclear-transport machinery. *J. Gen. Virol.* **2006**, *87*, 3209–3213.
151. Cohen, S.; Marr, A.K.; Garcin, P.; Pante, N. Nuclear envelope disruption involving host caspases plays a role in the parvovirus replication cycle. *J. Virol.* **2011**, *85*, 4863–4874.
152. Hansen, J.; Qing, K.; Srivastava, A. Infection of purified nuclei by adeno-associated virus 2. *Mol. Ther.* **2001**, *4*, 289–296.

ÚŘAD PRŮMYSLOVÉHO VLASTNICTVÍ
Antonína Čermáka 2a 160 68 Praha 6
Tel.: 220 383 111 Fax: 224 324 718
E-mail: posta@upv.cz

WWW.UPV.CZ

PŘIHLÁŠKA VYNÁLEZU
se žádostí o udělení patentu

Pořadové číslo: E267152
(Vyplní Úřad)

Spisová značka přihlášky:

Potvrzení o přijetí vydáno dne: 26.01.2016,17:45:38

MPT

Vyřizuje

Kód

1. DRUH PŘIHLÁŠKY

Přihláška NÁRODNÍ (vyplňte N) nebo ZAHRANIČNÍ (vyplňte Z) (1300) N

Vyberte druh:

Nová přihláška vynálezu

2. NÁZEV VYNÁLEZU

(5400) Vakcína založená na proteinové chimerické nanočástici proti prasečímu cirkoviru 2

3. POČET PŘIHLAŠOVATELŮ

(9007) 02

4. PŘIHLAŠOVATEL(-é)

Název firmy	(710101)	Přírodovědecká fakulta Univerzity Karlovy v Praze
Příjmení	(710201)	
Jméno	(710301)	
Titul před jm.	(710401)	
Titul za jm.	(711501)	
Ulice	(710501)	Albertov

Číslo	(710601)	6
Město	(710701)	Praha 2
PSČ (jen pro ČR)	(710801)	12843
Země	(710901)	Česká republika
IČ (nepovinný údaj)	(711701)	00216208
Datum narození (nepovinný údaj)	(712001)	
Telefon	(711201)	
FAX	(711301)	
E-mail	(711401)	
Přihlašovatel je i původce	(712101)	NE
Právnická / fyzická osoba	(711601)	Právnická

Název firmy	(710102)	Dyntec spol. s r.o.
Příjmení	(710202)	
Jméno	(710302)	
Titul před jm.	(710402)	
Titul za jm.	(711502)	
Ulice	(710502)	Klučovská
Číslo	(710602)	1280
Město	(710702)	Český Brod
PSČ (jen pro ČR)	(710802)	28201
Země	(710902)	Česká republika
IČ (nepovinný údaj)	(711702)	47548002
Datum narození (nepovinný údaj)	(712002)	
Telefon	(711202)	
FAX	(711302)	
E-mail	(711402)	
Přihlašovatel je i původce	(712102)	NE
Právnická / fyzická osoba	(711602)	Právnická

5. POČET PŮVODCŮ

(9008) 4

6. PŮVODCE(-i) (V případě, že je původce současně i přihlašovatelem, není nutné požadované údaje u tohoto původce vyplňovat.)

Příjmení	(730201)	Forstová
Jméno	(730301)	Jitka
Titul před jm.	(730401)	Doc. RNDr.
Titul za jm.	(731501)	CSc.
Ulice	(730501)	Pod Vrstevnicí
Číslo	(730601)	1527
Město	(730701)	Praha 4
PSČ (jen pro ČR)	(730801)	14000
Země	(730901)	Česká republika
Datum narození (nepovinný údaj)	(732001)	

Pokud si PŮVODCE NEPŘEJE BÝT ZVEŘEJNĚN, vyplňte ANO (732201) NE

Příjmení	(730202)	Fraiberk
Jméno	(730302)	Martin
Titul před jm.	(730402)	Mgr.
Titul za jm.	(731502)	
Ulice	(730502)	Arbesova
Číslo	(730602)	1583
Město	(730702)	Teplice
PSČ (jen pro ČR)	(730802)	41502
Země	(730902)	Česká republika
Datum narození (nepovinný údaj)	(732002)	

Pokud si PŮVODCE NEPŘEJE BÝT ZVEŘEJNĚN, vyplňte ANO (732202) NE

Příjmení	(730203)	Španielová
Jméno	(730303)	Hana
Titul před jm.	(730403)	RNDr.
Titul za jm.	(731503)	Ph.D.
Ulice	(730503)	Střední
Číslo	(730603)	184
Město	(730703)	Zdiby
PSČ (jen pro ČR)	(730803)	25066
Země	(730903)	Česká republika
Datum narození (nepovinný údaj)	(732003)	

Pokud si PŮVODCE NEPŘEJE BÝT ZVEŘEJNĚN, vyplňte ANO (732203) NE

Příjmení	(730204)	Pšikal
Jméno	(730304)	Ivan
Titul před jm.	(730404)	MVDr.
Titul za jm.	(731504)	CSc.
Ulice	(730504)	Zikova
Číslo	(730604)	3
Město	(730704)	Brno
PSČ (jen pro ČR)	(730804)	62800
Země	(730904)	Česká republika
Datum narození (nepovinný údaj)	(732004)	

Pokud si PŮVODCE NEPŘEJE BÝT ZVEŘEJNĚN, vyplňte ANO (732204) NE

7. ZÁSTUPCE PŘIHLAŠOVATELE

Název kanceláře	(7401)	Patentová a známková kancelář Novotný
Příjmení	(7402)	Novotný

Jméno	(7403)	Jaroslav
Titul před jm.	(7404)	Ing.
Titul za jm.	(7415)	
Ulice	(7405)	Římská
Číslo	(7406)	45/2135
Město	(7407)	Praha 2
PSČ	(7408)	12000
Země	(7409)	Česká republika
IČ (nepovinný údaj)	(7417)	
Datum narozeni (nepovinný údaj)	(7420)	
Telefon	(7412)	721307778
FAX	(7413)	222515659
E-mail	(7414)	novotny.patenty@centrum.cz
Číslo jednací zástupce	(7419)	
Číslo prezidiální plné moci	(7418)	14947

Prezidiální plná moc je podávána současně s touto přihláškou NE

8. ADRESA PRO DORUČOVÁNÍ (Kontaktní adresa pro styk s Úřadem - Vyberte jednu z uvedených možností a údaje VYPLŇTE jen v případě, že jde o ADRESU ODLIŠNOU od adresy přihlašovatele nebo zástupce.)

(•) adresa pro doručování **není** odlišná od adresy přihlašovatele nebo zástupce ANO

( ) adresa pro doručování **je odlišná** od adresy přihlašovatele nebo zástupce

9. PRÁVO PŘEDNOSTI PODLE MEZINÁRODNÍ SMLOUVY

Číslo přihlášky	(310001)
Datum podání přihlášky	(320001)
Země / Úřad	(330001)

10. POČET PATENTOVÝCH NÁROKŮ

(9032) 2

11. PODNIKOVÝ VYNÁLEZ

Pokud jde o PODNIKOVÝ VYNÁLEZ, vyplňte "ANO", v opačném případě vyplňte "NE"	(9031)	ANO

12. NABÍDKA LICENCE

Pokud NABÍZÍTE LICENCI, vyplňte "ANO", v opačném případě vyplňte "NE"	(9033)	ANO

13. SEZNAM PŘÍLOH

- Popis vynálezu	PV Vakcína založená na protei	(9009)	ANO
- Patentové nároky		(9010)	
- Anotace		(9011)	
- Obrázek k anotaci		(9012)	
- Výkresy		(9013)	

Pozn.: V případě papírové formy podání je třeba popis vynálezu, patentové nároky, anotaci, obrázek k anotaci a výkresy předložit ve třech vyhotoveních.

- Plná moc	(9015)
- Doklad o nabytí práva na patent	(9014)
- Prioritní doklad	(9019)
- Žádost o provedení úplného průzkumu	(9017)
- Potvrzení o deponování mikroorganismů	(9016)

Další přílohy: (Vyplňte název.)

Název

13A. ŽÁDOST O ÚPLNÝ PRŮZKUM (Není již nutné podávat samostatnou žádost o provedení úplného průzkumu.)

ŽÁDÁM O PROVEDENÍ ÚPLNÉHO PRŮZKUMU u této přihlášky vynálezu podle zákona č. 527/1990 Sb., o vynálezech a zlepšovacích návrzích, ve znění pozdějších předpisů.

(označte křížkem) ☐ANO ☒NE

13B. Souhlasím s předáním výsledků rešerše pro účely Pravidla 141 EPC přímo EPÚ.

(označte křížkem) ☒ANO ☐NE

Vysvětlivky (poznámka)

13B O úplný průzkum lze požádat buď při podání přihlášky (označením příslušného políčka ve formuláři křížkem) nebo formou samostatné žádosti kdykoli během následujících 36 měsíců.

V případě, že budete z této přihlášky nárokovat právo přednosti v následné evropské patentové přihlášce a máte zájem, aby požadavek podle Pravidla 141 EPC, tj. předložení výsledků rešerše Evropskému patentovému úřadu (EPÚ) provedl přímo náš Úřad, pak příslušné políčko označte křížkem. Jinak musíte požadavku z Pravidla 141 EPC vyhovět sami.

14. INFORMACE O VÝŠI SPRÁVNÍHO POPLATKU

Správní poplatek za podání přihlášky vynálezu přihlašovatelem je stanoven na 1200 Kč.
Správní poplatek za podání přihlášky vynálezu přihlašovatelem, který je současně i původcem, je stanoven na 600 Kč.

** **Způsob platby** (Vyberte jednu z uvedených možností.)

Převodem z účtu *

Pozn.: Správní poplatek je splatný při podání přihlášky. Kolky lze použít pouze pro platby do 5000 Kč (včetně).
*) Číslo účtu správních poplatků ÚPV: 3711-21526001/0710.
**) Ostatní informace o platbě jsou uvedeny v nápovědě.

Místo pro nalepení kolku

15. POZNÁMKA

(9034) Vynález byl vytvořen za podpory agentury TAČR, č. projektu 2013TA03010700.

Potvrzuji pravdivost a úplnost shora uvedených údajů a žádám o udělení patentu.

Vyberte jednu z uvedených možností:

○ Přihlašovatel(-é) (V případě více přihlašovatelů musí být uvedeny podpisy všech těchto přihlašovatelů.)

◉ Zástupce

26.01.2016	Ing. Jaroslav Novotný Digitálně podepsal Ing. Jaroslav Novotný DN: c=CZ, l=Praha 2-Nové Město, ou=P122034, cn=Ing. Jaroslav Novotný, serialNumber=P122034 Datum: 2016.01.26 17:45:57 +01'00'
Datum	Podpis (u právnické osoby případně i razítko)

Varování:

V návaznosti na zveřejnění Vaší přihlášky nebo ochranného dokumentu můžete obdržet nabídku - výzvu k úhradě, která může na první pohled vypadat jako dokument vystavený některým z patentových nebo známkových úřadů (ÚPV, WIPO, EPO, OHIM), a přitom jde pouze o pokus podvodně vylákat peníze.

Nabádáme tímto k maximální obezřetnosti.

Příklady nabídek - výzev jsou uvedeny např. na adrese:

http://www.upv.cz/cs/upv/aktuality/varovani/varovani-rejstriky.html

Pokud obdržíte takové podání, nejlepší obranou je podání trestního oznámení na jeho odesílatele (vzor získáte od ÚPV), popřípadě jej můžete zaslat Úřadu průmyslového vlastnictví (posta@upv.cz), který potřebné kroky učiní za Vás.

ČESKÁ REPUBLIKA
ÚŘAD PRŮMYSLOVÉHO VLASTNICTVÍ

OSVĚDČENÍ

O ZÁPISU UŽITNÉHO VZORU

Josef Kratochvíl
předseda
Úřadu průmyslového vlastnictví

Úřad průmyslového vlastnictví

zapsal podle § 11 odst. 1 zákona č. 478/1992 Sb., v platném znění, do rejstříku

UŽITNÝ VZOR

číslo

29249

na technické řešení uvedené v přiloženém popisu.

ÚŘAD PRŮMYSLOVÉHO VLASTNICTVÍ

V Praze dne 8.3.2016

Za správnost:

Ing. Jan Mrva
vedoucí oddělení rejstříků

Číslo zápisu: **29249** Datum zápisu: 08.03.2016

Číslo přihlášky: **2016-32039** Datum přihlášení: 26.01.2016

MPT:

A 61 K 39/12	(2006.01)
C 12 N 7/04	(2006.01)
C 07 K 14/01	(2006.01)
A 61 P 31/20	(2006.01)

Název: Vakcína založená na proteinové virové nanočástici odvozené z bovinního papilomaviru 1

Majitel: Přírodovědecká fakulta Univerzity Karlovy v Praze, Praha 2
Dyntec spol. s r.o., Český Brod

Původce: doc. RNDr. Jitka Forstová, CSc., Praha 4
Mgr. Martin Fraiberk, Teplice
RNDr. Hana Španielová, Ph.D., Zdiby
MVDr. Ivan Pšikal, CSc., Brno

UŽITNÝ VZOR

(11) Číslo dokumentu:

29 249

(13) Druh dokumentu: **U1**

(51) Int. Cl.:

A61K 39/12	(2006.01)
C12N 7/04	(2006.01)
C07K 14/01	(2006.01)
A61P 31/20	(2006.01)

(19) ČESKÁ REPUBLIKA

ÚŘAD PRŮMYSLOVÉHO VLASTNICTVÍ

(21) Číslo přihlášky: **2016-32039**
(22) Přihlášeno: **26.01.2016**
(47) Zapsáno: **08.03.2016**

(73) Majitel:
Přírodovědecká fakulta Univerzity Karlovy v Praze, Praha 2, CZ
Dyntec spol. s r.o., Český Brod, CZ

(72) Původce:
doc. RNDr. Jitka Forstová, CSc., Praha 4, CZ
Mgr. Martin Fraiberk, Teplice, CZ
RNDr. Hana Španielová, Ph.D., Zdiby, CZ
MVDr. Ivan Pšikal, CSc., Brno, CZ

(74) Zástupce:
Patentová a známková kancelář Novotný, Ing. Jaroslav Novotný, Římská 45/2135, 120 00 Praha 2

(54) Název užitného vzoru:
Vakcína založená na proteinové virové nanočástici odvozené z bovinního papilomaviru 1

Vakcína založená na proteinové virové nanočástici odvozené z bovinního papilomaviru 1

Oblast techniky

Technické řešení se týká vakcíny založené na proteinové virové nanočástici odvozené z bovinního papilomaviru 1, která slouží k vytvoření imunity hospodářských zvířat.

Dosavadní stav techniky

Proti bovinnímu papilomaviru 1, který se vyskytuje v chovech hospodářského skotu, neexistuje vakcína. Nanočástice, které by byly dostatečné a nahrazovaly virovou vakcínu proti bovinnímu papilomaviru 1, rovněž nejsou známy. Některá zvířata trpící touto chorobou se musí porazit. Jejich kůže a postižené sliznice se musí bezpečně zlikvidovat. Choroba postihuje nejčastěji kůži, dutinu ústní, penis a vemeno.

Úkolem vynálezců bylo vyvinout vakcínu založenou na proteinové virové nanočástici odvozenou z bovinního papilomaviru 1, která by preventivně ochránila zejména skot před virovou infekcí.

Podstata technického řešení

Uvedené nedostatky odstraňuje vakcína založená na proteinové virové nanočástici odvozené z bovinního papilomaviru 1, podle tohoto technického řešení, jehož podstata spočívá v produkci a izolaci nanočástic, složených z hlavního kapsidového proteinu L1 boviního papilomaviru, který se spontánně uspořádává do tvaru prázdné kapsidy (VLP).

K největším výhodám tohoto technického řešení patří jednoduchá příprava, dále to, že virová nanočástice není virulentní z důvodu chybějící genové virové informace. Další výhodou je snadná izolovatelnost.

Příklady uskutečnění technického řešení

Virové nanočástice jsou organizovaně uspořádané komplexy papilomavirového proteinu L1. Komplex se skládá z 360 molekul proteinu L1. Připraví se následujícím postupem.

Rekombinantní bakulovirus pro produkci chimerické nanočástice (složené z hlavního kapsidového proteinu bovinního papilomaviru 1 – L1) v hmyzích buňkách byl připraven metodou „Bac to Bac“ (Invitrogen). Pracuje se pouze s genem bovinního papilomaviru 1 – L1, kdy při výrobním procesu se nikde nepracuje s kompletním genomem BPV 1-L1. Nemůže tudíž dojít k replikaci viru. Hmyzí buňky Sf 9 adaptované na kultivaci v bezsérovém mediu se infikují v bioreaktoru inokulem rekombinantního bakuloviru s multiplicitou infekce 10. Po 5 dnech se buněčná suspenze lyzuje, a VLP částice se purifikují filtrací přes keramické filtry různých pórů. Rekombinantní bakulovirus není přítomen ve finálním produktu.

Průmyslová využitelnost

Uvedené technické řešení je využitelné pro prevenci papilomavirových chorob v chovech hospodářských zvířat, kde není dostupná vakcína.

NÁROKY NA OCHRANU

1. Vakcína založená na proteinové virové nanočástici odvozené z bovinního papilomaviru 1, **vyznačující se tím**, že je složena z hlavního kapsidového proteinu L1, přičemž se jedná o prázdnou kapsidu, která neobsahuje genom - DNA bovinního papilomaviru 1, přičemž kapsidový protein L1 se spontáně uspořádal do tvaru prázdné kapsidy - VLP.

Konec dokumentu

ČESKÁ REPUBLIKA
ÚŘAD PRŮMYSLOVÉHO VLASTNICTVÍ

OSVĚDČENÍ

O ZÁPISU UŽITNÉHO VZORU

Josef Kratochvíl
předseda
Úřadu průmyslového vlastnictví

Úřad průmyslového vlastnictví

zapsal podle § 11 odst. 1 zákona č. 478/1992 Sb., v platném znění, do rejstříku

UŽITNÝ VZOR

číslo

29310

na technické řešení uvedené v přiloženém popisu.

ÚŘAD PRŮMYSLOVÉHO VLASTNICTVÍ 8

V Praze dne 22.3.2016

Za správnost:

Ing. Jan Mrva
vedoucí oddělení rejstříků

Číslo zápisu: **29310** Datum zápisu: 22.03.2016

Číslo přihlášky: **2016-32043** Datum přihlášení: 26.01.2016

MPT:
A 61 K 38/02 (2006.01)
B 82 Y 5/00 (2011.01)
C 07 K 14/025 (2006.01)

Název: Vakcína založená na proteinové chimerické nanočástici proti prasečímu cirkoviru 2

Majitel: Přírodovědecká fakulta Univerzity Karlovy v Praze, Praha 2
Dyntec spol. s r.o., Český Brod

Původce: doc. RNDr. Jitka Forstová, CSc., Praha 4
Mgr. Martin Fraiberk, Teplice
RNDr. Hana Španielová, Ph.D., Zdiby
MVDr. Ivan Pšikal, CSc., Brno

UŽITNÝ VZOR

(11) Číslo dokumentu:

29 310

(13) Druh dokumentu: **U1**

(51) Int. Cl.:

A61K 38/02	(2006.01)
B82Y 5/00	(2011.01)
C07K 14/025	(2006.01)

(19) ČESKÁ REPUBLIKA

ÚŘAD PRŮMYSLOVÉHO VLASTNICTVÍ

(21) Číslo přihlášky: **2016-32043**
(22) Přihlášeno: **26.01.2016**
(47) Zapsáno: **22.03.2016**

(73) Majitel:
Přírodovědecká fakulta Univerzity Karlovy v Praze, Praha 2, CZ
Dyntec spol. s r.o., Český Brod, CZ

(72) Původce:
doc. RNDr. Jitka Forstová, CSc., Praha 4, CZ
Mgr. Martin Fraiberk, Teplice, CZ
RNDr. Hana Španielová, Ph.D., Zdiby, CZ
MVDr. Ivan Pšikal, CSc., Brno, CZ

(74) Zástupce:
Patentová a známková kancelář Novotný, Ing. Jaroslav Novotný, Římská 45/2135, 120 00 Praha 2

(54) Název užitného vzoru:
Vakcína založená na proteinové chimerické nanočástici proti prasečímu cirkoviru 2

Vakcína založená na proteinové chimerické nanočástici proti prasečímu cirkoviru 2

Oblast techniky

Technické řešení se týká vakcíny založené na proteinové chimerické nanočástici proti prasečímu cirkoviru 2, která nahrazuje inaktivovanou virovou vakcínu proti uvedenému viru.

Dosavadní stav techniky

Ke dnešku jsou na trhu 4 vakcíny proti prasečímu cirkoviru 2. Francouzká firma Merial vyvinula vakcínu Circovac založenou na inaktivovaném PCV2 viru. Firma Fort Dodge připravila vakcinu spočívající v chimerickém viru PCV1 ve kterém byl gen pro Cap (kapsidový protein) zaměněn za protein z PCV2. Produkty Circoflex (Boehrinhger, Ingelheim) a Circumvent (Intervet) jsou založeny na inaktivovaných chimerických bakulovirech produkujících cirkovirový Cap protein. Vzhledem k vysokým cenám těchto vakcín ani v České republice ani v celé řadě dalších zemí nedochází k plošné vakcinaci. Po levnější účinné vakcinaci je stále poptávka o čemž svědčí provedený průzkum trhu. Chimerická nanočástice – pentamer fůzního proteinu VP1 myšího polyomaviru a Cap proteinu prasečího cirkoviru 2 je produkována ve velkých množstvích v hmyzích buňkách z rekombinantního bakuloviru a díky připojené His-tag kotvě je snadno izolovatelná. Vzhledem k tomu, že se nejedná o virus, není třeba inaktivace. Při podobných vakcinačních účincích jako má nejlepší z dostupných vakcín (Circoflex), bude cena nižší.

Úkolem vynálezců bylo vyvinout vakcínu založenou na proteinové chimerické nanočástici proti prasečímu cirkoviru 2, která nahrazuje inaktivovanou virovou vakcínu proti uvedenému viru.

Podstata technického řešení

Uvedené nedostatky odstraňuje vakcína založená na proteinové chimerické nanočástici proti prasečímu cirkoviru 2, podle tohoto technického řešení, jehož podstata spočívá v tom, že nanočástice je složena z nosiče, který tvoří pentamer kapsidového proteinu VP1 myšího polyomaviru, na který jsou kovalentně připojeny molekuly kapsidového proteinu prasečího cirkoviru 2, neobsahující genom (DNA) prasečího cirkoviru 2, ani genom myšího papilomaviru a dále je připojena His-tag kotva. Chimerická nanočástice má kapsidový protein tvořen kmenem prasečího cirkoviru 2B.

K největším výhodám tohoto technického řešení patří jednoduchá příprava, dále to, že chimerická nanočástice není vůbec virulentní z důvodu chybějící genové virové informace. Další výhodou je snadná izolovatelnost.

Příklady uskutečnění technického řešení

Nanočástice je složena z nosiče, který tvoří pentamer kapsidového proteinu VP1 myšího polyomaviru, na který jsou kovalentně připojeny molekuly kapsidového proteinu prasečího cirkoviru 2 a dále je připojena His-tag kotva. His-tag kotva je řetězec po sobě jdoucích aminokyselin hystidinu. Tento řetězec je schopen vázat dvoumocné ionty kovů, nejčastěji Ni2+, Cu2+, Zn2+. Tyto ionty jsou ukotveny na nosiči v koloně a umožňují isolaci proteinu. Kapsidový protein je ve výhodném provedení tvořen prasečím cirkovirem 2B (v současnosti nejrozšířenějším kmenem). Chimerická nanočástice se připraví následujícím postupem:

Rekombinantní bakulovirus pro produkci chimerické nanočástice (složené z pentameru fůzního proteinu VP1 myšího polyomaviru a Cap proteinu prasečího cirkoviru) v hmyzích buňkách byl připraven metodou „Bac to Bac“ (Invitrogen). Hmyzí buňky Sf 9 adaptované na kultivaci v bezsérovém mediu se infikují v bioreaktoru inokulem rekombinantního bakuloviru s multiplicitou infekce 10. Po 5 dnech se buněčná suspenze lyzuje, opracuje DNasou a pentamery se izolují afinitní chromatografií s využitím His-tag kotvy. Rekombinantní bakulovirus není přítomen ve finálním produktu. Pracuje se pouze s geny pro kapsidové proteiny myšího polyomaviru

a prasečího cirkoviru 2. Při výrobním procesu se nikde nepracuje s kompletními genomy myšího polyomaviru a prasečího cirkoviru 2. Nemůže tudíž dojít k replikaci virů.

Průmyslová využitelnost

Uvedené technické řešení je využitelné pro prevenci virových chorob v chovech hospodářských zvířat, kde není dostupná (příliš drahá) vakcína, nebo je použití vakcíny riskantní z hlediska možného rozvoje choroby po její aplikaci.

NÁROKY NA OCHRANU

1. Vakcína založená na proteinové chimerické nanočástici proti prasečímu cirkoviru 2, **vyznačující se tím**, že nanočástice je složena z nosiče, který tvoří pentamer kapsidového proteinu VP1 myšího polyomaviru, na který jsou kovalentně připojeny molekuly kapsidového proteinu prasečího cirkoviru 2, přičemž tento neobsahuje genom DNA prasečího cirkoviru 2, ani genom myšího papilomaviru a dále je připojena His-tag kotva.

2. Vakcína podle nároku 1, **vyznačující se tím**, že kapsidový protein je tvořen kmenem prasečího cirkoviru 2B.

Konec dokumentu

PŘÍRODOVĚDECKÁ FAKULTA
Univerzita Karlova

DYNTEC

T A
Č R

Diagnostický antigen založený na rekombinantním proteinu VP1-Cap

Funkční vzorek připraven v rámci projektu TAČR (TA03010700)

1. Charakterizace vzorku:

Diagnostický antigen VP1-Cap je fúzní protein složený z hlavního kapsidového proteinu VP1 myšího polyomaviru (MPyV) a kapsidového proteinu Cap prasečího cirkoviru typu 2 (PCV2). Protein je produkovaný v bakulovirovém expresním systému ve formě pentamer. Antigen je určený pro diagnostiku - zjišťování koncentrace Cap proteinu v biologických vzorcích a také jako standarda v imunotestech používaných pro kvantifikaci Cap proteinu v jednotlivých šaržích vakcinačního antigenu k přesnému definování množství antigenní složky ve vakcíně.

2. Složení

Funkční vzorek obsahuje nativní antigen (pentamerní fúzní protein VP1-Cap), rozpuštěný v pufru PBS o definované koncentraci.

3. Příprava

3.1. Vytvoření rekombinantního bakuloviru produkující VP1- Cap (PřFUK)

Fuzní gen složený ze sekvencí kodujících MPyV VP1 a PCV2 Cap byly vloženy do transferového bakulovirového vektoru pFasBacI. Transferovým vektorem byly transfekovány bakterie DH10Bac pro vytvoření bacmidu (DNA obsahující genom rekombinantního bakuloviru). Rekombinantní bakulovirus byl připraven po transfekci bacmidu do hmyzích buněk Sf9.

3.2. Pomnožení antigenu VP1-Cap v kultuře hmyzích buněk SF9 (Dyntec spol. s r.o.)

Buňky Sf9 byly předpěstovány v bezsérovém médiu v 50 ml zkumavkách TS50 v kultivačním objemu 10 ml, inkubovaných na orbitálních třepačkách PZ-M/47-50 při teplotě 27°C ± 1°C a při rychlosti třepání 230 rpm. Pro osazení jednoho bioreaktoru TS600 bylo potřeba napěstovat buňky v deseti zkumavkách TS50 s minimální hustotou 2,0 x 10^6 /ml živých buněk s viabilitou ≥90%, která byla obvykle dosažena 4. až 5. den po nasazení (Graf, obr.1).

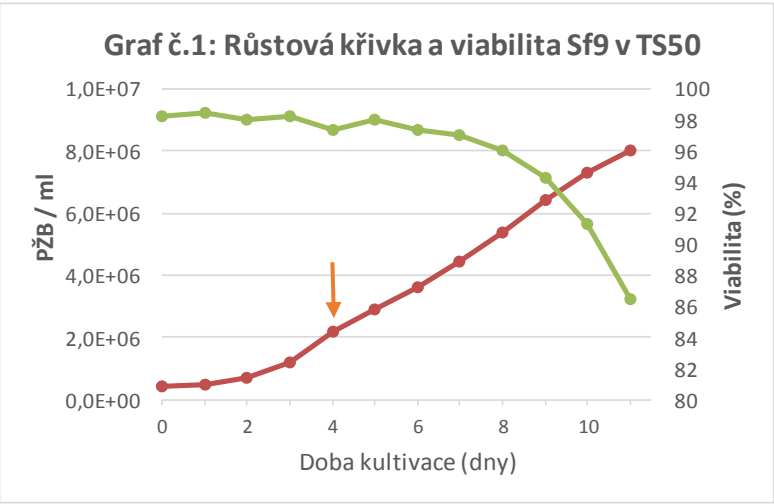

Obr. 1: Růstová křivka (červeně) a viabilita (zeleně)

Bioreaktor TS600 byl osazen 400ml buněčné suspenze SF9 o koncentraci 2,0 x 10^6 /ml. Následovala infekce buněčné kultury zásobním inokulem obsahujícím rBacV pro pomnožení antigenu VP1-Cap. Množství inokula potřebného pro infekci bylo vypočítáno dle vzorce:

$$rBacV\ inokulum\ (ml) = \frac{\text{MOI (PFU/buňku)} x\ počet\ buněk}{\text{titr virového inokula (PFU/ml)}}$$

Multiplicita infekce byla 5 PFU/buňka. Po 48 hodinách byla buněčná suspenze sklizena centrifugací 200xg, RT, 10minut po 50ml aliquotech. Aliquoty byly uchovávány zmrazeny při -20°C.

3.3. Výroba nativního lyzátu z infikovaných buněk SF9 a purifikace antigenu. (PřFUK)

- 50ml aliquot byl resuspendován celkem v 10ml vychlazeného pufru PBS.
- Následovala sonikace suspenze ve skříňovém sonikátoru na ledu 3x30s s 1 minutovým chlazením, amplituda 10.
- Nativní lyzát byl klarifikován centrifugací 8000xg, 15 minut, 4°C.
- Aliquot lyzátu byl testován na přítomnost antigenu metodou DotBlot (Obr.2).
- Supernatant byl zředěn na objem 60ml a zkoncentrován na ultracentrifuze Beckman, rotor SW28, 25000rpm, 4°C, 3h.
- Sediment byl rozplaven v celkem 10ml vychlazeného pufru PBS a zředěn pufrem PBS na hmotnost 32 g.
- Celkem 14,6g CsCl bylo rozpuštěno v 32 g rozplaveného sedimentu. Koncentrace CsCl byla zkontrolována refraktometricky (ref. Index = 1,365), popřípadě upravena přidáním pufru PBS.
- Směs CsCl a rozplaveného sedimentu byla rozdělena do 4 centrifugačních zkumavek, vyvážena a byla provedena ultracentrifugace na centrifuze Beckman, rotor SW40, 35000rpm, 18°C, 24h.
- CsCl gradienty byly rozebrány na celkem 8 frakcí. Frakce 4 gradientů, odpovídající stejným refraktometrickým indexům byly sloučeny.
- Byla provedena dvoustupňová dialýza jednotlivých frakcí s různými refraktometrickými indexy proti pufru PBS, 4°C, 48h.
- Jednotlivé frakce byly po dialýze testovány na čistotu a kvalitu antigenu SDS elektroforézou (SDS PAGE; Obr. 3).
- Frakce, které prokázaly vysokou čistotu (nepřítomnost kontaminujících proteinů) byly sjednoceny a koncentrace antigenu určena metodou Bradfordové (DCSOP 4313-1).

4. Testování kvality

Test přítomnosti antigenu metodou DotBlot (RMSOP129SBX216x)

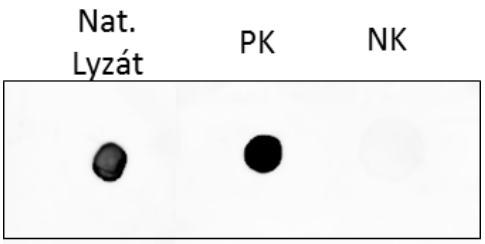

Obr. 2: Test přítomnosti antigenu: Dot Blot
PK – pozitivní kontrola, NK – negativní kontrola

Test čistoty a kvality antigenu metodou SDS PAGE (RMSOP128SDX2160)

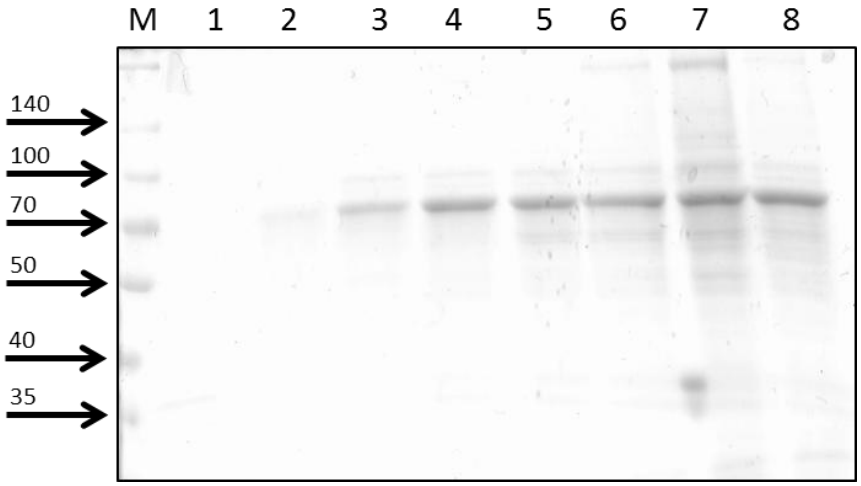

Obr. 3: Test kvality a čistoty antigenu metorou SDS-PAGE
Frakce, které obsahují antigenVP1-Cap (71 kDa) v požadované čistotě, byly sjednoceny (frakce 2, 3, 4, 5 a 6).

5. Ověření účinnosti

Studie účinnosti antigenu v „sandwich“ ELISA testu byla provedena na souboru vzorků odebraných pro mezioperační zkoušky při přípravě vakcinačního antigenu VP1-Cap- a v testech opakovatelnosti (intraassay) v různých ředěních antigenu. Koeficient variace absorbancí odečtených v různých ředěních antigenu (STD = VP1-Cap) nepřesahoval hodnotu 20% (viz tab. 1).

Číslo měření	STD (1:400)	STD (1:800)	STD (1:3200)	NK (1:400)	NK (1:800)	NK (1:3200)
1	0,779	0,300	0,121	0,076	0,062	0,084
2	0,696	0,298	0,132	0,064	0,067	0,067
3	0,684	0,288	0,102	0,06	0,062	0,066
4	0,72	0,286	0,101	0,061	0,061	0,073
5	0,749	0,262	0,099	0,073	0,06	0,065
6	0,794	0,272	0,097	0,063	0,061	0,066
7	0,811	0,268	0,101	0,059	0,06	0,066
8	0,761	0,270	0,118	0,063	0,064	0,069
9	0,791	0,291	0,106	0,071	0,073	0,068
10	0,806	0,261	0,102	0,063	0,065	0,07
11	0,813	0,271	0,098	0,061	0,065	0,065
12	0,696	0,251	0,093	0,062	0,062	0,069
13	0,688	0,281	0,098	0,063	0,062	0,067
14	0,702	0,276	0,095	0,064	0,064	0,074
15	0,767	0,262	0,091	0,065	0,061	0,075
16	0,827	0,272	0,099	0,064	0,065	0,07
X OD	0,755	0,276	0,103	0,065	0,063	0,070
SD	0,051	0,014	0,011	0,005	0,003	0,005
CV (%)	6,701	5,089	10,701	7,360	5,182	7,092
N(X+3SD)	NT	NT	0,136	0,079	0,073	0,084
Největší	0,827	0,300	0,132	0,076	0,073	0,084
Nejmenší	0,684	0,251	0,091	0,059	0,060	0,065
Počet	16	16	16	16	16	16

Tab 1: Test opakovatelnosti stanovení proteinu VP1-Cap (STD) a negativní kopntroly (NK) v různých ředěních.

6. Návod k použití

Standardní operační protokol je k dispozici ve firmě Dyntec pod označením RMSOP130SDX2170.

7. Balení, skladování

Diagnostický antigen je rozplněn po 0,2 ml do 0,5 ml mikrozkumavek utěsněných proti sublimaci parafilmem, které se uchovávají zmražené při -20°C. Mikrozkumavky jsou uloženy v krabičce a označeny štítkem, který obsahuje název výrobce, název přípravku, koncentraci antigenu a číslo šarže.

Autoři: Mgr. Martin Fraiberk, MVDr. Ivan Pšikal, CSc, Doc RNDr. Jitka Forstová, CSc.

Funkční vzorek byl vytvořen s podporou TAČR.

control - GFP expressing cells													
experiment 1							experiment 2						
Day	EGFP positive cells (%)	Normalization to 2nd day (%)	dead EGFP positive cells (%)	EGFP positive apoptotic cells (%)	EGFP positive apoptotic cells relative to dead cells(%)	% EGFP G2/M	EGFP positive cells (%)	Normalization to 2nd day (%)	dead EGFP positive cells (%)	EGFP positive apoptotic cells (%)	EGFP positive apoptotic cells relative to dead cells(%)	% EGFP G2/M
2	96.4	100	6.41	4.84	75.51	29.6	97.2	100	4.97	3.89	78.27	30.2
3	96	99.59	4.66	4.14	88.84	29	96	98.77	4.94	4.23	85.63	28.1
4	94.3	97.82	3.71	3.27	88.14	25	94.3	97.02	3.87	3.38	87.34	22.2
5	90.9	94.29	3.31	2.97	89.73	27	91.1	93.72	3.74	3.32	88.77	25.6
6	79.3	82.26	4.5	3.47	85.68	27.9	79.8	82.1	3.46	2.19	63.3	27.3
7	47.6	49.38	2.23	2.9	93.72	27.9	49.8	51.23	3.36	3.12	92.86	28.1
VP1/(EGFP) expressing cells													
experiment 1							experiment 2						
Day	EGFP positive cells (%)	Normalization to 2nd day (%)	dead EGFP positive cells (%)	EGFP positive apoptotic cells (%)	EGFP positive apoptotic cells relative to dead cells(%)	% EGFP G2/M	EGFP positive cells (%)	Normalization to 2nd day (%)	dead EGFP positive cells (%)	EGFP positive apoptotic cells (%)	EGFP positive apoptotic cells relative to dead cells(%)	% EGFP G2/M
2	93.3	100	7.75	5.54	71.48	30.9	91.7	100	5.69	4.54	79.79	33.8
3	89.2	95.61	8.48	6.8	80.19	29.2	87	94.87	5.18	4.33	83.59	31.3
4	78.1	83.71	4.8	3.51	86.03	28.4	76.9	83.86	4.81	4.22	87.73	32.8
5	56	60.02	5.41	4.94	91.31	28.2	54.1	59	4.92	4.5	91.46	31.3
6	31	33.27	4.49	3.95	87.97	34.2	30.4	33.15	6.68	6.11	91.47	34.6
7	13.1	14.4	4.9	4.35	88.78	39	12.7	13.85	5.69	5.29	92.97	38.4

mock	
Day	% G2/M
2	26.3
3	27.3
4	24.2
5	23.5
6	23.5
7	24.6

G2/M measurements

control - EGFP expressing cells

experiment 1

day 2

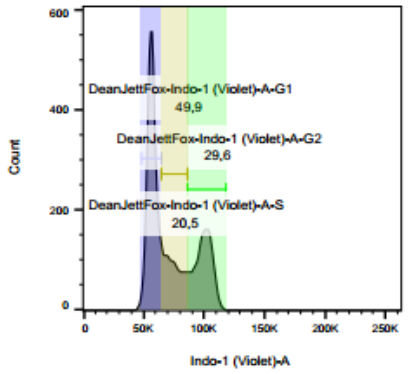

96.4% EGFP positive cells

day 3

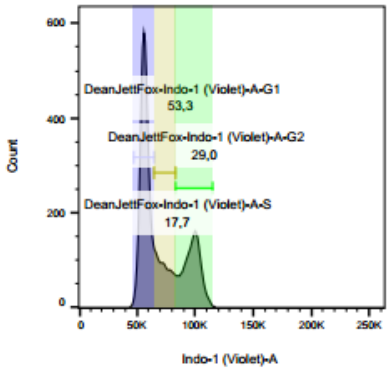

96% EGFP positive cells

day 4

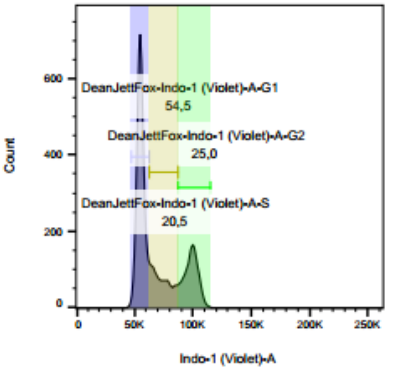

94.3% EGFP positive cells

day 5

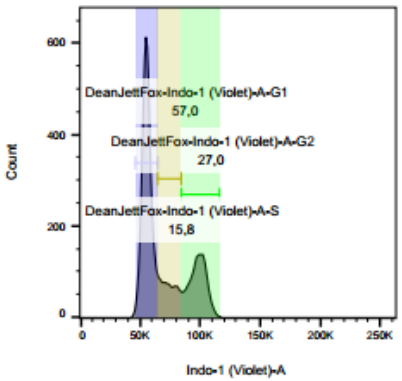

90.9% EGFP positive cells

day 6

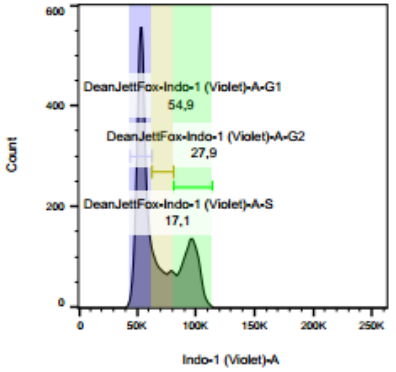

79.3% EGFP positive cells

day 7

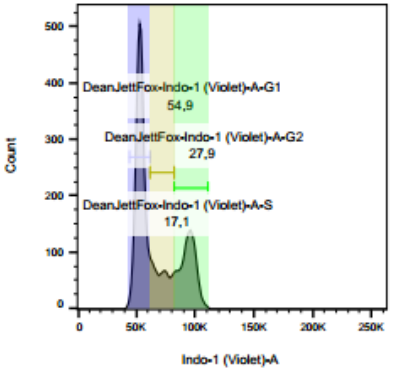

47.6% EGFP positive cells

VP1/(EGFP) expressing cells

experiment 1

day 2

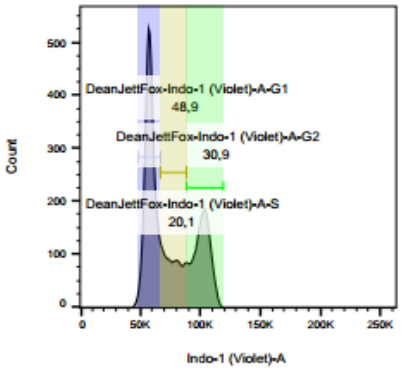

93.3% EGFP positive cells

day 3

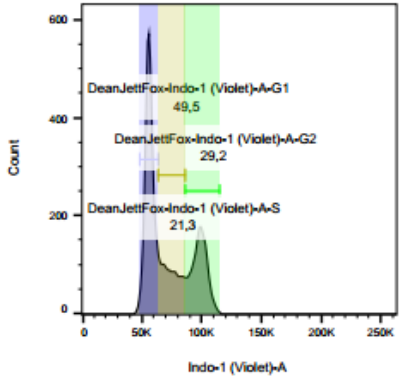

89.2% EGFP positive cells

day 4

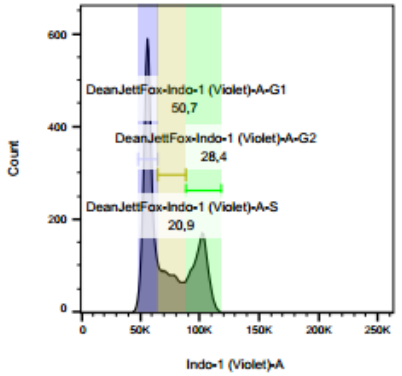

78.1% EGFP positive cells

day 5

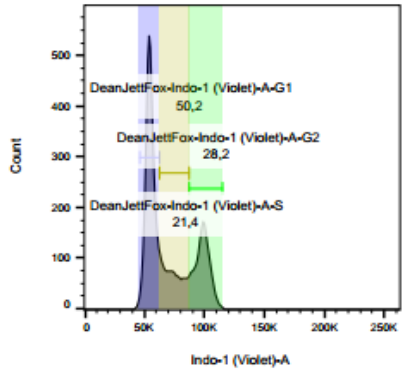

56% EGFP positive cells

day 6

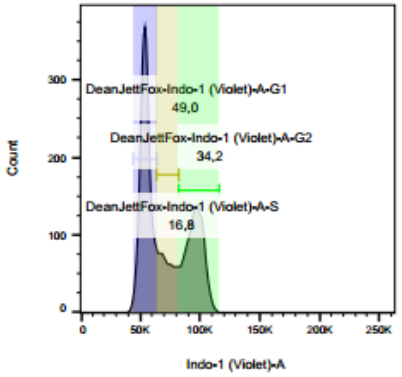

31% EGFP positive cells

day 7

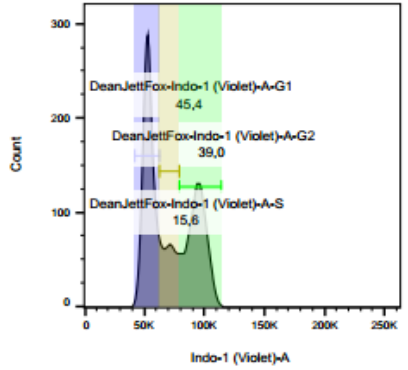

13.1% EGFP positive cells

control - EGFP expressing cells

experiment 2

day 2

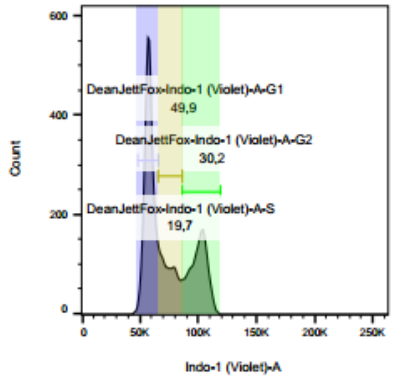

97.2% EGFP positive cells

day 3

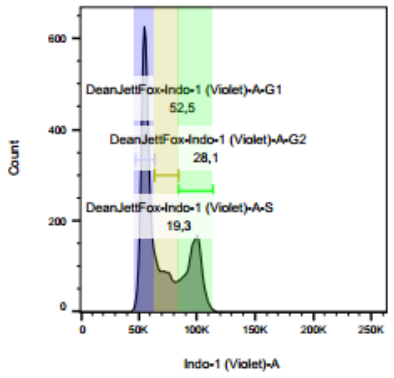

96% EGFP positive cells

day 4

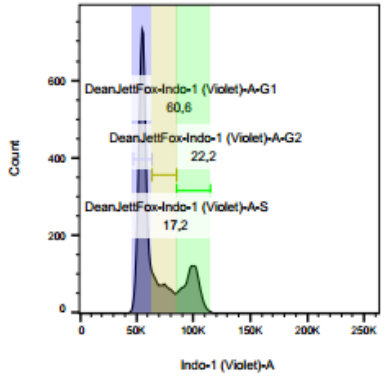

94.3% EGFP positive cells

day 5

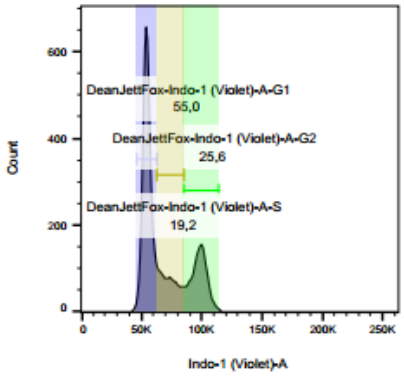

91.1% EGFP positive cells

day 6

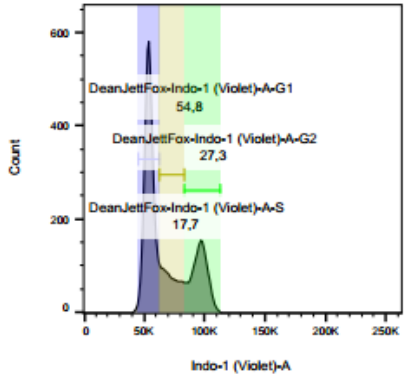

79.8 EGFP positive cells

day 7

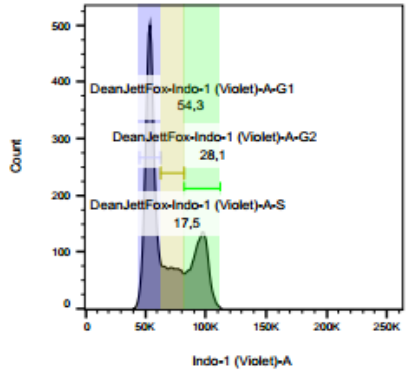

48.8% EGFP positive cells

VP1/(EGFP) expressing cells

experiment 2

day 2

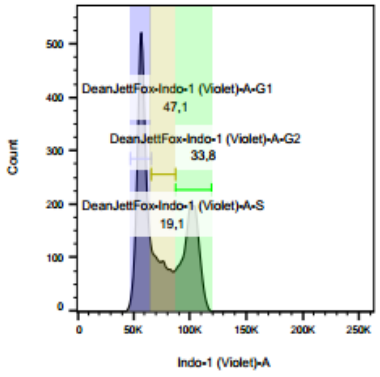

91.7% EGFP positive cells

day 3

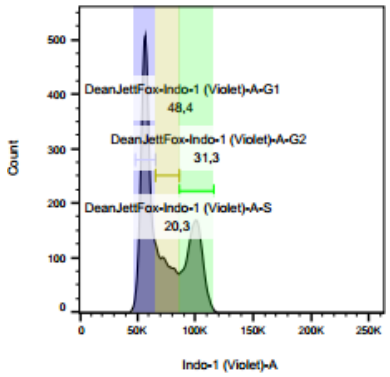

87% EGFP positive cells

day 4

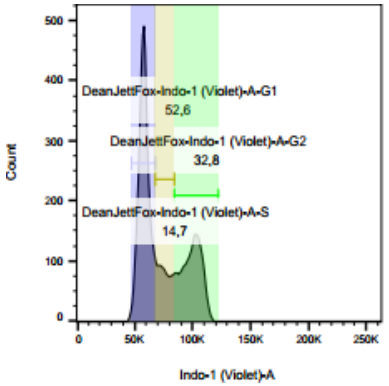

76.9% EGFP positive cells

day 5

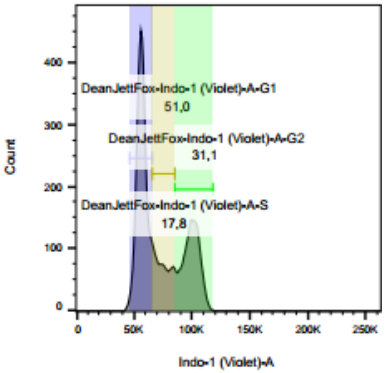

54.1% EGFP positive cells

day 6

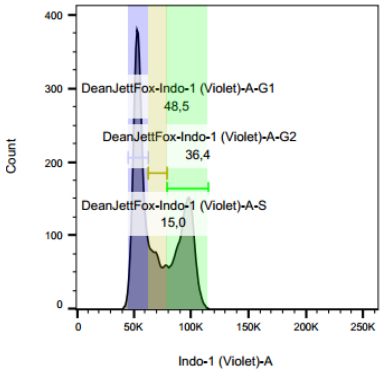

30.4% EGFP positive cells

day 7

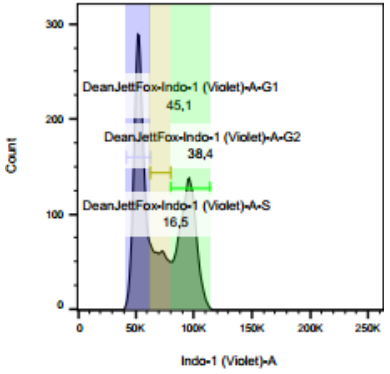

12.7% EGFP positive cells

MOCK transfected cells

day 2

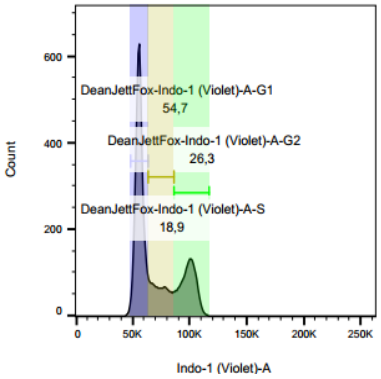

day 3

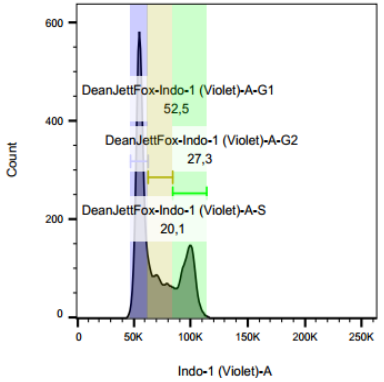

day 4

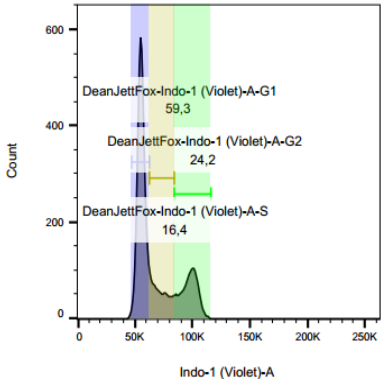

day 5

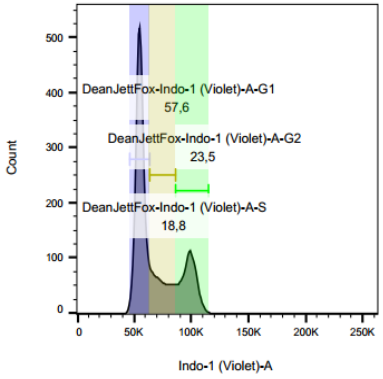

day 6

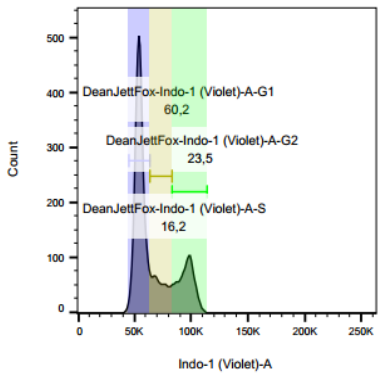

day 7

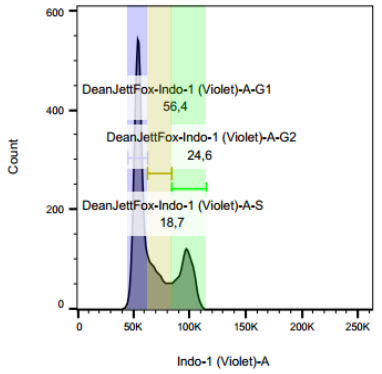

Cell death – annexin and DAPI staining

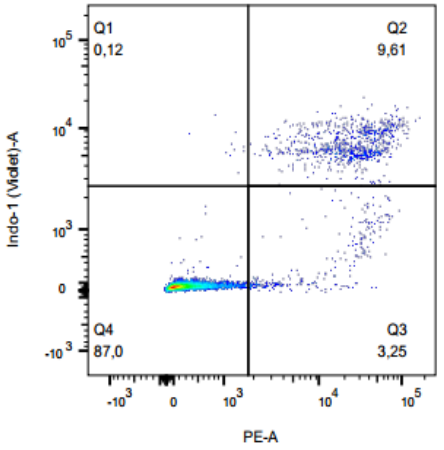

Annexin and DAPI staining Q2 – necrotic cells
Q3 - apoptotic cells
Q4 – living cells

Annexin V and DAPI staining adjustment

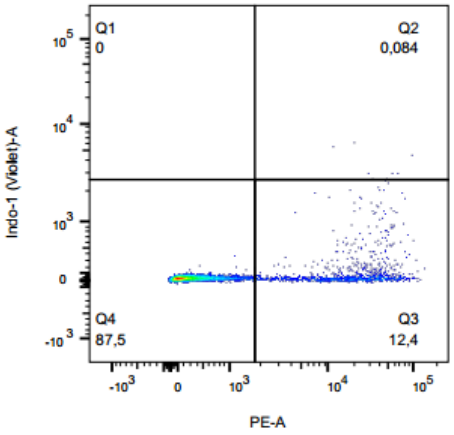

Annexin V staining Q3 - death cells
Q4 – living cells

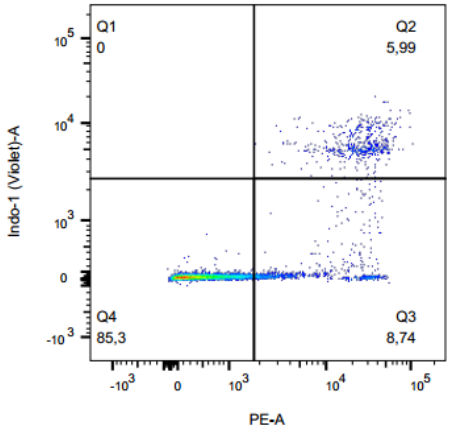

Annexin and DAPI staining, apoptosisi induction
Q2 – necrotic cells
Q3 - apoptotic cells
Q4 – living cells

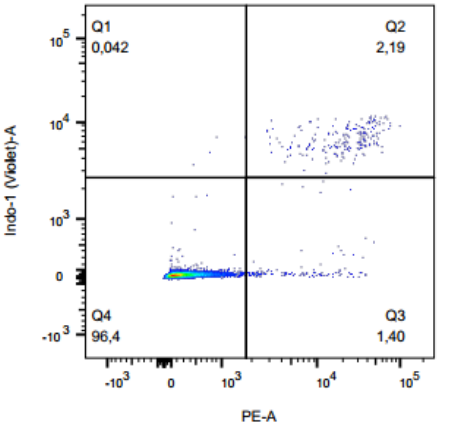

Annexin and DAPI staining, without apoptosisi induction
Q2 – necrotic cells
Q3 - apoptotic cells
Q4 – living cells

control - EGFP expressing cells

experiment 1

day 2

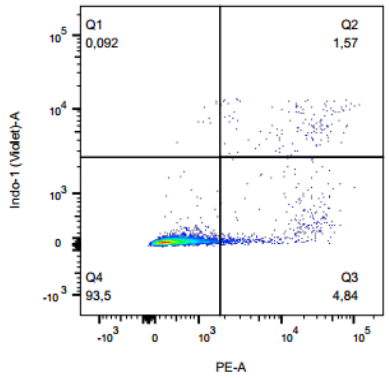

day 3

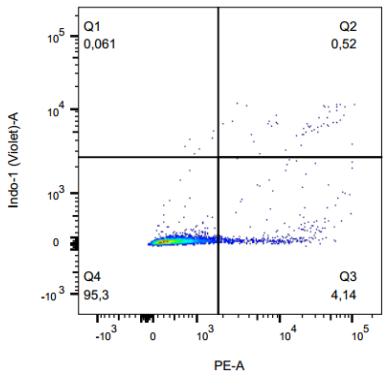

day 4

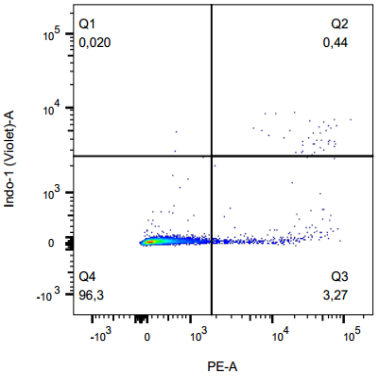

day 5

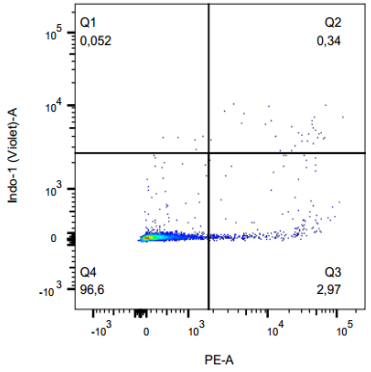

day 6

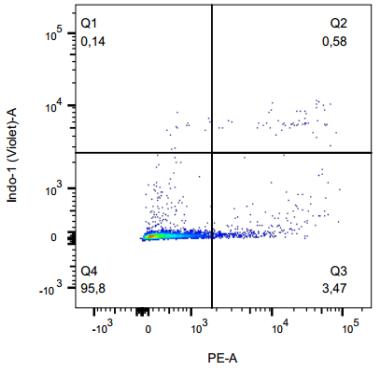

day 7

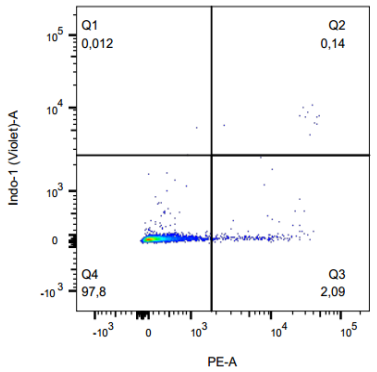

VP1/(EGFP) expressing cells

experiment 1

day 2

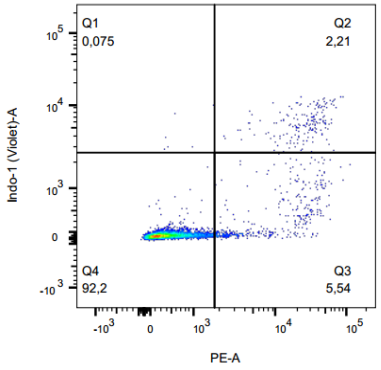

day 3

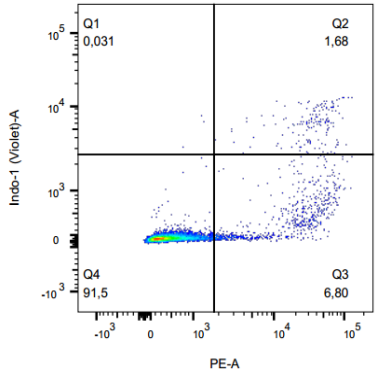

day 4

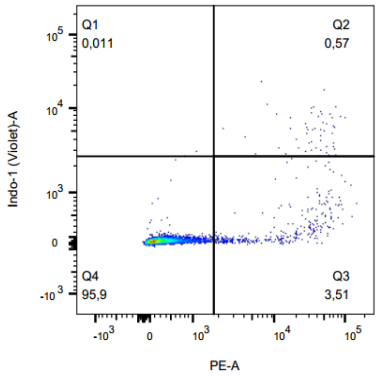

day 5

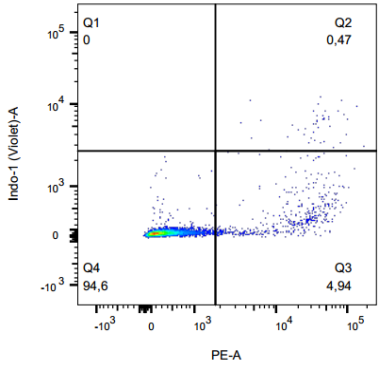

day 6

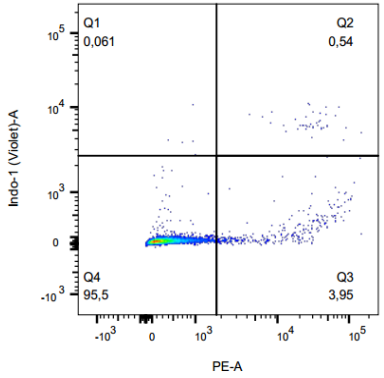

day 7

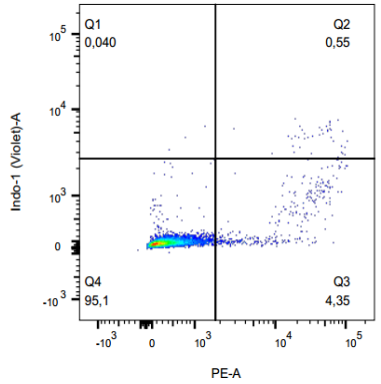

control - EGFP expressing cells

experiment 2

day 2

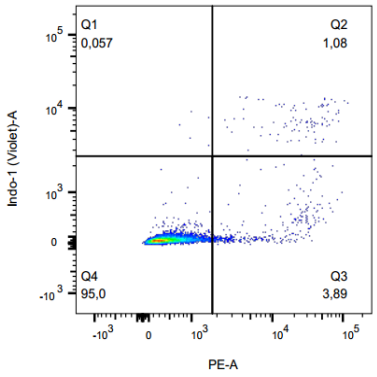

day 3

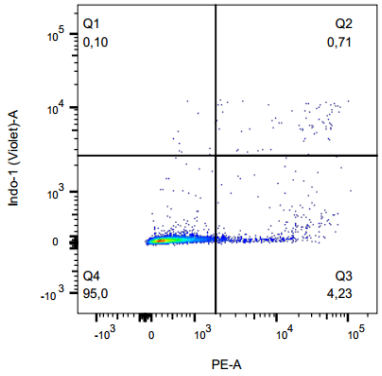

day 4

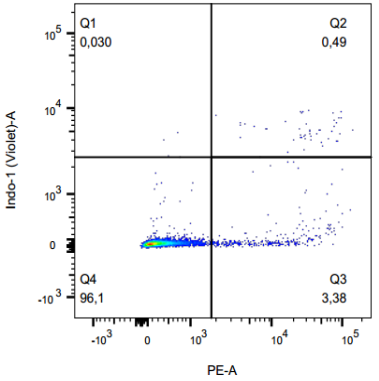

day 5

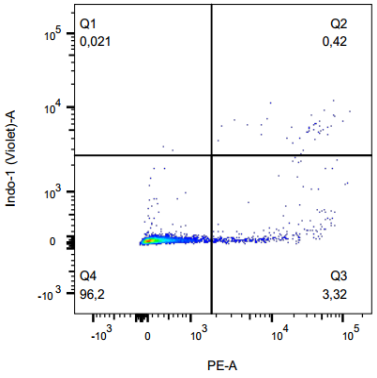

day 6

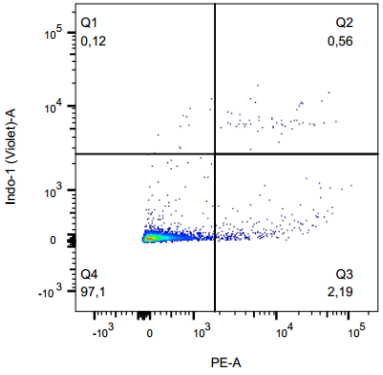

day 7

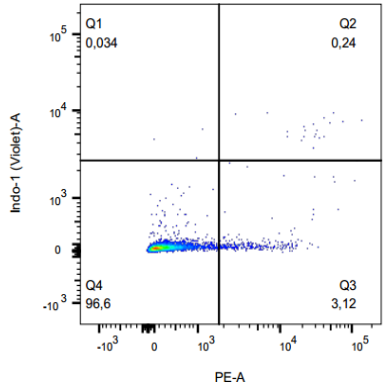

VP1/(EGFP) expressing cells

experiment 2

day 2

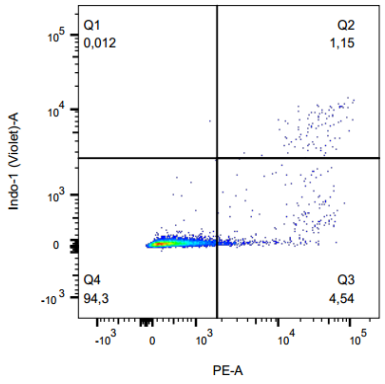

day 3

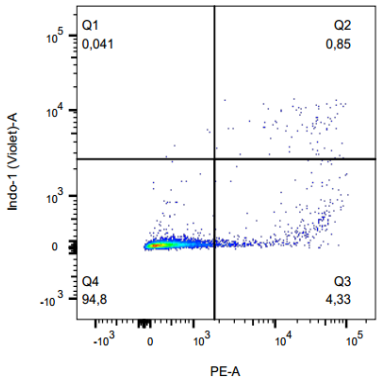

day 4

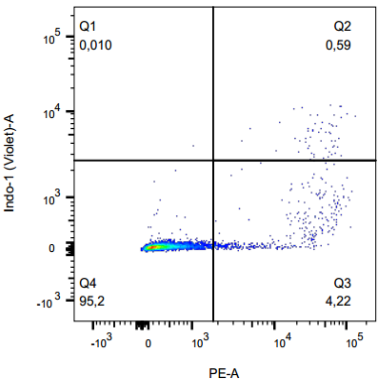

day 5

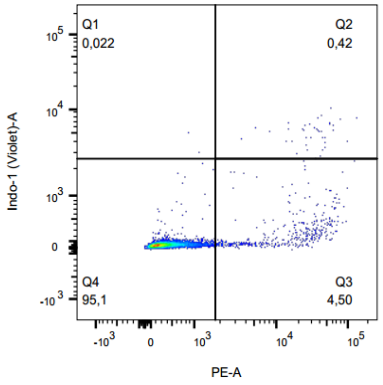

day 6

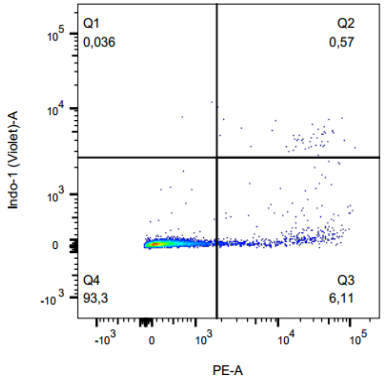

day 7